PhD Thesis

Ordered thin films of amphiphilic compounds and nanoparticles

Jan Paczesny

Advisor: prof. dr hab. Robert Hołyst

The dissertation was prepared within

the International PhD Studies at the

Institute of Physical Chemistry of the Polish Academy of Sciences

Kasprzaka 44/52, 01-224 Warszawa

Warsaw, April 2012

To my Parents, Friends and beloved Karolina

I gratefully dedicate this thesis

Acknowledgements

It was tricky to convince my Mother that it was good choice to become a chemist. I hope this thesis is convincing not only for her. Although it took a lot of work from me, it would not have been possible without the help that so many have contributed with. I would especially like to thank

Robert Hołyst, for being more than supervisor for me. Usually student is working in the main flow of research of the group; however I never had problems to work on my own ideas as well. I really appreciate that. I am especially thankful for the talks and how you inspired me to do my best both in science and in life. Thank you.

Andrzej Żywociński, a brilliant co-worker and great friend. You have had always time to help me with everyday work and answered all the question, even the stupid ones.

Krzysztof Sozański, the best undergraduate student ever. You have done excellent work in the drop casting project.

Patrycja Nitoń, who introduced me to the bolaamphiphile research.

Carsten Tschierske and his group (from Martin-Luther-University Halle-Wittenberg), for great contribution in bolaamphiphile part of the thesis.

Jacek Gregorowicz, who taught me so much in the field of polymer science. Our cooperation started serendipitously, however I really appreciate it.

Witold Adamkiewicz and **Katarzyna Winkler**, for being there to chat not only about work. Thank you for successful cooperation on SERS platform preparation. Witek was responsible for GaN nanowires growth and Kasia for gold microflowers deposition.

Ewa Górecka and **Damian Pociecha** (Warsaw University), for their trust and possibility to use equipment in the LBS laboratory.

Igor Dzięcielewski (Unipress PAS), for help with SEM and being so positive with all our ideas.

Agnieszka Kamińska, for help with SERS platform preparation.

Kostyantyn Nikiforov, for help with AFM imaging.

Michał Wójcik (Warsaw University) and **Volodymyr Sashuk**, for help with gold nanoparticles synthesis.

Wojciech Lisowski and **Janusz Sobczak**, for their contribution and help with XPS measurements.

All **co-authors** of my papers and manuscripts. Thank you for all the help.

The thesis was prepared as a result of work within:

The work was supported by the Foundation for Polish Science within „Team Programme" **TEAM/2008-2/2**, co-financed by the EU European Regional Development Fund.

Project partially supported by National Science Centre according to decision **DEC-2011/01/N/ST5/02917**.

Jan Paczesny is a scholar within Sub-measure 8.2.2 Regional Innovation Strategies, Measure 8.2 Transfer of knowledge, Priority VIII Regional human resources for the economy Human Capital Operational Programme co-financed by European Social Fund and state budget **DFS.VI.3361-4-37-033/10**.

Publications connected with the thesis:

1. *Formation of net-like patterns of gold nanoparticles in liquid crystal matrix at the air/water interface*
   Paczesny, J.; Sozański, K.; Dzięcielewski, I.; Żywociński, A.; Hołyst, R. *J. Nanopart. Res.* **2012**, **DOI**: 10.1007/s11051-012-0826-4.

2. *Stable, ordered multilayers of partially fluorinated bolaamphiphiles at the air-water interface*
   Paczesny, J.; Nitoń, P.; Żywociński, A.; Sozański, K.; Hołyst, R.; Glettner, B.; Kieffer, R.; Tschierske, C.; Pociecha, D.; Górecka, E. *Soft Matter* **2012**, **DOI:** 10.1039/C2SM00022A.

3. *Aggregation and layering transitions in thin films of X-,T-, and anchor-shaped bolaamphiphiles at the air/water interface*
   Nitoń, P.; Żywociński, A.; **Paczesny, J.**; Fiałkowski, M.; Hołyst, R.; Glettner, B.; Kieffer, R.; Tschierske, C.; Pociecha, D.; Górecka, E. *Chem. Eur. J.* **2011**, *17*, 5861.

4. *Reversible Aggregation of X-Shaped Bolaamphiphiles with Partially Fluorinated Lateral Chains at the Air/Water Interface*
   Nitoń, P.; Żywociński, A.; Hołyst, R.; Kieffer, R.; Tschierske, C.; **Paczesny, J.**; Pociecha, D.; Górecka, E. *Chemical Communications* **2010**, *46*, 1896.

5. *Three steps of hierarchical self-assembly towards stable and efficient SERS platform*
   Paczesny, J.; Sozański, K.; Dzięcielewski, I.; Adamkiewicz, W.; Winkler, K.; Kamińska, A.; Żywociński, A.; Hołyst, R. *Chemistry of Materials* **2012**, submitted.

6. *Phase transitions in monolayer formed by hyperbranched polyester with alkyl-terminated branches at air/water interface*
   Paczesny, J.; Gregorowicz, J.; Nikiforov, K. *Langmuir* **2012**, submitted.

7. *Self-assembly of Partially Fluorinated Bolaamphiphiles into Ordered Layered Structures*
   Paczesny, J.; Sozański, K.; Żywociński, A.; Hołyst, R.; Glettner, B.; Kieffer, R.; Tschierske, C.; Nikiforov K. manuscript in preparation.

8. *Formation of Nanoring Arrays by Self-assembly of Gold Nanoparticles with Bolaamphiphilic Moieties*
   Paczesny, J.; Wójcik, M.; Sozański, K.; Nikiforov, K.; Tschierske, C.; Górecka, E.; Mieczkowski, J.; Hołyst R. manuscript in preparation

Patent applications:

9. *Method for deposition of nanoparticles on solid substrates and surface covered by this method*
   Paczesny, **J.**; Sozański, K.; Żywociński, A.; Hołyst, R.; Dzięcielewski, I.; Adamkiewicz, W. *P-395009*, **25.05.2011**.

10. *Method for fabrication of 2D net-like patterns of nanoparticles on solid substrates and surface covered by this method*
    Paczesny, **J.**; Sozański, K.; Dzięcielewski, I.; Adamkiewicz, W.; Winkler, K.; Kamińska, A.; Żywociński, A.; Hołyst, R. *P-397169*, **29.11.2011**.

11. *SERS platform and its preparation method*
    Paczesny, **J.**; Sozański, K.; Dzięcielewski, I.; Adamkiewicz, W.; Winkler, K.; Kamińska, A.; Żywociński, A.; Hołyst, R. *P-397249*, **05.12.2011**.

Other publications:

12. *The interaction between G-quadruplex-forming oligonucleotide and cationic surfactant monolayer at the air/water interface*
    Juskowiak, B.; **Paczesny, J.** *J. Colloid Interface Sci.* **2012**, *365*, 150.

13. *Influence of detergents on development of domesticated plants – research project conducted by high school student*
    Paskal, W.; Malendowicz, E.; **Paczesny, J.** *Chemistry–Didactic–Ecology–Metrology* **2011**, *16*, 1 (corresponding author).

14. *Bystander Cell Death and Stress Response is Inhibited by the Radical Scavenger α1-Microglobulin in Irradiated Cell Cultures*
    Olsson, M. G.; Nilsson, E. J. C.; Rutardottir, S.; **Paczesny, J.**; Pallon, J.; Ákerström, B. *Radiat. Res.* **2010**, *174*, 590.

15. *Using microdispensing to manufacture a customized cell dish for microbeam irradiation of single, living cells*
    Nilsson, E. J. C.; Olsson, M. G.; Nilsson, J.; Pallon, J.; Masternak, A.; **Paczesny**, **J.**; Arteaga-Marrero, N.; Elfman, M.; Kristiansson, P.; Nilsson, C.; Ákerström, B. *Nucl. Instrum. & Meth. B* **2009**, *267(7)*, 1199.

16. *Interactions of sodium and potassium ions with oligonucleotides carrying human telomeric sequence and pyrene moieties at both termini*
    Hayashida, H.; **Paczesny**, **J.**; Juskowiak, B.; Takenaka, S. *Bioorganic & Medicinal Chemistry* **2008**, *16*, 9871.

17. *Fluorescence Resonance Energy Transfer (FRET) in the Studies of Tetraplex DNA Structures*
    Juskowiak, B.; Galezowska, E.; **Paczesny, J.** *Wiad. Chem.* **2006**, *60*, 547.

Table of contents

Abbreviations

AFM	atomic force microscopy
BAM	Brewster angle microscopy
CVD	chemical vapor deposition
VLS	vapor liquid solid mechanism
DB	degree of branching
DC	drop casting method
LB	Langmuir-Blodgett method
LS	Langmuir-Schaeffer method
LbL	layer by layer deposition
NMR	nuclear magnetic resonance
SAM	self-assemble monolayers
SAXS	small angle X-ray scattering
SEM	scanning electron microscopy
TEM	transition electron microscopy
SERS	surface enhanced Raman spectroscopy
STM	scanning tunneling microscopy
XPS	X-ray photoelectron scattering
XRR	X-ray reflectivity
ESP	equilibrium spreading pressure
Col_{hex}	hexagonal columnar phase
Col_{squ}	square columnar phase
Cr	crystalline solid
GS	glassy state
Iso	isotropic phase
Lam_{Iso}	lamellar isotropic phase
Lam_{N}	lamellar nematic phase
Lam_{Sm}	lamellar smectic phase
LC	liquid crystal, liquid crystalline
M	mesophase
A1-A2	anchor-shape bolaamphiphiles
T1-T2	T-shape bolaamphiphiles
X1-X6	X-shape bolaamphiphiles
8CB	4`-n-octyl-4-cyanobiphenyl
8OCB	4'-n-octyloxy-4-cyanobiphenyl
AA	arachidic acid
C1	12,12,13,13,14,14,15,15,16,16, 17,17,18,18,19,19,19 heptadecafluorononadecan-1-ol
NPs	nanoparticles
B-Au NPs	gold nanoparticles with covalently attached bolaamphiphilic domains
Au MFs	gold microflowers
THF	tetrahydrofuran
TMA	N,N,N trimethyl (11- mercapto undecyl) ammonium chloride
bis-MPA	2,2-bis (hydroxymethyl) propionic acid
H3200	hyperbranched polyester studied in **Chapter 6** (see **Figure 59**)
p-MBA	*p*-mercaptobenzoic acid
PTFE	poly (tetrafluoroethylene)
CPK	geometrical model of molecular shape from the names of Corey, Pauling and Koltun

Symbols

a, **b**, **c**	set of samples
w, l, t	geometrical dimensions
A_m	mean molecular area
A_L	area occupied by the film at the subphase
A_S	area of substrate
c	concentration
*c**	overlap concentration
C_s	compressibility
ε_s	static elasticity
d	density
d_n	thickness of film of n molecular layers
d_s	thickness of sublayer of film
EF	enhancement factor
I_{SERS}, I_{NR}	intensity of selected peak measured by SERS and regular Raman respectively
N_{SERS}, N_{NR}	number of molecules probed by SERS and regular Raman respectively
F	force
G	Gibbs free energy
g	gravity constant
L	number of layers in thin films
M	molecular weight
M_n, M_w	number and weight averaged molecular weight respectively
P	pressure
$P_{i,j}$	correlation coefficient
i, j	indexes of the spectra
k	the wave number index of the individual spectrum
σ_i	the standard deviation of the spectrum
Γ	spectra reproducibility
R_g	radius of gyration
T	temperature
T_m	melting point
ν	Flory`s exponent
V	surface potential
W	spectral range
γ	surface tension
ε	dielectric permittivity constant
ε_0	dielectric permittivity constant of vacuum
Θ	theta solvent
θ_c	contact angle
θ	angle of diffraction
θ_i	impinging angle
2δ	critical angle of incidence
λ, λ_{ex}	wavelength, excitation wavelength
μ	dipole moment
π	surface pressure
τ	transfer ratio
υ_{CS}, υ_{CC}	stretching vibrations
R_F, R_H	fluorinated segment and hydrocarbon segment of aliphatic chain, respectively

Abstract

Thin films have been of great interest for more than a hundred years because of their technological applications and possible usage as interesting system for physicochemical investigations. The possibility of direct observations of molecular arrangement, which came with the new imaging techniques in the 1980s (Atomic Force Microscopy, Scanning Tunneling Microscopy) resulted in a new wave of interest in thin films as a part of nanotechnology. Among the most promising areas for novel applications of thin films are organic semiconductors for use in field effect transistors, photovoltaics and spintronics.

Results of several research projects are presented in the thesis. The separated parts are linked by the main idea of utilization of the Langmuir-Blodgett technique to study the intriguing behavior of matter in 2D systems as well as the possible applications of the scientific findings. In the first part of the thesis, properties of thin films of a new class of liquid crystalline amphiphilic compounds, namely bolaamphiphiles, are presented. A study of the influence of fluorination on the film stability revealed unusual reversibility and reproducibility of the $\pi(A)$ isotherms of films of partially fluorinated bolaamphiphiles. Monolayers of these compounds did not collapse during compression at the air/water interface. Ordered lamellar structures were formed instead. The balance between rigidity and flexibility of the molecules, adjusted by partial fluorination and the shape of the molecules, was the key factor to avoid irreversible aggregation of the molecules and to create ordered multilayer structures. These investigations led to a vast improvement of the general understanding of multilayers formation. A new mechanism of formation of 3-, 5- and 7- layer films has been proposed.

Further work revealed that no compression was needed to form ordered 3-layer films of bolaamphiphiles. Simple drop casting experiments gave qualitatively identical results comparing to those based on the Langmuir-Blodgett method. The self-assembly of bolaamphiphiles induced ordering in thin films containing other species. Films of mixtures of gold nanoparticles and bolaamphiphiles exhibited enhanced ordering when compared to films of pure nanoparticles. Moreover, gold nanoparticles with covalently attached bolaamphiphilic domains formed ordered supramolecular assemblies over large areas in simple drop casting experiments.

The results presented in second part of the thesis originated from the above mentioned studies on mixtures of liquid crystalline compounds and nanoparticles. The Langmuir-Blodgett

technique was used to create 2D structures of gold nanoparticles. Thus prepared surfaces were afterwards used as substrates in the chemical vapor deposition process of gallium nitride (GaN) nanowires growth. On that scaffolding, a third step of material fabrication was performed. Gold microflowers (Au MFs) deposited from solution preferably appeared at the top of the GaN nanowires and not in the cavities among them. The obtained morphology of the final material could be controlled at each step of the preparation process to tailor its properties for desired purposes. The obtained surface was found to be active in surface enhanced Raman spectroscopy (SERS) with the enhancement factor around 10^7. Prepared platforms were also suitable for biological and biomedical applications. The label-free detection of DNA was demonstrated. Prepared substrates gave reproducible SERS spectra both across a single platform and between different platforms. The average spectral correlation coefficients (I) was 0.87. Moreover, the obtained material proved to be very stable.

The third part of the thesis deals with the behavior of a new class of polymers – hyperbranched polymers – at the air/water interface. Because of their novel molecular design, a number of unexpected phenomena were observed. The polymer molecules were bound through the interactions of the terminal alkyl tails. The strength of the interaction might be adjusted by changing their lengths. The mechanism of the collapse and its reversibility is discussed in detail. The temperature and/or surface pressure changes induced a first order phase transition in the monolayer. The overall picture of the transition resembled the solid – liquid phase transition in two dimensions. Large, organized structures of the polymer were transferred onto a solid substrate, ensuring stable and uniform coverage of the surface.

INTRODUCTION

1. Introduction

Nanotechnology is a part of science, which deals with self-organization processes, new materials of various shapes (spheres, rods, wires, half-shells, cubes) and compositions (organics, metals, oxides, and semiconductors) and devices, which at least one geometrical dimension is smaller than 100 nm. Such nanosystems can exhibit number of physical behaviors due to size scaling (superparamagnetism,[1] overlapping double layers in fluids[2]), which are often based on quantum phenomena (electron confinement,[3] near-field optical effects,[4] quantum entanglement,[5] electron tunneling[6] and ballistic transport[7]). Nanotechnology is present in everyday life, for instance all electronic devices use microprocessors that are built in the nanometer scale.[8] Despite that, there is still plenty of room for novel materials and devices, which might be created by means of nanotechnology. The possible applications are medicine, electronics, optoelectronics, biomaterials, energy storage and production. The best example is graphene, one atom thick planar sheet of sp2 bonded carbon atom. Graphene was explored in 2004,[9] and Nobel Prize in Physics was awarded to Andre Geim and Konstantin Novoselov “for groundbreaking experiments regarding the two-dimensional material graphene” in 2010.

The properties of the matter changes as the size of the system decreases as an effect of changes of magnitude of various physical phenomena. These include statistical mechanical effect, quantum size effect (mentioned previously), increase significance of surface tension and van der Waals interactions and decreased importance of gravity. Changes of properties often arise from changes of surface area to volume ratio.

Nanotechnology, as a concept, was started by Richard Feynman at an American Physical Society meeting on December 29, 1959.[10] The talk entitled “There`s Plenty of Room at the Bottom” described scaling issues. During his talk Feynman announced two awards, 1000 US dollars each, for the first who could solve them. First one, which involved construction of nanomotor, was completed by November 1960 by William McLellan. The second challenge – down-scaling the Encyclopedia Britannica to fit it on the head of a pin; was claimed in 1985 by Tom Newman.[11] The term “nanotechnology” was first used and defined by Norio Taniguchi at Tokyo University of Science in a paper from 1974.[12] He stated that "Nanotechnology' mainly consists of the processing of, separation, consolidation, and deformation of materials by one atom or by one molecule." In the 1980s Eric Drexler emphasized the technological significance of nanoscale phenomena and materials.[13] In the

same time new experimental techniques were invented, which gave nanotechnology a great boost.

The first observations and size measurements of nanoparticles were performed by Richard A. Zsigmondy in the beginning of 20th century. He used ultramicroscope with dark field method to study gold sols and other nanomaterials with size 10 nm and less (Nobel Prize in Chemistry in 1925).[14] In the 1920s Irving Langmuir and Katherine Blodgett focused on materials one molecule thick (Nobel Prize in Chemistry for Irving Langmuir in 1932).[15,16] The technique developed by them is still in use in modern laboratories. The invention of the scanning tunneling microscope (STM) in 1981 by Gerd Binning and Heinrich Rohrer (Nobel Prize in Physics in 1986)[17] and atomic force microscopy (AFM) in 1986 by Gerard Binning, Calvin F. Quate and Christoph Gerber had very big impact on the development of nanotechnology and nanoscience in general. Mentioned techniques allowed not only observation of nanoobjects, yet also precise manipulations of single atoms and molecules.[18] Nowadays also transition electron microscopy (TEM) and also scanning electron microscopy (SEM) are suitable for observation of the nanomaterials. More than eighty years of development of those techniques resulted in possibility of taking pictures with nanometer resolution. Nobel Prize in Physics was awarded to Ernst Ruska in 1986, more than 50 years after he constructed first electron microscope in 1928 and first with better resolution comparing to optical microscope in 1933.

For years the "top-down" approach has been the mainstream of nanotechnology.[19] "Top-down" approach uses larger devices to create smaller ones by directing their assembly from larger entities. Most of the electronic devices are produced this way. In 1965 Gordon Moore formulated rule, later codified as Moore`s law. It states that silicon transistors undergo a continual down scaling. Since then, transistors minimum sizes decreased from 10 um to the range of around 25 nm.[20] This seems to be the limit for "top-down" methods. Recently the "bottom-up" approach became more and more important. It takes advantage of molecular components properties to assemble into devices and materials by means of molecular recognitions.[21]

1.1. "Top-down" approach

"Top-down" methods are physical and chemical processes of different complexity. "Top-down" approach often utilizes the traditional workshop or microfabrication methods,

where externally-controlled tools are used to cut, mill, and shape materials into the desired shape and order.

One of the most straightforward concepts is to use high energy milling for the preparation of nanomaterials. Mechanochemistry as a branch of solid state chemistry deals with the processes which occur due to the application of mechanical energy. Mechanochemical technology has been applied in many industrial fields: preparation of metallic nanopowders, alloys, metallurgy, building industry, chemistry, especially catalysis, minerals engineering, agriculture industry, and pharmaceutical industry.[22]

The lithographical techniques give better control over the nanoobjects formation. The idea is based on patterning on large scale, while reducing the lateral dimensions to the nanoscale. Typically features smaller than 10 um are considered microlithographic, while smaller than 100 nm – nanolithographic. The most commonly used is photolithography. It uses light to transfer a geometric pattern from a photo mask to a light-sensitive polymer films (photoresists deposited on the solid substrate). Lasers or other sources of various wavelengths are used to create images or patterns in photoresist. Photoresist may become soluble or insoluble after light exposure, depending on the material used. Therefore it is possible to use different photoresists as templates for deposition of molecules, as well as mask for etching (dry – using plasma and wet – with use of aggressive liquid solutions). Afterwards photoresist is no longer needed. It might be removed by treatment with liquid "resist stripper" or with use of plasma in process called ashing.[23] In lithographic techniques UV light, X-ray, electron (electron beam lithography (EBL)) and ion (focus ion beam (FIB)) beam are used. Focused ion beams (typically using Ga ions, therefore samples are doped with Ga) can directly remove or deposit material.[24] The use of electron beam is expensive and relatively slow, therefore it has low potential for application in industrial manufacturing. Additionally the backscattering of electrons limits the resolution and contrast.[25] Laser patterning has been reported as mask less approach with a better resolution as compared to the classic photolithography. Such technique enables precise fabrication of materials, which are hard to machine, such as ceramics and semiconductors.[26]

For ultimate resolution AFM and STM techniques were employed. By moving individual nanoparticles or even molecules or atoms, patterns of precise arrangement might be prepared. These methods are far too slow for industrial applications.[18,27]

Another possibility to control the shape, size and matrix of the nanomaterials is "top-down" synthesis.[28] The set of techniques to control the synthesis of non-spherical particles or produce multi-component emulsion of monodisperse particles is given by microfluidics. Integrating microchannels with sensors, actuators or other electronics[29] and introducing new, smart geometries[30] gave new functionalities. This allowed investigating and using so called lab-on-chip systems.[31] For example, Doyle and co-workers[32] utilized shearing forces of a photopolymer in a continuous water phase at a specifically-designed microfluidics junction to produce non-spherical uniform polymer particles on the micron scale. Whitesides and coworkers[33] used similar method to control the size of monodisperse particles.

1.2. "Bottom up" approach

The technology of production of electronic devices based on the "top-down" approach is gradually reaching its limits. As device features are down-scaled into sub-100-nm regime the control over the process becomes limited. Fluctuations of size of manufactured nanodevices result in significant randomness in characteristics, affecting key parameters, such as *e.g.* threshold voltage and on/off currents in case of transistors.[34] Moreover, the costs of miniaturization associated with lithography equipment and operating facilities create an economical barrier for development of conventional processors and memory chips.[35] Therefore a lot of attention is currently paid to development of the "bottom-up" idea.[36,37] "Bottom-up" lithography, also denoted as "soft" lithography, has been recognized as complementary to the widely used "top-down" approach.[38] It takes advantage of properties of molecular components to induce assembly into complex structures due to principles of molecular recognitions. To achieve more sophisticated devices, hierarchical "building up" might be used.[39] Usually, the very first step of fabrication of complex nanostructures is surface treatment via chemical modification or thin film casting.[40]

It seems that the ideal way of preparation of future electronic devices will combine these two approaches *i.e.* facilitating a scaffold, obtained via lithography or other high-precision "top-down" technique, decorated with a functional pattern of precisely located nanoscale objects.[41] Selective, controlled patterning of surfaces is therefore a matter of significant importance. Much effort has to be directed to understand forces governing the self-assembly processes.[42] The very extensive review by Lu and Lieber describes the features and opportunities of "bottom up" approach for nanoelectronics, and presents were it could merge with today`s technology. Problems that have to be overcome to take such devices towards

commercial applications are also pointed.[21] Limited understanding of processes and interactions of self-assembly allows the usage of "bottom up" strategy only in case of relatively simple systems. To achieve more complicated devices hierarchical self-assembly might be used, where consecutive steps of self-assembly lead to desired system.

Whole nature is using "bottom up" approach to create as complicated systems as living cells. Biologically inspired self-assembly gives a variety of possibilities of utilization of specific interactions (molecular recognition[43]) in artificial system. For example nucleotide pairs formation is widely used. Recent review by Cha and coworkers[44] gives very deep insight into nanofabrication based on DNA. Also properties of oligopeptides and proteins were utilized *i.e.* the formation of peptide ion channels by self-assembly of cylindrical octapeptides tubes.[45] Another example is unique stability of porin MspA, channel protein from *Mycobacterium smegmatis*, which was used to form artificial nanopores of diameter of around 3.1 nm.[46]

There is a growing interest in using biomolecules as active components in preparation of new materials. Biotransformations are highly selective, site-specific and highly efficient under physiological conditions. For example enzymes can be deposited to form nanostructures of nucleic acid and proteins directly on the solid substrates.[47] While engineers race to downscale the size of transistors and memory chips, biologists and life scientists have started to use micro- and nanopatterning for high-throughput detection systems for genomic and proteomic studies.[48] The problems that still need to be overcome are incompatibility of biomolecules with conditions of industrial fabrication such as vacuum and non-aqueous environment.[49]

Another possible route for nanofabrication is to take advantage of other specific inter-molecular interaction, for instance of liquid crystals (LC) properties.[50] LC have been used across multiple disciplines of pure and applied science, including bioscience and material science. LC flow like a liquid while molecules are still ordered in long range. This results in anisotropy of physical properties. LC phases are thermodynamically stable states, hence often called the fourth state of matter. LC self-assemble into variety of structures due to almost all kinds of supramolecular interactions such as van der Waals, dipolar and quadrupolar, π-π interactions and charge transfer, metal coordination and hydrogen bonding etc.[51] Also molecular shape and microsegregation of incompatible parts are important factors for LC structures. The liquid crystalline states are intermediate phases between amorphous liquid and crystalline solid. LC phases are called mesophases. The molecules which are able to form LC phases are called mesogens. The most general classification of LC is based on the

way how the LC phase is obtained. In case of mesophase appearance due to changes of temperature – thermotropic; or by dissolving amphiphilic compounds in suitable solvents over the range of concentration and temperatures – lyotropic LC are distinguished. The LC phases are also classified due to molecular features (calamitic, discotic, bent core) or assemblies (nematic, smectic, columnar etc.). Very extensive review by Bisoyi and Kumar[50] gives number of examples of utilization of LC tendency for self-assembly. For instance new arrangement of gold nanoparticles stabilized with organic shell, which contains molecules with liquid crystalline moieties is described.

1.3. Surfaces and interfaces

The down-scaling of the dimensions results in different properties of the matter due to variation in magnitude of physical phenomenon. However, there is one more characteristic which distinguishes nanoobjects from macroscopic materials. The volume of the object is proportional to r^3 (r is characteristic length) and surface area to r^2. The down-scaling leads to structures with high percentage of their constituent atoms at a surface. In the most extreme case almost all atoms may be on the surface. Whitesides *et al.*[40] described surfaces as the state of matter, where the gradients of properties are greatest. In bulk phases the gradients are usually zero. The gradients arise from different environment of atoms or molecules at the surface comparing to those in bulk. This causes the differences of the physical properties *e.g.* free energies, electronic states, reactivities, mobilities and structures.[52] Therefore there is a great interest in physics and chemistry of the surfaces, interfaces and thin films.

In the ambient conditions the surface is continuously hit by the molecules of the gas. Freshly prepared surface becomes covered very quickly. The timescale of the process can be estimated on the basis of the kinetic theory of the gas. For the air, in room temperature and under atmospheric pressure, the frequency of the impacts equals 10^{27} m^{-2} s^{-1}. The 1 m^2 of the metal surface consists of 10^{19} atoms; therefore each atom is hit 10^8 times every second. Even when the adsorption ratio is very small the surface remains “fresh” and uncovered very shortly after exposure. Therefore, most of the techniques of molecular resolution work in the ultrahigh vacuum conditions. The impact frequency of the gas molecules drops to 10^5 to 10^6 m^{-2} s^{-1}(one for a day) in such conditions.

Bare surfaces are of importance in number of fields, for instance in catalysis. However, only a limited number of materials have surfaces with desired properties. Surface modification

allows adjusting its properties to specific needs. This is another reason why thin films have been of interest for more than a hundred years. The possibility of direct observations of molecular arrangement came with the new imaging techniques in 1980s (AFM, STM). It resulted in new wave of interest in field of thin films. Among the most promising and novel areas for application are organic semiconductors for use in field effect transistors, photovoltaics and, in general, the organic electronics. A vast amount of papers has already been published on the subject (for examples see the recent review by O'Neill and Kelly[53] and references therein). One of the most intriguing methods of fabrication of organic transistors is based on self-assembled monolayers and molecular junctions with π-conjugated molecules.[54] The limitation of this idea in attempts for miniaturization is unimolecular electronics, already reported in numerous papers[55,56] and described in a broad review by Metzger.[57] Another direction towards nanodevices is provided by spintronics which makes use of quantum properties of a single molecule. Supramolecular spin valves described in a very recent paper by Urdampilleta *et al.*[56] are an example of such spintronic devices.

Preparation of well-defined thin films composed of different kinds of molecules is therefore crucial to achieve functional nanoscale structures. Among the most widely used techniques of thin film preparation are: spin coating, layer-by-layer (LbL) deposition,[58,59] Langmuir-Blodgett (LB) technique,[15,16] electrochemical deposition[60] and self-assembled monolayers (SAMs).[40] All of them present some advantages for specific applications. Neither of them is universal and versatile enough to be appropriate for all purposes and to satisfy the rising requirements of all modern technological challenges. The choice of method of the thin film casting is dictated by the balance between cost (money and time) and control over the structure and quality of the created film. For example, assembly at the air/water interface (Langmuir films) and subsequent transfer of films onto a solid substrate assures very good control over the formation process and final structure of thin film.[61,62] Application of the method is however limited to fabrication on a small scale, since it is time consuming.

1.3.1. Self-assembled monolayers (SAM)

Bare metal and metal oxide surfaces tend to adsorbate organic materials. Such adsorbates lower the free energy of the interface between the metal or metal oxide and the ambient environment.[52] Additionally, such organic layers play role in stabilization of nanostructures of metals and metal oxides. The organic layers prevent the assemblies from aggregation (acting

as physical or electrical barrier) by decreasing the reactivity of surface atoms or acting like electrically insulating films.

Self-assemble monolayers (SAM) were introduced in 1980s by Nuzzo and Allara[63] and by Whitesides and co-workers.[64] SAMs are organic assemblies formed by the adsorption of molecular constituents from solution or gas phase onto the surface of metals, metal oxides, semiconductors and liquids (mercury and other liquid metals and alloys). The molecules need to have a chemical functionalization with a specific affinity for the substrate. The most interesting group of SAMs derives from the adsorption of alkanethiols on gold, silver, copper, palladium and mercury. The adsorbates organize spontaneously into crystalline or semi crystalline structures. Well defined organic surfaces with useful, reproducible and highly tunable chemical functionalities can be generated.[65]

The SAMs are the most elementary form of organic structures ordered at the nanoscale. They are easy to prepare and do not require specialized equipment or harsh conditions. The structure of the molecules of adsorbate determines the vertical composition of the SAM. It is possible to organize organic or organometallic structures at the surface with positional control of 0.1 nm. Regions of SAM, which are phase separated, can have more than 100 nm^2 [66] when microcontact printing (μCP),[67] scanning probes,[68] beams of fotons,[69] electrons[70] or atoms[71] are used.

1.3.2. Layer-by-Layer deposition

Layer-by-layer (LbL) method was first suggestively described by Iler[58] (paper published in 1966) and first performed and established by Decher and co-workers[59] at the beginning of the 1990s. The main idea of LbL method is to utilize electrostatic interactions to deposit the material in controllable manner. Several steps are repeated consecutively to obtain desired number of layers. First, a charged surface is placed in the solution of substance of opposite charge (substance A). Relatively high concentration of the substance in solution leads to excess adsorption of the substance and therefore to charge neutralization and resaturation. This results in the charge reversal.[72] Afterwards, the surface is rinsed with water to remove excess material. 10% decrease of mass after 5 minutes of washing is observed.[73] In the next step such modified surface is placed in the solution of the substance (substance B) of opposite charge (to substance A). After deposition of layer of substance B the surface is again washed with water. Described steps are repeated to obtain a desired number of A B bilayers.

Beside conventional polyelectrolytes such as poly (allylamine hydrochloride) (PAH), poly (diallyldimethylammonium chloride) (PDDA), and poly (ethyleneimine) (PEI), poly (sodium styrenesulfonate) (PSS), poly (sodium vinylsulfonate) (PVS), and poly (acrylic acid) (PAA)[74] also functional poly (*p*-phenylenevinylene) (PPV) for light-emitting diodes,[75] azobenzene-containing polycation and polyanion for non-linear optics,[76] and poly (amidoamine) dendrimer (PAMAM) and its metal composites[77] have been assembled via LbL method. Also biomaterials, such as proteins,[78] DNA,[79] and charged polysaccharides,[80] are appropriate for LbL deposition. The list of materials is not limited for polymeric materials; charged inorganic substances, including colloidal nanoparticles,[81] clay,[82] nanosheets,[83] modified zeolite crystals,[84] two-dimensional perovskite,[85] and polyoxometalates,[86] bolaamphiphile monolayers,[87] lipid bilayers[88] and stacked dye molecules[89] are appropriate for LbL method as well. The usage of the LbL is very broad in different fields of material science. Extensive review on the recent advances of LbL method has been published by Ariga *et al.*[90] The biological applications of LbL films have been presented in review by Kotov and coworkers.[91] Both reviews contain over 600 references.

The properties of films obtained via LbL method depend strongly on the thermodynamic conditions such as: pH, salt concentration, temperature or post processing. For example: thickness could vary from 0.4 nm to 8 nm over a very narrow pH range in case of weak electrolytes (PAA and PAH).[92] Important case is ionic strength and the type of the ionic species in solution. Also drying of the sample influences the film structure strongly. Drying at each step increases the thickness of the films due to enhanced surface roughness.[73] The technique is cheap and not sophisticated. It requires good control over the external parameters. The biggest drawback is limitation only to charged compounds.

1.3.3. Langmuir-Blodgett technique

Amphiphilic compounds are used as detergents, *i.e.* have "cleaning properties as dilute solutions". The mechanism of cleaning is well known. It is based on the fact, that amphiphiles have two domains – hydrophobic and hydrophilic. The hydrophobic parts interact with soil and hydrophilic with water in the same time. Thus soil particles become soluble in water. Surfactants are also used as emulsifiers. The shape of the molecules and the functional groups determine the properties and possible applications of surfactants. Depending on length to diameter ratio surfactants prefer to form micelles, membranes or monolayers in rather dilute regime.

The origin of the Langmuir method might be found in experiment conducted by Benjamin Franklin in 1773. He dropped about teaspoon of oil onto a pond. His intention was to test the protocol of popular myth of the sailors. Those days during the storm, the barrels of oil were spilled around the ship to calm down the water. In his original paper from 1774 Benjamin Franklin stated "the effect of smoothing the waves was not produced".[93] He was very close to much bigger discovery than just disproving of the oil-dropping myth. Since Franklin knew the volume of oil used in the experiment and the area of pond covered by oil, he could estimate the dimensions of the molecule just by dividing the volume by the area. Unfortunately the knowledge about the dimensions of the molecules was undiscovered for over one hundred years. Lord Rayleigh was first, who calculated the thickness of the oil layer in Franklin experiment to be around 2 nm. Additionally he confirmed Avogadro number. At the same time Agnes Pockels started her work on utilization of the tendency of the oils to form thin films at air/water interface to describe purity of the water. Her first paper was published in Nature in 1891.[94] She prepared the stage for Irving Langmuir, who continued the work on thin films of fatty acids, esters and alcohols. Langmuir found that the length of hydrophobic chain do not play important role in thin film formation, therefore molecules are oriented vertically.[15] He developed special equipment, called Langmuir trough, which is in use until today with only minor changes (**Figure 1**). In 1926 Katherine Blodgett, Langmuir`s student and co-worker, discovered the possibility of transfer of Langmuir films onto solid substrates. There are two main, complementary, techniques for the transfer: Langmuir-Blodgett – the solid substrate is oriented vertically to water surface[16]; and Langmuir-Schaeffer – solid wafer oriented parallel to the water surface.[95] Vincent Schaefer was Langmuir and Blodgett coworker, who joined the team in 1932.

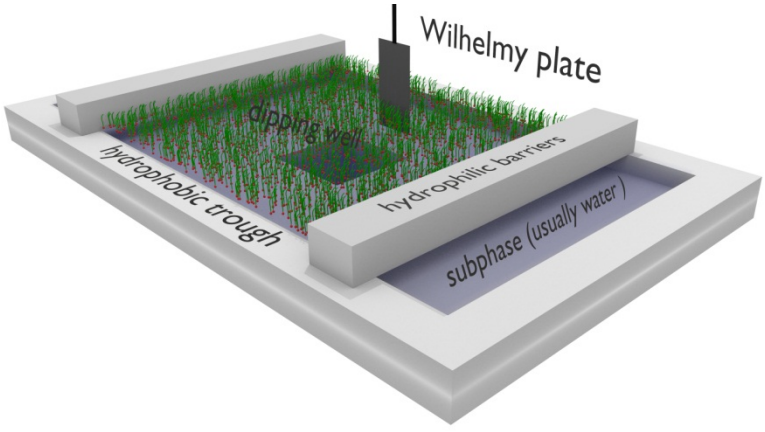

Figure 1 Scheme showing the most common Langmuir-Blodgett trough setup (equipped with two movable barriers for symmetrical compression). The film of amphiphilic molecules is

also presented; the green parts of molecules are hydrophobic tails, and red spheres correspond to hydrophilic head of the amphiphile. The well in the trough is needed for Langmuir-Blodgett deposition in order to dip the substrate into subphase.

The results of Langmuir experiments are usually depicted as plots of surface pressure versus mean molecular area. Surface tension is usually measured by means of Wilhelmy method.[96] The hydrophilic plate, preferably perfectly wettable (platinum is most popular, however filtration paper or even quartz and mica are in use) is immersed in subphase. The plate is connected to a very precise balance. The forces acting upon the plate are gravity and surface tension (downwards, into the water), and buoyancy due to displaced water (upwards). The measured force F is composition of those three forces. For rectangular plate of density d, which geometrical dimensions are w (width), l (length) and t (thickness), immersed in liquid of density $d`$ for high h (usually around one third of the plate is immersed in subphase; $h< l$), the force F is given by the equation:

$$F = dgwlt + 2\gamma w\cos(\theta_c) - d`gtwh \qquad \textbf{Equation 1}$$

where γ is surface tension, θ_c is wetting angle, and g is gravity constant. The Wilhelmy plate and the forces are depicted in **Figure 2**.

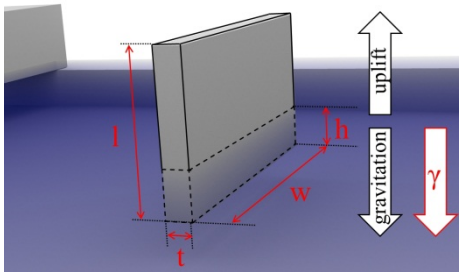

Figure 2 Cartoon showing surface pressure measurements by Wilhelmy method. Symbols correspond to **Equation 1**. The orientation of Wilhelmy plate (parallel or perpendicular to the barriers) was found to has influence on recorded $\pi(A)$ isotherm, especially in case of rigid films. [97] Recently simple new method for measuring the surface shear elasticity modulus and the dilatational modulus was established. It utilizes the anisotropy of surface tension measured in different orientations of Wilhelmy plate.[98]

Surface pressure π is defined as difference of F between pure solvent (γ) and solvent with compound applied (γ*) divided by the perimeter of the sensing plate. Since the gravity and

uplift part of **Equation 1** are constant during the experiment, therefore in case of perfect wettability ($\cos(\theta_c) = 1$):

$$\pi = \frac{2w(\gamma - \gamma^*)}{(2t + 2w)} \qquad \textbf{Equation 2}$$

For very thin plate ($t = 0$)

$$\pi = \gamma - \gamma^* \qquad \textbf{Equation 3}$$

Surface pressure is a result of a subtraction of surface tension of solvent and solvent with compound of interest applied at the interface. The only parameter that vary during the experiment is surface tension γ^* (after surfactant application), due to changes of available area per molecule.

Surface tension could be described as model force which pulls molecules from the interface towards the bulk. This force arises from the lack of symmetry of interactions at the interface. In the bulk of the liquid phase, each molecule is pulled equally in each direction by neighboring liquid molecules, resulting in a zero net force. However, at the interface the interactions with gas molecules are weak. Therefore the molecules at the interface are pulled down, towards the phase interior. As a result the surface area is minimalized (liquid form droplets). In case of strong intermolecular interactions the value of surface tension is high (*i.e.* for water $\gamma = 72.8$ mN m^{-1} at 25^{0}C). Factors like temperature or impurities (especially surfactants) cause decrease of interaction forces between molecules and therefore decrease of the surface tension.

Another way to describe the surface tension is in terms of energy. The interior molecules have as many neighbors as the geometry allows, while at interface half of the neighbors are missing. The intermolecular interactions lower the energy. In case of a liquid system, the number of higher energy boundary molecules is minimized to minimize its energy. Therefore droplet is formed as shape of minimal surface area at given volume.

The same conclusion arises from thermodynamics. Surface tension is defined as a work needed to change the surface area (work per unit area):

$$dW = \gamma dA \qquad \textbf{Equation 4}$$

It might be written as changes of Gibbs free energy *G*:

$$\gamma = \left(\frac{\partial G}{\partial A} \right)_{P,T,n} \qquad \textbf{Equation 5}$$

Thermodynamics requires that all spontaneous processes occur with decrease of *G*. Since γ is constant in given conditions (*T, P*), from **Equation 5** it is clear that the liquid system is always minimalizing its surface area.

The experimental setup for investigations on thin films, which was developed by Irving Langmuir, remained almost immutable. The most commonly used equipment consists of hydrophobic trough, made of PTFE, which is fulfilled with subphase (water, water – alcohol and water –glycerol mixtures, mercury or even ammonia). On the edges of the trough, perpendicular to its long axis, the movable barriers are positioned (see **Figure 1**). The barriers are usually made of material, which is wettable by the subphase. Beside most common rectangular troughs with one or two barriers, also round setups are in use with barriers moving engine in the center of the trough[99] or constant perimeter trough with the tape as a barrier, which folds during compression.[100]

The studied amphiphilic compound is applied as a solution in volatile solvent (usually chloroform) onto the subphase, between the barriers. Usually the working solutions are of concentration ca. 1 mg ml^{-1}, therefore less than 100 µl is applied onto the subphase in case of troughs of standard dimensions. The standard pipettes are not suitable for volatile solvents, thus microsyringes or drop-counters are used.

During the experiment the barriers move towards each other, thus surface area between them decreases. In case of system with non-symmetrical compression only one barrier is present, which moves towards the edge of the trough. Changes of the surface pressure as a function of surface area per molecule are recorded. Since the temperature is constant during the experiment the resultant plot is called $\pi(A)$ isotherm. Preferably the speed of barrier movement should be as slow as possible. In such a case the system is as close equilibrium as possible. In fact usually non-equilibrium processes are observed during compression/decompression cycles. Another way to conduct experiments is titration of studied amphiphile while barriers remain static. This method is preferred when very small changes of the surface pressure are investigated.

The stability of thin films mainly depends on two factors: on the tendency of molecules for dissolution into the subphase; and on the mechanical stability of the layer, in order to resist over-compressions. For insoluble amphiphilic molecules, the equilibrium between Langmuir film and saturated subphase might be approached very slowly. To consider the stability criteria the equilibrium spreading pressure (ESP) should be introduced. The equilibrium spreading pressure is defined as spontaneously generated, when a crystalline phase is placed in contact with surface of a pure subphase.[101] The equilibrium spreading pressure corresponds to the equilibrium pressure between the monolayer (2D state), and the crystal (3D state). To be in stable equilibrium, the monolayer should not be compressed to the surface pressure higher than ESP. At any surface pressure higher than ESP, the monolayer has a tendency to aggregate into crystals by a nucleation and crystalline growth process. Luckily, during Langmuir experiments, when the monolayer is compressed beyond ESP, the equilibrium is approached very slowly. Therefore the ESP is generally not attained in the course of experiments and films could be compressed to higher values of surface pressure. To conclude, the processes responsible for the monolayer instability occur in long time scale. However, it is important to consider a floating film as a metastable system rather than an absolutely stable equilibrium phase.[102]

The behavior of the film during compression depends on the nature of the amphiphile, temperature, subphase composition and compression speed. At the early stage of the experiment the value of mean molecular area is high and molecules form a two-dimensional gaseous state (surface pressure lower than 0.1 mN m^{-1}). During compression the mean molecular area decreases and therefore molecules are forced to interact. First phase, beside gaseous, is a "liquid expanded" and afterwards "liquid condensed". Further compression results in the formation of monolayer in solid state, where molecules are densely packed on the interface. More reliable classification of states of Langmuir films were given by Davies and Rideal.[103] Their approach is based on modulus of compressibility C_s, called static elasticity ε_s. The static elasticity is defined as:

$$\varepsilon_S = -\frac{1}{A}\left(\frac{\partial A}{\partial \pi}\right)_T \qquad \textbf{Equation 6}$$

and can be calculated from $\pi(A)$ isotherms. The values of static elasticity ε_s for different phases of the monolayer are given in the **Table 1**. Great attention is paid especially to the

self-assembly of Langmuir films and to the alignment mechanism typical for liquid crystals (LC).[104,105,106]

Table 1 Values of static elasticity corresponding to different 2D phases.

Monolayer state	ε_s / mN m^{-1}
Gaseous	0 – 12
Liquid expanded	15-50
Intermediate	50 – 100
Liquid condensed	100 – 250
Solid	250 – 2000

1.3.3.1. Layering transition and collapse of the LB films

When the mean molecular area becomes smaller than the area occupied by a single molecule the molecules explore the third dimension upon compression. The term "collapse" is usually used to describe a phenomenon of disruption of the monolayer. Understanding this 2D to 3D transition provides insight into the origin and nature of defects in thin films. Because of technological (for example coating of optical fibers[107]) and biological (protection of the eyes,[108] the ears,[109] inner surface of the lungs[110]) importance of thin films, much effort has been devoted into understanding of the collapse phenomena.

The two-dimensional film finally reaches its stability limit on compression. Usually at this point a steep $\pi(A)$ isotherm abruptly becomes horizontal. The process usually occurs at high surface pressure. The molecular area reaches a limiting value beyond which the monolayer cannot be compressed further without destabilizing its 2D nature and yielding the structure in the third dimension. The surface pressure at collapse determines the minimum surface tension for the interface. The collapse mechanism determines its reversibility (*i.e.* how well the monolayer respreads upon expanding the film). Fluid monolayers collapse at relatively low surface pressure via the ejection of materials to the subphase.[111] More ordered and rigid monolayers collapse at higher surface pressure, usually by fracturing, followed by a loss of materials in the subphase or the formation of multilayered aggregates at the air side of the interface.[62,112] The collapse occurring via fracturing or solubilization is irreversible.[113] The collapsed materials do not incorporate into the monolayer as the surface pressure is decreased. When the material spread at the interface contains more than one component it may happened

that at the collapse some of the components are squeeze out from the monolayer. That leaves the film enriched in the more rigid components.[114]

At least one biological system needs to take advantage from the reversible collapse of the film. Lung surfactants are complex mixture of lipids and proteins that line the alveoli and are responsible for proper functioning of the lung.[115] They adsorb rapidly at the air/fluid interface of the alveoli after being secreted. The functions of lung surfactants are to lower the surface tension, to reduce the work of breathing and to stabilize the alveoli against changes of alveolar volume. Therefore the lung surfactants need to form a film which cannot be destroyed upon changes of surface pressure. Those conditions are fulfilled by the specific composition. Special proteins are involved in the process of reversible folding/unfolding of the film during breathing cycles. The foldings are in facts reservoirs where the excess material is stored during the compression of the film.[116] Studies on lung surfactants are great example of Langmuir technique possibilities in variety of applications.

The monolayer that contains continuous network of the fluid phase separating islands of ordered and rigid phase, collapses via a reversible, localized, large amplitude buckling (folding). In such a case the monolayer is flexible enough to bend but retains enough cohesion to prevent loss of material to the subphase or to the air side of the monolayer. The mechanism of folding collapse is similar to the behavior of a thin sheet of paper after applying lateral stress – the paper buckles and folds. The conclusion is that proper rigidity of the film is needed to observe buckling; the monolayer cannot be too rigid (broken sheets of monolayer sliding onto each other) or too fluid. Similar collapse mechanism has been also found in case of films of pure compounds[117] and described theoretically.[118] In fact the buckling of the polymer films were reported for the first time in 1954. However the authors did not connect the foldings with the reversibility of the collapse. The investigations were performed not *in situ*, yet after deposition of collapsed film onto solid substrate.[119]

There are only few examples of well-defined multilayer structures formation upon compression beyond a monolayer collapse.[120,121,122,123] To distinguish the phenomenon of real collapse of a monolayer (random 3D-aggregation) from the formation of ordered multilayers, the term “the layering transition” (after Möhwald[124]) is used throughout the thesis for ordered transition between monolayers and thicker films. The layering transition is a specific type of phase transition. This term was introduced for the first time to describe gas adsorption on solid surfaces and building-up of additional layers on the adsorbed monolayer. The analogy of

formation of multilayers in Langmuir films to the above is very close. There are however doubts if it is justified to consider it simply as a phase transition in a common sense, because of the change of dimensionality of the system during the process. The properties of the system are changing discontinuously when new layers are being built up to the former ones. In this context a substantial question arises: how many layers the system should consist of to be treated as a bulk? Gallani *et al.*[125] considered the layering transitions in Langmuir films of the paramagnetic molecules known as TEMPO. They concluded that these transitions "can shed a new light on their behavior in the bulk". This conclusion is closely related to the question above, but an answer is still unknown.

Trilayers are often formed during compression of monolayers at the air/water interface if no disordered (irreversible) collapse takes place.[121,126,127,128] The *roll over* mechanism, which explains formation of trilayer and not bilayer films, was for the first time proposed in 1979 by H. E. Ries, Jr (ref. 126). Elongated structures and wrinkles in the film of 2-hydroxytetrecosanoic acid were found with use of electron microscopy after compression of the film beyond its collapse point and transfer onto solid substrate. The scheme of the molecular alignment of 8CB (4'-n-octyl-4-cyanobiphenyl) molecules during *roll over* process is shown in Figure 4 in ref. 113. The scheme of *roll over* mechanism is also shown in **Chapter 3.2.4** in **Figure 19b**.

Layering transitions in Langmuir films were intensively studied for a liquid crystalline compound, well known as 8CB, using: ellipsometry,[104] BAM,[121,129,130,131] surface potential measurements,[131,132] and optical second harmonic generation (SHG).[104,133] The SHG technique was also used to confirm spontaneous organization of 8CB molecules evaporated onto solid substrate into multilayer stacks.[134] Multilayers were observed for other liquid crystals from the group of cyanobiphenyls as well.[120,135] Layering transitions of compound similar to 8CB (containing a siloxane group attached to the aliphatic chain) at the air/water interface were also thoroughly studied using the Langmuir technique.[104,122] A stepwise change of the layer thickness was found and additionally proved by X-ray reflectivity (XRR) measurements.[136]

1.3.3.2. Interactions with the species within the subphase

The example of Langmuir technique for biological studies of lung surfactants was mentioned. The Langmuir trough is not suitable for study of a transport across the membrane. The

monolayers are perfect for studies of interactions between biomolecules and membranes.[137] The Langmuir films might be considered as perfect model of biological biomembrane. For example DNA was found to influence the $\pi(A)$ isotherms[138] and very recently different types of four stranded DNA (G-quadruplexes) were distinguished with use of Langmuir technique.[139]

Large numbers of experiments were conducted in physiological or pseudo physiological conditions. Not only pure water is used as a subphase, but also electrolytes and polymer solutions. Such additives change the $\pi(A)$ isotherm when compared to one recorded on water surface. The ions charged oppositely to polar groups of amphiphile form double electrical layer. This modifies the local dielectric constant and dissociation of the amphiphile. In case of water the main counter ions to cationic monolayer in the subphase are strongly hydrated OH^-. Ahuja *et al.*[140] performed the systematic studies on the interactions between halogen anions and head groups of dioctadecyldimethylammonium monolayers. Souza *et al.*[141] studied others anions in this system. The changes of shape of the isotherm were explained as a function of hydration layer of the anion. The smaller hydratation the bigger influence the anion has on the behavior of the monolayer. For subphase in which ions like Br^-, Cl^- and NO_3^- (which interact strongly with micelles and liposomes of dioctadecyldimethylammonium cations) are present, recorded isotherms have different general shape and slopes comparing to isotherm recorded on water subphase. The layers are additionally more condensed. This suggests presence of different phases during compression. On the other hand the isotherms recorded on solutions of F^- and Ac^-, which interact weakly with dioctadecyldimethylammonium cations are very similar to ones recorded on pure water, yet shifted towards bigger values of mean molecular area.

The interactions of cations and anionic monolayer have been studied for years and hundreds of papers were published on the topic. This case was intensively studied because the first Langmuir-Blodgett experiments were performed with use of fatty acids. Here only recent paper on specific ions effects is cited.[142] For more details see references therein.

1.3.3.3. Transfer of the LB films onto solid substrates

The Langmuir-Blodgett (LB) and Langmuir-Schaeffer (LS) methods are used to transfer films onto solid substrate. During the LB deposition the solid substrate is oriented vertically. The transfer occurs during down- and up-stroke of solid wafer in case of hydrophobic or

hydrophilic substrates, respectively. During the process the surface pressure is constant. The novel equipment might automatically compress film to balance the effect of decreased amount of the compound on the surface of water. Amphiphilic molecules are pushed onto a solid substrate with constant force. Consecutive steps of immersing and looming of the substrate might lead to deposition of up to tens of layers.

The LB transfer could be affected by the nature of studied compound (how strong does it interact with the surface); temperature (influence on rigidity of the film) and surface pressure (type of 2D phase of the film and average area per molecule affect the surface coverage). Another important factors are: type of solid surface (how hydrophilic/hydrophobic the surface is), speed of deposition (too fast dipper speed results in nonuniform coverage), time interval between deposition cycles (drying of the film affects roughness) and orientation of the solid substrate (orientation parallel to the barriers ensure the best quality of the transferred films).

The deposition process is described by the transfer ratio τ:

$$\tau = \frac{A_L}{A_S} \qquad \textbf{Equation 7}$$

where A_L is the change of surface area occupied by thin film at subphase and A_S is the area of solid wafer. For perfect coverage of the solid substrate the transfer ratio equals 1.

During deposition of several layers three main types of deposition are observed. The most common are films Y, where layers are deposited during both down- and up- stroke. In such a case the orientation of consecutive layers ensure the maximal stability of multilayer coverage. The molecules from neighboring layers interact via compatible parts, *i.e.* hydrophilic heads or hydrophobic tails. The nature of the solid substrate (hydrophobic or hydrophilic) affects only the orientation of the first layer. The films Z and X are deposited only during down-stroke and up-stroke, respectively. Therefore hydrophobic and hydrophilic parts of molecules of different layers are forced to be close to each other.[143]

In case of unsuccessful Langmuir-Blodgett deposition it is possible to utilize Langmuir-Schaeffer method.[95] In this approach solid substrate is oriented horizontally to the surface of water and moves towards the film from above. The deposition occurs when the solid substrate touches the interface. The wafer does not go any deeper. The whole area of solid substrate is in contact with transferred film at the same time. Since the hydrophobic parts of molecules are exposed towards air, the solid wafers used in this method are usually

also hydrophobic to ensure satisfying transfer ratio. After deposition hydrophilic parts of the molecules are exposed, thus surface becomes hydrophilic.

In case of LB technique the hydrophilic head groups may have a stronger affinity for the water subphase than for the hydrophilic substrate. This results in a poor adhesion of the first layer on a hydrophilic support. During the second immersion the film may be peeled off the substrate and respreads on the air/water interface.[144] Under such circumstances, despite the repeated dipping, only one monolayer could be deposited. To solve this problem, Tamm and McConnell[145] proposed a combined approach to elaborate phospholipid bilayers on hydrophilic substrate. The first layer is transferred by vertical Langmuir-Blodgett deposition and the second one by horizontal Langmuir-Schaeffer method. After LB deposition of monolayer the orientation of the substrate is changed to horizontal. The substrate horizontally oriented with the face coated by the first layer is slowly lowered until it becomes in contact with the floating monolayer. Due to tail-to-tail interactions the bilayer is formed. This method is perfect for the preparation of mixed bilayers, which consist of different types of amphiphilic compounds (for example second layer might be labeled or doped).

Other approaches have been used, yet not very widely. For example solid substrates oriented at the different angles to the surface of water have been tested in pseudo Langmuir-Blodgett setup during up-stroke.

1.3.4. Other methods of thin films fabrication

A great number of techniques of thin film fabrication are available depending on the requirements. The most trivial are dip coating (immersing the substrate in the solution of compound of interest or through its film at the interface) and spray deposition. Although they do not require any specific equipment, the control over the casted films properties is very limited. Among most commonly used is spin coating (for example to prepare the photoresist masks for photolithography). The solid substrate is rotating with high rpm speed providing the uniform spreading of the liquid solution applied on it. The calibration curves correlate the rpm speed and the viscosity of the applied solution with the thickness of obtained films. The biggest disadvantage is that up to 95% of material is lost in the process and it is difficult to obtain layers thinner than 1 μm.

The sol-gel deposition is used in fields of materials science and ceramics engineering. It was also recognized as appropriate for thin films preparation.[146] The colloidal solution (sol) acts as precursor for an integrated network (gel) of either discrete particles or network polymer.

The short review of the methods of thin film preparation presented here was restricted to the techniques which do not require harsh conditions and complicated equipment. As mentioned previously depending on the balance of the cost, time and control over the obtained material properties, the choice of appropriate method should be done. Techniques based on vacuum evaporation (conventional, electron beam evaporation, molecular beam epitaxy (MBE), reactive evaporation), sputtering (reactive sputtering, ion beam deposition, bias sputtering and other), plasma processes, whole set of chemical vapor deposition (CVD) techniques (metaloorganic CVD (MOCVD), laser induced CVD, electron enhanced CVD, low pressure and atmospheric pressure CVD and other), electro processes (electroplating, electrolyte anodization, electrophoretic deposition and other) or thermal processes (thermal oxidation and polymerization among others) are utilized to prepare thin film of desired material (some techniques are suitable only for inorganic compounds), thickness, porosity or uniformity at reasonable time scale.[147]

EXPERIMENTAL SECTION

2. Experimental section

2.1. Materials

Commercially available solvents and chemicals were purchased from Sigma Aldrich or Merck and used as received (if not specified).

2.1.1. Bolaamphiphiles

Bolaamphiphiles[148,149] represent a special type of amphiphiles possessing two hydrophilic groups attached to both ends of an elongated hydrophobic segment. One of the most promising classes of rod-like bolaamphiphiles are compounds composed of a rigid π-conjugated aromatic core which is terminated at both ends with hydrophilic, hydrogen-bonding glycerol moieties.[150,151,152] The shape of the core can be linear[150,151] or bent.[152] This general arrangement may be modified by attachment of additional lateral chains at different positions. Such modifications give T- (T),[150] X- (X),[151] or anchor-shaped[152] (A) molecules (**Figure 3**). The shape of the molecule, combined with the segregation of the lateral chains into distinct compartments, determines the bulk properties of the compound. Such concept of polyphilic bolaamphiphiles leads to a wide variety of highly complex liquid crystalline soft-matter structures as described recently.[153]

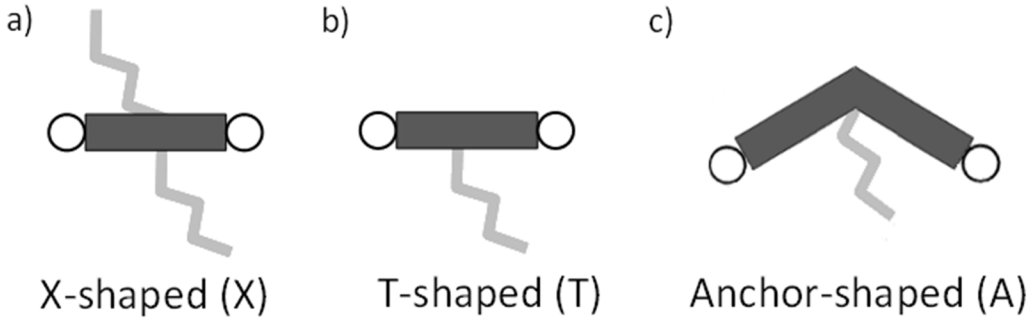

Figure 3 Cartoon showing the shapes of bolaamphiphilic molecules studied in **Chapter 3**.

In **Chapter 3** the results of studies of ten bolaamphiphiles are presented. The molecular structures of investigated compounds are presented in **Figure 4**. The figure is repeated in the thesis for readers' convenience. Bolaamphiphiles were synthetized in the group of Professor Tschierske from Martin-Luther-University Halle-Wittenberg. The bulk phase behavior of studied compounds is presented in **Table 2**. In case of nonfluorinated compounds **X5** and **A1** no mesophases were found. In case of nonfluorinated **X1** the mesophase was metastable.

Eight out of ten of studied bolaamphiphiles were partially fluorinated. All fluorinated analogues were stable liquid crystals with first phase transition temperature below 100°C.

Table 2 Phases and transition temperatures observed in the investigated compounds.

Compound	Phase transitions T [°C][a]				
X1	Cr	83	(M	65)	Iso
X2	Cr	70	$Col_{squ}/p4mm$	94	Iso
X3	Cr	< 20	GS 50 $Col_{hex}/p6mm$	67	Iso
X4	Cr	64	$Col_{squ}/p4mm$	92	Iso
X5	Cr	113	-	-	
X6	Cr	96	$Col_{hex}/p6mm$	110	
T1	Cr	87	$Col_{hex}/p6mm$	229	Iso
T2	Cr	99	M 180 Col	218	
A1	Cr	113	-	-	Iso
A2	Cr	63	$Col_{hex}/p3m1$	190	Iso

[a] Abbreviations: Cr = crystalline solid, Iso = isotropic liquid, $Col_{squ}/p4mm$ = square columnar phase with simple $p4mm$ lattice, $Col_{hex}/p6mm$ = hexagonal columnar phase with $p6mm$ lattice, $Col_{squ}/p3m1$ = hexagonal columnar phase with trigonal $p3m1$ lattice, Col = columnar phase with unknown lattice, M = mesophase of unknown structure, GS = glassy state; values in parenthesis refer to monotropic (metastable) phases.

Molecules of compounds **X1**-**X4** contained a bolaamphiphilic unit consisting of a rigid linear p-terphenyl core terminated with two polar groups (glycerol moieties) at both ends. In the central part of the core two lateral lipophilic chains were attached. The fluorination ratio of lateral chains increased from **X1** to **X4**. Compounds **X5** and **X6** consisted of a linear rigid core which was significantly longer than that in case of compounds **X1**-**X4.** The two additional ethinyl groups were introduced between the phenyl rings. Compound **X6** contained one chain (partially fluorinated) which was much longer than the other (hydrocarbon chain). Compound **X5** had two relatively short, identical hydrocarbon chains. Compounds **X1**-**X6** were solids in a bulk phase at room temperature and melted at elevated temperatures (between 60 and 115°C). When melted, the fluorinated analogues formed columnar liquid crystalline phases (**Table 2**).

Compound **T1** had only one partially fluorinated side-chain attached to the same linear core as in the case of **X1**-**X4** molecules (shorter). At elevated temperature, *i.e.* above the melting point at T_m = 87ºC, the bulk phase of this compound exhibited a liquid crystalline hexagonal columnar phase (**Table 2**). Compound **T2** had identical side chain as **T1**, however the core was longer (with two ethinyl groups as in case of **X5** and **X6**). Mesophases of **T2** were observed between 99ºC and 218ºC.

The oligo (phenylene ethynylene) cores of compounds **A1** and **A2** were bent. One lateral chain was attached inside an angle created by the bent core (bay position in anchor-shaped molecules). Compound **A2** was a fluorinated analogue of compound **A1**. Both compounds had the same core and the same length of the aliphatic chains. The only difference was the fluorinated segment introduced in the lateral chain of compound **A2**.

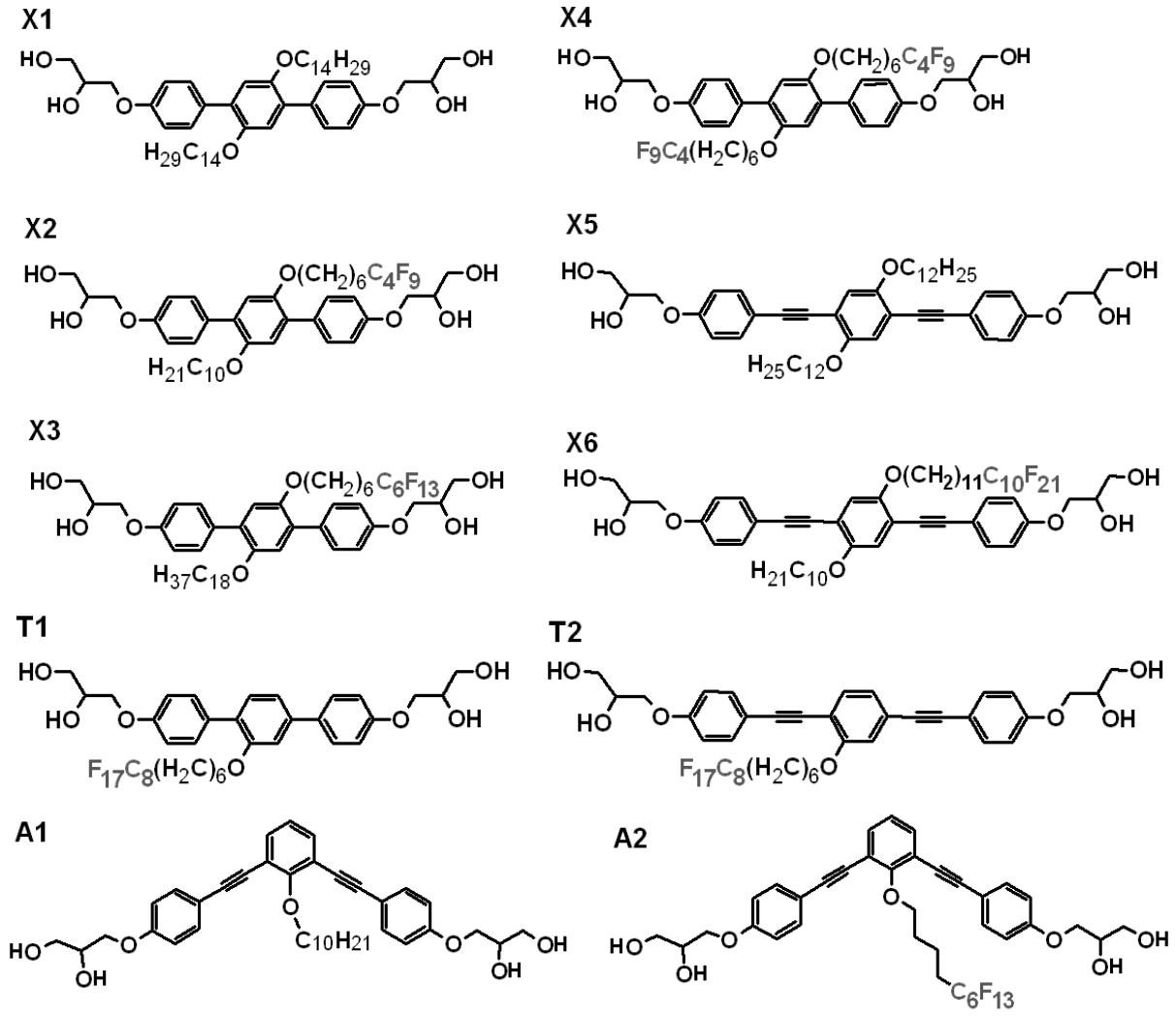

Figure 4 Structures of bolaamphiphiles studied in **Chapter 3**.

2.1.2. Gold nanoparticles

Gold nanoparticles (**Au NPs** – bold font is used to distinguish nanoparticles used in experiments presented here and the literature data) were synthesized according to a procedure described elsewhere.[154] The primary grafting was subsequently substituted for N,N,N-trimethyl (11-mercaptoundecyl) ammonium chloride (TMA). Around 10% of original undecanethiol ligands were substituted for TMA.[155] Mean diameter, assessed by means of SAXS measurements (not shown) and AFM images analysis was 8.9 nm ± 0.8 nm. **Au NPs** exhibited a single, moderately narrow peak of zeta potential at +35 mV.

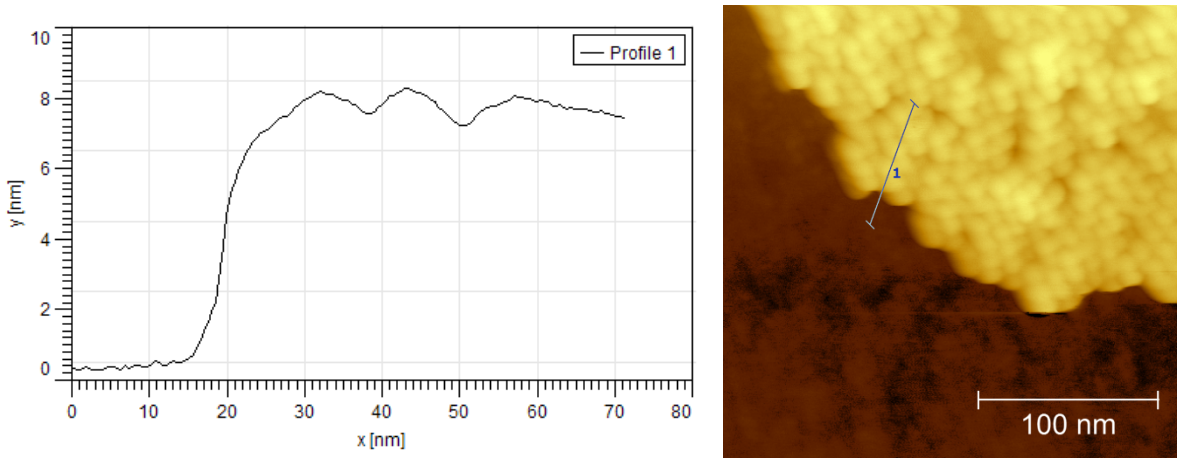

Figure 5 Size of **Au NPs** was determined with use of AFM. Values obtained with AFM and SAXS were in good agreement.

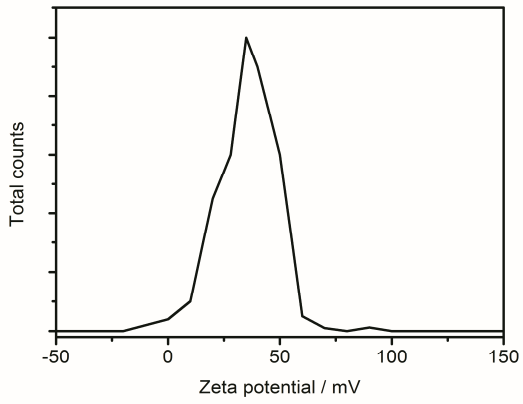

Figure 6 The positive value of zeta potential confirmed the amphiphilic character of **Au NPs**. At the end of 10% of thiol chains the polar group was introduced to ensure increased hydrophilicity of the particles.

In all the experiments, 1:1 chloroform/methanol solutions of concentration of around 0.5 mg Au per ml of solution were used. The amphiphilic **Au NPs** formed stable Langmuir films. Upon spreading at the air/water surface the thiols rearranged, so that the polar groups were in contact with the water surface.[156]

When known volume of solution of **Au NPs** was spread onto the water surface and compressed, the collapse point (kink at the isotherm) indicated the point corresponding to a dense monolayer (see **Figure 7a**). The area between the barriers at the moment of film collapse was equal to the maximal area which could be covered by a dense monolayer with applied amount of solution. If volume of the applied solution was divided by the collapse point area, the result was the concentration (which can be expressed in µl cm^{-2} *i.e.* how much solution was needed to cover 1 cm^2 with dense monolayer). Such notation was used in drop casting part of the thesis, since it was difficult to determine the absolute concentration of gold nanoparticles with required accuracy.

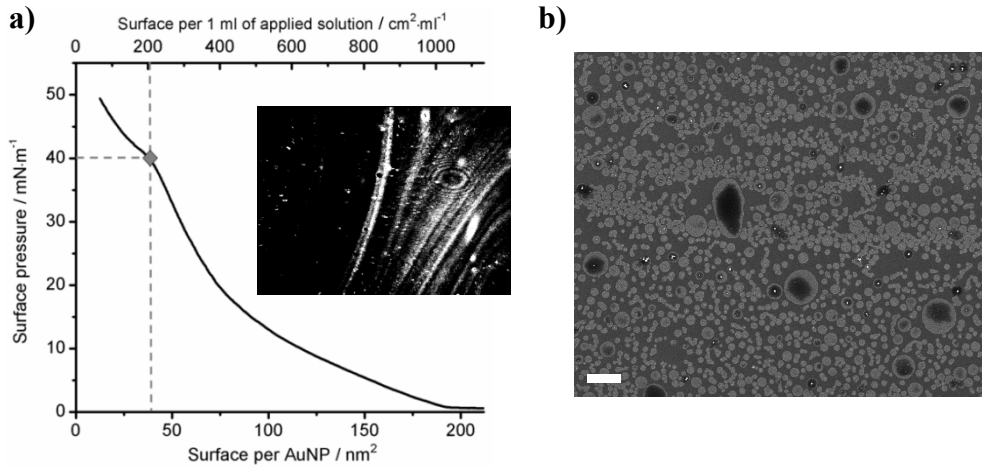

Figure 7 a) The $\pi(A)$ isotherm of used **Au NPs**. The BAM picture of film of pure **Au NPs**, taken at around 5 mN m^{-1} is shown as inset; **b)** SEM image of film transferred at 30 mN m^{-1} revealed formation of circular domains at the air/water interface; scale bar 2 µm.

2.1.3. Gold nanoparticles with bolaamphiphilic domains attached covalently

The synthesis of gold nanoparticles with covalently attached bolaamphiphilic domains (**B-Au NPs**) was performed by Michał Wójcik from the Warsaw University in cooperation with Professor Carsten Tschierske. Therefore detailed synthetic route and full analytical data concerning this material could be found in PhD thesis of Michał Wójcik.[157]

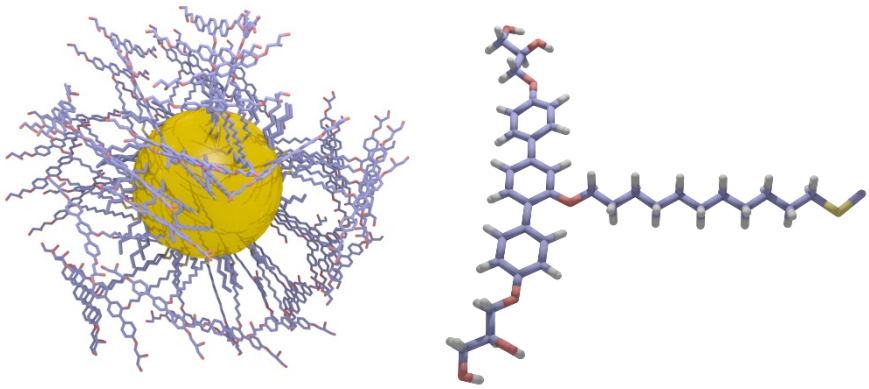

Figure 8 Cartoon showing gold nanoparticles with around 50% of the n-hexanothiol ligands substituted with bolaamphiphilic ligands (which structure is also shown).

In the first step **Au NPs** were synthesized according to the Brust method,[158] using n-hexane thiol to passivate metal surface. The diameter of the metal particle core (average size of 2.6 nm) was determined from the SAXS measurements and confirmed by TEM imaging (not shown). The thio-bolaamphiphilic secondary ligand for surface modification of gold nanoparticles was synthesized from phenolic templates obtained as described in the literature.[151,157] The molecules of primary grafting layers were partially exchanged for mesogenic thiols by a ligand exchange reaction.[159] Exchange ratio in the reaction is known to depend mainly on starting concentration of incoming thiols and time of reaction.[160] For chosen reaction conditions, a 50% exchange ratio was obtained. The ratio of mesogenic to n-alkyl thiols was determined from integration of ^{1}H NMR signals characteristic for both molecules. The structure of obtained material is shown in **Figure 8**. The **B-Au NPs** were used as THF solution for Langmuir-Blodgett and drop casting experiments.

2.1.4. Gallium nitride nanowires growth

Thins films containing **Au NPs** on the silicon wafer were used as a substrate for the **GaN** nanowires growth. The experiments were performed with use of a horizontal quartz tube as a CVD reactor.[161] Gallium nitride powder (99.99%, Alfa Aesar) and metallic gallium (99.999%, Alfa Aesar) were placed in a quartz boat. The solid substrate was placed on top of the quartz boat in a face-down position, located in the center part of the heating zone. The system was heated to 930°C under a constant flow of nitrogen (0.6 dm^3 min^{-1}). After 45 minutes the reactor was cooled down to 730°C and gaseous ammonia (99.995%, Air Liquide) was introduced with a flow rate of 0.02 dm^3 min^{-1} (1 minute). Afterwards, the reactor was cooled down to ambient temperature under a constant flow of nitrogen (1 dm^3 min^{-1}).

2.1.5. Gold microflowers deposition

Gold microflowers (**Au MFs**) were deposited from a freshly prepared reaction mixture containing aqueous solutions of chloroauric acid ($HAuCl_4$) and hydroxylamine hydrochloride ($NH_2OH{\cdot}HCl$). In the process, hydroxylamine reduced the gold ions to metallic gold. The formation of flower-like gold microclusters was observed. The reaction was in addition accelerated[162] by the Au-Ga alloy droplets immobilized on the top of **GaN** nanowires.[163] Solution of chloroauric acid was added dropwise to the solution of hydroxylamine hydrochloride. As soon as the reagents were stirred, plates covered with **GaN** nanowires were placed at the bottom of a vial containing this mixture. After 20 hours the plates were washed subsequently with water and methanol and then dried in air. The as-prepared surfaces were then used as platforms in SERS measurements without additional cleaning.

In **Chapter 5** three different rates of Au MFs coverage were prepared. The amount of deposited Au MFs increased from sample **a** to **c**. An exemplary mixture used for the process consisted of one part of 8 mM $NH_2OH{\cdot}HCl$ and 0.6 parts of 5 mM $HAuCl_4$. In case of coverage **a** the height of the solution column above the substrate was about 10 mm. To fabricate coverage **b**, the same ratio and volume of aqueous solutions of $NH_2OH{\cdot}HCl$ and $HAuCl_4$ was used, but the concentrations were 40 mM and 25 mM, respectively. The same reaction mixture (higher concentrations) was employed in preparation of coverage **c**, however the height of the solution column above the substrate was about 20 mm.

2.1.5. Hyperbranched polymer Boltorn H3200

Perstop AB (Sweden) produces a series of hydroxyl-functional hyperbranched polyesters based on 2,2-bis-methylpropionic acid with an ethoxylated pentaerythriol core, designated as Boltorn H20, H30, and H40. **Boltorn H3200**, the hyperbranched polymer used in this work, was synthesized from Boltorn H30 through the esterification of the OH-end groups with a mixture of eicosanoic and docosanoic acid leading to C20/22 alkyl chains as end groups.

The investigated polymer was characterized with Nuclear Magnetic Resonance (NMR) spectroscopy. For all samples ^{1}H and ^{13}C spectra were recorded on a Bruker DRX Avance 300 MHz. The spectra of the polymer were measured in CD_2Cl_2 and DMSO-d6 solutions at 298 K. All polymer solutions were prepared in the same way. An appropriate amount of the polymer was placed in a 5 mm NMR tube which was connected to the vacuum line through a ball joint. The tube with the polymer was kept at high vacuum at 343 K for about 24 hours

to remove any traces of water. The dry solvent was vacuum transported to the NMR tube. Then the tube was sealed. The concentration of the solution was established by weight.

Gel permeation chromatography measurements were performed on an Agilent chromatographic setup coupled to two detectors: a Knauer Refractive Index Detector and a Wyatt Technology DAWN multi-angle laser light scattering (MALLS) detector. A Polymer Laboratories PLGel 5 micron MIXED-C column with a length of 300 mm and inner diameter of 7.5 mm was used. Methylene chloride served as the mobile phase with a flow rate of 0.80 ml min^{-1}. The measurements were performed at 303 K.

2.2. Methods

2.2.1. Langmuir films experiments

All solutions for the monolayer spreading were prepared by dissolving the compounds in chloroform (HPLC grade) to the concentrations ca. 1 mg ml^{-1}. If a mixture of two solutions was required, it was prepared before applying onto the subphase.

To ensure reproducibility of achieved results, prior to every experiment the trough was carefully cleaned with chloroform, ethanol and rinsed with water. Ethanol 95% (Merck), used for cleaning the trough and the barriers, as well as the other solvents were of analytical grade. Ultra-pure water characterized by surface tension 72.75 $mN \cdot m^{-1}$ at 20°C and resistivity 18.2 MΩ·cm was obtained from the Milli-Q water purification system. Such water was used as a subphase in all experiments. Any remaining impurities floating on the subphase were removed in iterated process of putting the barriers together as close as possible and removing the surface layer of water from in-between the barriers with an aspirator.

The Langmuir-Blodgett trough together with Brewster angle microscope (Nanofilm) and Kelvin electrode (Treck) were placed on an active anti-vibration table (Newport) and closed in a Plexiglas box to prevent the films from dust and air-currents.

2.2.1.1. Compression isotherms

Experiments were carried out using the equipment from Nima Technology. The PTFE trough of size 50 mm × 750 mm × 10 mm was equipped with two hydrophilic barriers for symmetric compression. The film balance for surface pressure (π) measurements was of resolution

0.005 mN m^{-1}. A rectangular piece of analytical filtering paper (20 mm × 10 mm × 0.1 mm) was used as a surface pressure sensor. Sensor was calibrated before every experiment.

Langmuir experiments were performed using two different strategies (modes) of measurements: static and dynamic modes. In the dynamic mode only one portion (usually around 40 μl) of chloroform solution was carefully spread on the surface of water using a microsyringe (Hamilton). The deposition was performed at the maximal distance between the barriers, *i.e.* maximal surface area of the trough. The time delay allowing chloroform to evaporate after applying the solution was always around 15 minutes. Then the surface area of the trough available was reduced by a slow uniform motion of the barriers. Usually, films were compressed/decompressed at a rate of 5 $cm^2 \cdot min^{-1}$ which corresponds to approximately 0.05 - 0.25 $nm^2 \cdot molecule^{-1} \cdot min^{-1}$ (exact value depended on the amount and molecular mass of substance spread in the film). For all the studied compounds, the isotherms of compression and decompression (hysteresis loops) were recorded at temperature of 23°C (otherwise it is specified). The temperature was controlled with accuracy ± 0.2 °C by using a cooling/heating circulating bath (Thermo Scientific). Temperature was measured with two Pt100Ω resistance thermometers immersed at both ends of the trough and connected to Keithley multimeter.

The static experiments were performed with maximal surface of the trough and the barriers motionless. Portions of the solution of a volume from 2 to 5 μl were successively deposited at the air/water interface. After the deposition the system was equilibrated for about 30 minutes and then the surface pressure was measured.

2.2.1.2. Brewster angle microscopy (BAM)

The trough was equipped with a Brewster angle microscope from Nanofilm Technology (MiniBAM) of the resolution of 8.3 μm per pixel. The technique allowed direct observations of the films during compression/decompression. Moreover, it was used to qualitatively distinguish between areas of water surface covered with monolayer or multilayer. Also liquid and solid phases of the films were distinguished based on the shape of the domains (circular versus irregular) and the patterns observed at the interface. Magnification of MiniBAM was not high, so the field of observation was relatively large, *i.e.* 4.8mm × 6.4mm.

2.2.1.3. Surface potential

The Kelvin electrode was used to measure the surface potential (ΔV). A measuring head with a vibrating electrode from Treck Inc. was mounted on the Langmuir trough. A counter electrode made of stainless steel was placed on the bottom.

The measured surface potential is related to vertical component of the molecular dipole moment by Helmholtz equation:

$$\mu_{\perp} = \Delta V A_m \varepsilon \varepsilon_0 \qquad \textbf{Equation 8}$$

where: $\mu_{\perp} = \mu \cdot \cos\beta$ is the average component of the molecular dipole moment normal to the plane of the monolayer (β is the angle between the surface normal and the dipole axis), A_m is the area per molecule, ε and ε_0 are dielectric permittivity constants of the monolayer (which is usually taken as 1) and vacuum, respectively. Throughout the thesis no ΔV to $\mu\perp$ conversion was done because the dielectric permittivity of the film was unknown. Moreover, it changed significantly during layering transitions and strongly affected the curve of $\mu\perp(A)$. The signal of surface potential was extremely sensitive to the distance between the vibrating electrode and the water surface. Therefore it was "zeroed" at the beginning of each experiment and its stability was always checked before and after cleaning the surface. The level of water was constant during experiments in Langmuir trough. To assure this, reservoirs with water were placed inside the protective box, where whole setup was installed.

2.2.1.4. Langmuir-Blodgett technique

The films were transferred onto silicon and mica substrates according to the Langmuir-Blodgett technique. The dipper speed was always 10 mm minute^{-1}. The silicon wafers used for the experiments were provided by the Institute of Electronic Materials Technology (Warsaw, Poland). The wafers were cleaned with acetone, then dipped in nitric acid (30% solution) for 30 minutes and rinsed several times with water. Pieces of mica were freshly cleaved using scotch tape. Afterwards the mica was rinsed with only water. Both types of substrates prepared according to above described protocols were hydrophilic. The solid substrate was immersed in subphase before the spreading of the chloroform solution. Transfers onto solid substrate were always performed during the upstroke.

2.2.2. Drop Casting (DC)

In **Chapters 3.3**, **3.4** and **3.5** the films were casted by spreading a precisely calculated amount of chloroform solution directly onto the surface of water or hydrophilized silicon wafers. This method is denoted as drop casting (DC). Volumes of solution spread, v, were calculated according to the formula:

$$v = \frac{A_w L}{A_m N_A c} \qquad \textbf{Equation 9}$$

where: A_w – area of casted film (wafer area or water surface area), A_m – area per molecule in a densely packed monolayer (obtained from Langmuir isotherms), c – concentration of solution mol dm^{-3}, N_A – Avogadro number, L – demanded number of molecular layers in the film (1, 2, 3, 5, 7 or 9). The letter L was used to underline the number of molecular layers that could be formed if a perfectly ordered film was formed.

When the amount of solution calculated according to **Equation 9** was spread onto the silicon surface and the solvent evaporated, XRR patterns were recorded. In case of drop casting (DC) onto the water surface, the films were transferred onto silicon wafers at a constant surface pressure, according to the Blodgett method (without compression),[15,16] prior to the XRR measurements.

The spin coating method is known to assure good and homogeneous surface coverage. However the control over the thickness of the film in demanded regime of several molecular layers is very limited. Therefore DC was chosen over spin coating to precise control the L parameter.

In case of films of mixtures of at least two constituents the following methodology was used. First reference LB experiments were performed *i.e.* known volumes of solutions of pure components were spread onto the water surface and compressed. The collapse point (kink at the isotherm) indicated the point corresponding to a dense monolayer. The area between the barriers at the moment of film collapse was equal to the maximal area that could be covered by a dense monolayer by applied amount of solution. If volume of applied solution was divided by the collapse point area, the result was the concentration (expressed in µl cm^{-2}).

Relations between amounts of components in mixed solutions were denoted throughout the thesis as ratio of above described concentrations. Such ratios were in fact fractions of surface occupied of distinct mixture components.

2.2.3. X-ray reflectivity measurements (XRR)

Interference of the waves reflected from the sample surface and the interface between the thin film and the substrate results in oscillations of the reflected intensity as a function of the incident angle. The maximum of intensity appears when the phase difference is multiple of the incident wavelength λ, according to the formula:

$$m\lambda \cong 2d_S\sqrt{\theta_i^2 - 2\delta_1}, \qquad m = 0,1,2... \qquad \textbf{Equation 10}$$

where: d_s is the sublayer thickness, θ_i is the wave impinging angle at which the maximum intensity of reflected beam was measured, and 2δ is equal to critical angle of incidence. It is related to index of refraction, n, by approximate relation $n \approx 1 - \delta$. For the sample, which consists of N ideally smooth layers the Parratt approach was used.[164] In the kinematical approximation the reflected X-ray intensity is related to electron density profiles. These profiles are estimated according to expected structure of the layer. Distribution of electron density as a function of z-coordinate *i.e.* distance from the substrate gives the starting parameters for fitting procedure which simulates the real profile corresponding to the measured curve of intensity vs. 2θ angle. Software package Leptos 4.02 (from Bruker-AXS, Karlsruhe, Germany) allows to evaluate the layer thicknesses from the angular interval between the Kiessig fringes recorded for the layer. Detailed description of the basis of X-rays reflectivity measurements are given in the reference [165] and articles quoted therein.

Samples of monolayers and multilayers for XRR measurements were prepared on silicon wafers by direct transfer from water surface onto the solid substrate using LB or by DC technique. The measurements were performed using the X-ray diffractometer Bruker D8 Discover. Cu K_α radiation was used and the monochromatic parallel beam was formed by parabolic Goebel mirror. The system was equipped with Eulerian cradle and reflectometry sample-stage, which ensured precise sample positioning. Scintillation counter together with automatic absorber of primary beam allowed for linear dynamic range better than 10^8 cps; data were analyzed by fitting to theoretical model using the Leptos 4.02 software package. The "box model" in which the film was subdivided into slabs of various electron densities was used. The starting parameters were roughly calculated according to the structure of the

molecules within the films. The CPK model (from the names of Robert Corey, Linus Pauling and Walter Koltun) was used for modeling of molecular structures and estimation of molecular dimensions.

Some fits did not overlap perfectly with measured XRR profiles in a region of very small 2θ angles. The area of silicon wafer used for film deposition was smaller than a cross section of incident beam in plane parallel to the wafer. The incident beam covered not only investigated sample, but also a part of the stage. This caused a decrease of the reflected wave intensity when compared to fitted curves. When angles became greater, the area covered by incident beam decreases and measured signal corresponded to X-rays reflected from the films only (thus overlapped with theoretical curves).

2.2.4. Scanning electron microscopy (SEM)

Due to Abbe limit the resolution of classical optical microscopes is limited to half of the wavelength used (around 200 nm). To make it possible to directly observe smaller structures the beam of electrons of wavelength shorter than light is used. The higher energy of the electrons the shorter corresponding wavelength is.

Scanning electron microscopy (SEM) images were taken with use of a Zeiss LEO 1530 scanning electron microscope in the InLens detection mode. Since most of the samples were covered with organic compounds or residues, the energy of electron beam used was relatively low *i.e.* lower than 3 kV.

2.2.5. Atomic force microscopy (AFM)

The idea of atomic force microscopy (AFM) measurements is as follow. The tip is placed on the end of the cantilever. The position of the cantilever is measured by the position of the laser beam which is reflected on the cantilever top. When the cantilever bends the light is deflected. The tip is attracted or repulsed from the surface due to electrostatic and van der Waals interactions. Therefore the surface does not need to be conductive. The measurements can be performed in three basic modes: contact mode – the tip is in constant contact with the studied surface and changes its position due to roughness of the sample (appropriate for the stiff and rigid materials); non-contact mode – the tip is always in some distance from the surface and the changes of its position occur due to the interactions; and tapping mode – the tip touches the surface for very short period of time and the movement in

the XY directions is done when the tip does not touches the sample, what allows the investigations on the soft materials, which could be scratched otherwise.

The AFM images were acquired both in non-contact (FM) and tapping (AM) mode with the UHV-350 AFM/STM microscope (RHK Technology, Troy, MI, USA) at room temperature with base pressure in the low 10^{-10} mbar range. The AFM tips were Al-coated silicon cantilevers Nanosensors PPP-NCHR with a radius of curvature <10 nm, frequency 330 kHz, force constant 42 N m^{-1} (nominal values as reported by manufacturer). The topography, frequency, phase and amplitude of the cantilever were registered independently. XPMPro 2.0 software was used to control the hardware and to process the obtained scans.

2.2.6. X-ray photoelectron spectroscopy (XPS)

In the photoelectric effect the electrons are emitted from matter as a result of absorption of energy from electromagnetic radiation. Such electrons are called photoelectrons. Depending on the used wavelength the ultraviolet photoelectron spectroscopy (UPS) and X-ray photoelectron spectroscopy (XPS) are distinguished.

The XPS measurements were performed on PHI 5000 VersaProbe spectrometer with microfocused and monochromatic Al K_α radiation. The spectrometer was equipped with a spherical capacitor energy analyzer with multi-channel detection within a 100 μm × 100 μm area for XPS analysis. The X-ray beam was incident at the surface at the angle of 45° with respect to the surface normal. The analyzer axis was also located at 45° with respect to the surface normal. In the AR mode, the spectra were collected at electron take-off angles 15–70° relative to the surface plane. Shirley background subtraction and peak fitting with Gaussian-Lorentzian shaped profiles was performed for all considered photoelectron peaks. The data were analyzed using the Casa XPS software. Details on the spectrometer and its arrangement were recently reported by Jablonski.[166]

2.2.7. Surface enhanced Raman spectroscopy (SERS)

p-mercaptobenzoic acid (***p*-MBA**) and malachite green isothiocyanate were purchased from Sigma and used as received DNA oligomers ST20N2 (SHC6TTTTTTTTTTTTTTTTTTTG CGGCAATCAGGTTGACCGTACATCATAGCAGGACTAGTTGGTCGCAGTC) were purchased from Genomed and used as received.

SERS measurements were carried out on dried samples using a Renishaw InVia Raman system. The setup was equipped with a 300 mW diode laser emitting a 785 nm line used as the excitation source. The light from the laser passed through a line filter, and focused on a sample mounted on an X-Y-Z translation stage with a 20× microscope objective. The Raman scattered light was collected by the same objective through a holographic notch filter to block out Rayleigh scattering. A 1800 groove per mm grating was used to provide a spectral resolution of 5 cm^{-1}. The Raman scattering signal was recorded by a 1024 per 256 pixels RenCam CCD detector. The beam diameter was approximately 5 μm. The regular Raman spectra were acquired for 20 min; for SERS experiments the spectra were acquired for 30-60 s with the laser power measured at the sample being 5 mW. For presentation of the results, the spectra were normalized by the laser power and the collection times.

The normal Raman and SERS spectra of ***p*-MBA** were observed by excitation with a 785 nm laser. The enhancement factors (*EF*) were calculated according to the formula:

$$EF = \frac{I_{SERS} N_{NR}}{I_{NR} N_{SERS}} \qquad \textbf{Equation 11}$$

where N_{SERS} and N_{NR} – number of molecules adsorbed on the SERS probe within the laser spot area and the number of molecules probed by regular Raman spectroscopy, respectively; I_{SERS} and I_{NR} –the SERS intensity of ***p*-MBA** onto studied surface and to the normal Raman scattering intensity of ***p*-MBA** in bulk. I_{NR} and I_{SERS} were measured at 1077 cm^{-1}.

The SERS samples were prepared by dipping the substrate in 9.0 mL of 1.0×10^{-6} M solution of ***p*-MBA**. The number of molecules contained in this amount of the solution was 5.4×10^{15} and the surface area irradiated by a 5 μm diameter laser beam was around 19.6 μm^2. Therefore around 4.2×10^6 molecules were present in the laser beam spot.

The regular Raman spectrum was observed for a 100 μm thick cell filled with pure ***p*-MBA** of density of 1.06 g cm^{-3}. The molecular mass of ***p*-MBA** is 154.19 g mol^{-1}. Assuming cylindrical shape of the laser beam in the probe, the irradiated volume was estimated to be approximately 1.96×10^3 μm^3. This value was confirmed by registering Raman spectra of silicon while varying the distance from the focal plane. Under these conditions, $N_{NR} = 8.1 \times 10^{12}$ molecules were irradiated (volume × density × Avogadro's number/molar mass).

Prior to reproducibility analysis all SERS spectra were processed with a Savitzky-Golay second derivative method (window size of 50 date points with second order polynomial). Correlation coefficients between all nonidentical spectral pairs ($i \neq j$) in the same date set were determined from the data[167] according to the formula:

$$P_{i,j} = \frac{\sum_{k=1}^{W} (I_i(k) - \overline{I_i})(I_j(k) - \overline{I_j})}{\sigma_i \sigma_j} \qquad \textbf{Equation 12}$$

where i, j were the indexes of the spectra in the data matrix, k was the wave number index of the individual spectra, I was the spectral intensity, W was the spectral range, and σ_i was the standard deviation of the spectrum. Once the correlation coefficients $P_{i,j}$ were calculated, Γ, the average of the off-diagonal correlation coefficient, was determined:

$$\Gamma \equiv \frac{2\sum_{i=1}^{N} \sum_{j=i+1}^{N} P_{ij}}{N(N-1)} \qquad \textbf{Equation 13}$$

Thus defined Γ was an easily determined and very useful parameter for quantitative assessment of spectral reproducibility. Γ varied between 0 and 1, where 1 was the case of identical spectra and 0 the case of completely uncorrelated spectra. Γ as defined in **Equation 13** was used to evaluate the reproducibility of multiple measurements.

RESULTS

3. Results: Bolaamphiphiles

Modern technologies, along with constantly diminishing scale of processes they implement, bring new requirements for materials with very special properties. Industry and science are now concentrated mainly on design and processing at the micro- or even nanoscale. To reach this level of scaling, new functional materials have to be designed, starting from the molecular level. Progress in organic synthesis can fulfill such requirements. It is now possible to synthesize new molecules designed for specific purposes. However, for future technical applications, far more complex and better organized molecular assemblies are necessary.

An observation that partially fluorinated alkanes act like surfactants[168] gave an impulse for intensive studies on behavior of fluorinated compounds.[169,170,171] The Langmuir films of fluorinated compounds have been intensively studied for the past decade. Films of fluorinated amphiphiles gained a great importance[172] with the realization of their various possible biomedical applications. For example such partially fluorinated surfactants were used for producing the medium with air microbubbles used as a contrast for sonography of living tissues (like lungs).[173] Systematic studies showed an unusual behavior of thin films of fluorinated compounds. For example $\pi(A)$ isotherms of Langmuir films of fluorinated surfactants appeared to be reversible when decompressed before the film collapse. An important way to increase stability of the monolayer and to prevent an irreversible 3D aggregation was a fluorination of particular parts of the amphiphilic molecules.[174] The fluorination of parts of the molecules enhanced the stability of these layers due to an increase of hydrophobicity.[175]

In this chapter compounds belonging to the new group of amphiphiles, namely bolaamphiphiles are investigated. Results of both partially fluorinated and nonfluorinated analogues are described to evaluate the influence of fluorination on the properties of thin films of bolaamphiphiles.

Bolaamphiphiles may be regarded as dimeric end-to-end connected amphiphiles. They stabilize membranes significantly (*e.g.* monolayer lipid membranes of archaebacteria[176]) and form other interesting self-assembled structures, such as liquid crystalline phases in the bulk state,[177] and gels[148] or helical fibers[178] in aqueous systems. Formation of nanowells and pores in lipid membranes represents an additional example of unique self-assembly capability of bolaamphiphiles.[148] Flexible bolaamphiphiles can adopt different conformations: a linear or,

if the hydrophobic moiety is sufficiently long and flexible, also a reversed U-shape.[179] Introduction of a rodlike rigid segment as a hydrophobic moiety between the polar groups inhibits deformation to a U shaped conformation. A reversed U-shape conformation was also observed for bolaamphiphiles with a rigid biphenyl moiety and flexible siloxane units decoupling the rigid core from the head groups. In the monolayers the biphenyl cores are arranged parallel to the water surface, similar to p-terphenyl amphiphiles reported previously.[180,181]

The compounds studied here have potential for applications in organic electronics. This originates from the molecular structure of the core, which consist of stiff π-conjugated structures. The rod-like π-conjugated moieties introduce extended functionality due to their possible fluorescent and semiconducting properties, which are of interest with respect to the potential applications of the formed thin films.[182,183] Conjugated systems are typically utilized for preparation of conducting polymers and compounds applied as organic semiconductors, capacitors, transistors, rectifiers or other nanodevices.[55-57,153]

3.1. Reversibility and reproducibility of $\pi(A)$ isotherms

The detailed work on reversibility and reproducibility of Langmuir isotherms of bolaamphiphiles of different shapes is the main topic of the PhD thesis of Patrycja Nitoń. My part of the work in this project was the XRR and XPS measurements and data analysis. Therefore in this chapter I focused on the alignment of the molecules upon layering transition (part of the project done by me). The reversibility and reproducibility of $\pi(A)$ isotherms of the films of partially fluorinated bolaamphiphiles are just mentioned as the starting point for my own research presented in **Chapters 3.2** to **3.5**.

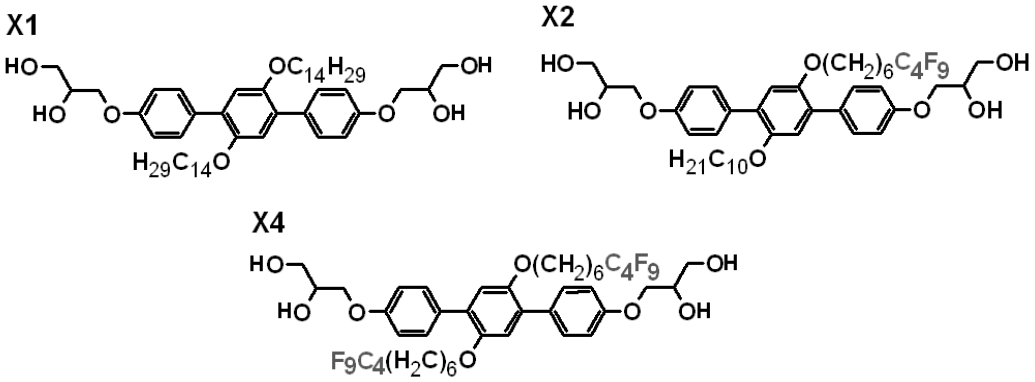

The isotherms of compounds with partially fluorinated segments were found to be reversible and reproducible in spite of the compression far beyond collapse point. The Langmuir-Blodgett technique has been used for more than one hundred years and no one reported such reversibility and reproducibility of the isotherms before. Even for the highest possible compression/decompression rates of 1.50 nm^2 $molecule^{-1}$ min^{-1} (usually experiments were carried out at much lower speed of the barriers of approximately 0.05 nm^2 $molecule^{-1}$ min^{-1} for system to be as close equilibrium as possible) the compression and decompression curves perfectly overlapped. This indicated perfect reversibility of the collapse. Only polyphiles with fluorinated lateral chains gave such perfectly reversible isotherms. In case of nonfluorinated compound **X1** this process was irreversible.

Three compression/decompression cycles for compound **X2** were recorded with high speed (1.50 nm^2 $molecule^{-1}$ min^{-1}). The $\pi(A)$ isotherms exhibited almost horizontal plateau typical for the phase transition (**Figure 9**). A careful analysis of isotherm gave a ratio of area at the beginning and at the end of the plateau equal to around three in case of all X-shaped partially fluorinated bolaamphiphiles. Therefore, the process corresponding to the plateau at the

isotherms was related to the trilayer formation. It shall be therefore called "the layering transition" and not a collapse (according to **Chapter 1.3.3.1**).

Formation of the trilayer structure was additionally verified by means of XRR measurements. The samples were prepared by transfer of the films at an appropriate surface pressure onto a silicon substrate according to LB method. For each compound the monolayer was transferred at the surface pressure below the plateau. The expected trilayer was transferred well above the plateau, but below the next singularity in the isotherm. Transfer ratios were always close to unity, often slightly bigger than 1. This indicated that the films on the silicon wafer (after transfer) were even better organized than on the water surface. For the detailed results see **Chapter 3.2**. The obtained reflectivity curves were very similar to those recorded for freely suspended liquid-crystalline smectic films,[187] indicating a perfectly layered structure. A film thickness was obtained as one of the parameters in the equation used to fit the experimental XRR data.

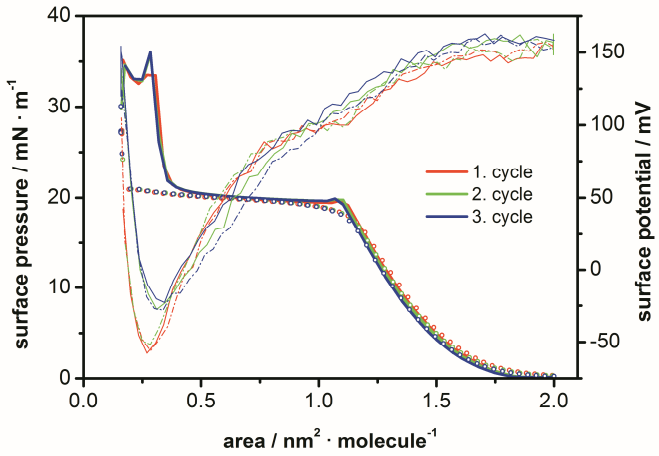

Figure 9 Reversible isotherms of compound **X2**; solid and dotted lines correspond to compression and decompression runs, respectively.

The biggest challenge was to determine the orientation of the molecules before and after layering transition within the films. The results obtained for compound **X4** were most appropriate for data analysis because of the symmetry of the molecules. For the experimental data see **Figure 15** in **Chapter 3.2**. The film transferred at π = 20 mN m^{-1} (below the plateau region) had a thickness of 1.45 nm. This value was in good agreement with a monolayer structure, where the terphenyls lay flat on the surface and the two lateral chains were perpendicular to the water surface. The film transferred at surface pressure π = 40 mN m^{-1} had a thickness of 4.32 nm (approximately three times thicker than monolayer film). The

presented conformity indicated formation of a well-defined trilayer stack with relatively small interdigitation of the neighboring layers.

X-ray reflectivity measurements are very sensitive to film thickness, roughness and density variations in the direction perpendicular to the surface. The method is therefore very suitable for thin film investigation. The biggest disadvantage is that the data simulation is nonunique, in the sense that a change of one parameter can be compensated by other subsequent changes throughout the model structure. Therefore it is crucial to set the starting parameters within physically reasonable values or determine them by means of other techniques.

The electron densities of the parts of the molecules were roughly estimated by dividing the number of all electrons by the volume of the parts of the molecule calculated as purely geometrical values (CPK model). The starting parameters were allowed to vary only in a reasonable, restricted range (±10%). Box model was used for fitting XRR patterns of monolayer films. The molecule was divided into rigid, core section (with glycerol moieties), R_H and R_F segments. The electron densities of such sublayers differed significantly. Fitting confirmed the above mentioned arrangement of the molecules in monolayers. The cores were found to be oriented horizontally and the lateral chains vertically (or slightly tilted) to the surface.

Much more difficult task was to fit the data obtained for 3-layer films. The number of sublayers of different electron density increased. It became possible to obtain relatively good fits from at least two different sets of starting parameters.

In case of the alignment presented in **Figure 10** the molecules fulfilled the requirement of minimization of conformational energy. The X conformation of the molecules was energetically preferable over the π orientation. The orientation of molecules in the bottom layer was constrained by the presence of the water surface. For such arrangement a lot of free space was available between the rigid cores (area of the core was around 1.25 nm^2, area of aliphatic chain around 0.2 nm^2 and area of the fluorinated chain around 0.4 nm^2).[52] The lateral chains, which belonged to molecules from different layers, were strongly interdigitated and tilted. Such conclusion was also justified by the analysis of thickness of the layer and the size of the molecule. If no interdigitation was assumed the thicknes of the trilayer film should be around 7 nm, *i.e.* much larger than in fact measured. If maximal interdigitation of side chains and no tilt were assumed the thickness of the trilayer film of compound **X4** should be around 4.5 nm (4.32 nm was in fact measured). It was difficult to estimate the electron density

in regions between the cores. Therefore the starting parameters for overlapping chains were allowed to vary strongly during the fitting process. This lack of constrains resulted in good quality of the XRR fits.

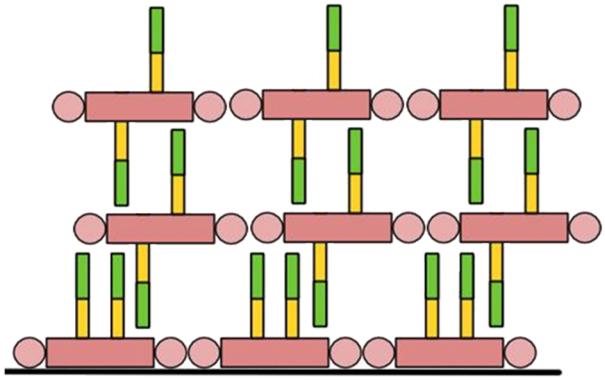

Figure 10 Hypothetical alignment of X-shape molecules (compound **X4**) within 3-layer stacks. Presented alignment is based on the assumption, that X geometry is energetically more preferred than π geometry. Pink color – cores, yellow – R_H segments, green – R_F segments.

The second proposed orientation of the molecules in 3-layer film of compound **X4** originated from the analysis of *roll over* mechanism (**Figure 11**). This was used as a hint, and the true mechanism of multilayer stacks formation is discussed in details in **Chapter 3.2.4**. The assumption was that the air/water interface influenced not only the bottom layer, but all molecular layers. Moreover, the molecules created pairs with back-to-back organization of the aromatic cores, additionally associated through hydrogen bonds between the glycerol moieties. Similar structures with a bilayer on top of a monolayer were obtained in computer simulations[184] for arachidic acid (AA) on water in a presence of calcium ions (chemical bonds AA-Ca-AA stabilized such structure). Even more ordered trilayer structure was obtained for AA/pure water system in longer time-scale simulations (see Figure 18 in ref. 184). Similarly to bolaamphiphiles, the AA molecules in this system were also associated in bilayers through hydrogen bonds (but in this case formed between carboxylic groups). Another example of pair formations was described in case of liquid crystalline cyanobiphenyls due to the π-π stacking as a bilayer forming factor.

The possibility of the glycerol moieties to be exposed as a top sublayer of the film of X-shaped bolaamphiphiles was excluded by the contact angle measurements described in details in **Chapter 3.2.3**.

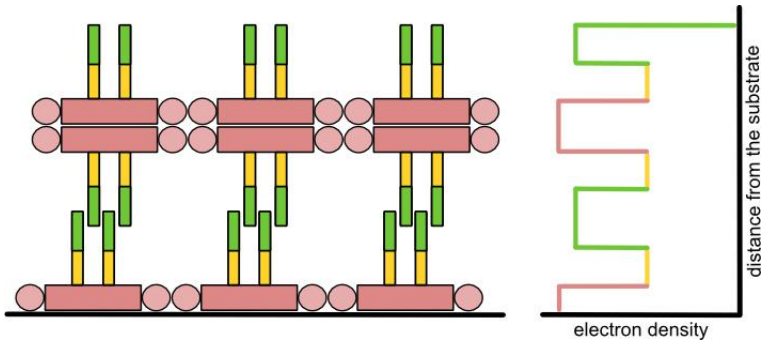

Figure 11 Schematic structure of 3-layer film of X-shaped molecules (compound **X4**) (left) and corresponding electron density profile (right). The assumed distribution of electron density was used as set of starting parameters for fitting procedure. Electron density is the highest for the sublayer of aromatic cores (pink), medium for the sublayer of the fluorinated segments (green), and the lowest for the sublayer of the aliphatic segments (yellow).

To distinguish two possible organizations of the molecules in 3-layer films (**Figure 10** and **Figure 11**) the XPS technique was employed. The samples of films of **X4** for XPS were prepared according to the same protocol as for XRR measurements, *i.e.* monolayer was transferred at 20 mN m^{-1} and trilayer at 40 mN m^{-1}. In case of XPS, the silicon wafers appeared to be inappropriate due to silicon dioxide layer at the surface. This made the F/O atomic concentration ratio analysis unreliable due to additional source of oxygen. Therefore glass covered with chromium as a sublayer and gold as a top layer was used. Such substrates were also hydrophilic, therefore LB procedure remained unchanged.

In the arrangement shown in **Figure 10** the fluorine atoms should be distributed randomly within the film interior due to the overlapping of the molecular layers as mentioned previously. On the other hand in case of arrangement of molecules presented in **Figure 11** almost no overlapping was predicted and regions of higher atomic concentration of oxygen (from glycerol units) and fluorine (R_F segments) should be observed. In fact XPS revealed fluorine and oxygen rich regions within 3-layer film of compound **X4**, as shown in **Figure 12**. Therefore the π orientation of the molecules in 3-layer films of X-shaped bolaamphiphiles was confirmed (arrangement shown in **Figure 11**).

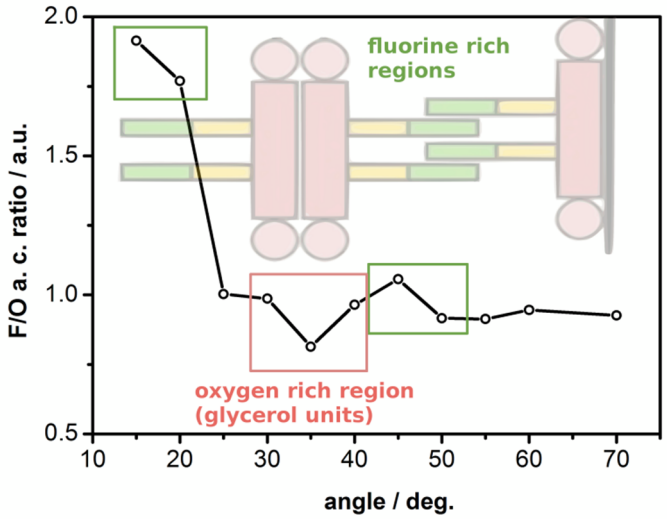

Figure 12 The relative atomic concentration ratio of fluorine to oxygen at various depth of the surface and subsurface regions of the trilayer film of **X4** is shown. Angles do not correspond directly to *z* position of the sublayers in the trilayer film. Cartoon of the molecules arrangement is shown to illustrate the oxygen and fluorine rich regions in proposed molecular alignment.

XPS sputter depth profiling was done using 500 eV argon ion beam with the slowest profiling speed (0.36 nm per minute) and the lowest possible energy. The films of bolaamphiphiles were found to be very soft and fragile. Therefore the sublayers of 3-layer film were not removed in controlled way. Disruption of the whole film occurred during the ion bombardment. Such experiments provided only additional confirmation of π orientation of the **X4** molecules in monolayer film (not shown).

3.1.1. Conclusions

The reproducibility and the reversibility of the trilayer films formation of bolaamphiphiles was assured by fluidity of the layers. Therefore the reversible layering transition depended on shape and rigidity/flexibility of different parts of the molecules. The function of the semi-perfluorinated chains was twofold: 1) they increased the film stability by increasing the amphiphilicity and 2) the fluorinated chains of medium size increased film fluidity due to the mismatch of chain diameter (R_H versus R_F), and probably, due to the dipole moment introduced at the R_H–R_F junctions.[170] Hence, beside the presence of an anisometric rigid unit, also the partial fluorination of the lateral chains turned out to be a key factor for reversible formation of stable and well-defined mono- and trilayers. Reversible transition to a bilayer was reported earlier by Gallani *et al.*[185] for a mesogenic compound with rigid core and two

chains at both its ends. The fact that one of the aliphatic chains of the molecule of Gallani *et al.*[185] contained even stiffer segment of alkylosiloxane confirmed presented reasoning. However, the conclusion of Gallani *et al.*[185] about bilayer created in their film seems somewhat doubtful. The results presented in Figures 2 and 3 of ref. 185 indicated rather formation of the trilayer.

The arrangement of molecules in monolayer and trilayer films of X-shaped bolaamphiphiles was proved as a result of careful analysis of XRR and XPS measurements.

3.2. Multilayers formation at the air/water interface

In this chapter detailed studies on layering transitions within thin films of compounds belonging to the groups of X-shaped, T-shaped and anchor-shaped bolaamphiphiles (**Figure 3**) are described. Investigated molecules contained a hydrophobic, rod-like or bent rigid core with two polar groups (glycerol units) on both ends. One or two lateral chains were attached in the central part of the molecules. The side chains were partially fluorinated.[172] For comparison, one X-shaped and one anchor-shaped compounds as nonfluorinated analogues were also studied. A tendency of fluorinated compounds to create very stable and well defined multilayers was proved. Stacks consisting not only of 3- but also 5-, 7- or even 9-layers were formed by compression of monolayer at the air/water interface. A very important finding of conducted experiments was a possibility of transferring them onto solid substrates in a one-step procedure.

3.2.1. Results and Discussion

The studied compounds differed in shape (X-, T- and anchor-shaped) and hence their properties varied as well. The results for each of three types of molecules are described in separate sections. The structures of the studied molecules are shown in **Figure 4** and repeated in the beginning of each section. All studied compounds formed stable Langmuir films at the air/water interface. The partial fluorination in the lateral aliphatic chains prevented them from a collapse into undefined aggregates even at high compression ratio. During compression the monolayer films underwent layering transitions to well defined lamellar structures.[153] This was surprising, since studied compounds formed predominately columnar LC phases in bulk.[149,151]

Laminated phases (Lam phases) represent a special type of smectic LC phases whereby the aromatic cores are arranged parallel to the smectic layers. Lam_{Iso}, Lam_{N} and Lam_{Sm} phases are distinguished as having no order (isotropic), only orientational order (nematic), or orientational and positional in-plane order (smectic), respectively.[186] These mesophases can be regarded as laminated analogues (2D analogues) of the corresponding isotropic, nematic and smectic bulk phases.[149] The data concerning bulk properties of studied bolaamphiphiles is shown in **Table 2**.

3.2.1.1. X-shaped bolaamphiphiles

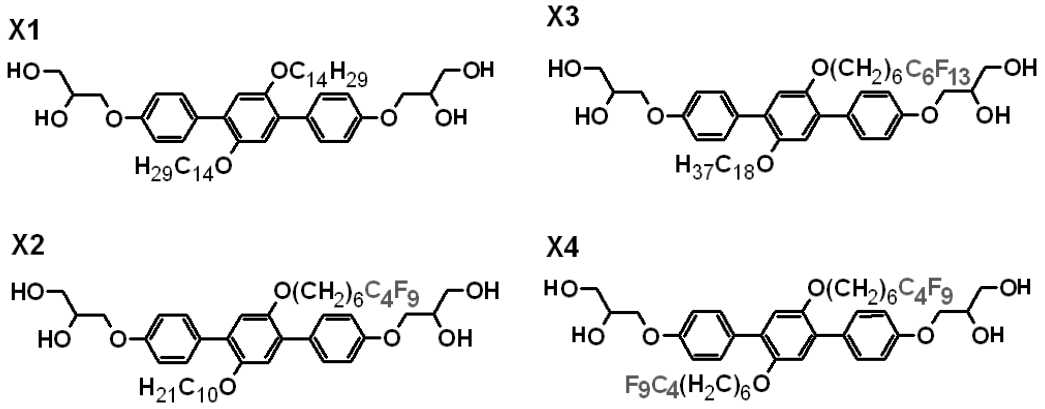

The measurements were performed on the films transferred onto silicon wafers using Langmuir-Blodgett technique.[15,16] It was important to transfer the homogenous (one-phase) films. Thus the surface pressures chosen for the transfer (given on the graphs) corresponded to the slopes of the isotherms. Compound **X1** had two nonfluorinated side chains of the same length. The isotherms of surface pressure, π, and surface potential, ΔV, plotted against molecular area, A_m, for **X1** are shown in **Figure 13a**. A proof for the trilayer formation during compression of a monolayer of compound **X1** was provided by the XRR measurements, presented in **Figure 13** (graphs **d** and **e**). In case of **X1** the minima/maxima on the XRR curves were smeared-out and not well shaped, when compared to the results obtained for fluorinated X-shaped compounds (verify **Figure 14** and **Figure 15**). The films gave deformed profiles due to disorder in the layers. The thickness of the films was roughly estimated; it was related mainly to the locations of the minima of XRR patterns.[187] The values of thicknesses estimated from the fits were: for the monolayer d_1 = 1.52 nm and for the trilayer d_3 = 4.23 nm. The ratio d_3/d_1 = 2.78 was slightly less than 3, probably because of partial interdigitation of the molecules in neighboring layers.

Another way to confirm the formation of trilayer of compound **X1** was a comparison of the molecular areas at both ends of the plateau. The plateau region corresponded to the layering transition. The area occupied by one molecule in a monolayer corresponded to the A-coordinate of the kink at π = 15.9 mN·m^{-1} and it was equal to A_1 = 1.07 nm^2·molecule^{-1}. The molecular area in a trilayer was estimated as A-coordinate of the intersection of a horizontal line tangent to the curve in the plateau region (here at π = 15.9 mN·m^{-1}) and the extrapolated linear part of the curve corresponding to the trilayer compression (here, in range of $\pi \approx$ 20.5 - 23.0 mN·m^{-1}) and was equal to $A_3 \approx$ 0.38 nm^2·molecule^{-1}. The ratio of these two

values A_1/A_3 was equal to 2.8 (within uncertainty of the estimation it was considered as close to 3). This supported the formation of the trilayer in the plateau of $\pi(A)$ isotherm.

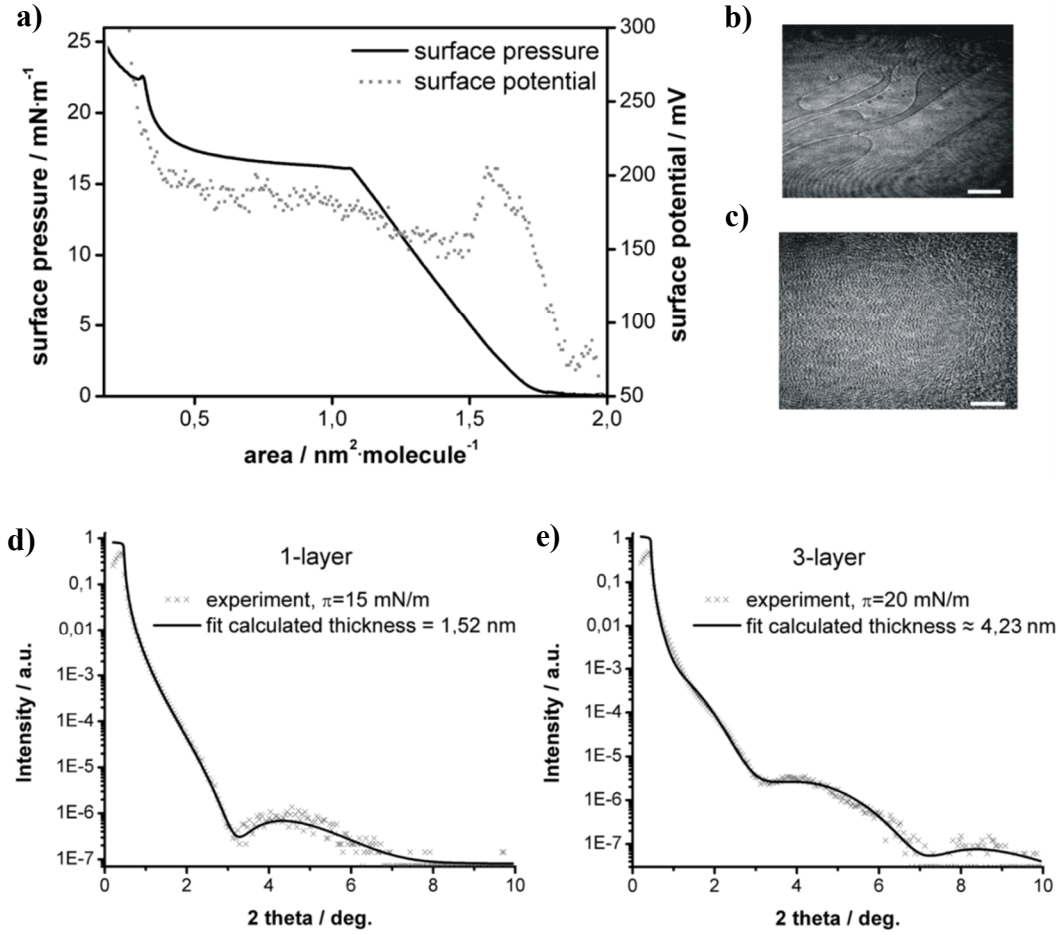

Figure 13 Results for compound **X1** (nonfluorinated): **a)** isotherms of surface pressure, π, and surface potential, ΔV, plotted against molecular area, **b)** the BAM image taken at π = 0 mN·m^{-1} showing coexistence of liquid monolayer and gas phase, **c)** the BAM image taken at π = 24 mN·m^{-1} showing the collapsing trilayer; scale bars in BAM images correspond to 500 μm. **d)-e)** the XRR measurements for monolayer and trilayer transferred to silicon wafers at 15 mN·m^{-1} and 20 mN·m^{-1}, respectively.

The film of compound **X1** compressed beyond the second kink in the $\pi(A)$ isotherm at π = 24 mN·m^{-1} was also transferred onto the silicon wafer. XRR studies did not give any regular profile. The kink at π = 23 mN·m^{-1} corresponded to collapse. Also BAM observations (image **c** in **Figure 13**) showed a rough surface with aggregates.

The isotherm of the surface potential, $\Delta V(A)$, presented in **Figure 13a** revealed that the signal increased during compression of the monolayer. This was a result of the reorientation of

aliphatic chains to a tilted/vertical orientation. The surface potential remained almost constant during trilayer formation. It justified the conclusion that the molecules in the bilayer created on top of the monolayer had the aliphatic lateral chains in anti-parallel orientation. Their dipole moments were almost compensated.

Experimental data concerning compounds **X2** and **X3** is presented in **Figure 14** in a similar manner as for compound **X1**. All results obtained for compounds **X2** and **X3** are compared in **Figure 14**, showing an incredible similarity. Hence the following discussion of compound **X2** applies to compound **X3** as well.

The $\pi(A)$ isotherm of **X2** seems analogous to the one obtained for **X1**. The first broad plateau on the $\pi(A)$ curve corresponded to the layering transition, *i.e.* to the coexistence of domains of different thickness. The inclined parts of the isotherm corresponded to the compression of the film of uniform thickness. The A-coordinates for the monolayer and the trilayer films were estimated for constant surface pressure π = 20.0 $mN \cdot m^{-1}$, the same way as in the case of compound **X1**. The following values were obtained: A_1 = 1.06 $nm^2 \cdot molecule^{-1}$ and A_3 = 0.35 $nm^2 \cdot molecule^{-1}$ for mono- and expected trilayer, respectively. The ratio A_1/A_3 = 3.0 proved that at the first plateau the monolayer transforms into a trilayer. On further compression of the film another kink or inflexion point was visible. The same behavior was seen even more clearly for compound **X3** (see **Figure 14**). Estimation of the A-coordinate at this point gave the value A_5 = 0.20 $nm^2 \cdot molecule^{-1}$ and the ratio $A_1/A_5 \approx 5$. This gave a strong inclination that a 5-layer film was observed. As expected, the same analysis for the compound **X3** gave the values of A-coordinates for 1-, 3-, and 5-layer equal to 1.07 $nm^2 \cdot molecule^{-1}$, 0.35 $nm^2 \cdot molecule^{-1}$, and 0.21 $nm^2 \cdot molecule^{-1}$, respectively. These values indicated a decrease of the molecular area by 3.05 and 5.09 times, showing the formation of 3- and 5- layer films. Also the 2D compressibility of a trilayer was 3 times smaller than that of a monolayer, 5 times smaller than that of a 5-layer, and so on. In such a case the extrapolation of A-coordinate for the 5-layered film to lower surface pressure was not necessary because the extrapolated line is almost vertical. The curve $\pi(A)$ for compression of 5-layer and thicker films was so steep that the correction would be small and negligible.

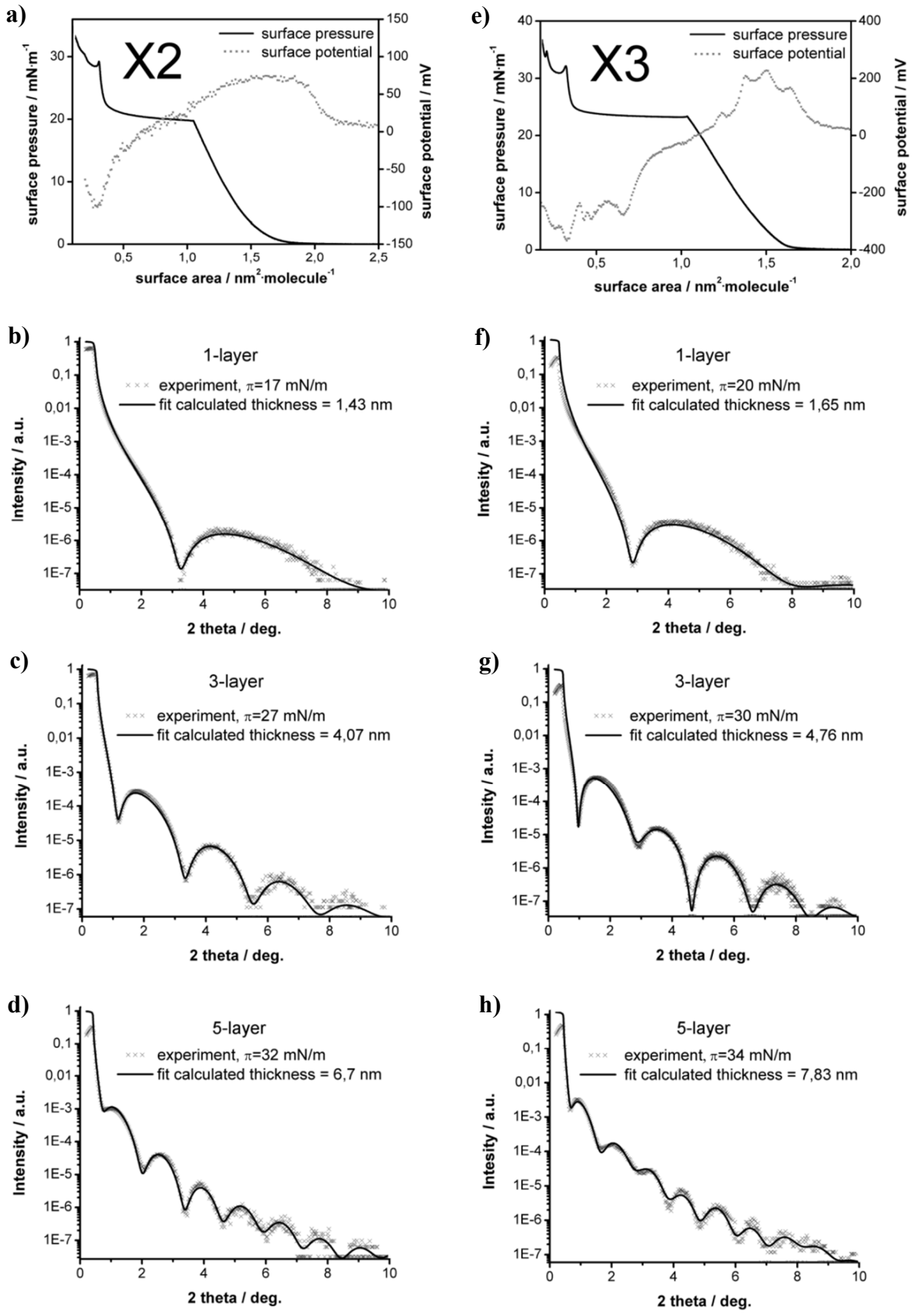

Figure 14 Comparison of results for two X-shaped compounds: **a)-d)** for **X2** and **e)-h)** for **X3**; **a)** and **e)**: the isotherms of surface pressure and surface potential plotted against molecular area for **X2** and **X3**, respectively; **b)-d)**: X-ray reflectivity measurements (XRR)

for 1-, 3- and 5-layer films of compound **X2** transferred from air/water interface onto silicon wafers at surface pressures 17 mN m^{-1}, 27 mN m^{-1} and 32 mN m^{-1}, respectively; **f)-h)**: XRR measurements for 1-, 3- and 5-layer films of compound **X3** transferred from air/water interface onto silicon wafers at surface pressures 22 mN m^{-1}, 30 mN m^{-1} and 34 mN m^{-1}, respectively.

For each compound the films were transferred at a surface pressure corresponding to the well-defined multilayered structures. The films of compound **X2** were deposited at 17 mN·m^{-1} (monolayer), 27 mN·m^{-1} (trilayer) and 32 mN·m^{-1} (5-layer). These of compound **X3** were transferred at pressures of 20 mN·m^{-1} (monolayer), 30 mN·m^{-1} (trilayer), and 34 mN·m^{-1} (5-layer). The XRR patterns together with fits and film thicknesses are given in **Figure 14 (b-d)** for **X2** and in **Figure 14 (f-h)** for **X3**. The results confirmed the numbers of layers predicted from the shape of the isotherm. Corresponding ratios of thicknesses between particular multilayers are collected in **Table 3**. All results of thickness measurements using XRR technique are collected in **Table 4**.

Table 3 The ratios of thicknesses of particular multilayers and monolayer for compounds X2 and X3.[a]

compound X2	**compound X3**
$d_3/d_1 = 4.07/1.43 = 2.85$	$d_3/d_1 = 4.76/1/65 = 2.89$
$d_5/d_1 = 6.70/1.43 = 4.69$	$d_5/d_1 = 7.83/1.65 = 4.74$
$d_3/d_5 = 4.07/6.70 = 0.608 \approx 3/5$	$d_3/d_5 = 4.76/7.83 = 0.608 \approx 3/5$

[a] Above values of the ratios are the approximate results because it was neglected in this estimation that the layer being in contact with air (top layer or monolayer) is thicker than the other layers, which create the interdigitated bilayers. For that reason the ratios $d_3/d_1 < 3$ and $d_5/d_1 < 5$ were found. The very close similarity between results for **X2** and **X3** has to be noted.

The surface potential isotherms of compounds **X2** and **X3** differed from these recorded for compound **X1** because of the presence of fluorinated segments in one of the lateral chains. For both compounds the surface potential initially increased because of closer packing of the molecules. Next the surface potential started to decrease. This was caused by the negative contribution of the C-F dipoles[188] coming from the strongly electronegative terminal fluorine atoms (the dipoles of C-F in $-CF_3$ and C-H in $-CH_3$ have opposite signs). Weak inflexions were visible in the $\Delta V(A)$ curves at the beginning of the plateau. The potential continued to

decrease to negative values, showing that the compensation of the dipoles in the second and third layers was not complete. It could be explained by a lack of symmetry in the lengths of the chains as well as by an imperfect ordering of the chains in the layers. Orientation of the chains was to some degree random. This means that the fluorinated segment could be directed "upwards" or "downwards." However, the "upwards" orientation giving a negative contribution to the vertical component of dipole moment was apparently preferred.

Compound **X4** contained two partially fluorinated lateral chains with the same length and the same degree of fluorination. This made this molecule symmetrical, thus similar to **X1**. Comparison of the isotherms of surface pressure, $\pi(A)$, and surface potential, $\Delta V(A)$, for **X1** (shown in **Figure 13a**) and for **X4** (shown in **Figure 15a**), revealed that in spite of the symmetry of both molecules their behavior is very distinct.

In the curve of $\pi(A)$ of compound **X4** (**Figure 15a**) three layering transitions were clearly distinguished. Only the first one was represented by a broad plateau of coexisting films of distinct thickness. The subsequent transitions were manifested as loops of van der Waals type. The peaks of metastable states, typical for gas/liquid phase transitions, were visible. The estimated equilibrium surface pressures of these layering transitions were: 25.5 $mN \cdot m^{-1}$, 38.0 $mN \cdot m^{-1}$, and 48.3 $mN \cdot m^{-1}$. Respective values of A-coordinates corresponding to well packed films of different thickness were as follows: 1.12 $nm^2 \cdot molecule^{-1}$, 0.37 $nm^2 \cdot molecule^{-1}$, 0.22 $nm^2 \cdot molecule^{-1}$, and 0.16 $nm^2 \cdot molecule^{-1}$. Calculated ratios of the molecular areas showed that the kinks on the isotherm corresponded to the formation of trilayer (decrease of molecular area by 3.02 times), 5-layer (5.09 times) and 7-layer (7.00 times). Such behavior indicated that further compression of the fluorinated bolaamphiphiles might result in even thicker films. However, it was impossible to perform such experiments due to technical limitations of compression ratio of the Langmuir trough used.

The formation of multilayered structures during compression of the monolayer of **X4** was also verified in XRR measurements. The films were transferred onto silicon wafers at surface pressures: 20 $mN \cdot m^{-1}$ (monolayer), 35 $mN \cdot m^{-1}$ (trilayer), 45 $mN \cdot m^{-1}$ (5-layer), and 55 $mN \cdot m^{-1}$ (7-layer). All results of thickness measurements using XRR technique are given on the graphs with X-ray reflectivity profiles (**Figure 15**) and also collected in **Table 4**. The ratios of thickness d_n/d_1 of the films confirmed their expected structures and showed partial interdigitation of the molecules between the layers. These ratios are 2.98, 4.64, and 6.39 for 3-, 5-, and 7-layered films, respectively.

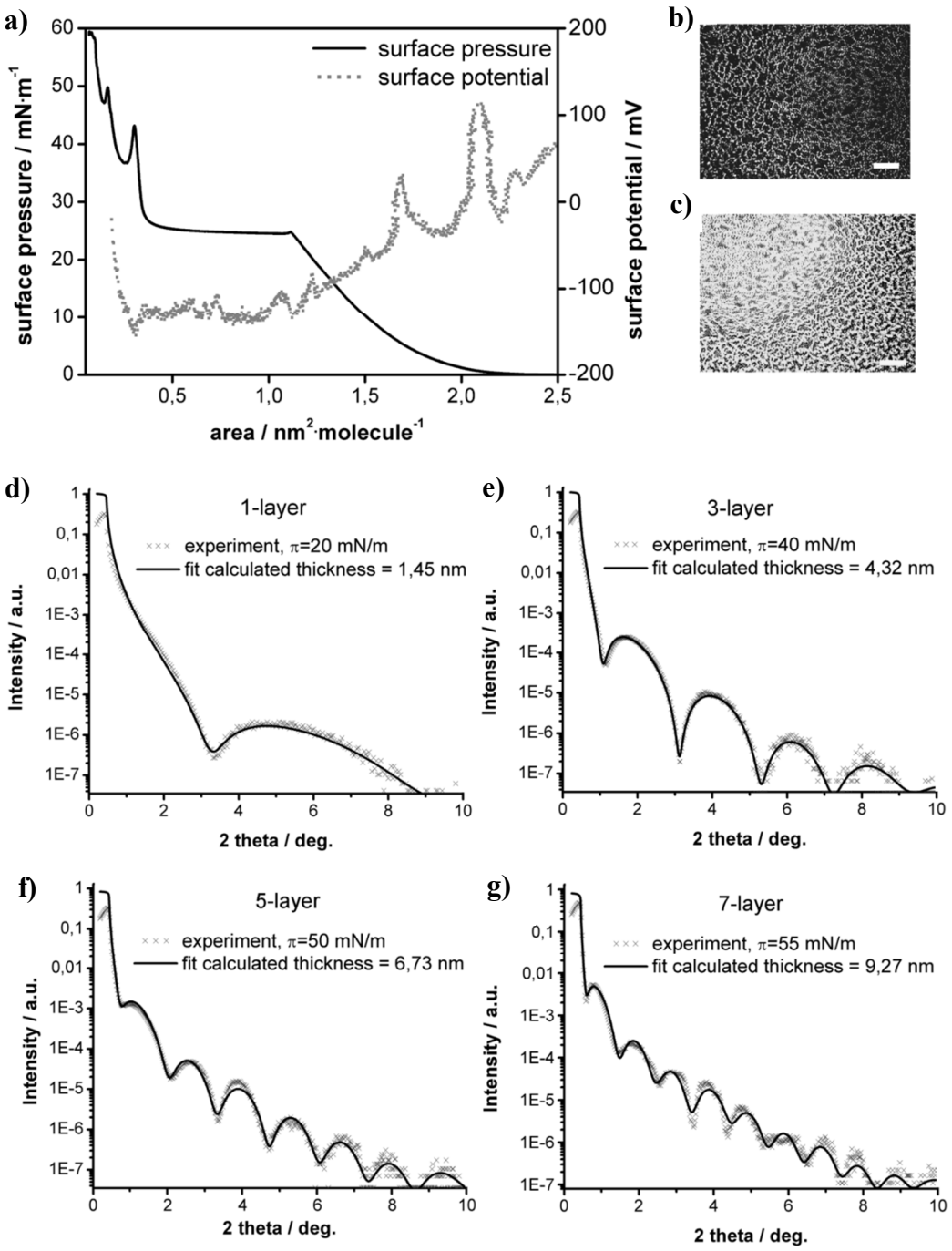

Figure 15 Results for compound **X4** (two fluorinated lateral chains): **a)** isotherms of surface pressure, π, and surface potential, ΔV, plotted against molecular area, **b)** BAM image taken at $\pi \approx 20$ mN·m^{-1} and $A \approx 1.1$ nm^2·molecule^{-1} showing coexistence of monolayer and trilayer at the beginning of the plateau, **c)** BAM image taken at $\pi \approx 20$ mN·m^{-1} and $A \approx 0.5$ nm^2·molecule^{-1}showing an increasing area of the trilayer still coexisting with the monolayer (scale bars in BAM images correspond to 500 μm). **d)–g)** XRR measurements for

monolayer, trilayer, 5-layer and 7-layer films transferred to silicon wafers at 20 $mN \cdot m^{-1}$, 40 $mN \cdot m^{-1}$, 50 $mN \cdot m^{-1}$, and 55 $mN \cdot m^{-1}$, respectively.

3.2.1.2. T-shaped bolaamphiphiles

T1

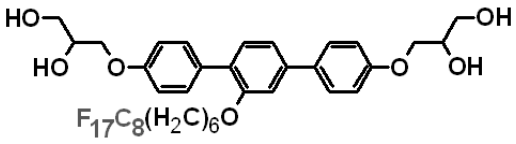

The $\pi(A)$ isotherm of compound **T1** (**Figure 16a**) was similar to the isotherms of the X-shaped molecules. Careful analysis of the shape of the curve indicated an unexpected behavior of the T-shaped molecules. The "collapse" of the monolayer film occurred at $A_1 = 0.39$ nm^2 $molecule^{-1}$ which was much less than the projection of the aromatic core lying flat on the water surface. However, this value agreed with the cross section of the core and the lateral chain standing perpendicularly to the water surface.[189] The area at which the surface pressure started to increase rapidly (lift-off) was equal to 1.15 nm^2 $molecule^{-1}$. This corresponded to the area of the molecules lying flat on the surface. The molecules changed their orientation to tilted and next to vertical upon compression. Very high compressibility (small slope of the isotherm) just after the point of lift-off also supported the assumption about rapid decrease of molecular area caused by a change of the molecular orientation. Next the compressibility decreased to usual values, typical for 2D liquid phases. The "collapse" of the monolayer of vertically oriented molecules occurred after a small peak. This indicated that the film became metastable at the onset of the phase transition manifested by the following plateau. The area at the end of this plateau was $A_3 = 0.13$ nm^2 $molecule^{-1}$ which supported the assumption about the formation of a trilayer film in the plateau region (area ratio equals $A_3/A_1 = 3.0$). Though the LB trough used was characterized by a high compression ratio, it was impossible to reach the next layering transitions to obtain thicker stacks of **T1**.

The BAM images taken for compound **T1** and shown in **Figure 16** (**b** and **c)** were very different from those obtained for other bolaamphiphiles. At the beginning of the plateau very bright curved lines appeared. High contrast of such structures indicated significant differences in thickness of the coexisting 1- and 3-layer films. The T-shaped compound **T1** formed 3-layer film, analogous to an isolated three layers-stack of a bulk smectic A or smectic C phase (the molecules are vertical or tilted, respectively). There was no indication of any in-plane anisotropy, which supported a smectic A like structure instead of a tilted

smectic C-like structure. The unusual appearance of the thin films of compound **T1** in the BAM images might be explained in terms of high stability and rigidity of the monolayer. It underwent a first order layering transition which needed nucleation (the metastable state analogous to "overcooling" was observed as a peak before the plateau) and occurred at relatively high surface pressure. The trilayer film was formed by nucleation at some defects (dust particles) present in the film. Afterwards the wrinkles spread parallel to the barriers. The trilayer film remained fluid even despite the increased rigidity/decreased elasticity.

The T-shaped compound **T1** was transferred onto silicon wafers at 40 mN m^{-1} (monolayer) and at 53 mN m^{-1} (trilayer). The XRR profiles (**Figure 16d** and **e**) of the films were very regular. The profile of the film of expected trilayer consisted of more minima and maxima than it was observed for trilayers of X-shaped molecules. In fittings of the XRR profiles to theoretical equation,[190] a vertical orientation of the molecules was assumed. The thickness of monolayer and trilayer films calculated from XRR profiles was 2.72 nm and 7.22 nm, respectively. The ratio of these thickness values is equal to 2.65, indicating partial interdigitation of the molecular cores. An analysis of the molecular dimensions of **T1** showed that the thickness of a trilayer film corresponded to three times the length of the cores. Thus the molecules were standing vertically. The glycerol units of neighboring layers were interdigitated.

The curve of surface potential, $\Delta V(A)$, of **T1** shown in **Figure 16a** was nearly constant at the beginning of compression in a wide range of values of area per molecule. A decrease of the surface potential to negative values began at the place where the slope of $\pi(A)$ significantly changes. Such behavior of $\Delta V(A)$ indicated that the beginning of the compression occurred without significant change in orientation of those parts of the molecules which contain strong electric dipoles. Reorganization of aromatic cores occurred with detachment of one of the glycerol groups from the water surface. The stiff cores remained strongly tilted. The rapid decrease of the surface potential with simultaneous increase of the surface pressure was related to the reorganization of the side chains and aromatic cores perpendicularly to the air/water interface.

Such reorientation process was additionally confirmed by the analysis of the compressibility C_s of the $\pi(A)$ isotherm. The compressibility was unexpectedly high in the regions corresponding to the 2D gas phase and, surprisingly, also in this part of the $\Delta V(A)$ isotherm

where the surface pressure started to increase. Upon further compression (but before kink) the compressibility decreased smoothly to values typical for a 2D liquid phase.[62]

Both $\pi(A)$ and $\Delta V(A)$ curves reached the plateau at around 0.4 nm^2 $molecule^{-1}$. This confirmed the formation of trilayer film. The compensation of the dipoles in the second and third layers was complete as expected for *roll over* process.

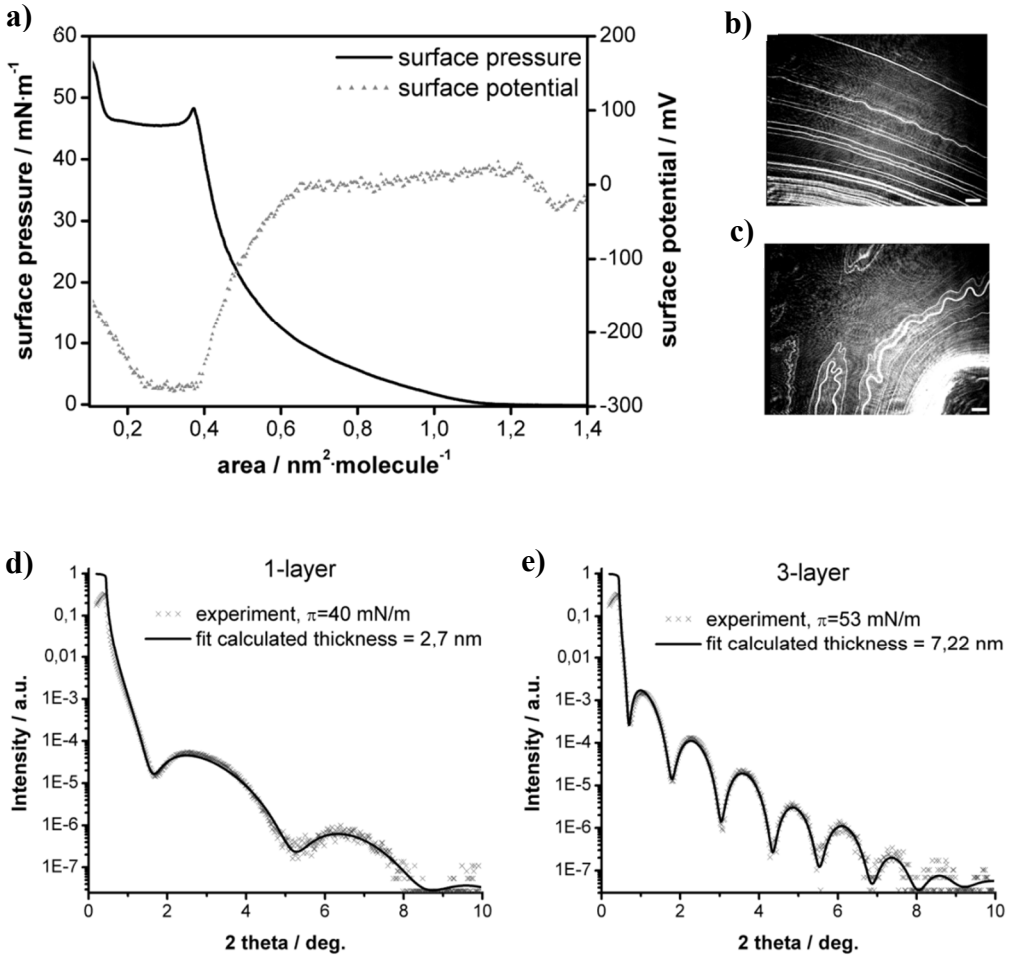

Figure 16 Results for compound **T1** (one partially fluorinated lateral chain): **a)** isotherms of surface pressure, π, and surface potential, ΔV, plotted against molecular area; small slope of $\pi(A)$ isotherm at the beginning of compression corresponds to continuous transformation from planar to vertical orientation of the molecular cores, **b)** BAM image taken at $\pi \approx 47$ $mN \cdot m^{-1}$ and $A = 0.36$ $nm^2 \cdot molecule^{-1}$ showing the wrinkles created during trilayer formation by *roll over* mechanism, **c)** BAM image taken at $\pi \approx 47$ $mN \cdot m^{-1}$ and $A = 0.17$ $nm^2 \cdot molecule^{-1}$showing an increasing number of wrinkles with very high contrast caused by a big difference of thickness. Scale bars in BAM images correspond to 500 μm, **d)** and **e)** The XRR measurements for monolayer and trilayer transferred to silicon wafers at 40 $mN \cdot m^{-1}$ and 53 $mN \cdot m^{-1}$, respectively.

3.2.1.3. Anchor-shaped bolaamphiphiles

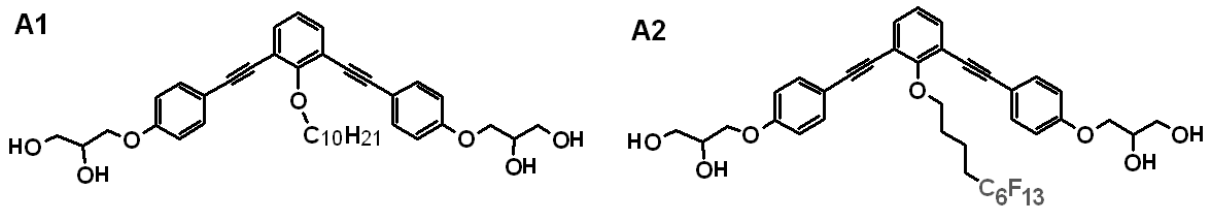

The $\pi(A)$ isotherm of the nonfluorinated compound **A1** (**Figure 17**) showed a broad plateau at low surface pressure π = 12.5 mN·m^{-1}. This indicated a low stability of the monolayer. The plateau ended with an abrupt increase of the surface pressure at an unreasonably small value of molecular area. It was an artifact coming from random and irreversible aggregation. In this case the plateau represented a simple collapse of the monolayer. Transfer of the monolayer onto silicon wafer at π = 10.0 mN·m^{-1} allowed XRR measurements. A thickness of the monolayer equal to 1.56 nm could be estimated.

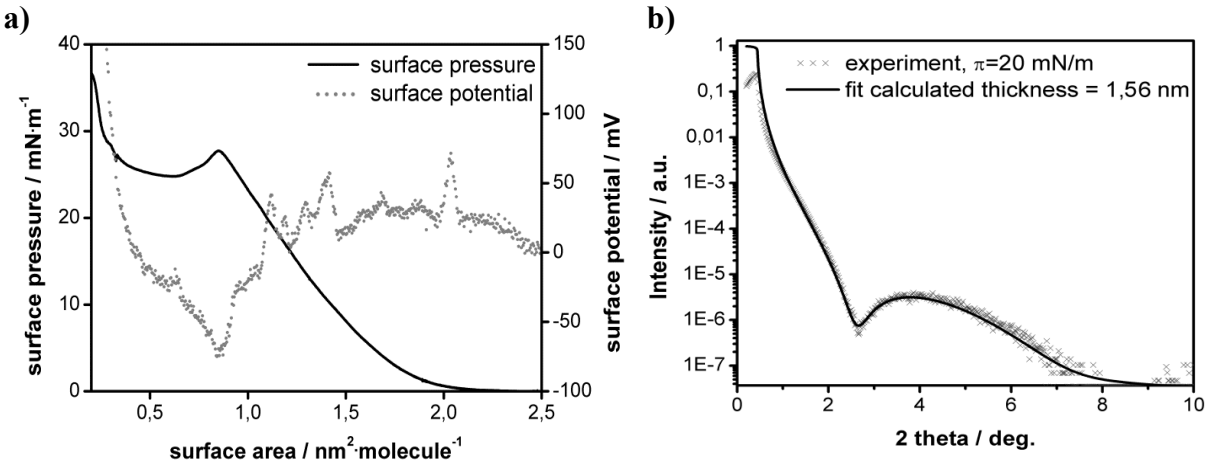

Figure 17 Results for compound **A1**: **a)** the isotherms of surface pressure and surface potential plotted against molecular area; **b)** XRR measurements for the monolayer transferred onto silicon wafer at surface pressure π = 20 mN m^{-1}. The film of **A1** was also transferred at π = 30 mN m^{-1}, where the 3-layer film was expected. In this case XRR measurements did not show any regular pattern, proving that only disordered aggregates were created in the film during compression beyond the local maximum (peak) visible on the $\pi(A)$ isotherm.

The partially fluorinated anchor-shaped compound **A2** was thoroughly investigated. The behavior of **A2** was very different when compared to fluorinated T- and X-shaped bolaamphiphiles. The results are presented in **Figure 18**. Two broad plateaus in the $\pi(A)$ isotherm of the anchor-shaped compound **A2** separated the steep parts of the compression

curve. Values of molecular areas corresponding to both ends of the first plateau at $\pi = 20$ mN·m^{-1} were 1.09 nm^{2}molecule^{-1} and 0.36 nm^{2}molecule^{-1}. Their ratio is equal to 3.02. The *A*-coordinates of the second plateau at $\pi = 33$ mN·m^{-1} were equal to 0.33 nm^{2}molecule^{-1} and 0.12 nm^{2}molecule^{-1}, giving the ratio 2.75. This analysis suggested the formation of a trilayer film by *roll over* mechanism at the first plateau and subsequent *roll over* of the trilayer film at the second plateau. As a result the 9-layer film was formed (ratio of molecular areas in monolayer and 9-layer is 1.09/0.12 = 9). The constant value of surface potential (also shown in **Figure 18a**) in both plateau regions was an additional confirmation of film folding by *roll over*. *Roll over* of well-organized monolayer and trilayer resulted in well-ordered and compensated dipole moments.

Validity of the above observation was checked by XRR measurements on the films transferred onto silicon wafers. The recorded XRR profiles are presented in **Figure 18 (e-g).** Measurements were performed on uniform films transferred after compression to proper pressures on the steep part of the $\pi(A)$ curve: 20 mN·m^{-1}, 30 mN·m^{-1} and 40 mN·m^{-1}. Assuming that the estimation of the number of layers in the films based on the estimation of molecular areas was correct, the respective thicknesses should be: d_1, $d_3 = 3d_1$, and $d_9 = 9d_1$. Obtained values were $d_1 = 1.43$ nm, $d_3 = 3.71$ nm, and $d_9 = 10.5$ nm. The average thickness of each single layer calculated from the thickness of trilayer and 9-layer is equal to $d_3/3 = 1.24$ nm and $d_9/9 = 1.17$ nm, respectively. These values, when compared to $d_1 = 1.43$ nm, showed that the layers were interdigitated. The other calculated ratios, $d_3/d_1 = 2.59$ and $d_9/d_3 = 2.83$, proved that the *double roll over* mechanism of folding of the monolayer and next, of the trilayer was observed.

Analysis of the layer thickness is carried out in the section dealing with the mechanism of layering transition. It is shown that the thickness of the monolayer, d_1, and the top layer in the multilayer is always larger than that of the other layers, so the value of d_3/d_1 is less than d_9/d_3 (verify with **Table 4** and **Table 5**).

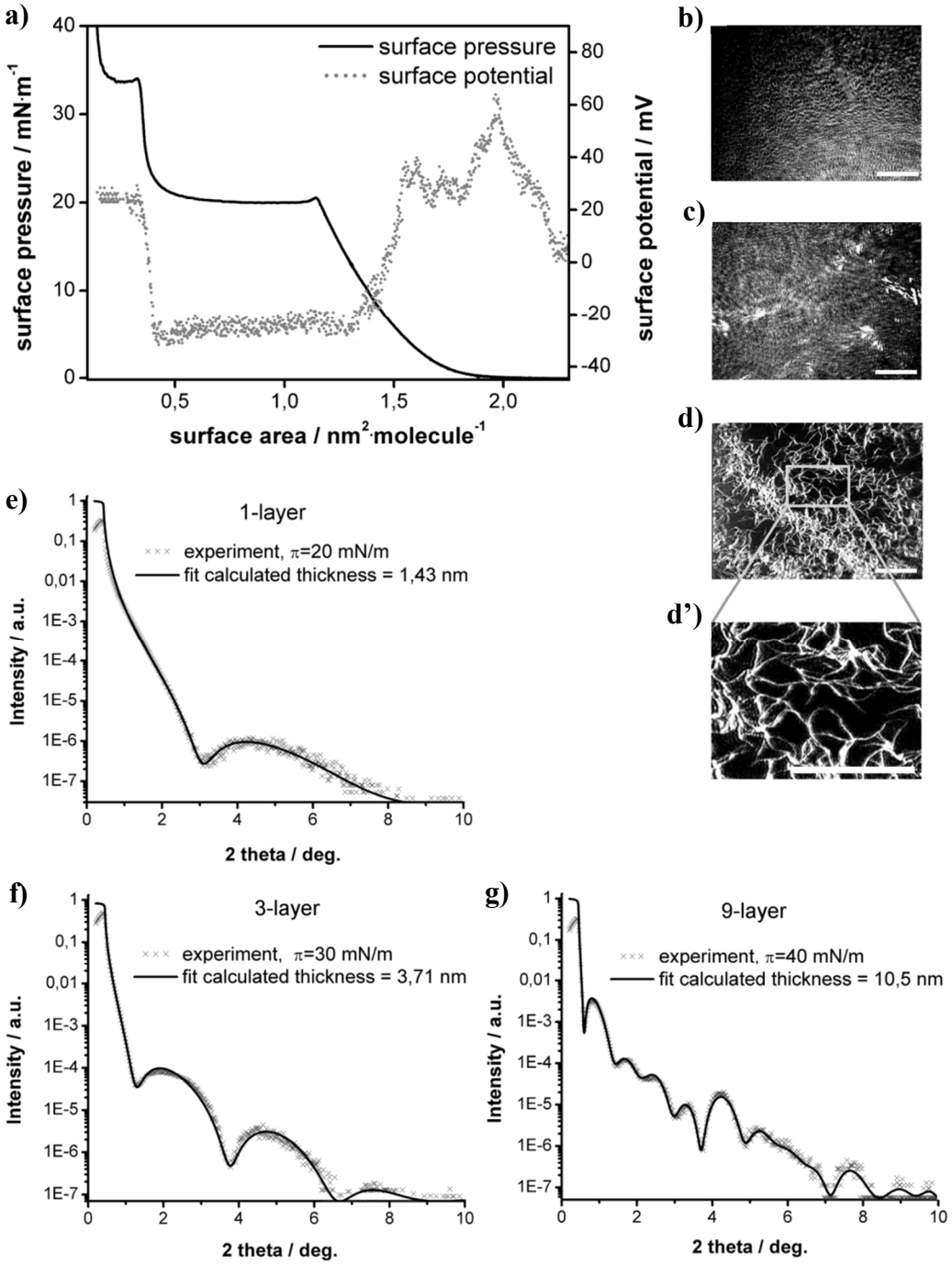

Figure 18 Results for compound **A2** (one partially fluorinated lateral chain): **a)** isotherms of surface pressure, π, and surface potential, ΔV, plotted against molecular area: **b)–d)** BAM images taken at: **b)** the beginning of the first plateau, **c)** the end of the first plateau, **d)** central part of the second plateau (fibrous domains are visible at high contrast). Scale bars in BAM images correspond to 500 μm, **e)-g)** XRR measurements for monolayer, trilayer and 9-layer films transferred to silicon wafers at 20 $mN \cdot m^{-1}$, 30 $mN \cdot m^{-1}$ and 40 $mN \cdot m^{-1}$, respectively.

The XRR profiles obtained for the 1- and 3-layers of compound **A2** were very similar to the profiles of partially fluorinated X-shaped compounds. However the profile of the 9-layer film (**Figure 18e**) differed significantly. This profile resembled very much the profiles obtained from thin free-suspended films of liquid crystals[187] in the smectic phase. In **Figure 18e** three higher peaks, corresponding to Bragg reflections, and three lower peaks between each two of the higher ones were visible. The lower peaks corresponded to typical Kiessig fringes due to the interference in the film thickness. In thin films it was hard to distinguish between Bragg reflections and Kiessig fringes. On the other hand, in the limit of infinite thickness the Kiessig fringes disappeared. The width of the Bragg signals became smaller and limited by the apparatus resolution. A relation of the number of Kiessig fringes to the number of layers was given by Hołyst.[187] The XRR profile shown in **Figure 18e** allowed determining the total thickness of the layer. The discussion presented above proved the existence of nine layers in the film of **A2** transferred at π = 40 mN·m^{-1}. The compound **A2** seems to be the first example of an amphiphilic compound for which *the double roll over* mechanism at the air/water interface was proven experimentally.

3.2.2. Comparison of XRR analysis results

Simple comparison of the numbers in **Table 4** showed that the thicknesses of the multilayers were not completely commensurate with the thickness of the monolayer for particular compounds. It supported the assumption about partial interdigitation of molecules in the multilayered films. **Table 5** presents the results of another analysis of measured thicknesses. The increments of thicknesses between trilayer and monolayer, 5- and trilayer, 7- and 5-layer were calculated and then divided by 2 to obtain an average thickness of each layer in particular bilayers. Another parameter used in the analysis was the averaged thicknesses of a single layer in the *n*-layered film calculated for each film separately. Here the thickness of the monolayer was subtracted and result divided by *n*-1. It was assumed that thickness of monolayer corresponded to the thickness of top layer in multilayer stack. The values of averaged thicknesses of a single layer of particular compounds were very consistent. This proved that the top layer in each film was the same as a corresponding monolayer. The bilayers with partial interdigitation of the molecules were really well defined.

Table 4 Thickness of the films (nm) of investigated bolaamphiphiles transferred on silicon wafers determined by means of XRR measurements; numbers of layers in the films given in top row of the table were estimated from the ratios of molecular areas at both ends of the plateau corresponding to layering transitions.

compound	1-layer	3-layer	5-layer	7-layer	9-layer
X1	1.52	4.23[a]			
X2	1.43	4.07	6.70		
X3	1.65	4.76	7.83		
X4	1.45	4.32	6.73	9.27	
T1	2.70	7.22			
A1	1.56[b]				
A2	1.43	3.71			10.5

[a] Thickness of the trilayer of nonfluorinated compound **X1** was estimated in spite of deformed XRR profile (poorly defined layers). [b] For nonfluorinated compound **A1** only monolayer could be analyzed; The film transferred on the second slope of the isotherm (above plateau) did not give any regular XRR profile proving that only disordered aggregates were created in the film during compression beyond the local maximum (peak) corresponding to the collapse of the monolayer.

Table 5 Comparison of thicknesses (nm) of the top and the single layer composed in the interdigitated layers as a proof of bilayered structure of multilayers.

	averaged thickness of one layer calculated for two neighboring layers				
compound	top layer[a]	1. and 2. layer[b]	3. and 4. layer[c]	5. and 6. layer[d]	average of *n*-1 layers[e]
X1	1.52	1.36			1.36[h]
X2	1.43	1.32	1.32		1.32
X3	1.65	1.56	1.54		1.55
X4	1.45	1.44[f]	1.21[g]	1.27	1.30
T1	2.70	2.26			2.26[h]
A1	1.56				
A2	1.43	1.14			1.13

[a] thickness of a monolayer, d_1, taken as thickness of top layer in each multilayer, [b] average thickness of a single layer in the interdigitated 1st and 2nd layers calculated as

$d_{1,2} = (d_3-d_1)/2$, [c] average thickness of a single layer in the interdigitated 3rd and 4th layers calculated as $d_{3,4} = (d_5-d_3)/2$, [d] average thickness of a single layer in interdigitated 5th and 6th layers is calculated as $d_{5,6} = (d_7-d_5)/2$, [e] average thickness of a single layer in the multilayer composed of $(n-1)/2$ interdigitated layers (n is number of the layers) calculated as $d_{1,n-1} = (d_n-d_1)/(n-1)$, [f] thickness of the trilayer in compound **X4** was probably overestimated (experimental error), so this value of $d_{1,2}$ is also overestimated and, as a consequence, the value of $d_{3,4}$ is underestimated, [g] average thickness calculated for 4 bottom layers in the 5-layer as $d_{1,4} = (d_5-d_1)/4 = 1.32$ nm, [h] in case of compounds **X1** and **T1**, in which only trilayers were detected, these values are the same as $d_{1,2}$ by definition.

3.2.3. Wetting of the deposited films

Measurements of contact angle of water droplets deposited on the films of bolaamphiphiles were performed. Possible orientations of the molecules in the upper layer of the multilayered films were analyzed. Two hypotheses were verified: 1) if the glycerol groups were exposed then the film should be hydrophilic and the water contact angle should be smaller than 90º; 2) if the upper layer consisted mainly of $-CF_3$ groups then the film should be strongly hydrophobic and the contact angle with water should be greater than 90º.

According to Israelachvili and Gee,[191] who considered the problem of "molecular roughness", it is assumed that surfaces are chemically heterogeneous and not flat on atomic level (have some roughness). Each chemical moiety present at the surface has contribution to its hydrophilic/hydrophobic properties. The influence of the distinct parts of the molecules on the contact angle is expressed as function of the nature and area occupied by the moiety of interest. Theoretical prediction can be done according to Cassie-Baxter model[192] of the surface according to the equation:

$$\cos\theta_c = \sum_i x_i \cos\theta_i \qquad \textbf{Equation 14}$$

where: x_i is the area fraction occupied by the chemical moiety of type i and θ_i is the contact angle on this fraction i of the surface. Contact angles, θ_c, for the relevant chemical moieties are collected in **Table 6**.

The exact areas occupied by the moieties of the molecules were not known. It was assumed that in a monolayer the X-shaped molecules adopt a π-conformation[179,180,181] (in a monolayer the horizontally oriented cores with both lateral chains sticking-out in the air resembled the reverse letters π). Assuming area fractions as 0.4 for glycerol and 0.6 for aromatics, and

contact angles for these parts as 15º and 86º (see **Table 6**), respectively, the contact angle $\theta_c = 65°$ was estimated from the **Equation 14**. In the monolayer a part of the aromatic cores was covered by the hydrophobic hydrogenated or fluorinated lateral chains. Therefore the contact angle should be even higher than the estimated 65º. The above mentioned protocol did not consider that water molecules could be incorporated within the glycerol units. This should result in increased area fraction of glycerol units and reduce the resulting contact angle. Also, the ether-type oxygens connecting the alkyl chains to the aromatics were not considered. This explains why for all monolayers small contact angles were measured, as shown in **Table 7.**

Table 6 Values of contact angles of relevant chemical moieties appearing in the bolaamphiphiles reported here.

	Polymer	**SAM on Au**	**SAM on Si [193]**
Glycerol		Dendritic oligoglycerol: 20.0º [194] ROH: <15° [195]	
Aromatics	PS: 87.4° [196] PS: 86° [197]		Ph: 73.9° CH_2CH_2Ph: 87.9°
R_H	PE: 96° [196] Paraffin: 108.9° [196]	$C_{10}H_{21}$: 113° [195]	98.2°
R_F	PTFE: 109.2°[196]	C_8F_{17}: 118° [195]	109.6°

Table 7 Contact angles (θ_c,) of water droplets deposited on films of investigated bolaamphiphiles transferred on silicon wafers.

compound	**1-layer**	**3-layer**	**5-layer**	**7-layer**	**9-layer**
X2	52º	72º	69º		
X3	48º	72º	73º		
X4	51º	70º	67º	75º	
T1	45º/90º[a]	89º			
A2	52º	55º			49º

[a] The monolayer of T-shaped compound **T1** was transferred to silicon wafers at two different surface pressures: at π = 15 mN·m^{-1} and π = 33 mN·m^{-1} the contact angles 45º and 90º, respectively, were measured.

Relatively small values of contact angles around 50º±2º were obtained for all monolayers of the X-shaped bolaamphiphiles. For thicker films contact angles were always close to 70º±5º, and obviously greater than for all monolayers. Such value was obtained independently of the number of layers. The contact angles for the top layer of the multilayers of X-shaped molecules were still smaller than expected for alkyl or fluorinated chains. Higher wettability of the monolayers might be explained by a stronger hydration of the glycerol moieties in the monolayers because they were in contact with bulk water. Such hydratation increased the hydrophilicity of the monolayer, also after transfer onto the solid substrates.[198] Additionally the lateral chains in the top layers were probably more tilted and covered the hydrophilic moieties of the molecular cores more than in the monolayers.

An interesting result was obtained for compound **T1**. Because of the intriguing shape of the isotherm the monolayer of this compound was transferred onto the silicon wafers at two different surface pressures: at small slope of the curve (π = 15 mN·m^{-1}) and at its steep part (π = 33 mN·m$^{-1)}$. The contact angles 45º and 90º, respectively, were measured. It proved that initially the core was horizontally oriented on the water surface and the partially fluorinated chain stuck-out into the air (similarly as in case of X-shaped compounds). The hydrophobic chain did not (or not completely) cover the hydrophilic glycerol moieties (therefore contact angle was smaller than in case of X-shaped compounds). Upon compression the molecular cores were forced to a vertical or tilted orientation (attached to the water surface at one end only). The lateral chains were approximately parallel to the cores, closely packed and also tilted. In compound **T1** the chain was significantly longer than half of the aromatic core. The lateral chain (with –CF_3 group at the end) was exposed above the glycerol moiety of vertically oriented core. Hence the hydrophobic chains covered the hydrophilic glycerol groups. It led to contact angle equal to 90° (hydrophobic surface).

The same contact angle (within experimental error) as for the closely packed monolayer was obtained for the trilayer of **T1**. This supported the *roll over* mechanism. There was no difference in character of the top layer between mono- and trilayer during this type of layering transition. In this mechanism the top layer of the multilayered film was the same as in the monolayer (verify with **Figure 19** in next section). Therefore the fluorinated chains of the T-shaped compound **T1** represented a main component of the hydrophobic top sublayer in both, mono- and trilayer.

The anchor-shaped compound **A2** exhibited a contact angle around 50º for the monolayer. Similar angles were measured for X-shaped compounds in monolayers, only. For thicker layers of X-shaped molecules this angle was greater. This suggested that the multilayers are less hydrophilic than the monolayer. For compound **A2** the contact angle was approximately the same for 1-, 3-, and 9-layered films. The values of contact angle 50º±2º indicated some degree of hydrophilicity. There was always a bonding of water molecules to the glycerol moieties on top of the layers. Only one side chain did not cover the hydrophilic glycerol unit to the same extent as in case of X-shaped compounds. This strongly supported the proposed *roll over* mechanism without reorganization of the molecules. There was not (and it should not be) any change in the hydrophilic character of the monolayer and the top layers of the multilayers created by *roll over*.

3.2.4. Mechanisms of layering transitions

The $\pi(A)$ isotherms and XRR analysis of transferred films provided solid evidence that multilayer stacks were formed during compression of thin films of partially fluorinated bolaamphiphiles. 1-, 3-, 5- and in one case 7-layer stacks were formed in case of the X-shaped compounds **X2** - **X4** and 1-, 3- and 9-layers for the anchor shaped compound **A2** (**Table 4**). In this section a new insight into the mechanisms of the formation of distinct multilayered films at the air/water interface and their layering transitions is demonstrated. Two mechanisms are explained here *i.e.* lifting and permeation of the molecules (**Figure 19a**), and *double roll over* (**Figure 19b**).

Disordered collapse was found if the films were either completely fluid (*e.g.* amphiphiles with branched alkyl chains) or too rigid (crystalline). It appeared that chaotic collapse could be avoided by a well-balanced relation between order and mobility of the molecules. Hence monolayer-to-multilayer transition was often observed in thin films of molecules combining rigid and flexible elements *e.g.* liquid crystalline compounds. For the described molecules this combination of order and mobility was provided by the combination of rigid aromatic units with hydrocarbon and semi-perfluorinated chains. The mismatch of cross sectional area of fluorinated segments R_F and hydrocarbon spacers R_H led to the required fluidity. This was against intuition, since fluorination made the chains stiffer.

The well-defined multilayers were odd numbered as only in this case the dissymmetry of the layers was retained. The more hydrophilic parts of the molecules in the first layer were

exposed to the water surface. The hydrophobic parts of the molecules in the top layer were exposed to air. This explained why the trilayers existed as a preferred configuration after an "ordered" (reversible) collapse of the monolayer, eventually followed by formation of 5-layers, 7-layers etc. Bilayers, in which either the polar groups or the lipophilic groups had to be exposed to both, the water surface and the air, have been rather scarce.[199,200,201] The molecules of very specific structure, like calixarenes,[199] were reported as self-assembling to bilayer structures at the air/water interface. Stable bilayers on water surface could be formed by lipids,[200] which were also able to create vesicles and membranes in bulk water. Similarly, the mixtures of phospholipids and cholesterol derivatives were able to form mixed bilayers at air/water interface.[201]

The properties of monolayers (like rigidity and viscosity), as well as a interactions in three dimensions were the key factor deciding whether a bilayer, a trilayer or 3D aggregates were created during compression. The *roll over* mechanism was also proposed by de Mul and Mann[121] to explain a trilayer formation in liquid crystalline cyanobiphenyl derivative **8CB**. The authors presented BAM images with circular domains of a trilayer in coexistence with a monolayer. The mechanism of *double roll over* leading to a 9-layered film created by folding of the trilayer was proposed (see Figure 4 in ref. 121). The existence of a 9-layer film was not proved by experimental methods.

It seems that the first convincing example of formation of a trilayer and next of a 9-layer by *double roll over* is presented here in case of compound **A2**. The main difference between the case of **A2** and the case of **8CB** was the appearance of BAM images. The circular domains were not seen for films of **A2**, but the fibrous domains *i.e.* the wrinkles in the film (**Figure 18d**). Another case of trilayer formation (compound **T1**) was presented in **Figure 16** (images **b** and **c**). Here also the wrinkles caused by folding of the monolayer and following *roll over* were perfectly visible in BAM pictures. The mechanism of trilayer formation might be therefore different in **8CB** and in **A2** or **T1**.

The liquid crystals from the group of cyanobiphenyls have a strong tendency for pairing.[202] The pairs of molecules are present even in their bulk phases. The smectic A_d phase of cyanobiphenyls has a periodicity ranging from $1.3 \cdot l$ to $1.7 \cdot l$ (l is the length of the molecule). Each layer consists of associated pairs of partially overlapping anti-parallel molecules.[124,202] In a monolayer at air/water interface a strong interactions of polar cyano- group with water stabilize the monolayer of single molecules. During compression the molecules are

pushed-out of the interface. The lateral interactions between biphenyls occur to be weaker than the interactions of –CN with the π-electrons of the phenyl ring, which favor the association process. During collapse of the monolayer the molecules are removed from the interface and immediately associate into anti-parallel pairs. Bilayer on top of a monolayer is created. Further compression of the trilayer of cyanobiphenyls leads to 5-layer formation, as it was proved by ellipsometry and SHG.[104] Similar behavior leading to formation of odd numbers of layers only was observed by de Garcia Lux *et al.*[170] in case of partially fluorinated alkanes (diblock molecules). Surprisingly, these non-polar compounds, called "primitive surfactants",[203] are able to create monolayers at the air/water interface. According to the hypothesis of El Abed *et al.*[204] a monolayer of diblock partially fluorinated alkanes on the water surface is built of anti-parallel molecules. In the papers from the group of M. P. Krafft[169b,170,174] a mechanism different from the *roll over* type leading to formation of odd numbers of layers (1, 3, 5, and so on) is proposed. First, the bilayer of associated pairs is created on top of the monolayer (trilayer is formed at this stage). Next the bilayer only is sliding over the monolayer, bending and winding-up to create the 5-layer (see Figure 16 in ref. 170). This mechanism would leave the bottom layer unchanged. This is unlikely, because during compression of Langmuir films a simultaneous compression of all layers takes place. At each infinitesimal step of compression the same number of molecules has to be removed from each bottom layer to the next subsequent upper layer. This problem does not arise during a *roll over* mechanism.

The *roll over* mechanism allows only for creation of the sequence 1, 3, and 9 layers (as proved for compound **A2** and shown schematically in **Figure 19b**), but not of 5- and 7-layers (as in case X-shaped bolaamphiphiles). 1-, 3-, 5-, and 7-layered films in X-shaped bolaamphiphiles were observed. The system had to be in a LC state with a thermodynamically stable smectic (lamellar) organization. Thin LC films could be compressed in the direction parallel to the layers with expansion in the perpendicular direction (and vice versa). In the very thin films on the water surface this took place in a well-defined stepwise manner. A probable mechanism of multilayer formation in which the number of layers is stepwise increasing by 2 is shown schematically in **Figure 19a**. When the monolayer of molecules in reverse π-conformation was compressed to maximum, the molecules were forced to "escape into the third dimension". They created pairs with "back-to-back" organization of the aromatic cores (**Chapter 3.1**). On further compression of the X-shaped bolaamphiphiles, after the available area was completely covered with a trilayer, the next bilayer was formed. The

formation of the second and following bilayers (leading to 5-layer, 7-layer etc.) took place during simultaneous compression of all previously formed layers. Therefore some molecules from each previously formed lower layer had to move to the next upper and the top layers during compression. This allowed the creation of thicker films in the shape of circular islands, as observed for liquid crystals.[121,122] This process always takes place if the layers have a sufficient fluidity. Also the barrier for the jumping from one layer to the next should be sufficiently low. If these requirements are not fulfilled other reorganization processes can become more favorable. This was the case of compound **A2**, where a *roll over* process took place. In line with this, elongated wrinkles were observed in the BAM images instead of the circular domains. This indicates an increased layer rigidity, though the layers were still fluid.

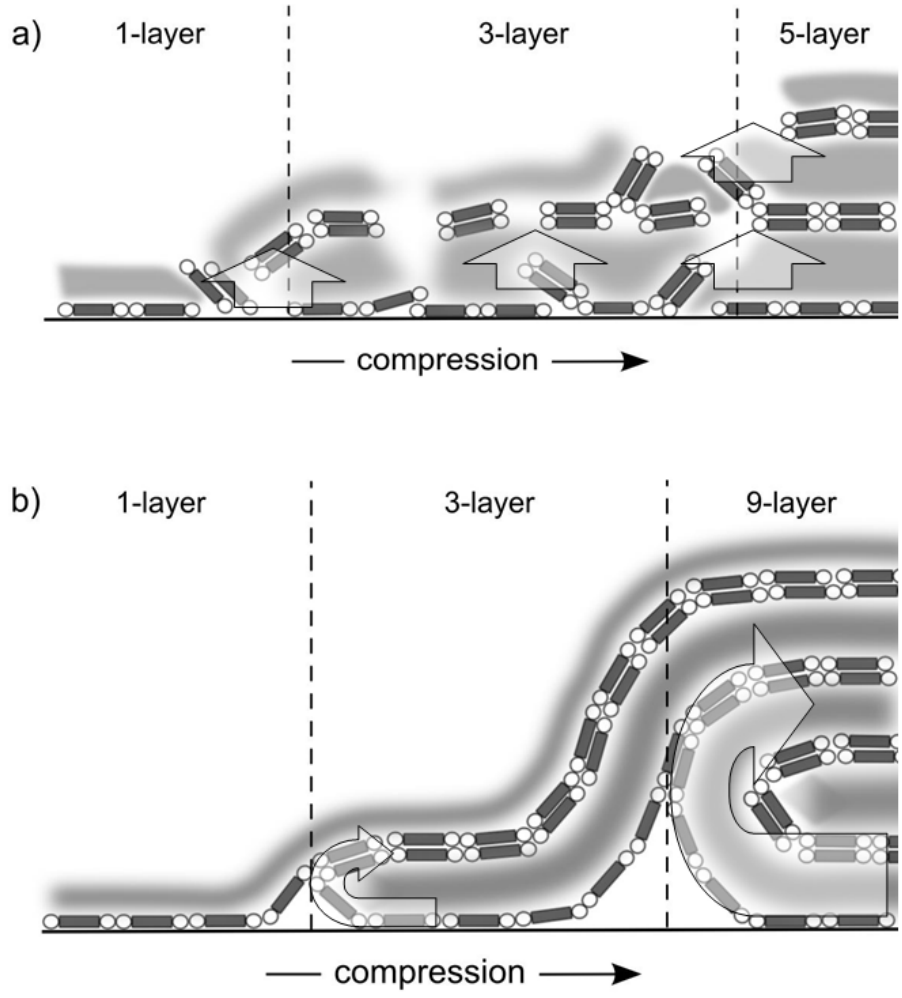

Figure 19 Schematic presentation of two versions of possible mechanism allowing formation of odd numbers of layers with different sequence of thicknesses: dark gray = rigid aromatic cores (simplified); white circles = polar glycerol groups; light gray = regions of semi-perfluorinated chains and alkyl chains; **a)** example of X-shaped molecules exhibiting

a creation of the tri- and 5-layered films during compression of the monolayer by permeation mechanism with simultaneous "back-to-back" pairing of the molecules, **b)** *double roll over* of the monolayer of compound **A2** - the trilayer and next the 9-layer are formed during compression.

Hence, BAM images give a first indication of the type of layering transition. Accordingly, circular domains appear to be typical for the layering transitions in fluid films, leading to the sequence 1- 3-, 5,- 7-…. layers upon compression. These films are in thermodynamic equilibrium. Hence, these transitions (and the corresponding $\pi(A)$ isotherms) are reversible. *Roll over* can only take place under special conditions; if monolayers and odd-numbered (2n+1) multilayers are not in equilibrium. In this case the structure of the multilayer film is determined by the mechanism of its formation. The BAM images do not show fluid circular domains, but instead elongated wrinkles. Confirmation of a *roll over* mechanism is provided by the sequence of 1-, 3-, and 9- layers of **A2** upon compression. However, it is questionable if further compression could possibly lead to 27-layer films. The stiffness of 9-layer film is expected to lead to a complete collapse, instead.

3.2.5. Multiple transfers of monolayers/multilayers

The defined multilayers obtained by compression of monolayers were quantitatively transferred onto silicon substrates by the LB technique. However it was not possible to obtain multilayered structures by consecutive transfer of the monolayers. The monolayer deposited during up-stroke was always flushed out during down-stroke. It was possible to obtain thick films (even 30-layered film) by consecutive deposition of multilayers. This might be caused by the rigidity of such thicker films. The fact that multilayers, in contrast to monolayers, were not easily removed from the solid substrate during down-stroke can be explained by the wettability difference between monolayer and multilayer. All linear bolaamphiphiles (except the bent compound **A2**) exhibited larger contact angle on the top surface of the multilayer, than on the monolayer, *i.e.* multilayer had a less hydrophilic surface. This multiple transfer of well-defined multilayers onto solid substrates opens new possibility for preparation of functional surfaces.

3.2.6. Conclusions

The unique feature of partially fluorinated bolaamphiphiles was that the compression of their Langmuir films led to formation of stable and well defined multilayered structures. All

fluorinated X-shaped compounds exhibited similar behavior with small differences depending on the degree of fluorination. Compounds **X2** and **X3** with only one perfluorinated chain and a second alkyl chain created 3- and 5-layers. The more symmetric compound **X4** with two perfluorinated chains could be compressed even to a 7-layer film. The T-shaped compound, **T1**, with only one fluorinated chain showed very distinct behavior. It created a trilayer after preceding tilt of the molecular core to vertical/tilted position. In case of the anchor-shaped molecule **A2**, 1-, 3-, and 9-layer films were created in the sequence. In two compounds, **X1** and **A1**, which were not fluorinated, only poorly organized monolayer and trilayer (**X1**) or only monolayer (**A1**) were found.

The 3-, 5-, 7- and 9-layer films, created by compression of a monolayer, were transferred onto solid substrates in a one-step procedure. Such prepared films were afterwards analyzed using XRR technique and by measurements of water contact angle. Analysis of these results definitely confirmed the findings concluded from Langmuir isotherms, surface potential measurements and BAM images.

These studies lead to an improved general understanding of layering transitions in Langmuir films. Accordingly, trilayer formation is usually observed during compression of monolayers if a disordered collapse does not take place. Trilayers represent the first step in layering transitions of liquid crystalline films. By subsequent formation of additional bilayers on top of the existing layer(s) thicker odd-numbered films (5-layers, 7-layers, etc.) are formed. If such layering transitions take place under thermodynamic equilibrium conditions, the BAM images are characterized by the appearance and growth of circular domains with uniform thickness. Such structures finally coalesce to the next uniform bilayer on top of the existing layer(s). However, neither the formation of such trilayers nor the observation of these circular domains can be regarded as a firm proof of a *roll over* process, as proposed in ref. 121. Only in cases where a sequence of 1-, 3- and 9-layers is observed during compression, as reported here for compound **A2**, one can be sure that the layering transition must occur via a *double roll over mechanism*. However, this type of layering transition is rare and seems to be only possible under special circumstances. Compound **A2** provides the first experimental evidence. The typical BAM images of such transitions are characterized by elongated wrinkles which can be regarded as a first hint on a *roll over* process. This also leads to the conclusion that observation of circular domains during compression excludes a *roll over* mechanism.

3.3. Drop Casting

Direct self-assembly on the solid substrate has been reported as an efficient method for obtaining complex structures from specially designed molecules.[205] The preparation of desired structures as a result noncovalent self-assembly is promising for fabrication of novel materials. The main problem is that very often random, disordered aggregation takes place instead of the self-assembly. The outcome of the self-assembly process should depend mostly on the properties of the molecules. However, there is no clear answer, which parameters are crucial nor how can the dependence be described. Such knowledge is necessary to properly design the molecular structure desired for self-assembly and enabling a formation of functional complex materials.

Aiming to make a contribution to the subject, the unique behavior of molecules from the group of partially fluorinated bolaamphiphiles was examined.[148,149] Also compounds of simpler structure were studied for comparison. Studied bolaamphiphiles revealed an unusual tendency for self-organization into ordered stacks directly on the silicon wafers and at the air/water interface. No initial compression was needed. Simple drop casting resulted in trilayer films formation of similar quality as in case of LB.

3.3.1. Results

The methodology described in **Chapter 2.2.2** was used to prepare films according to very simple drop casting procedure. Three distinct surface coverage protocols were compared in this chapter: 1) Lagmuir-Blodgett (LB) and 2) drop casting onto water and 3) silicon surface (**Figure 20**). Parameter L (see **Equation 9**) corresponded to the number of molecular layers, that a) was established based on the $\pi(A)$ isotherms in case of LB films, b) was calculated for drop casting of the films. In case of DC number L did not always equal number of ordered layers of molecules in the films. In such case it simply stated how much molecules were casted onto the surface.

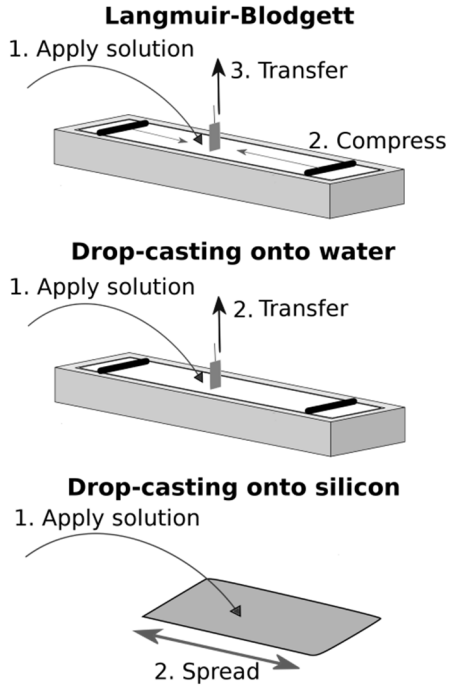

Figure 20 Cartoon showing three used approaches of thin films preparation.

XRR patterns of drop casted samples were compared with these obtained via Langmuir-Blodgett method. In most cases small differences were observed. The general shape of XRR patterns of corresponding samples obtained by different methods was preserved. The minima of XRR patterns were slightly shifted towards higher values of 2θ angle for DC samples. Such shift corresponded to small decrease of the film thickness. There was no external force applied in DC method, which could impose formation of densely packed structures. Therefore the resultant structures were looser, molecules were tilted and films were slightly thinner in comparison with samples prepared via LB method. Such tendency was noticeable for all studied compounds, both fluorinated and nonfluorinated. The quality of the films obtained with use of different methods was compared by means of roughness, obtained as an XRR fitting parameter.

3.3.1.1. X-shaped bolaamphiphiles

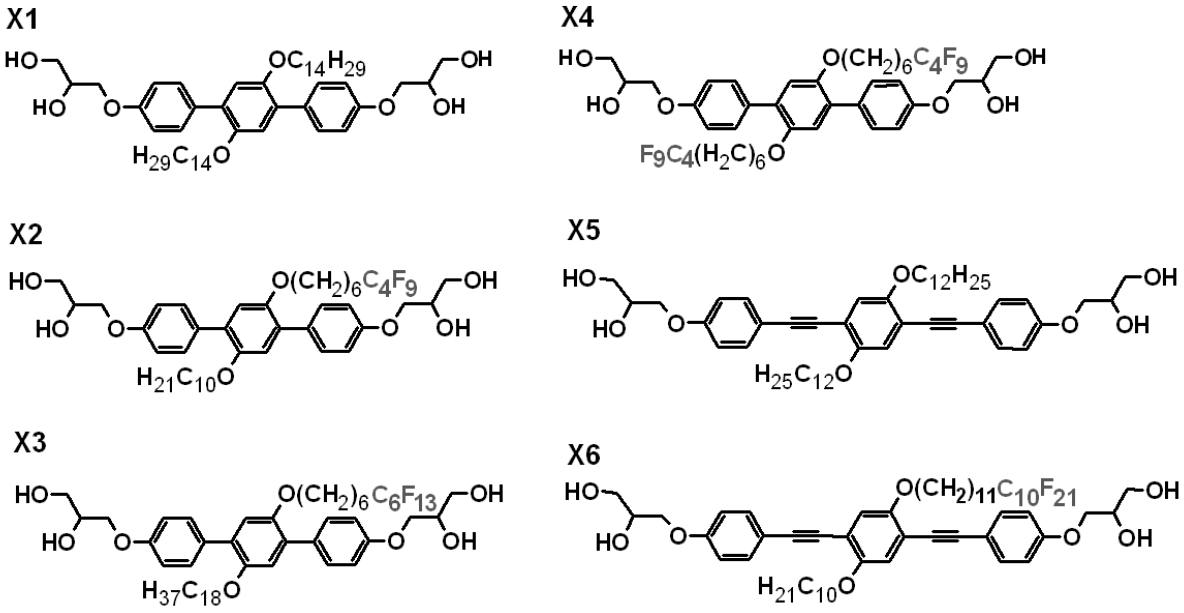

Values of thickness of films formed by the LB and the DC on the water and silicon surfaces are compared in **Table 8** at the end of the chapter.

Nonfluorinated compounds **X1** and **X5** formed stable monolayer films both in LB and DC experiments. Results of XRR measurements of films of **X1** are presented in **Figure 21a** (**X5** is not shown). Thicknesses of monolayer films of **X1** obtained by LB method and by DC onto the water surface were around 1.5 nm and 1.3 nm, respectively.[187] The electron density profile, used in the XRR fitting procedure, confirmed the reverse π orientation of the molecules. The cores were lying flat on the water surface with lateral chains pointing towards the air (both in LB and DC on water).

Surprisingly, films of compound **X1** prepared via DC on silicon differed significantly from these presented above. The thickness of the obtained layer was around 2.3 nm. This value corresponded to the length of the core of the **X1** molecule. Fitting of XRR profiles confirmed, that the cores in the monolayer drop casted onto silicon were not parallel to the surface, but oriented perpendicularly. The explanation for that might originate in competitive interactions between cores of the molecules and the surface. The Lam-like monolayer (cores parallel to the surface) was formed when interactions between glycerol moieties and hydrophilic interface were favorable. The smectic C-like monolayer (cores aligned perpendicularly to the surface) was formed in case of stronger interactions between the molecules due to the π-π stacking.

The surface of silicon was not hydrophilic enough (two week interactions with glycerol domains) for **X1** molecules to prefer the parallel alignment as opposite to the surface of water.

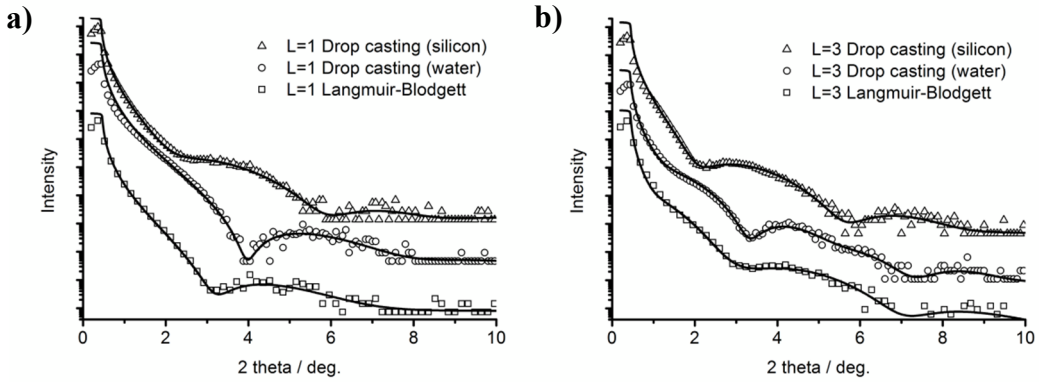

Figure 21 Comparison of XRR profiles of **a)** $L = 1$ and **b)** $L = 3$ films of compound **X1** prepared with use of various methods. In case of LB experiments L stands for the number of molecular layers. It was estimated from the ratios of molecular areas at both ends of the plateaus on $\pi(A)$ curves. In case of DC experiments it was equal to the number of demanded molecular layers calculated according to **Equation 9** from the amount of solution casted on the known area of water or solid surface.

Trilayer stack of **X1** was also observed upon DC onto the water surface. However, the layers within the film were poorly defined. Similar behavior was observed in case of LB films of **X1 (**see **Chapter 3.2.1.1**). The thicknesses (around 4.2 nm) were only roughly estimated due to deformed XRR patterns without any well pronounced minima. DC of film of $L = 3$ of **X1** onto silicon gave smectic C-like monolayer only (d_3 = 2.34 nm). In case of **X5** only monolayers were observed irrespective of the film preparation procedure (d_1 around 1.4 nm). When the amounts of solution sufficient to form multilayers were drop casted, aggregates preserving no specific order were formed. This is in line with LB experiments, which revealed collapse of film of **X5** to a disordered state.

More interesting results were obtained for X-shaped molecules containing partially fluorinated lateral chains (compounds **X2**, **X3**, and **X4**). When the amounts of solutions used for drop casting were sufficient only for monomolecular coverage ($L = 1$), monolayer films were indeed formed. The orientation of the molecules was the same as in case of LB films (reverse π orientation). Irrespective of surface type (silicon or water) the cores were lying flat and side chains were oriented perpendicularly to the surface (see **Table 8**). The different behavior of fluorinated and nonfluorinated compounds drop casted onto silicon originated in

the enhanced amphiphilicity of fluorinated compounds. Increased hydrophobicity of the side chains due to fluorination resulted in increased general amphiphilicity of molecule. In case of fluorinated X-shaped compounds the interactions with the silicon were sufficient to induce parallel alignment and to overcome the intermolecular interactions. The amount of solution sufficient for obtaining a trilayer ($L = 3$) was drop casted both onto water and silicon surface. XRR revealed films of thickness matching perfectly the trilayer stacks ($d_3 \approx 3d_1$). The recorded patterns corresponded to the stacks of predicted thickness (around 4 nm for **X2** and 4.3 nm for **X4**), with well-defined layered structure. The XRR patterns of trilayer films were fitted with use of the same electron density profiles as in a case of LB films (see **Figure 11** and discussion in **Chapter 3.1**). This proved that the alignment of the molecules of partially fluorinated X-shaped bolaamphiphiles was identical irrespective of preparation method.

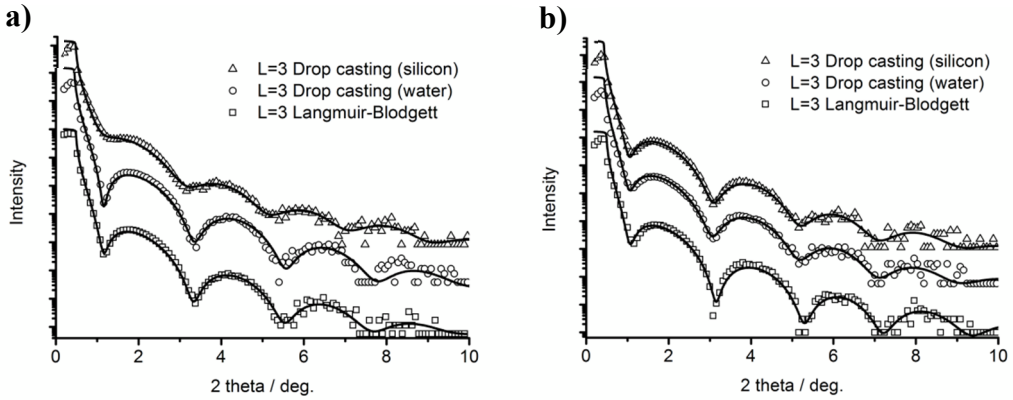

Figure 22 Comparison of XRR patterns of trilayer films obtained via Langmuir-Blodgett deposition and drop casting of compounds **a) X2**, **b) X4**.

XRR patterns of films of partially fluorinated compounds **X2-X4** had much more clearly visible minima (see **Figure 22** for **X2** and **X4** and **Figure 26** for **X3**) than in case of nonfluorinated compound **X1**. This indicated small roughness of these films. The fitting provided values of roughness below 0.5 nm for **X2-X4** and more than 1 nm for X**1**.

There was no significant difference in structure of trilayer films ($L = 3$) of **X2** and **X4** obtained with use of LB and DC methods. Covering the surface with **X2** and **X4** to form 5-layer stacks ($L = 5$) gave unexpected results. Applying more molecules of compound **X4** than necessary for trilayer stack ($L>3$), up to $L = 7$, did not change the general shape of XRR pattern (see **Figure 23b** and **Figure 25b**). Only small shifts of minima towards lower 2θ angle values were observed. The fitted values of thickness of the films varied moderately, *i.e.* from 4.25 nm ($L = 3$) to 4.30 nm ($L = 7$). In case of compound **X2** drop casted on the water surface

for $L = 5$, a highly deformed pattern was recorded (see **Figure 23a**). Such film was much more distorted comparing to one obtained via Langmuir-Blodgett method, while trilayer films ($L = 3$) were of very similar quality. The explanation might be as follow. Compound **X2** (one fluorinated chain) was more flexible than compound **X4** (two fluorinated chains). Therefore it was possible for the **X2** molecules to adjust to form thicker stacks. The obtained deformed pattern might be in fact a superposition of signals from trilayer and other, thicker stacks. Still **X2** was more rigid than **X1**, so the formed trilayer stacks were relatively stable and did not collapse into disordered aggregates. Compound **X4** formed well-ordered trilayer films in drop casting. The stiffness of both fluorinated chains prevented self-assembly into thicker stacks (L>3). Such conclusion is in a good agreement with previous observations: **X2** presented enhanced reversibility and reproducibility over **X4** (more flexible molecules could better adjust during the dynamic process); whereas **X4** formed thicker multilayer stacks upon compression (stiffer molecules were better building blocks for thicker films in LB).

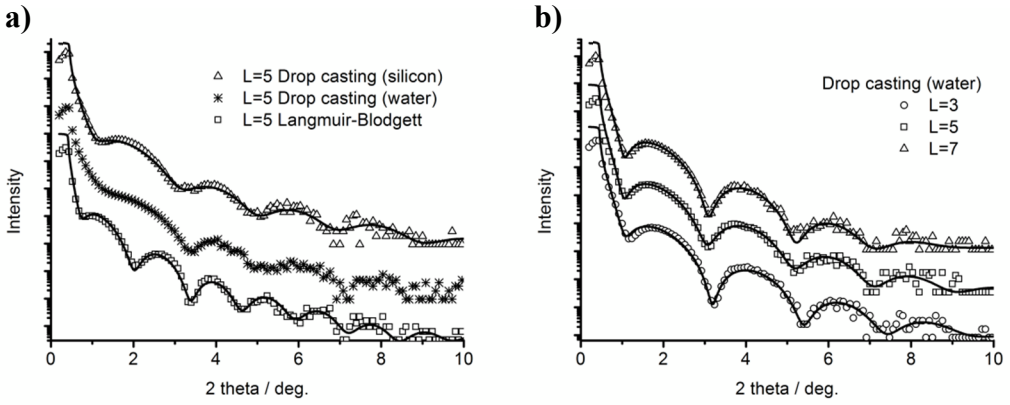

Figure 23 a) Comparison of XRR patterns of films obtained via Langmuir-Blodgett and drop casting method of compound **X2**, **b)** XRR patterns of films of compound **X4** drop casted onto water surface and transferred onto silicon surface. The number L corresponded to the expected number of casted layers in DC or was estimated from isotherms in LB experiments.

The constant value of thickness (around 4.3 nm) of the films of $L = 3$, $L = 5$ and $L = 7$ of compound **X4** raised the question concerning the alignment of the excessive molecules in L>3 films. Compound **X2** behaved similarly when drop casted onto a silicon wafer (**Figure 25**). The formation of trilayer was confirmed by XRR for L = 3 to L = 7. Excessive molecules should be somehow stockpiled on top of the trilayer. Why they were not detected in XRR measurements? AFM was employed to solve this apparent paradox. **Figure 24** shows the AFM images of L = 7 films of **X4** obtained with use of **a)** LB (transferred at 55 mN m^{-1}) and **b)** DC onto the water surface. The roughness of a 7-layer film obtained via LB was of the

order of 1 nm. This value was in a good agreement with data obtained from fitting of the XRR profile. In case of film $L = 7$ prepared by means of DC only an ordered trilayer was formed (confirmed by XRR). The excessive molecules formed random, disordered aggregates on top of the trilayer film. Such structures were randomly located and covered only a minor part of the area; they were not detected by the XRR method. Elongated shapes of the aggregates indicated presence of a columnar phase as in bulk. The trilayer was formed spontaneously, independently of the excess of molecules applied on top of it.

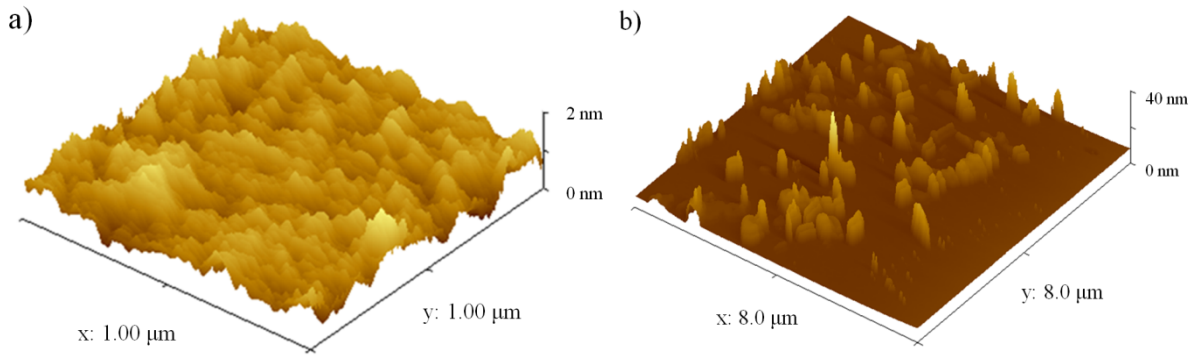

Figure 24 AFM pictures of films of $L = 7$ of compound **X4** obtained with use of **a)** LB, **b)** DC methods. One should notice different z scales.

5-layer and 7-layer films were not formed during DC directly onto the silicon surface. This fact needs additional explanation. In case of drop casting of **X2** on water it was claimed that thicker stack could be formed. The surface of water was more appropriate for the self-assembly of thin films comparing to silicon. Water surface was more hydrophilic and interacted stronger with glycerol units of the bolaamphiphiles. Moreover, it fluctuated; if aggregates appeared they could be reassembled.

A proper amount of solution of **X2**, sufficient only for two molecular layers, $L = 2$, was spread on the surface of silicon. Subsequent XRR measurements indicated formation of the trilayer film. No changes of general shape of XRR patterns for $L = 2$ to $L = 7$ was observed for **X2**, as depicted in **Figure 25**. The value of thickness of these films was nearly constant (around 4 nm). This showed that the formation of the trilayer was energetically favorable. The molecules aligned as trilayer stacks, even if there were neighboring patches of film of only monomolecular thickness. This was in line with description of the process of formation of multilayers in Langmuir experiments presented in **Chapter 3.1** and **3.2**.

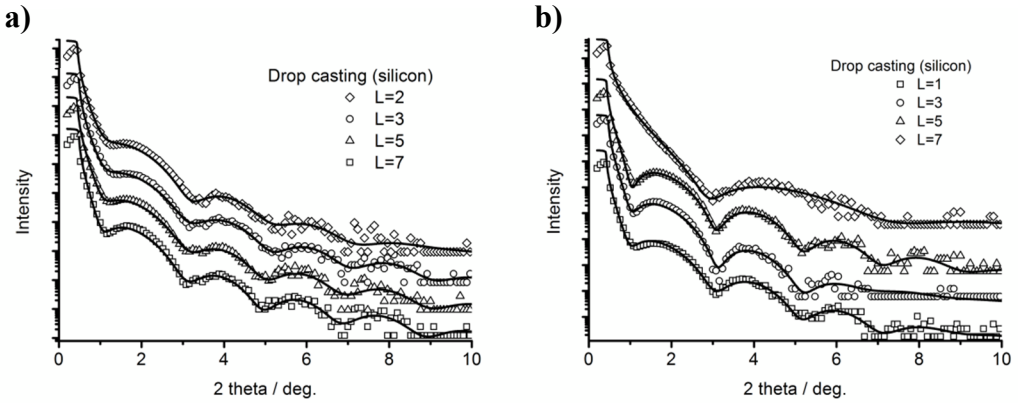

Figure 25 Results of XRR measurements of films of compounds **a) X2** and **b) X4** drop casted directly onto a silicon wafer. *L* stands for the calculated number of layers casted. In range of *L* = 2 to *L* = 7 the XRR patterns always corresponded only to ordered trilayer film.

Compounds **X3** and **X6** contained two chains of different length. These compounds were studied as examples of X-shaped bolaamphiphiles with lower symmetry. In the LB experiments compound **X3** formed 3- and 5-layer films (see **Chapter 3.2.1.1**). The compound **X6** was not discussed in previous chapter, since no multilayers were found during Langmuir experiments. The behavior of **X6** was determined by the molecular structure. Fluorinated chain of **X6** was twice as long as the hydrocarbon chain. This asymmetry made the **X6** similar to T-shaped compounds. During compression one of the glycerol moieties detached from the water surface and the core of the molecule became perpendicular (or slightly tilted) to the surface of water. In case of **X3** the differences in length of chains were not as pronounced. Therefore the symmetry was preserved and **X3** behaved similarly as other X-shaped compounds.

Compound **X3** formed well defined mono- and trilayer films in DC experiments (**Figure 26**). A thicker film was observed only when drop casted onto the water surface (*L*=5). This was in good agreement with results obtained for **X2** (both **X2** and **X3** have only one fluorinated chain). This observation additionally justified the assumption of formation of 5-layer films in DC experiments in case of X-shaped compounds with only one partially fluorinated chain. Surprisingly, the film obtained via DC onto the water surface had smaller surface roughness comparing to LB method. In case of direct drop casting onto a silicon wafer, the XRR pattern was distorted and poorly developed.

In case of compound **X6** both Lam-like monolayer (with cores lying flat on the surface) and smectic C-like monolayer (with cores perpendicular to the surface) were prepared via DC

(**Figure 27**). Multilayer stacks were not observed. This was in agreement with LB experiments. Only in case of DC onto silicon unexpected behavior of compound **X6** was found. Smectic C-like monolayer was formed even when there was enough space to form a Lam-like monolayer. As mentioned previously this was caused by the fact that the lack of symmetry made the **X6** behave as a T-shape compounds (see following chapter). Such behavior was also similar to **X1** drop casted onto a silicon wafer (stronger interactions between cores than cores and surface).

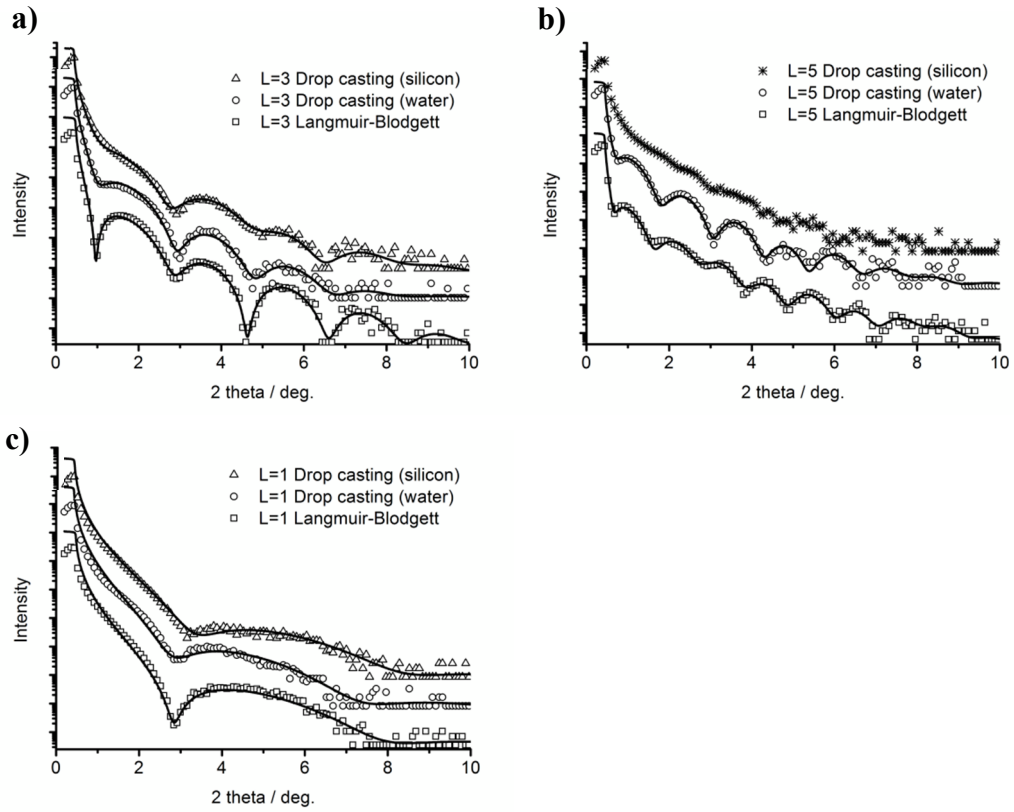

Figure 26 Comparison of XRR patterns of films of compound **X3** prepared via LB and DC. **a)** $L = 3$, **b)** $L = 5$, **c)** $L = 1$.

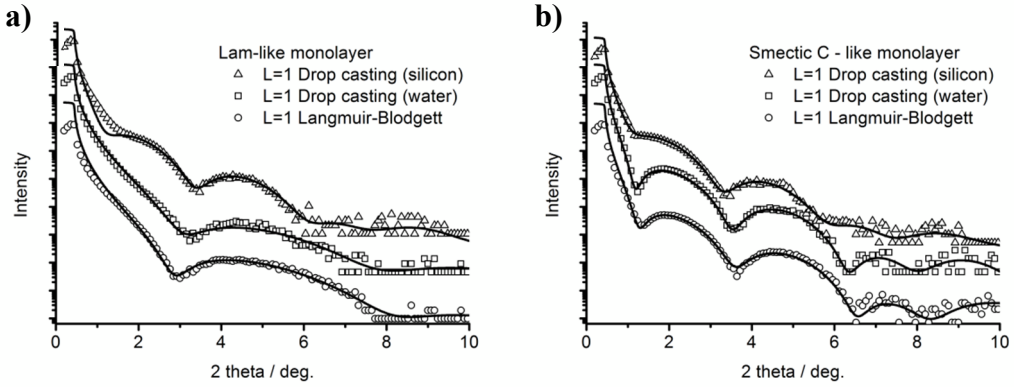

Figure 27 Comparison of XRR of the films of compound **X6** when amounts of solution applied corresponded to **a)** Lam-like monolayer and **b)** smectic C-like monolayer.

Table 8 Thicknesses of films (nm) of X-shaped bolaamphiphiles prepared with use of LB and DC methods determined by means of XRR measurements. Number of layers in the films given in the top row of the table was estimated from the ratios of molecular areas at both ends of the plateaus corresponding to layering transitions upon compression in Langmuir experiments, whereas in DC experiments the number of layer of prepared films was controlled by application of precisely calculated amounts of chloroform solutions.

compound	method	1-layer	3-layer	5-layer	7-layer
X1	LB	1.52	4.23[a]		
	DC H_2O	1.27	4.10[a]		
	DC Si	2.28	2.34		
X2	LB	1.43	4.07	6.70	
	DC H_2O	1.38	3.97		
	DC Si	1.36	4.15	4.15	4.17
X3	LB	1.65	4.76	7.83	
	DC H_2O	1.61	4.55	7.28	
	DC Si	1.52	4.52		
X4	LB	1.45	4.32	6.73	9.27
	DC H_2O	1.42	4.29	4.32	4.35
	DC Si	1.34	4.25	4.27	4.3
X5	LB	1.42[a]			
	DC H_2O	1.40[a]			
	DC Si	1.37[a]			
X6	LB	1.57[b]/ 3.51[c]			
	DC H_2O	1.51[b]/ 3.55[c]			
	DC Si	2.39[b]/ 3.44[c]			

[a] Thickness of the films of nonfluorinated compounds **X1** and **X5** was estimated in spite of the deformed XRR profiles (poorly defined layers). In case of multilayer films of **X5** it was not even possible to estimate the values of thickness of [b] Lam – like monolayer and [c] smectic C-like monolayer of compound **X6**.

3.3.1.2. T-shaped bolaamphiphiles

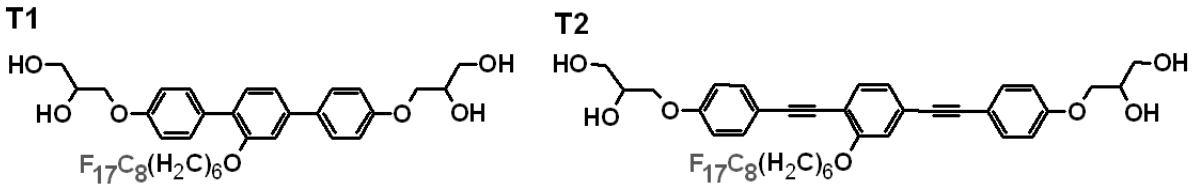

The behavior of Langmuir films of T-shaped bolaamphiphiles was affected by the asymmetry of the molecular structure. The lateral chain was attached slightly closer to one end of the core. Thus glycerol moieties were not energetically equivalent. This made the detachment of one of the polar groups from the water surface much easier. The rigid cores of the molecules reoriented to tilted and finally to vertical position during the compression of the film. Therefore **T1** and **T2** formed two types of monolayer films: Lam-like monolayer at a low surface pressure (cores aligned horizontally) and smectic C-like monolayer at a high surface pressure (cores perpendicular to the surface of water). **T1** actually did form a trilayer film in Langmuir-Blodgett experiments. Molecules' alignment was vertical in all the layers, which resulted in a very densely packed, thick structure. Smectic C-like trilayer was not detected in case of **T2**, probably due to the technical limitation of the compression ratio of the Langmuir trough used. The core of **T2** was much longer comparing to **T1**, therefore it required a higher compression ratio to align it vertically. The influence of lowered symmetry on the properties of thin films was described in case of compound **X6** as well.

The results of the DC experiments of compound **T1** are shown in **Figure 28** (results for compound **T2** were qualitatively identical, therefore not shown). It was possible to prepare both Lam-like and smectic C-like monolayer films of both **T1** and **T2**. Attempt to form trilayer film ($L = 3$) via drop casting resulted in only smectic C-like monolayer formation. It was very unlikely for T-shaped molecules to self-assemble into the smectic C-like trilayer film without any external force. The fluctuations of values of thickness of DC films (silicon and water) might be caused by difficulties in determination of area per molecule values from LB experiments. There was no apparent kink or collapse on $\pi(A)$ isotherms corresponding to the transition between Lam- and smectic C-like monolayers (see **Chapter 3.2**). The calculation of expected number of layers L, according to **Equation 9**, was therefore uncertain. Probably calculated L did not correspond to dense Lam-like nor smectic C-like films. The summary of the XRR fitting results is given in **Table 9**.

Two effects influenced the process of film formation via DC. The lack of symmetry resulted in energetically nonequivalent glycerol units. Therefore the cores reoriented to vertical position. Other reason is lowered amphiphilicity of the molecules with only one lateral chain when compared to X-shaped bolaamphiphiles. Therefore the interactions between such molecules and hydrophilic surface were not sufficiently strong to overcome the interactions between adjacent cores.

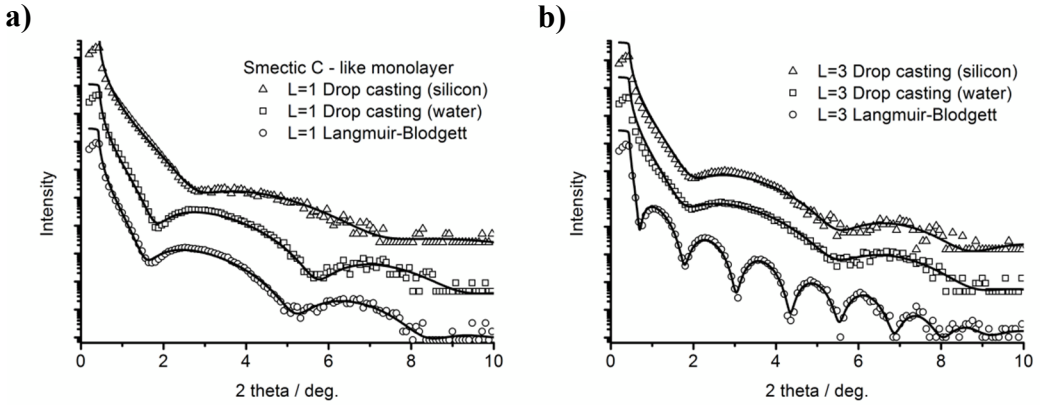

Figure 28 XRR profiles of films of compound **T1**. The amounts of solutions used in DC experiments corresponded to **a)** smectic C-like monolayer and **b)** trilayer films. Fitting of the patterns revealed that only monolayer films were well-ordered in case of DC method. *L* corresponds to the expected number of casted layers in DC or is estimated from LB compression experiments.

Table 9 Values of thickness of films of T-shaped bolaamphiphiles prepared with use of LB and DC methods and measured by means of XRR.

compound	method	1-layer	3-layer
T1	LB	1.16[a]/ 2.70[b]	7.22[c]
	DC H_2O	1.52[a] / 2.41[b]	2.51[b]
	DC Si	1.27[a] / 2.07[b]	2.45[b]
T2	LB	1.27[a] / 2.76[b]	
	DC H_2O	1.50[a] / 2.49[b]	2.60[b]
	DC Si	1.25[a] / 1.98[b]	

[a] Lam – like monolayer [b] smectic C-like monolayer [c] smectic C-like trilayer.

3.3.1.3. Anchor-shaped bolaamphiphiles

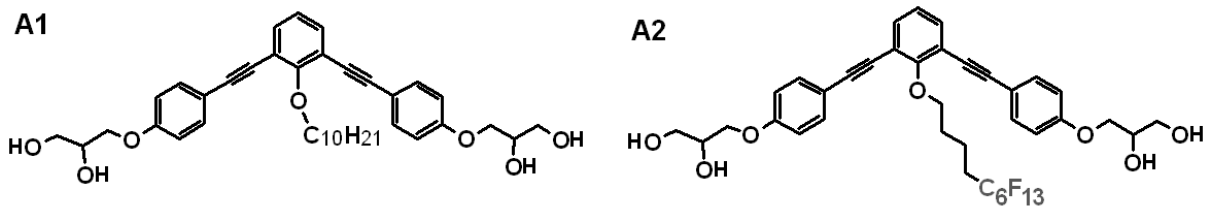

The influence of the shape of the core on thin films formation of the anchor-shaped compounds **A1** and **A2** was studied. Nonfluorinated compound **A1** did not have any interesting self-assembly properties (not shown). Compound **A2** formed a trilayer and 9-layer film at the air/water interface upon compression in LB experiments.

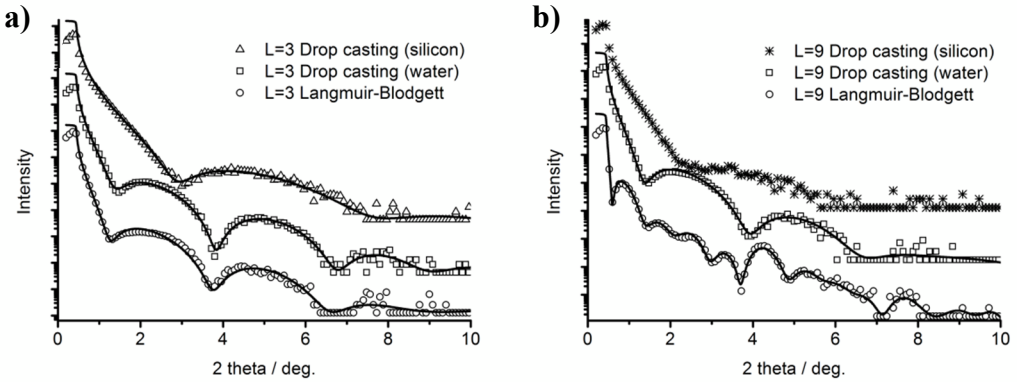

Figure 29 The results of XRR measurements of films of compound **A2**. Surprisingly, a trilayer film is formed in DC experiments on the water surface only; *L* corresponds to the expected number of casted layers in DC or is estimated from LB compression experiments.

Compound **A2** (**Figure 29)** spontaneously formed trilayer films when drop casted onto the water surface, even when excessive molecules were applied ($L>3$). Drop casting onto a silicon wafer did not give any interesting results. There were no indications of formation of stacks thicker than trilayer in DC experiments. Again water surface appeared more appropriate for self-assembly of multilayer stacks. Compound **A2** did not form smectic C-like films, even despite it had only one lateral chain as T-shaped compounds. This was caused by shape of the molecules, which limited the interactions between adjacent cores. Moreover, in case of **A2** the symmetry of the molecules is preserved.

The values of thickness of films obtained with use of LB and DC methods for compound **A2** are given in **Table 10**.

Table 10 Thickness (nm) of multilayers estimated from fitting of XRR patterns of films of anchor-shaped bolaamphiphiles obtained by DC and LB methods.

compound	method	1-layer	3-layer	9-layer
A1	LB	1.56		
A2	LB	1.43	3.71	10.5
	DC H_2O	1.39	3.62	3.73
	DC Si	1.40	1.42	

No tendency for self-assembly in DC experiments was found in case of compound **A1**

3.2.3. Discussion and Conclusions

The experimental studies were aimed to evaluate the influence of shape, core length and fluorination of part of the molecules on the self-assembly properties of bolaamphiphiles. Literature provided some examples of formation of stable multilayers of other compounds in Langmuir-Blodgett system.[120-122,129] One of the widely studied was **8CB**.[104,129,131-134] Therefore it was chosen as reference compound for test of self-assembly properties in DC experiments. Surprisingly not even a well-organized monolayer was obtained with use of the DC method. Also experiments with **8OCB** (4'-n-octyloxy-4-cyanobiphenyl) and perfluorinated **8OCB** (to test a stiffer analogue) were performed. Still no tendency for self-assembly in DC experiments was found. A specially designed, partially fluorinated nonadecanol abbreviated as **C1** (12,12,13,13,14,14,15,15,16,16,17,17,18,18,19,19,19 heptadecafluorononadecan-1-ol) was examined (**Figure 30**). The compound might be considered as an analogue of side chains of partially fluorinated bolaamphiphiles. Although compound **C1** formed a trilayer film in Langmuir-Blodgett experiments, it did not reveal any self-assembly properties when drop casted directly onto the water and silicon surface.

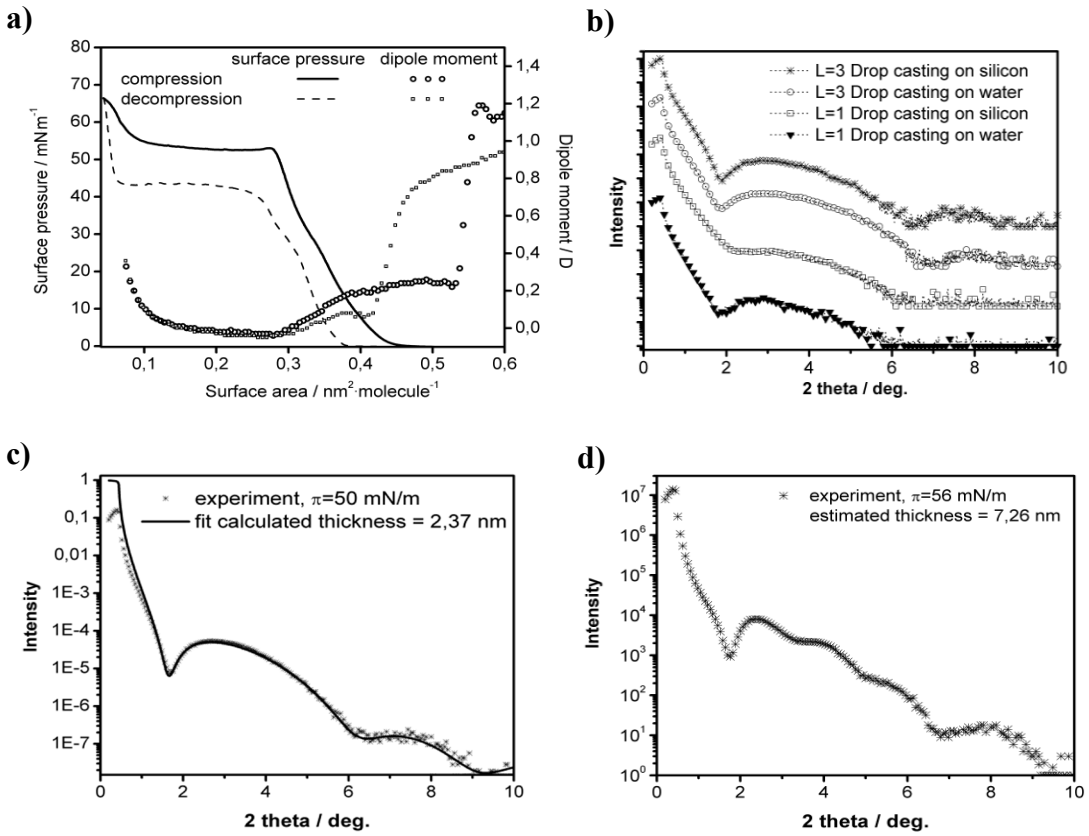

Figure 30 Set of results for compound **C1** (partially fluorinated nonadecanol). Picture **a)** shows $\pi(A)$ isotherms and surface potential recorded during compression/decompression cycle. Characteristic plateau indicates that the layering transition to trilayer film occurred (ratio of values of area at the beginning and end of the plateau close to 3). This was confirmed with use of XRR (patterns presented in **c)** for monolayer and **d)** trilayer film). It was impossible to fit the XRR pattern obtained for trilayer film with use of reasonable set of parameters. Therefore only estimated thickness is presented. Picture **b)** shows the results of drop casting experiments – only monolayer films were formed with use of this method.

The original idea was to establish, which part of the molecule of a bolaamphiphile was responsible for its unique properties. The following paragraphs are an attempt to answer this question.

Nonfluorinated compounds **X1**, **X5** and **A1** gave unsatisfying results both in LB and DC experiments. Only the monolayers of **X1** and **X5** were formed via DC. In case of **X1** the trilayer stack was formed upon DC onto water surface, however not well ordered. Such behavior is coherent with Langmuir-Blodgett experiments in which fluorination of the lateral

chains was the key factor for reversibility of Langmuir films and for multilayer stacks formation.

The partially fluorinated bolaamphiphiles were able to self-assemble into ordered thin films. The structure of the stacks varied depending on the shape of the molecules. Symmetrical X-shaped and anchor-shaped bolaamphiphiles tended to form Lam-like, whereas unsymmetrical X-shaped and T-shaped – smectic C-like films. The surface of water was more appropriate for the self-assembly process comparing to silicon surface. For example **A2** formed trilayer films ($L = 3$) when drop casted onto the water surface and not onto the silicon surface. There might be several factors which explain such observation. The interactions between water molecules and the glycerol units of the bolaamphiphilic cores were stronger than interactions between silicon surface and glycerol units. Flexibility of the water surface might have a positive impact on the molecules' alignment process as well.

Compounds **X2**-**X4** formed monolayer and trilayer films in drop casting experiments (on both water and silicon surface) as long as appropriate amounts of the solution were used. Further increase of amount of applied compound obviously increased the thickness of the film. XRR profiles however still revealed ordering within only a trilayer stacks. It indicated that molecules above the well-ordered trilayer films remained in a disordered state. This was confirmed by the AFM measurements.

Compounds which were found to form both Lam-like and smectic C-like films in Langmuir-Blodgett experiments (**X6**, **T1** and **T2**) behaved similarly in drop casting experiments as well. By changing the amounts of applied solution, Lam-like and smectic-C-like monolayers were prepared. No multilayers were found in this case. **X6** behaved as a T-shape compound. One of chains of **X6** is significantly longer and fluorinated, therefore it influenced the properties of the molecule much stronger than the second chain.

Results of drop casting experiments were in line with previously described Langmuir-Blodgett experiments. In case of LB, increased rigidity of molecules enhanced the tendency for multilayer stacks formation. However, the stiffer compound (**X4**) exhibited a hysteresis loop during the compression/decompression cycles, while the more flexible (**X2**) did not. The good balance of the molecules' rigidity and flexibility was the key factor to reconcile the possibility of formation (flexibility is needed) and stability (improved by increased rigidity) of multilayer stacks in LB experiments. The same factors were found to be important in DC experiments. The non-covalent bondings were not strong enough to stabilize

the ordering in case of very flexible molecules. On the other hand, if the molecules were too rigid, they could not adopt the proper orientation in space. At least two structural domains of the molecule should be stiff to trigger the spontaneous self-assembly. Probably the bolaamphiphilic properties and the shape of the studied molecules are not the only ones that allow the self-assembly into ordered stacks.

The DC experiments confirmed the assumption made in previous chapter, that the molecules create pairs with back-to-back organization. Attempt to form the 2-layer stack of compound **X2** in drop casting experiments was performed. The obtained film was in fact a trilayer with patches of just monomolecular thickness or just clean silicon surface. The relation of interactions between molecules and between molecules and surface were important factor for thin films formation. The interactions between the cores are weaker than between the hydrophilic surface and the molecules in case of symmetrical X-shaped and anchor-shaped and stronger for unsymmetrical X-shaped and T-shaped bolaamphiphiles. This reasoning explained formation both Lam-like and smectic C-like films.

The observation of spontaneous formation of ordered stacks might be of great importance, *e.g.* as an alternative to SAM formation. The very simple procedure of coverage preparation provides uniform films of practically no limitations in terms of the coated area. This procedure seems to be ideal for industrial applications. As has been proved, self-assembly properties can be tuned by careful adjustment of few parameters at the stage of designing the structure of the molecules. There are no apparent obstacles on the way to utilizing hereby described phenomena in a much wider range of new compounds. This can lead to preparation of different functional molecules capable of efficient and non-demanding self-assembly into well-ordered thin films.

3.4. Ordering of gold nanoparticles in thin films of bolaamphiphiles

Gold nanoparticles have recently attracted a lot of interest due to their possible applications in electronic and optoelectronic devices.[206] Moreover, they have bio-nanotechnological potential, which stems from versatile synthetic routes for surface bio-functionalization.[207] The Au NPs are applicable in preparation of logic gates,[208] catalysts,[209] biosensors,[210] fuel cells,[211] solar cells,[212] super hydrophobic surfaces,[213] nanotips[214] and platforms used in SERS.[215] Various concepts concerning organization of Au NPs at the nanometer scale have already been described: Langmuir-Blodgett method,[216] electrodeposition,[217] covalent bonding to surface, organization at the interface (solvent-air,[218] water-hydrocarbon,[219] water-alcohol[220]) or on variety of templates such as block copolymers,[221] DNA,[222] peptides,[223] nanotubes[224] and many more.[225] Described methods have limitations, which influence possible applications to very specific purposes or allow only small scale fabrication. The easy and fast method for the preparation of the uniform 2D nanostructures of Au NPs with the control over the parameters of the process (like interparticle distance, shape and size of the domains, the percentage coverage) is needed for the industrial purposes.

The tendency of the bolaamphiphiles for self-assembly into ordered thin films, described in **Chapter 3.3**, can be transferred onto other species. The preparation of ordered patterns of nanoparticles in bolaamphiphilic matrix is presented. The method is based on the drop casting of mixtures of amphiphiles and nanoparticles directly onto the solid substrate.

Yang and coworkers[226] reported the enhanced ordering in gold nanoparticles 2D lattices. Excess free ligands added to the mixture improved significantly properties of the obtained films. The work was focused on the Langmuir-Blodgett films. In hereby presented case, partially fluorinated bolaamphiphiles gave qualitatively the same results in LB and drop casting experiments. Tests with other amphiphiles proved that there was no trivial link between these two methods. The tendency of bolaamphiphiles for self-assembly into thin films was rather unusual. Other examples of surfactant that enhanced ordering of **Au NPs** lattices directly at solid surface were not found. In this chapter the results obtained for bolaamphiphiles are compared to those obtained for arachidic acid and liquid crystalline amphiphilic compound **8CB**, as the ordering compounds in the mixtures with **Au NPs**.

3.4.1. Results

The protocol describing preparation of mixtures of surfactants and **Au NPs** was described in **Chapter 2.2.2.** The ratios of surface concentrations were used to describe the DC mixture composition. Such concentrations were expressed in terms of amounts of solutions needed to cover 1 cm^2 of surface with dense monolayer in ($\mu l\ cm^{-2}$). The values of surface concentrations were determined according to the $\pi(A)$ isotherms of compounds of interest (dividing the area of the film at the collapse point by the amount of applied solution). The ratio of surface concentrations indicated the surface fractions covered by mixture constituents. This description was used for the clarity of the presentation and for readers` convenience. Moreover, there was no need to determine the exact molar concentration of the **Au NPs** solutions, which could cause unnecessary errors.

The mixtures of bolaamphiphiles and **Au NPs** were prepared before the experiments. The microsyringe was used to apply proper amounts of two-component solutions directly onto the silicon wafers. The volume of applied solution was a controllable parameter. It strongly affected the obtained morphology. For example in case of mixture of concentration ratio 1:1 (the same area covered by both components) the most intuitive was film in which each component (**Au NPs** and additive) covered 50% of the area of the substrate. As a result dense monolayer was formed, and the **Au NPs** surface coverage was 50%. However, it was easy to apply twice as much solution to provide as much **Au NPs** to cover 100% of the available surface. In such a case the relatively small molecules of the second component were forced to be located in the empty voids between the **Au NPs**, or at the top or bottom of **Au NPs** lattice. Usually the amount of applied solution was no greater than to obtain only dense monolayer, and not multilayer stacks. Otherwise it was specified (as for example in case of film presented in **Figure 31b**).

Two films are compared in **Figure 31** to prove the enhanced ordering in drop casted films of mixtures of bolaamphiphiles and **Au NPs**. Picture **a** shows SEM image of the pure **Au NPs** drop casted directly onto the silicon wafer. The amount of the **Au NPs** was calculated to cover 100% of the area of the silicon substrate. The film was strongly distorted. Big voids with no **Au NPs** and regions of multilayers stacks were present. The image **b** shows the morphology of the film of the mixture of **Au NPs** and bolaamphiphile **A2** prepared via DC method. The amount of **Au NPs** was the same as in case of picture **a**, and **A2** was an additive (ratio 1:1). The ordering of **Au NPs** in bolaamphiphilic matrix is obvious.

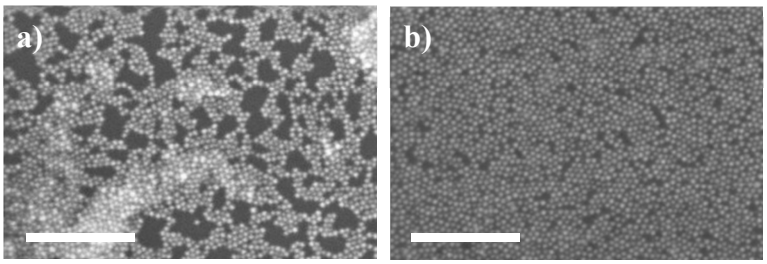

Figure 31 SEM images of drop casted films of **Au NPs** obtained with use of **a)** pure **Au NPs** solution and **b)** mixture of **Au NPs** and bolaamphiphile **A2** (concentration ratio 1:1, total applied amount of solution is greater than needed to cover the substrate with composite film of monomolecular thickness). Scale bar 200 nm.

As described previously (**Chapter 3.3**) the films of bolaamphiphiles obtained via Langmuir-Blodgett and drop casting methods were very similar. In hereby presented case the formation of ordered films of bolaamphiphiles induced the ordering of the **Au NPs**. Therefore there was possibility to overcome the Langmuir-Blodgett technique limitation and prepare the patterns of **Au NPs** in a very simple, one step procedure. Moreover, the drop casting allowed preparing films, which could not be obtained via LB method. For example films of the mixture of **Au NPs** and **A2** of surface concentration ratio 1:1 (as in **Figure 31b**) were transferred according to Langmuir-Blodgett method at surface pressure 21 mN m^{-1} (**Figure 32a**), 30 mN m^{-1} (**Figure 32b**) and 37.5 mN m^{-1} (**Figure 32c**). Even despite the Langmuir trough used in the experiment offered big compression ratio, it appeared impossible to compress the film so far to obtain 100% **Au NPs** coverage. The limitations of LB technique allowed forming of the films of only up to 85% **Au NPs** surface coverage (**A2** formed multilayers, therefore it could effectively cover smaller area than 50% even despite 1:1 ratio). The films of 100% **Au NPs** coverage were obtained via DC method just by applying properly calculated amounts of solution (**Figure 31b**).

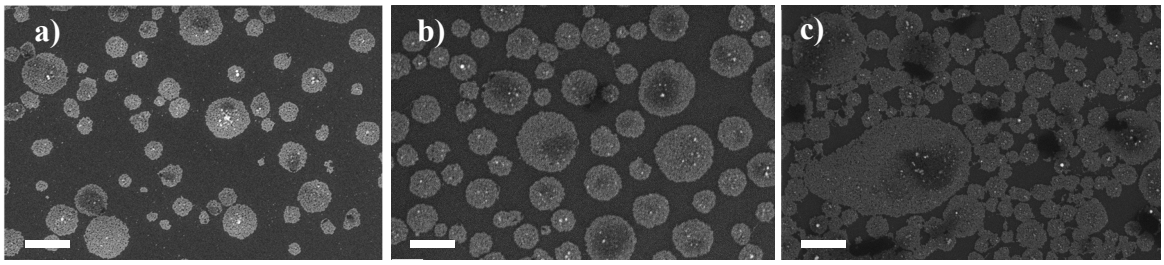

Figure 32 The comparison of films of **Au NPs** : **A2** mixtures obtained with use of LB method transferred at different surface pressure a) 21 mN m^{-1}, b) 30 mN m^{-1} and c) 37.5 mN m^{-1}. Scale bar 500 nm.

The $\pi(A)$ isotherms of mixtures of bolaamphiphile **A2** and **Au NPs** are shown in **Figure 33**. The shape of the curves evolved from characteristic for pure **Au NPs** towards pure **A2**. The controllable parameters were: concentration ratio and surface pressure at which the transfer was performed. In case of 1:1 surface fraction of each component in monolayer film was ½. The amount of applied solution was adjusted to obtain monolayer composite film. However **A2** tended to form multilayer stacks upon compression. The coverage fractions were changing due to layering transitions of **A2**. Only one third of the **A2** molecules were still in contact with surface upon first layering transition (*i.e.* **Au NPs** coverage should equal around 75%).

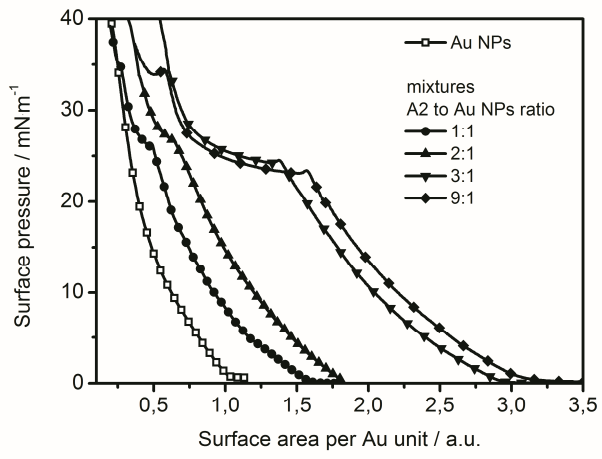

Figure 33 $\pi(A)$ isotherms of mixtures of **Au NPs** and bolaamphiphile **A2** of different surface concentration ratios.

In the drop casting method the controllable parameters were: concentration ratio and the amount of solution applied directly onto the surface. The parameters for DC method were adjusted to fit the LB condition. The morphologies and surface coverage obtained with use of LB and DC methods were very similar (**Figure 34)**. The concentration ratio of the mixture was 1:3 (**Au NPs** : **A2**) and surface pressure at which the transfer was performed 30 mN m^{-1}.

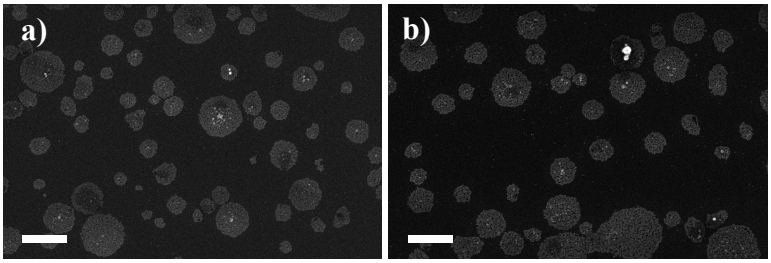

Figure 34 Films of mixtures of **Au NPs** and bolaamphiphile **A2** of concentration ratio 1:3; **a)** pattern obtained with use of LB technique and **b)** corresponding film prepared with use of drop casting method. Scale bar 500 nm.

Among bolaamphiphiles **A2** gave the best enhancement of the ordering. In **Figure 35** the drop casted films of mixtures of surface concentration ratio 1:1 of bolaamphiphile **X2** (**Figure 35a**) and liquid crystalline **8CB** (**Figure 35b**) are shown. The amount of applied solution was calculated to obtain 100% of **Au NPs** surface coverage. The images in **Figure 35** should be compared with **Figure 31b** for **A2**. The influence of surfactant structure was obvious. However, there were no guidelines what the dependence was. Even in relatively small group of compounds, such as partially fluorinated bolaamphiphiles, the differences of behavior were very big. Probably the main factors were general shape and rigidity of the molecules. In **Chapter 4** results of the Langmuir-Blodgett experiments of **8CB** and **Au NPs** mixtures are described. The LB films of **8CB** and **Au NPs** mixtures differed dramatically from those obtained via DC.

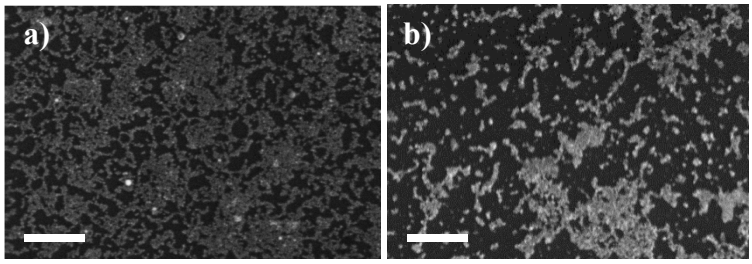

Figure 35 SEM images of drop casted films of mixtures of **Au NPs** and **a)** bolaamphiphile **X2**, **b) 8CB**. Surface concentrations ratio 1:1, the volume of applied solution was enough to cover 100% the of desired surfaces with **Au NPs**, therefore it was greater than to form monomolecular mixed films. No ordering was visible. Scale bar 200 nm.

3.4.2. Conclusions

The presented work was focused on example of system, which was efficient for simple surface patterning with **Au NPs**. The method of preparation of controllable 2D patterns of **Au NPs** with use of direct drop casting of mixtures of nanoparticles and surfactants (in general, not only bolaamphiphiles) were main topic of patent application, submitted to the Polish Patent Agency in June 2011.

Previous reports on the colloidal particles with non-zero charge at the surface revealed the tendency for rafts formation. The patterns evolved towards net-like structures with increase of surface coverage.[227] In case of pure **Au NPs** the same behavior was noticed (compare **Chapter 2.1.2** and **Figure 31a**). For films of mixtures of **Au NPs** and bolaamphiphile **A2** the enhanced ordering of **Au NPs** was observed. The mechanism involved was similar as

described by Lau and coworkers,[226] *i.e.* excess of surfactant reduced the attractive forces between the **Au NPs** moving the system from kinetically trapped state to an ordered state, which was thermodynamically more favorable. The authors found the ordering only in microscale droplets. They utilized LB method and could not reach the 100% **Au NPs** surface coverage. The DC method allowed to overcome this problem and simplified the whole process. Also multilayer films formation was possible with use of DC method.

The presented **Au NPs** patterns were used as substrates for chemical vapor deposition (CVD) process of gallium nitride (**GaN**) nanowires growth. Gold was catalyst in this process; **GaN** nanowires appeared only in spots where **Au NPs** were deposited. An example is shown in **Figure 36**. Presence of additional amphiphilic compounds did not influence the process of **GaN** growth.

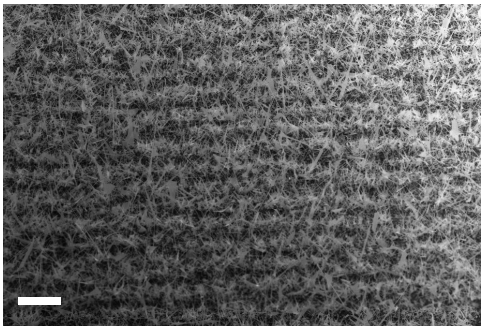

Figure 36 GaN nanowires prepared on the surface shown in **Figure 31b**. Scale bar 10 μm.

Results presented in this chapter are rather preliminary. More efforts are needed to evaluate the influence of the controllable parameters, as type of surfactant, solvent, temperature or concentrations (not only concentration ratios) on the process and obtained morphology. The biggest advantage of presented method is that it does not require any equipment beside microsyringe. It might be used as complementary method for spin coating for patterning of parts of the scaffold prepared according to "top-down" approach.

3.5. Gold nanoparticles with covalently attached bolaamphiphilic domains

Ordered structures of nanoparticles could be obtained either by the self-organization of particles capped with specific thiols, assembly on modified substrates or with use of templates.[228] Self-assembly of ligand-protected nanoparticles is a relatively simple and well established technique. The interparticle distance is typically tuned by changing the ligand molecules. Several research groups evaluated the effect of monofunctional ligands, such as alkyl thiols (or dithiols), alkylamines, ammonium salts, and alkyl silanes on the self-assembly of nanoparticles.[229] Also the ligands baring the aromatic domains,[230] liquid crystalline moieties[50] or allowing the multiple H-bonding were investigated.[231] Number of applications of nanoparticles arrays such as catalysts for templated nanowire growth for dye-sensitized solar cells,[232] catalyst layers in fuel cells,[233] electrical transducers of chemical or biological binding processes[234] etc., required control over interparticle spacing in the 10–50 nm regime. Ligands based on alkane chains allowed the adjustment of the interparticle spacing in the sub-5 nm range.[235] The diblock copolymer method assured the spacing control only in a range above 25 nm.[236] Here the results on controlled self-assembly of Au NPs functionalized with bolaamphiphiles are presented. Such ligands influenced not only interparticle distance, but also the arrangement of the particles in 2D films.

3.5.1. Results and Discussion

Only one paper published until now on bolaamphiphiles – Au NPs system was found.[237] The authors reported that the adsorption of a bolaamphiphilic surfactant at the surface of Au NPs increased the stability of the system and allowed a reversible aggregation upon pH changes. In this chapter Au NPs with covalently attached bolaamphiphilic ligands were investigated. The ligand consisted of a terphenyl rigid core with two hydrophilic glycerol domains at the end, and a side chain with thiol group as a linker (see **Figure 8**). The surface behavior of gold nanoparticles comprising unusual coating ligand with a bolaamphiphilic domain (**B-Au NPs**) was investigated as a continuation of work presented earlier in the thesis. The ligand, which was used, was in fact a T-shaped bolaamphiphile. Therefore it was expected to enhance ordering of the **B-Au NPs** due to bolaamphiphiles tendency for self-assembly. The bolaamphiphilic ligands constituted 50% of all ligands at the surface of Au NPs. The bolaamphiphilic ligands were introduced in exchange reaction, and the primary grafting

consisted of classical thiols. The best amphiphilic properties were assured by the hexanothiol ligands as primary grafting.

The THF solutions of **B-Au NPs** were spread at the air/water interface. The $\pi(A)$ isotherms were recorded simultaneously with the BAM picture acquisition – both are shown in **Figure 37**. The shape of the $\pi(A)$ isotherm revealed two different compression regions. Up to 10 mN m^{-1}, the slope of the isotherm was small. It corresponded to the rearrangement of ligands on the surface of **B-Au NPs**. This part of the isotherm corresponded to the compression of liquid expanded phase. It was possible to observe this process, because the ligands were large comparing to the metallic core of the **B-Au NPs** (core diameter of around 2.6 nm). Narrow plateau at around 10 mN m^{-1} was visible. It corresponded to the liquid expanded – liquid condensed phase transition. Further compression caused a steep increase of the surface pressure and corresponded to packing of non-overlapping spheres of nanoparticles. Because of very high compressibility of the film (significant changes of available area resulted in small changes of the surface pressure) it was impossible to reach a collapse pressure and record full isotherm. Further compression above 42 mN m^{-1} was impossible due to technical limitations of the Langmuir trough, *i.e.* limited ratio of maximal to minimal available area between movable barriers. However, a bend of the $\pi(A)$ isotherm was observed above 40 mN m^{-1}. It probably corresponded to the onset of the collapse of the film. Similar isotherms were observed by others in case of Au NPs[238] as well as Ag NPs,[239] NiCo alloy NP[240] or FePt alloy NP.[241]

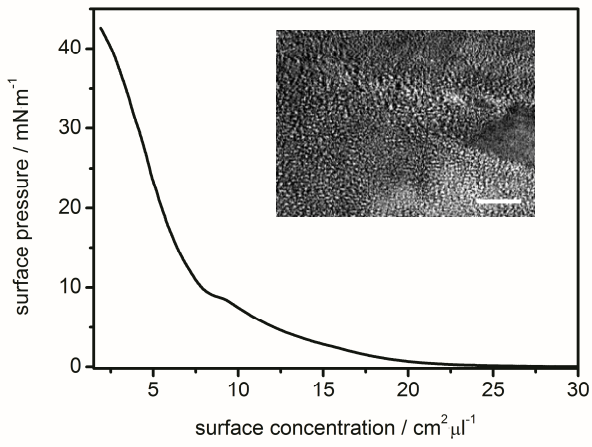

Figure 37 The $\pi(A)$ isotherm of the **B-Au NPs**. The inset shows the BAM picture taken at around 30 mN m^{-1} (scale bar 500 µm).

The Langmuir-Blodgett method was used for film deposition at surface pressures up to 41 mN m^{-1}. The transfer ratio was insufficient (less than 0.3) and surface coverage was not

satisfactory even in case of very high values of surface pressure. Therefore a very simple alternative method of film formation was used, *i.e.* drop casting of precisely calculated amounts of a solution directly onto the solid surface.[242] To determine the proper parameters for such sample preparation the $\pi(A)$ isotherms were analyzed.

Thus prepared samples were further studied with use of XRR and AFM. The AFM images shown in **Figure 38** revealed the uniform morphology of the film over large area (image **a**). The film of single particle thickness was formed. The circular and densely distributed domains were observed. The diameter of such domains was highly monodisperse (around 30 nm). The interior of the domains was empty (images **c** and **d**). The **B-Au NPs** were located at the rim, forming ordered array of nanorings at the silicon surface.

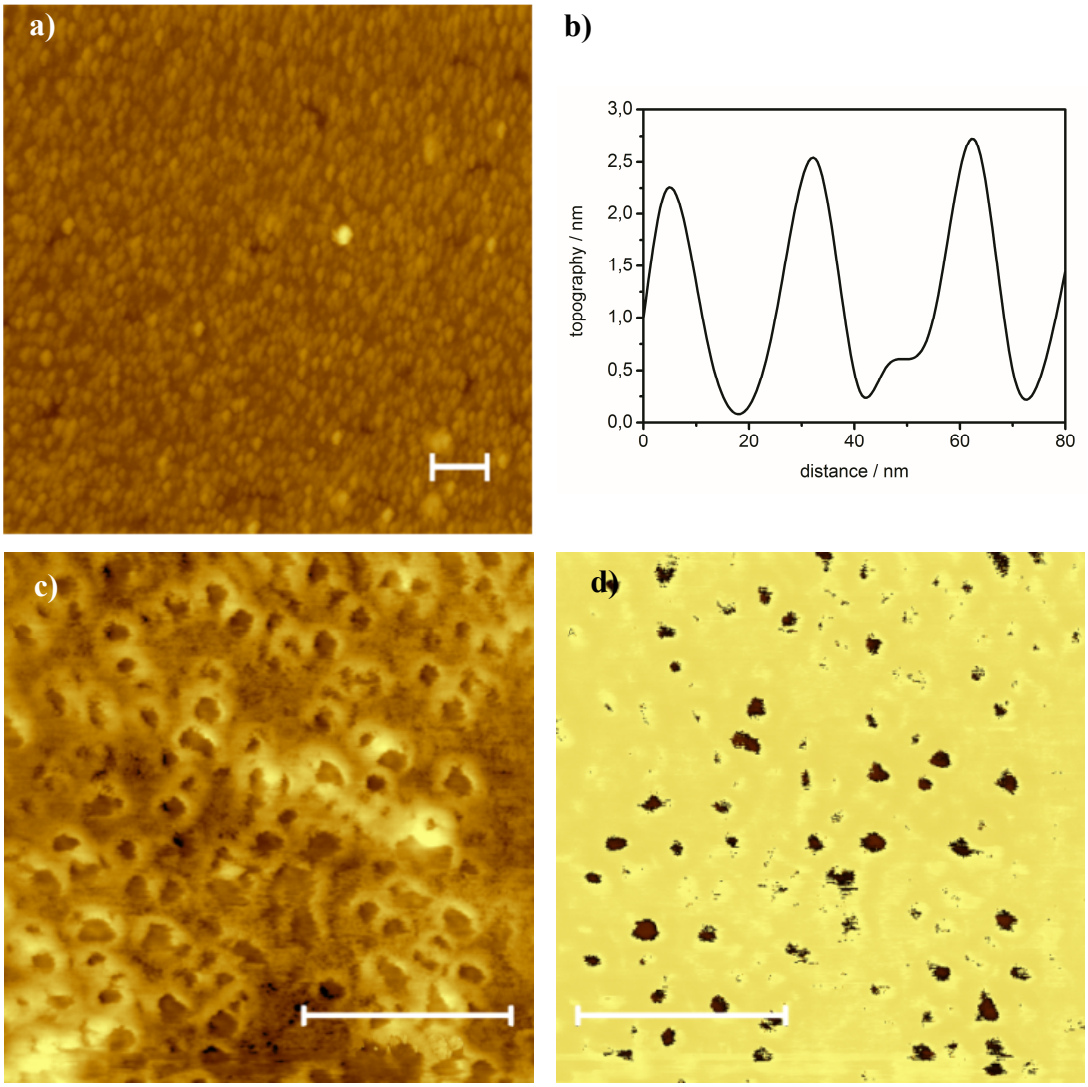

Figure 38 a) AFM non-contact mode image of large area of the thin film of **B-Au NPs**, **b)** topography obtained in tapping mode, **c)** AFM tapping mode and **d)** phase contrast image. Scale bar 200 nm.

Topography of the sample and phase of the cantilever oscillations, measured relative to the drive signal oscillations, were registered simultaneously during a tapping mode AFM scan (**Figure 38c** and **Figure 38d**). Strong phase contrast observed in tapping mode scan is usually attributed to difference in mechanical properties of materials on the heterogeneous surface[243] – in this case between the Si substrate and the layer of **B-Au NPs**.

To obtain reliable results of XRR fitting it was crucial to set the starting simulation parameters within physically reasonable values. The geometrical model, which takes into account only length of bonds and the angles between them (CPK model) was used. The starting parameters were based on the dimensions of primary and secondary ligands of the **B-Au NPs**. The starting parameters could vary only in a reasonable, restricted range (±10%). Only the diameter of the metallic core of the gold nanoparticles was kept constant (2.6 nm). This value was obtained from SAXS measurements of Au NPs with primary ligand. The obtained thickness of the **B-Au NPs** film, *i.e.* 5.01 nm (see **Figure 39**) was in good agreement with the SAXS measurements of the diameter of the **B-Au NPs** proving ordered monolayer formation.

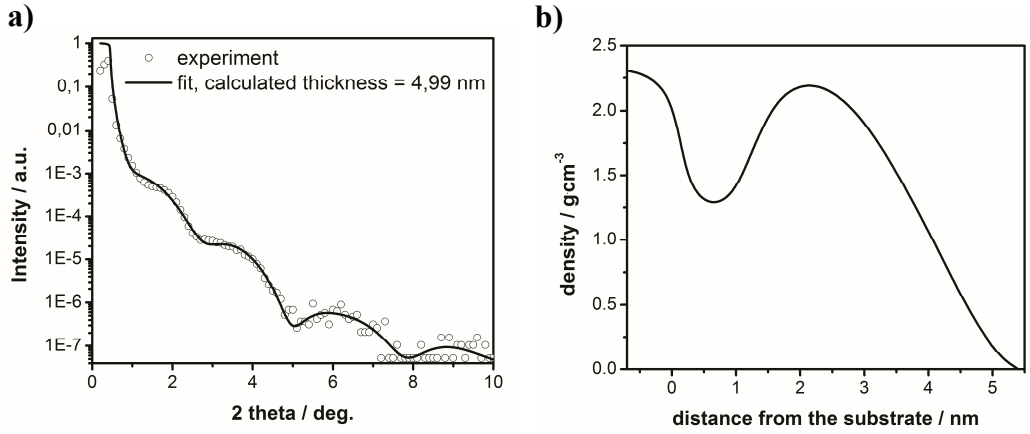

Figure 39 a) The XRR pattern and fit curve. The calculated thickness of the film was 5.01 nm, **b)** density profile used for fit preparation.

As a result of fitting of XRR patterns, the density of the Au sublayer was obtained (it was allowed to vary, while its thickness was constant).[244] In case of a perfect coverage of the surface with gold, this value should be equal to the density of gold (for dense 2D lattice of Au NPs 0.74 x density of gold). The decrease of the simulated values corresponded to the decrease of the **B-Au NPs** surface coverage. Influence of the organic moieties on the density profile at the same *z* distance from the substrate as gold sublayer was practically neglectable. The density profile obtained as a result of XRR fitting is shown in **Figure 39b**. The obtained

density of the metallic core sublayer was 2.16 g cm^{-3}. This value corresponded to the surface coverage of 11.1%. To compare this value with the experimental results a simple geometrical model of the **B-Au NPs** arrangement was used (see **Figure 40**). It was assumed that the **B-Au NPs** centers were located 15 nm from the center of the round shape domain. This assumption was based on the surface topography determined with use of AFM (see **Figure 38b**). Since the diameter of the **B-Au NPs** was around 5 nm, the diameter of the domain was 32.5 nm. The metallic cores of the **B-Au NPs** were on average 2.6 nm in diameter. Therefore they only covered a part of the domains – a ring of inner and outer diameters equal 28.7 nm and 31.3 nm, respectively. As a result only around 14.8% of the domain was covered with the sublayer of gold. If close packing of the domains at the surface was assumed, this value should be multiplied by the factor 0.74 for the domains array. This procedure gave a total surface coverage of 10.9%. Presented conformity and the very good quality of the fit gave great confidence in the obtained simulated parameters.

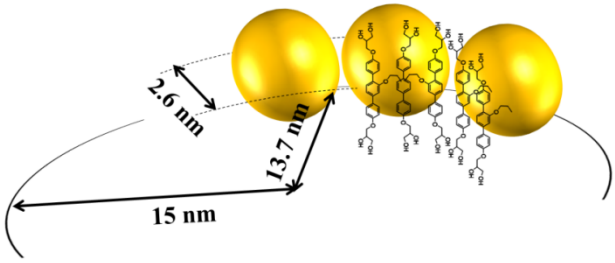

Figure 40 Model of the **B-Au NPs** arrangement in 2D system. The nanorings form a densely packed array upon simple drop casting.

The formation of rings of NPs was already reported and several mechanisms were proposed. Microrings were formed by kinetic processes driven by solvent evaporation, such as hole nucleation in unstable wetting layers,[245] cell wall formation by Rayleigh–Benard convection,[246] "breath figures"' created by the condensation of water droplets on the rapidly cooling wetting layer[247] and contact line pinning during surface dewetting.[248] Till now the formation of nanorings was reported only in case of magnetic NPs due to dipole-directed assembly.[249] Moreover, the rings obtained in all of these cases were sparsely distributed at the surface. Above explanations did not apply to **B-Au NPs**. They did not have any magnetic properties, observed nanorings were far too small to be formed by a kinetic process and the obtained arrays were densely packed.

The formation of nanoring arrays of **B-Au NPs** was governed by the interactions between

rigid cores of bolaamphiphilic moieties. Used bolaamphiphilic ligand belonged to the group of T-shaped bolaamphiphiles and had similar structure as the compounds studied previously in **Chapters 3.2.1.2** and **3.3.1.2**. Partially fluorinated T-shaped bolaamphiphiles formed two types of monolayer films: Lam-like monolayer (cores aligned horizontally) and smectic C-like monolayer (cores perpendicular to the surface). It was assumed that the reason for such behavior was the balance of interactions between cores comparing to interactions with the surface. Moreover, the T-shaped bolaamphiphiles formed columnar phases in bulk with the cores forming stems and the side chains in the space between the columns. In case of **B-Au NPs** the ligands were attached covalently, what restricted the possible alignment. However the linkers were flexible, what might allow the proper orientation in space of the liquid crystalline domains. In such a confined system the estimated distance between rigid cores was very similar as in case of a bulk phase. As well as in case of bulk Col_{Hex} phases of the T-shape bolaamphiphiles, the π-π stacking between terphenyl cores of **B-Au NPs** governed the nanorings formation at the surface. In Col_{Hex} phase the distance between terphenyl cores of T-shape bolaamphiphiles was around 0.5 nm. Taking into account the fact that the rigid terphenyl core was not perfectly flat and the influence of glycerol moieties, this value was in reasonable agreement with the distance predicted for π- π stacking (around 0.4 nm).[250] The inner radius of the circular domain of the **B-Au NPs** was around 13.7 nm, what corresponded to the circumference of 86 nm *i.e.* around 172 bolaamphiphilic domains arranged perpendicularly to the surface. On the other hand it was easy to calculate how much ligands could be attached to the metallic core. The metallic core area was around 21.22 nm^2 ($4\pi r^2$) and the minimal area occupied by one hydrocarbon chains was 0.205 nm^2.[52] Therefore the number of bolaamphiphilic ligands (50% of all ligands) per one **B-Au NP** was around 50. In case of only 6 major directions around 8 bolaamphiphilic moieties of one **B-Au NP** should be inside the circular domain (in the orientation schematically depicted in **Figure 40**). Therefore there should be around 19 **B-Au NPs** at the rim of the domain. This corresponded to the circumference of the rim of 94.81 nm. That gave the radius of the domain (to the center of the **B-Au NPs**) of 15.1 nm, *i.e.* great agreement with the experimental data and with the model based on assumption that the bolaamphiphilic domains were oriented in the same manner as in Col_{Hex} phase. This track led to the conclusion, that the bolaamphiphilic moieties of the **B-Au NPs** inside the circular domains had the same orientation as in Col_{Hex} bulk phase, *i.e.* the same interactions played role in the thin film formation of **B-Au NPs**.

3.5.2. Conclusions

For the first time the assembly of bolaamphiphiles – Au NPs hybrid structures on a solid surface was shown. The thin film was prepared according to a simple procedure of drop casting of a precisely calculated volume of a solution (based on LB experiments) directly onto the solid surface. The obtained films were of uniform morphology over large area. The **B-Au NPs** self-assemble into nanorings of diameter of around 30 nm with an empty interior. Such pattern, schematically depicted in **Figure 40**, was confirmed by means of AFM and XRR measurements.

The ability to produce nanostructured surfaces over macroscopic areas is likely to be of crucial importance for the integration of nanotechnology into commercial devices.

4. Results: Formation of net-like patterns of Au NPs in liquid crystal matrix

4.1. Introduction

Thin films of periodically organized nanoporosity are very important topics in contemporary research.[251] One- and two-dimensional networks of nanoparticles are among the most applicable ones. Cellular structures were obtained in case of Au NPs[257] as well as Ag NPs[252] or Co NPs.[253] In the review by Srivastava and Kotov the authors described the possible applications of unique optical (spectroscopy), magnetic (bio-imaging) and electronic (single electron transistors) properties of such structures.[254] 1D array of Pd NPs was used to manufacture a gas sensor.[255] In another example, a DNA detection sensor was based on a 2D structure of Au NPs.[256] An interesting paper by Kane *et al.*[257] described the Au NPs net, which exhibited electronic switching based on gating by metabolic activity of yeast cells deposited on the structure. The cells played the role of a moiety sensor. Coupling between biochemical processes of cells and electronic properties of the net was predicted to have potential applications in electrodes of biofuel cells and biosensors.

Net-like structures were also found in Langmuir-Blodgett systems. Gold nanoparticles were mixed with amphiphilic molecules such as polymers[258] or phospholipids,[259,260] what resulted in net-like morphology of the films. Hassenkam *et al.*[259] described a mechanism of formation of a net-like structure by hydrophobic Au NPs. Authors proved it to be invalid in case of NPs with hydrophilic ligands. The main idea was that the nanoparticles acted as impurities. As such they were repulsed to the edges of domains solidifying during compression of the LB films. Mogilevsky *et al.*[260] confirmed such explanation by systematic studies on behavior of Au NPs in LB films of a number of phospholipids. Net-like structures were observed only in case of the Au NPs mixtures with phospholipids exhibiting liquid expanded – liquid condensed phase transition. The Au NPs were “frozen out” to the borders of the domains of the condensed phase. The mechanism of formation of the observed maze-like structures was based on the following assumptions. 1) It was energetically favorable for the amphiphilic molecules to occupy the entire water surface. 2) The Au NPs formed close packed 2D hexagonal rafts; direct contact between the hydrophobic Au NPs and water surface was unfavorable. In such case the surfactant molecules served as a template. The nanoparticles were lifted from the water surface and accumulated on the edges of the condensed phase.

Lifting was confirmed by means of XRR measurments.[258] In this model the increase of hydrophilicity of the Au NPs should result in different morphology of the film. The Au NPs should compete for the area at the water surface with phospholipids, rather than be easily lifted. This was in fact the case – amphiphilic Au NPs (15% of OH groups at the ends of coating molecules) were found not to create any net-like structures in a matrix of phospholipids.

In this chapter a new system for preparation of net-like structures of controlled morphology based on amphiphilic **Au NPs** is presented. When mixed with a liquid crystalline **8CB** and compressed, the stable Langmuir films were formed. During the decompression a net-like structure appeared. It was easily transferred onto solid substrates according to LB method. The average area of a unit cell of the net was controllable. It depended on the value of the surface pressure and, therefore, on the total available area of the water subphase during the transfer of the structure.

The liquid crystals were recognized as an ideal template for the "bottom-up" approach of preparation of more complex nanostructures. The recent review by Kumar and Bisoyi[50] concerning LC as an emerging avenue of soft self-assembly refers to around ninety articles showing possibilities of utilization of LC properties.

Chain-like structures were observed in bulk liquid crystal matrix before. Described mechanism of formation of such structures was however based on colloidal interactions. Such explanation arose from the orientational elastic energy of the anisotropic host fluid, within which the particles were suspended.[261] Therefore it was not applicable in case of Langmuir-Blodgett films of Au NPs – LC mixtures.

The mixtures of Au NPs and liquid crystals in 2D systems were also studied previously. However, no net-like structure was described until now in such system. For instance Vijayaraghavan and Kumar described the ordered structure of Au NPs in a matrix of a discoitic LC.[262]

Pressure induced layering transitions in thin films of **8CB** have been intensively studied.[104,121,129-133] Thus behavior of **8CB** in LB systems is well known and described. Behind the collapse point the molecules do not form disordered aggregates. Instead a process of formation of a well-defined multilayer occurs. The plateau region of the $\pi(A)$ isotherm corresponds to formation of liquid domains of a trilayer film. At the end of this plateau, the

entire film consists of a trilayer stack. Upon further compression a rise of surface pressure is observed. The second collapse point corresponds to a very close packed trilayer film. Further decrease of available area leads to a break of the trilayer film and formation of even thicker multilayer stacks.[121,129]

4.2. Results

A study of thin films of mixtures of **Au NPs** and **8CB** is hereby presented. **Au NPs** used in the experiments were of diameter 8.9 nm. Around 10% of dodecanothiol ligands was substituted with TMA (N,N,N trimethyl (11-mercaptoundecyl) ammonium chloride). This assured the amphiphilic character of **Au NPs**. For the sake of convenience, concentrations of solutions used in LB experiments were expressed as volumes of the solution needed to cover 1 cm^2 of the surface with a dense monolayer (see Experimental section; **Chapter 2.1.2**). Such description made it easy to follow the evolution of patterns with changes of the **Au NPs** surface coverage. For example, a ratio of 1:1 corresponded to film in which both components covered the same area in the monolayer. In case of ratio 1:27 area covered by **8CB** was 27 times greater than by **Au NPs** (as long as film is no thicker than monolayer). Such ratios corresponded in fact to surface fractions of mixtures constituents.

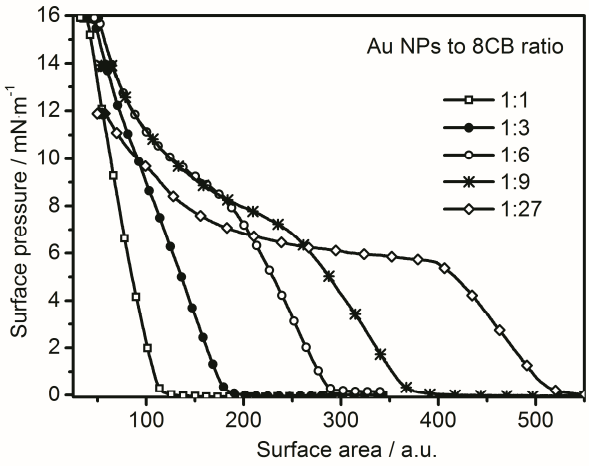

Figure 41 The $\pi(A)$ isotherms of mixtures of **Au NPs** and **8CB** of different composition. The *x* axis is scaled so that the amount of **Au NPs** per area unit is the same in all the plots, and the amount of **8CB** vary.

The influence of changes of the concentration ratio of the components on the obtained $\pi(A)$ isotherm was investigated. The results are presented in **Figure 41**. The isotherms were scaled with respect to the area occupied by **Au NPs**. It was assumed that the diameter of **Au NPs** did

not change significantly during the compression/decompression process. Therefore the scaling, based only on the area occupied by both **8CB** molecules and **Au NPs**, was linear. With changes of proportions of the two components, the shape of the isotherm evolved from one characteristic for pure **Au NPs** (see Experimental section) towards the shape obtained for pure **8CB** (see Figure 1 in Ref. 121). The isotherm of sample of a 1:27 ratio had a characteristic plateau, which corresponded to the formation of a trilayer film of **8CB**. In case of an isotherm of a 1:1 sample the character of the curve was predominantly determined by the compression of a film of **Au NPs**; no plateau was visible.

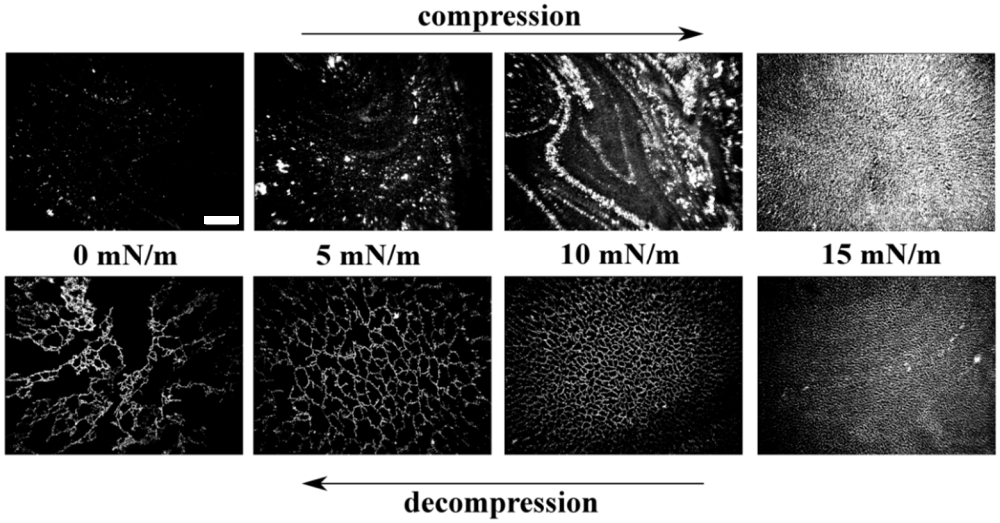

Figure 42 BAM pictures of a film of a mixture of **Au NPs** and **8CB** of composition 1:9. The net-like structure is visible only during the decompression. Scale bar 500 μm.

The brighter domains observed in the BAM images corresponded to the more reflective regions, populated by the **Au NPs**.[263] BAM images were captured in real time during. Exemplary BAM pictures taken during compression/decompression cycle (film of a 1:9 mixture) are shown in **Figure 42**. The morphology observed during compression did not differ from the one for pure **Au NPs** spread at the air/water interface (for comparison see **Figure 7b**). The BAM pictures shown in the bottom row of **Figure 42** revealed the formation of the net-like structure of **Au NPs** in **8CB** matrix during decompression. The film was initially compressed to 18 mN m^{-1} and then immediately decompressed. The net-like structure was visible in BAM pictures during the decompression starting from around 15 mN m^{-1}. It was not visible in range of surface pressure from 18 mN m^{-1} to 15 mN m^{-1} due to the limited resolution of the used equipment. This was overcame by using SEM. Very similar patterns of far smaller unit cells were observed, when the samples were transferred at surface pressures

up to 17 mN m^{-1}. However, initial compression to higher values of surface pressure (at least 18 mN m^{-1}) was needed.

The SEM images of mixtures of different compositions are presented in **Figure 43**. The films were transferred according to the Langmuir-Blodgett method. Films were initially compressed to 18 mN m^{-1} and then decompressed to the surface pressure of 15 mN m^{-1}. Then the transfer was started after a time interval of 3 minutes. The SEM images of films prepared from mixtures of composition ratio 1:6 (**Figure 43c**) and 1:9 (**Figure 43d**) revealed the net-like structure of **Au NPs** of very similar morphology as that observed with use of BAM. As the amount of **Au NPs** in the mixture increased, aggregates started to appear and the structure was strongly deformed (**Figure 43a** and **Figure 43b**). On the other hand, in case of a film of composition 1:27 (small amount of **Au NPs**) the net units were open and not well marked (**Figure 43e**).

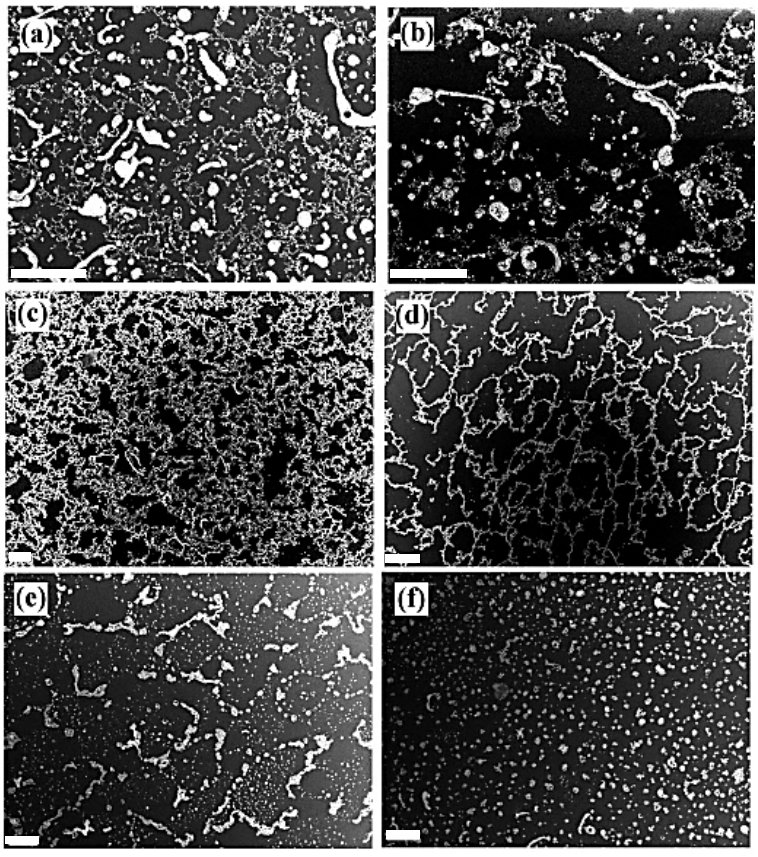

Figure 43 SEM pictures of films transferred at 15 mN m^{-1} of **Au NPs** and **8CB** mixtures of different compositions: **a)** 1:1, **b)** 1:3, **c)** 1:6, **d)** 1:9, **e)** 1:27 compressed initially to 18 mN m^{-1} and **f)** 1:9 without initial compression and no time interval before the transfer. Scale bar represents 20 μm.

SEM picture of a film transferred at 15 mN m^{-1} without initial compression step and no time interval is shown in **Figure 43f**. The sample prepared according to such protocol corresponded to the structure of the film observed during compression (see **Figure 42**). No net-like structure was detected, which was in line with the BAM observations. The net-like structure was not present during the compression step, up to approximately 18 mN m^{-1}. In case of a film transferred immediately after reaching the target surface pressure of 18 mN m^{-1}, the **Au NPs** were relatively densely distributed at the surface. It was difficult to determine whether the net-like structure was present. If this was the case, the size of a unit cell of the net was very small – in the range of dimensions of the net "frames" composed of **Au NPs** (**Figure 45a**). Therefore any kind of structure was practically undistinguishable.

The influence of time interval between reaching the target pressure and transfer was investigated. The films were transferred onto solid substrates without the initial compression above the target surface pressure (equal 15 mN m^{-1}). The films were conditioned at such pressure, prior to the transfer, for a certain period of time. The pictures in **Figure 44** show the evolution of morphology towards the net-like structure. SEM pictures of films of composition ratio 1:9 after 10 to 90 minutes of time interval prior to the transfer are presented.

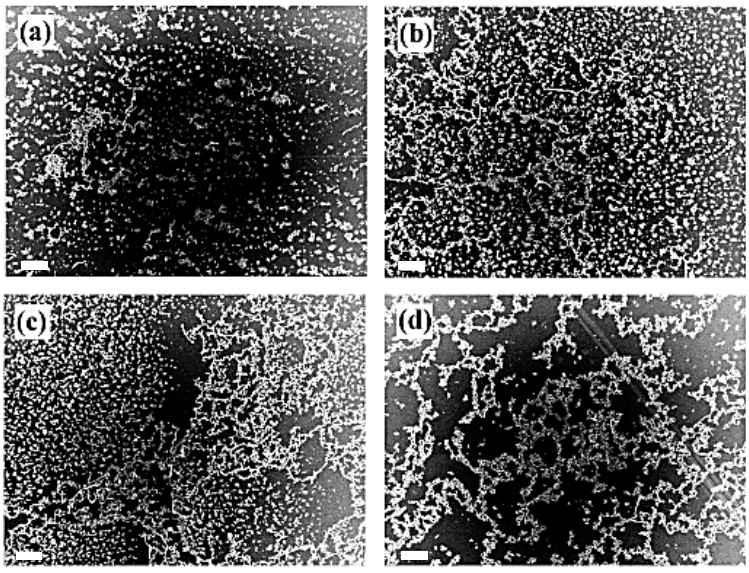

Figure 44 SEM images of films of 1:9 composition transferred after **a)** 10 min, **b)** 30 min, **c)** 60 min, **d)** 90 min of conditioning at a surface pressure equal 15 mN m^{-1} without initial compression; scale bar 20 μm.

Presence of organic compounds (**8CB** and thiols at the **Au NPs** surface) might be undesirable for further usage of the surface covered with **Au NPs** net-like structure. Therefore the samples

were dipped in the $NaBH_4$ solution for 2 hours. Such preparation was recognized to reduce the S-Au bonds. This procedure resulted in a bare gold surface without any organic residues. The net-like patterns were preserved (**Figure 45b**).[264]

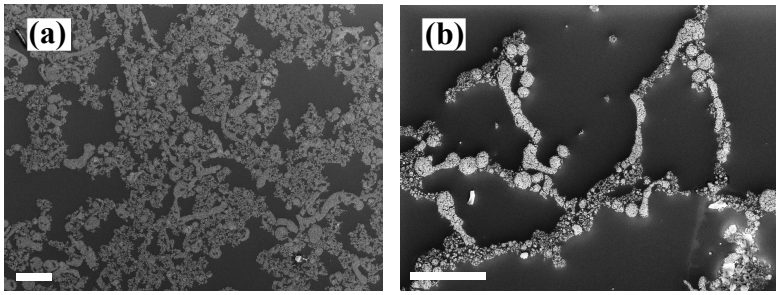

Figure 45 SEM images showing **a)** net-like structure transferred at 18 mN m^{-1} and **b)** net-like structure shown in **Figure 43d** after treatment with $NaBH_4$. Scale bars 10 µm.

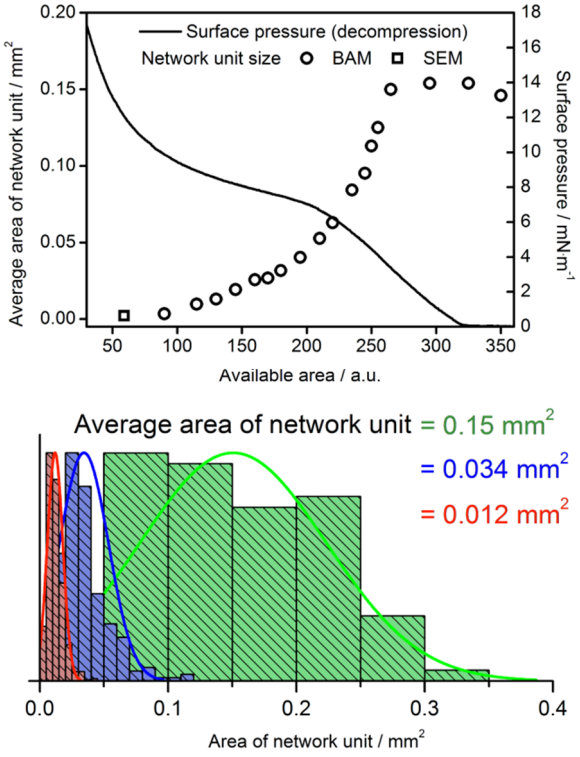

Figure 46 Average size of a unit of a net-like structure versus area of the water subphase upon decompression of a film of mixture of composition 1:9 from 15 mN m^{-1}.

During the decompression process the area of the unit cell of the net-like structure increased, as could be noticed in **Figure 42**. Therefore the morphology of the films was controlled not only by means of the composition ratio of the **8CB** and **Au NPs** mixture. Also the surface pressure during the decompression and available area of the subphase influenced the morphology of the films. The average area of the net unit cell within the film of composition

ratio 1:9 during the decompression from 18 mN m^{-1} was determined. The decompression started just after reaching the surface pressure of 18 mN m^{-1}. The barriers moved at a speed of 4 cm^2 min^{-1} (the slowest possible). The result of analysis of unit cell size correlated with the $\pi(A)$ decompression curve is shown in **Figure 46**. The first point at the plot was based on the analysis of the SEM picture of the film transferred onto solid substrate at 15 mN m^{-1}. Further analysis was based on the BAM images. The increase of the average size of the net unit cell could be stopped at desired positions of the movable barriers.

In the beginning of the decompression process the single cell of the net grew and the "frames" were thinning. At some point the net units began to merge. There was a limit of the expansion of the structure (maximal average area of the unit cell was around 0.15 mm^2). The histograms show a significant increase of polydispersity of the unit cells upon decompression.

XRR pattern was recorded for film of composition ratio 1:9 transferred at 15 mN m^{-1} after initial compression to 18 mN m^{-1} (**Figure 47**). The CPK model was used for determination of the simulation starting parameters based on the dimensions of **8CB** and the organic shell of the **Au NPs**. Additionally the radius of the metallic core of the gold nanoparticles was kept constant and equal to the value obtained from SAXS measurements. The starting parameters could vary only in a reasonable, restricted range (±10%) Only the density of the sublayer of the metallic core of **Au NPs** was not restricted at all. Three different models of molecular arrangement of the net-like structure were tested: 1) the **Au NPs** were in contact with the surface of the substrate, 2) the **Au NPs** were placed on the top of a monolayer of **8CB**, 3) the **Au NPs** were placed on the top of a trilayer of **8CB**.

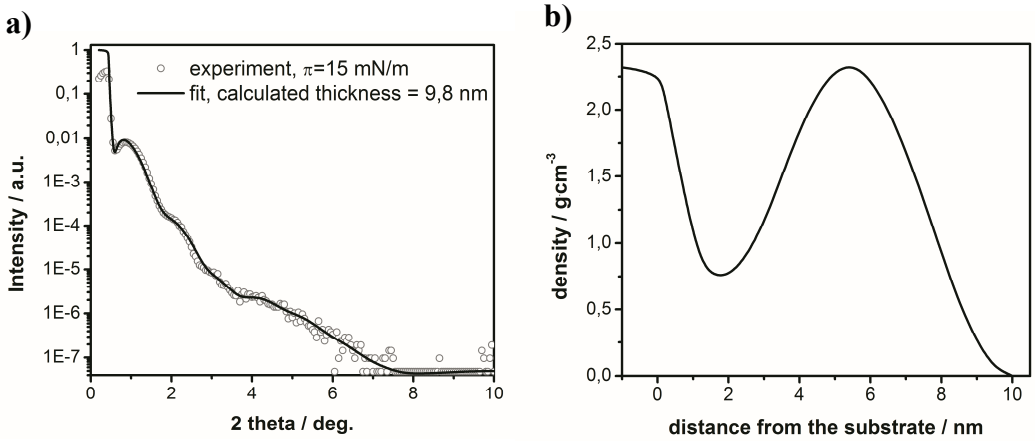

Figure 47 a) Open circles – XRR profile of sample of mixture composition 1:9 transferred at 15 mN m^{-1}; solid curve – simulated curve, **b)** density profile used for XRR pattern simulation, corresponding to **Au NPs** located on the top of **8CB** monolayer.

The best fit was obtained in case of a model that assumed **Au NPs** placed on the top of the monolayer of **8CB**. The film thickness (9.8 nm) was greater than the dimensions of the nanoparticles (8.9 nm). The maximum density of the metallic core sublayer was found at a distance of 5.4 nm from the substrate. This was where, on average, the centers of the **Au NPs** were located. Therefore the distance from 5.5 nm to 9.8 nm from the substrate surface (*i.e.* 4.3 nm) corresponded to the radius of an Au NP. Thus the thickness of the layer placed underneath the **Au NPs** was around 1.2 nm. In a fully extended conformation the **8CB** molecule is around 1.8 nm long. Therefore some interdigitation of aliphatic chains of **8CB** and organic shell of **Au NPs** was observed.

The lifting of Au NPs during the net-like structures formation was observed previously by Hansen *et al.*[258] This observation is discussed in more detail later as a part of the discussion on the mechanism of formation of the **Au NPs** net-like structures (**Chapter 4.3**).

Moreover, detailed studies on the distribution of the nanoparticles within a composite film were performed. XRR was an optimal technique for such investigations due to its sensitivity to electron (and hence mass) density variations perpendicular to the solid substrate. As a result of fitting of XRR patterns, the density of the Au NPs sublayer was obtained.[244] In case of a perfect coverage of the surface with gold, this value should be equal to the density of gold. The value of the simulated density of the gold sublayer corresponded to the decrease of the coverage of the surface with **Au NPs**. Influence of the presence of the organic moieties at the same distance from the substrate as the metallic core was practically neglectable. The value of density of the **Au NPs** sublayer was compared with the expected density for a single layer of **Au NPs**. The value 2.3 g cm^{-3} indicated that 12% of the surface was covered with **Au NPs**. The coverage of the surface with **Au NPs** estimated from the SEM image (see **Figure 43d**) was around 13.5 % (based on the image analysis). The results obtained with use of SEM and fitting of XRR patterns were in a very good agreement.

4.3. Discussion

The Langmuir films of mixtures of **8CB** and **Au NPs** formed a net-like structure, wherein **Au NPs** aggregated around nanoparticle-free areas. The SEM images indicated that the obtained structure was uniform over large film area. Similar structures were previously found in phospholipids and polymer matrixes at the air/water interface.[258,259,260] In case of relatively small amounts of **Au NPs** incorporated within the LC matrix analysis of the $\pi(A)$ isotherms

indicated no significant alterations of compression properties and layering transitions of **8CB**. Only in such case the well-ordered net-like structures were formed. Increased amount of the **Au NPs** in the mixture led to disordered films with large aggregates. Too small amount of **Au NPs** was insufficient to form a complete net.

The gold nanoparticles acted as impurities dissolved in a 2D solvent. The limited solubility of the particles in the LC film might cause diffusion-limited growth of a fractal, net-like structure.[265] The model proposed by Hassenkam *et al.*[259] was found to work in case of hydrophobic Au NPs. The authors did not find any structure of this kind in case of mixtures of surfactants and Au NPs of increased hydrophilicity. It was explained in terms of competition of the interactions between Au NPs themselves and Au NPs and the water surface. For instance the hydrophobic Au NPs did not interact strongly with the water surface. Therefore they could be lifted and "frozen out" from the domains of the condensed phase of second constituent of the mixture. Lifting was confirmed by means of XRR measurements. The increased hydrophilicity of the Au NPs resulted in different morphology of the film. In such case the Au NPs competed for the area at the water surface with template molecules. Therefore they were not easily lifted. Amphiphilic Au NPs (15% of OH groups at the ends of coating molecules) were found not to create any net-like structures in a matrix of phospholipids.

The model presented in the aforementioned publication was still valid for system studied here. Lifting of the **Au NPs** from the water surface was observed in **8CB** (**Figure 47**), even despite the used **Au NPs** were amphiphilic. Moreover, similarly as in case of completely hydrophobic Au NPs, the **Au NPs** used during presented studies (10% of polar groups in the outer shell) tended to form rafts at the air/water interface. Such behavior indicated that the interactions between **Au NPs** were stronger comparing to interactions between **Au NPs** and the water surface.[227] Such statement raised a question: why Hassenkam and coworkers did not find the net-like structure in case of amphiphilic **Au NPs** and phospholipids mixtures? The interactions between OH groups introduced to the outer shell of the Au NPs (15% of coating thiols) were fairly strong, comparing to the interactions between phospholipid molecules and the water surface. Therefore the phospholipid could not act as a template. Au NPs were not lifted from the water surface during the compression of the Langmuir film. In presented case the balance between these interactions was different. This was because 1) different amphiphile (**8CB**) as the matrix and 2) only 10% of the thiols coating the **Au NPs** had a polar group attached at the end of the chain.

In case of phospholipids the 2D liquid expanded phase decreased in size, whereas the 2D condensed phase increased as the compression proceeded. The Au NPs were frozen out of the liquid phase and end up in the boundaries between the condensed phase domains. The analysis of the isotherms of the films of mixtures of **8CB** and **Au NPs** indicated a slightly different mechanism. The domains of multilayer stacks, and not a 2D condensed monolayer, acted as the phase that caused the net-like structures formation. Net-like structures appeared upon film compression to more than 15 mN m^{-1}. In case of mixture compositions 1:6, 1:9 and 1:27 such value of surface pressure corresponded to a point at the second slope of the isotherm, behind the plateau. It is well known and proven that the plateau in the isotherm of **8CB** corresponds to formation of a trilayer. In case of film of 1:9 composition, the observed surface coverage upon trilayer formation should equal 1:3 (**8CB** occupied 3 times smaller area than in monolayer film), *i.e.* around 25% of the surface should be covered with Au NPs. However at π = 15 mN m^{-1} the Au NPs coverage of around 13% was observed. This corresponded to a coverage ratio around 1:7. Not all of the **8CB** molecules formed densely packed trilayer domains in the observed film. This could be easily explained by the fact that the net-like structure was decompressed (from 18 mN m^{-1}) prior to the transfer (at 15 mN m^{-1}). As a result, a decrease in density of the packing of the molecules was observed. Therefore the densely packed trilayer film should not be observed. Rather a coexistence of a trilayer and a monolayer film of **8CB** as a matrix for the structure of **Au NPs** should be expected. The fitting of XRR profile indicated that the **Au NPs** were lifted from the surface by around 1.2 nm. Therefore **Au NPs** were placed on the monolayer of **8CB** and the particle-free cavities were filled with the trilayer domains of **8CB** of rather loose compaction of molecules.

The **Au NPs** surface coverage in case of sample of composition ratio 1:9 transferred at 18 mN m^{-1} reached a value of around 28% (**Figure 45b**). As was already mentioned, in case of formation of a trilayer film of **8CB** at the whole available area of the water surface, the **Au NPs** surface coverage should equal 25%. The observed, higher value indicated that the **8CB** exhibited a layering transition to thicker films. Such behavior of **8CB** was previously recognized.[121,129] The second plateau at the $\pi(A)$ isotherm was not visible as the **Au NPs** altered the compression properties of the composite film. The effective surface fraction of **Au NPs** was larger in case of multilayer films of **8CB**, and determined the properties of the composite **Au NPs/ 8CB** multilayers films.

Overall, the process of the formation of **Au NPs** net-like structures required the initial compression of the films of **Au NPs** and **8CB** mixtures. During this process the trilayer film of **8CB** was formed and **Au NPs** were "frozen out" and appear at the domains` border. The compression to around 18 mN $m^{-1}$ was sufficient for the process to take place. When the initial compression was stopped at 15 mN $m^{-1}$, the process took much more time. An interval of 90 minutes was needed for the **Au NPs** to rearrange and appear at the domains` border. This was probably caused by the difference in the compaction of the molecules – the higher the surface pressure was the more condensed phase was formed at the air/water interface and the faster the "freezing out" process was. The image analysis of the films of composition ratio 1:9 transferred at 15 mN m^{-1} with no initial compression with varying time interval prior to transfer (3 min to 90 min) revealed that the **Au NPs** surface coverage was almost constant even despite different morphology of the samples (see **Figure 43d**, **Figure 43f** and **Figure 44**). This confirmed 2D rearrangement ("freezing out") of the **Au NPs** during the net-like structure formation due to condensed domains formation.

The decompression of the films of studied mixtures resulted in an increase of average size of the unit cell of the structure. This was due to a layering transition within the **8CB** domains, *i.e.* formation of a monolayer from thicker stacks. As a result, the **8CB** molecules occupied a larger area. Due to the decompression of the multilayer stacks the average area of unit cell could increase by factor smaller than 10 (depending on the number of layers in multilayer stacks). However, SEM and BAM observations revealed an increase of the unit cells from around 2200 μm^2 (at 15 mN m^{-1}) to around 0.15 mm^2 (at 0 mN m^{-1}). This implied an increase of the unit cell by a factor of around 70. Such effect was caused by further decompression of the **8CB** monolayer from 2D solid to a 2D liquid phase. The process of unit cells growth stopped at some point (see **Figure 46**) – probably when the 2D gaseous phase of **8CB** appeared.

4.4. Conclusions

This study presents a systematic investigation of self-assembly of amphiphilic **Au NPs** in a liquid crystalline matrix of **8CB** at the air/water interface. The Langmuir films of mixtures of **8CB** and **Au NPs** formed a net-like structure, wherein Au NPs aggregated around **Au NPs** free areas. The net-like patterns appeared due to the initial compression to at least 18 mN m^{-1}, as a result of formation of condensed phase of domains of a multilayer film of **8CB**. The

nanoparticles acted as impurities in the liquid crystalline matrix and were “frozen out” to the edges of the LC domains. At lower surface pressures such process was very slow.

An analogous mechanism of formation of net-like patterns was reported previously for hydrophobic Au NPs. Its validity was hereby confirmed also in case of amphiphilic **Au NPs** (with 10% of charged ligands). The average size of the unit cell proved to be fully controllable during film decompression. The net-like patterns of the desired average unit cell area were easily and effectively transferred onto a solid substrate with use of the Langmuir-Blodgett technique. SEM images indicated that the structures were uniform over large areas.

5. Results: Three steps of hierarchical "bottom up" self-assembly towards stable and efficient SERS platform

Introduction of the significant enhancement of the intensity of the vibrational spectra by a rough metal surface transformed Raman spectroscopy into an ultra-sensitive, ultra-rapid and universal analytical technique.[266] The typical enhancements obtained due to this phenomenon were in the range of 5 to 8 orders of magnitude compared to regular Raman signal. Higher values, up to 10^{14} were reported in case of single molecule Surface Enhanced Raman Spectroscopy (SERS). Such strong signal came from molecules located in the "hot spots".[267] Although SERS was discovered more than 30 years ago,[268] the dramatic increase in research activity in this field occurred very recently, mostly due to development of nanotechnology and improved instrumentation. Proper design of the platforms – surfaces, on which measurements were performed – was the key factor for the practical use of SERS. Although a number of excellent reviews discussed the considerable progress that has been made towards improving and optimizing SERS substrates,[269] the construction of ultra-sensitive, stable and highly reproducible SERS substrates still remains a challenging problem. Carefully designed nano- and microstructures easily assembled in "bottom-up" processes can be one of its best solutions.

The platform based on **Au MFs** deposited on flat surface, which was developed in Department of Soft Condensed Matter IPC PAS by Katarzyna Winkler, was SERS active and reproducible, however relatively unstable and difficult to handle. The reason why much effort was done to introduce three steps of material preparation and to optimize parameters of each of them, was to reach the desired balance between stability and enhancement factor of the SERS platform. **Au MFs** deposited on a flat surface were SERS active, yet unstable. **Au MFs** deposited on a surface covered completely with **GaN** nanowires were stable and reproducible, but enhancement factor dropped to around 10^2. Therefore scaffold of **GaN** nanowires, which covered only some part of the substrate, was chosen for new SERS platforms based on **Au MFs**.

5.1. SERS platform fabrication – three steps of "bottom up" self-assembly

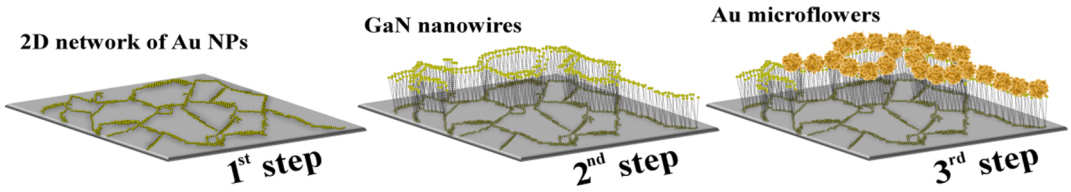

Figure 48 Cartoon showing three steps of SERS platform preparation

5.1.1. 1st step – Net-like patterns of Au NPs

Formation of 2D pattern of Au NPs on solid substrate was a first step of the hierarchical self-assembly of SERS platform preparation. The Langmuir-Blodgett technique was used to deposit the Au NPs onto a silicon wafer. First Langmuir films of pure **Au NPs** were transferred. The Au NPs formed two dimensional droplets. Upon compression the **Au NPs** surface coverage increased. Eventually the droplets merged. Films were transferred at surface pressures ranging from 1 mN m^{-1} to 39 mN m^{-1}. By changing the surface pressure at which the transfer was performed, the fraction of surface covered with gold was adjusted. Since used **Au NPs** had amphiphilic character they were easy to handle in Langmuir-Blodgett experiments (see Experimental section).

Transfer of films of pure **Au NPs** even at very low surface pressures resulted in minimal surface coverage of around 20%. To obtain smaller values mixtures of **Au NPs** and liquid crystalline amphiphilic compound **8CB** were used. The **8CB** matrix acted twofold: 1) it diluted the **Au NPs** in 2D system (decreased **Au NPs** surface coverage) and 2) induced formation of net-like patterns of **Au NPs**. The **Au NPs** behaved as impurities in liquid crystalline matrix and were "frozen out" from the condensed domains of **8CB** upon compression to at least 18 $mN \cdot m^{-1}$. As a result net-like patterns appeared. The average area of unit cell was easily controllable as the pattern expanded during the decompression of the film. The thin films of mixtures of **Au NPs** and **8CB** were described in **Chapter 4.**

5.1.2. 2nd step – GaN nanowires

Some of the possibilities of further application of net-like structures of metal nanoparticles were shown in the literature, *e. g.* a bio-detector utilizing electronic switching based on gating

by metabolic activity of yeast cells deposited on such a structure.[257] A novel route of modification of such structures transferred onto the solid substrate that could extend its possible usability is demonstrated. The CVD method was employed to grow **GaN** nanowires on the silicon surface covered with a net of **Au NPs**. The CVD process utilized gold droplets as a catalyst for **GaN** nanowires growth, due to the VLS mechanism.[161] Therefore the **GaN** nanowires appeared only where the **Au NPs** were deposited. SEM pictures of the obtained morphology after the CVD process are shown in **Figure 49a** and **Figure 49b**. Presence of organic compounds (**8CB** and thiols at the **Au NPs** surface) did not interfere with the CVD process – similar morphology for samples that were dipped in the $NaBH_4$ solution for 2 hours prior to the **GaN** growth was observed. Such preparation of the sample was recognized to reduce the S-Au bonds and resulted in a bare gold surface without any organic residues.[264]

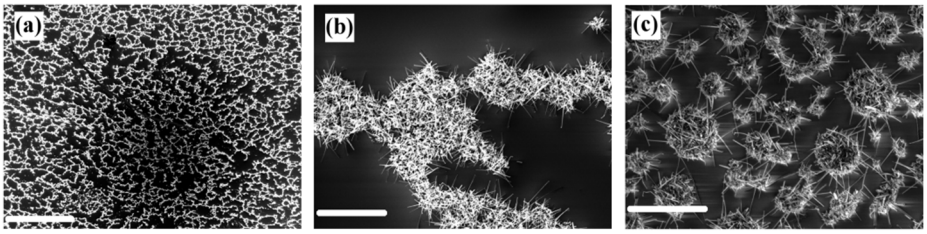

Figure 49 SEM images of the surface prepared by **Au NPs** pattern deposition followed by induced growth of **GaN** nanowires with use of CVD method. Scale bars **a)** 250 μm, **b)** 5 μm, (**Au NPs** and **8CB** mixtures – net-like patterns), **c)** 2.5 μm (pure **Au NPs** – circular domains).

5.1.3. 3rd step – Au microflowers

The third step of the nanostructure fabrication was the deposition of **Au MFs**, based on a protocol described elsewhere.[163] The morphology of single **Au MF** is shown in **Figure 50b**. The **Au MFs** were preferably deposited at the **GaN** nanowires and not in the cavities between them. This was a result of the **GaN** nanowires formation procedure which results in Au-Ga alloy droplet on the top of each nanowire.[161] **Figure 50a** shows **Au MFs** deposited on the net of **GaN** nanowires of relatively large average area, therefore the hierarchical structure is clearly visible (this sample was not used as SERS platform).

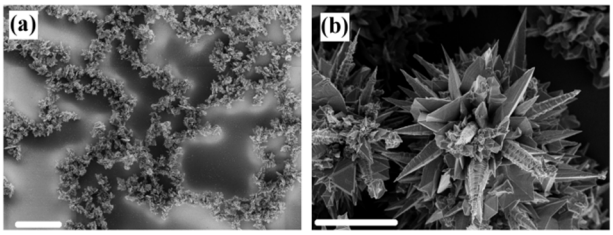

Figure 50 a) Au MFs deposited on the network of **GaN** nanowires of large average area of unit cell. The interiors of the network unit cells are empty. Hierarchical structure of the obtained material is clearly visible; scale bar 50 μm, **b)** SEM image of a single **Au MF**; scale bar 2.5 μm.

The surface coverage with **Au MFs** was easily controlled by changing the parameters of the deposition process (like time of deposition and the concentration of the solution used). It was possible to cover the obtained **GaN** scaffold completely with **Au MFs**. In such a case the morphology of the film was very similar as in samples obtained in a procedure omitting the CVD process. However, the presence of **GaN** nanowires significantly improved the stability of the **Au MFs** at the surface.

Using reaction mixtures of different concentration of reagents three different surface morphologies were prepared. The amount of deposited **Au MFs** increased from surface **a** to **c**. In case of sample **a** the amount of **Au MFs** was very limited. The **Au MFs** were located only on the **GaN** nanowires. In case of sample **c** the surface coverage was almost complete, and the **Au MFs** were deposited also in cavities of the **GaN** scaffold. The pictures **b** (surface **b**) and **c** (surface **c**) in **Figure 52** show the morphology of obtained SERS platforms.

5.2. SERS platform properties

Molecules of *p*-mercaptobenzoic acid (***p*-MBA**) were adsorbed from a 10^{-6} M ethanol solution onto prepared surfaces. SERS spectra are presented in **Figure 52**. The spectra of ***p*-MBA** were dominated by the bands around 1077cm^{-1} and 1587cm^{-1}, which were assigned to ν_{CS}, and ν_{CC} stretching vibrations, respectively (a_1 vibrational modes).[270] In the SERS spectra an apparent enhancement of the bands around 1432, 1394 and 1142 cm^{-1} (b_2 vibrational modes) was also observed. The enhancement of the b_2 modes, which were closely related to the thiol group vibrations, suggested that the ***p*-MBA** molecules were adsorbed onto the **Au MFs** film through their sulfur atoms and were perpendicular to the surface.

The main motivation to introduce the additional steps of preparation of SERS platforms based on **Au MFs** was to improve their stability and at least preserved the enhancement factor at the same level as for **Au MFs** deposited on flat surface. As reported previously such platforms were sensitive and reproducible, however they were not stable enough for commercial applications. The idea was to deposit the **Au MFs** on the **GaN** nanowires. The stability was expected to increase because the tip of the **GaN** nanowire was in fact a nucleation center for **Au MFs** growth. It appeared however that when a substrate completely covered with **GaN** nanowires was used to deposit **Au MFs** on it (**Figure 51**), the material was almost inactive as a SERS platform (*EF* did not exceed 10^2). Therefore the coverage of **GaN** nanowires was decreased to find the proper balance between *EF* (0% of **GaN**) and stability (100% of **GaN**).

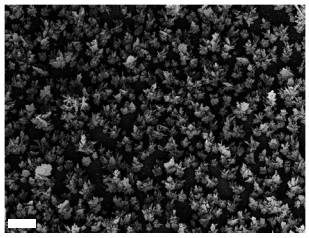

Figure 51 The morphology of the film of **Au MFs** deposited on the surface completely covered with **GaN** nanowires. Scale bar 20 μm. The **Au MFs** coverage corresponds to sample **c** (highest studied coverage). Obtained SERS enhancement factor was not higher than 10^2.

5.2.1. Optimization: Au MFs surface coverage

Au MFs were expected to be responsible for Raman enhancement. Therefore three surfaces, which differed only in the amount of applied **Au MFs** were tested. As a scaffold the net-like structure of **GaN** nanowires was judiciously chosen. **GaN** nanowires were grown on the Langmuir-Blodgett film of mixture of **8CB** and **Au NPs** transferred at 15 mN m^{-1}, after initial compression to 18 mN m^{-1} .

The highest *EF* of SERS intensity was obtained for ***p*-MBA** adsorbed on surface **c** (**Figure 52c**) – of highest **Au MFs** coverage. *EF* in this case was 7.2×10^6 and was more than 100 to 1000 times greater than for morphologies **b** and **a**, respectively. A low *EF* value was obtained on the surface **a**, characterized by the lowest surface coverage and **Au MFs**' size. The value of *EF* obtained for sample **c** was compared to the *EF* of a platform based on **Au MFs** deposited on a flat surface (around 2×10^6). The net-like scaffold of **GaN** nanowires, which

covered around 15% of the surface of the substrate, had only a minor influence on the SERS enhancement properties of **Au MFs**.

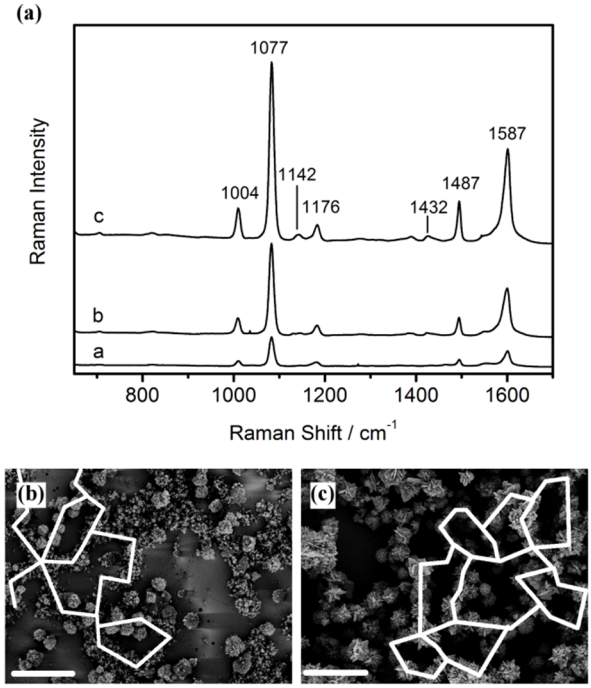

Figure 52 a) SERS measurement of ***p*-MBA** at three surfaces obtained with use of a three-step hierarchical self-assembly process. The surfaces **a**, **b**, **c** based on the 2D net of **Au NPs** (in **8CB**, transferred at 15 $mN \cdot m^{-1}$, composition ratio 1:9) with **GaN** nanowires and **Au MFs** coverage ranging from the lowest (**a**) to almost complete (**c**). The morphologies of surfaces **b** and **c** are depicted in **b** and **c** respectively; scale bars 20 μm and 10 μm, respectively. The artificial white lines correspond to the net at which the **Au MFs** are preferably deposited.

5.2.2. Optimization: stability

First the influence of GaN pattern on enhancement factor and platform stability was investigated. Afterwards, the most stable and efficient SERS platform was further tested. It appeared that obtained platform was extremely time stable and resistant for mechanical damage.

The influence of the amount of **GaN** nanowires on the SERS platform properties was evaluated. All the compared platforms were covered with **Au MFs** as surface **c** (the largest used coverage). They differed only in the pattern of **Au NPs** deposited on the solid wafer in the first step of platform preparation. Variations in **Au NPs** coverage corresponded to the percentage of area covered by **GaN** nanowires. Two parameters – *EF* and stability were

compared. As mentioned *EF* should decrease and stability increase with increasing amount of **GaN** nanowires. Therefore the balance between these two opposite features should be maintained.

The stability of prepared platforms was studied over a period of 12 days. Samples were stored in 10^{-6} M ***p*-MBA** solution at room temperature. SERS spectra were captured every 24 h from the same sample (λ_{ex} = 785 nm, t = 60 s). In **Figure 53** the stability of **Au MFs** deposited on roughened silicon and on GaN net-like scaffold is compared. The ***p*-MBA** spectral band positions and relative intensities did not vary significantly over the course of 12 days. Although the peak intensities of ***p*-MBA** on both surfaces were comparable on the first day (see inset in **Figure 53**), peak intensities for the **Au MFs** on the bare surface decreased dramatically as time passed. By the third day, the 1077 cm^{-1} peak intensity of the ***p*-MBA** diminished to the point where no data could be acquired. On the other hand the 1077 cm^{-1} peak intensity of the ***p*-MBA** on the **Au MFs/GaN** scaffold remained nearly constant over the period of 12 days.

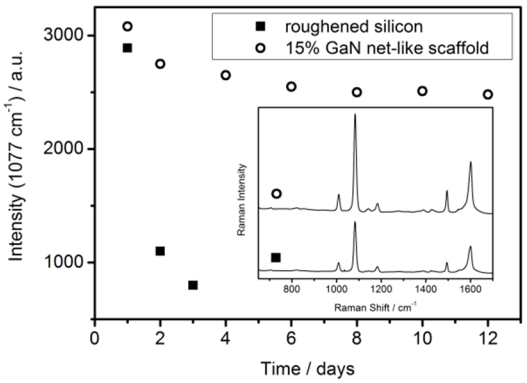

Figure 53 The peak intensity at 1077cm^{-1} of samples stored in ***p*-MBA** solution. During the 12 days of the test, **Au MFs** deposited on **GaN** scaffold remained SERS active. Inset shows the initial ***p*-MBA** spectra on **Au MFs** and **Au MFs** on the net based **GaN** scaffold.

In **Figure 54** the complete comparison of properties of **Au MFs** deposited on **GaN** scaffold is presented. The stability was determined by comparing the changes of 1077 cm^{-1} peak intensity of the ***p*-MBA** after three days of storage in 10^{-6} M ***p*-MBA** solution at room temperature. The stability is expressed as percentage of the intensity measured at third day in relation to first day.

In case of LB film of pure **Au NPs** (2D droplets) the lowest coverage was around 20%. To obtain smaller values of **Au NPs** surface coverage **8CB** as a matrix was used. The highest

Au NPs coverage of net-like pattern (in **8CB** matrix) was around 28%. The net-like patterns (**Au NPs** and **8CB**) gave better stability of the platforms than 2D droplets (pure **Au NPs**) of similar surface coverage. Here the Au NPs coverage is compared since it corresponded directly to the amount of GaN nanowires after second step of platforms preparation.

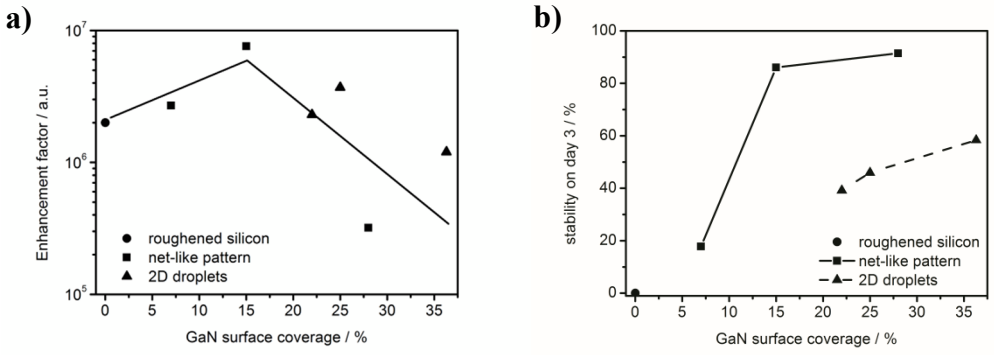

Figure 54 The comparison of properties of obtained SERS platforms as a function of **GaN** nanowires surface coverage: **a)** *EF* (line shows only trend), **b)** stability as a percentage of *EF* on day 3 in respect to initial *EF*.

To examine strength of immobilization/adhesion of Au MFs to the Si-GaN a "scotch tape" test was performed. The morphologies of the films of **Au MFs** on silicon wafer and on the **GaN** scaffold were observed using SEM before and after putting and peeling a scotch tape off it. The **Au MFs** were removed almost completely from the surface of roughened silicon. The presented material (**Au MFs**/**GaN**) was only slightly affected by the tape (**Figure 55**).

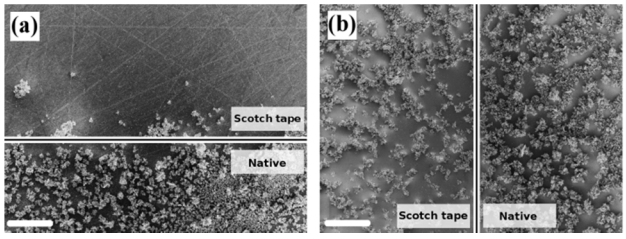

Figure 55 Au MFs deposited on **a)** roughened silicon, **b) GaN** net-like scaffold. Scotch tape had only small influence on the morphology of the studied platform. In case of roughened silicon almost 100% of **Au MFs** was removed by the scotch tape. Scale bar 50 μm.

Moreover, the obtained surfaces retained their SERS enhancement properties over time (**Figure 56**). Over a period of more than six months of storing at room temperature the enhancement factor of surface **c** (around 15% of GaN net-like scaffold) decreased very moderately, from 7.2×10^6 to 1.8×10^6.

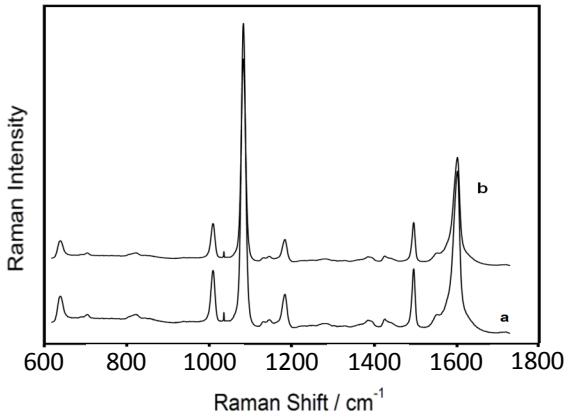

Figure 56 Comparison of SERS spectra of ***p*-MBA** recorded on **a)** of fresh platform and **b)** after six months of storage in ambient conditions.

5.2.3. Reproducibility of SERS spectra

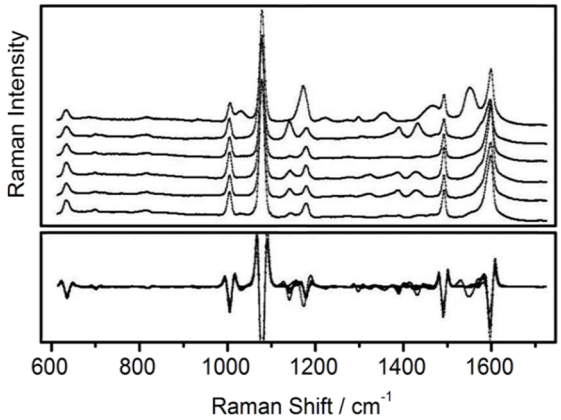

Figure 57 SERS spectra of ***p*-MBA** from six different measurements and second derivative of SERS spectra with calculated cross correlation coefficient Γ of 0.87

For all the spectroscopic experiments, presented in following parts of the chapter, the best platform was used. The highest **Au MFs** coverage (as in surface **c**) was prepared on **GaN** net-like scaffold, which covered around 15% of the substrate. A series of vertically displaced SERS spectra of ***p*-MBA** is shown in **Figure 57a**. The spectra were acquired at various positions on the same substrate and also on different substrates. In each sampled region the same modes appeared with extremely high reproducibility with only a slight variation in amplitude for some of the higher wavenumber modes. The normalized second derivatives of the SERS spectra are shown in **Figure 57b** (displayed without offset). The almost complete overlap in features observed in the second derivative spectra indicated that the differences in the SERS spectra were primarily caused by intensity and/or baseline variations. The

possibility of variations in peak positions or in relative peak intensities was excluded. A quantitative metric of the high degree of reproducibility was observed. Γ was calculated as a cross-correlation between all pairs of spectra. An average Γ of 0.87 was obtained. Similar results of excellent reproducibility were found in case of SERS spectra acquired for the other analytes (malchit green; not shown).

5.2.4. Label-free detection of DNA

To examine the viability of prepared surface as a general SERS platform for a variety of biological applications the DNA sequence was tested. Most of the methods of DNA analysis required the use of a sensitive and specific label. Often a fluorescent dyes were used, which were attached to either the 5'or 3' terminus, or to one of the bases. In the case of molecular fluorophores, overlapping spectral features and nonuniform fluorophore photo-bleaching rates led to several potential complications. The Raman spectroscopy offered a very useful alternative technique with several important advantages as an analytical tool. This method provided rapid analytical capability and allowed measuring of structural fingerprinting owing to its narrow and resolvable bands. It led to a label-free strategy based on the potentially great sensitivity of SERS.

The crucial aspects of the SERS based method of DNA detection are reproducibility and stability of SERS signals from SERS-active surfaces in time. Especially reliable reproducibility and good time stability of SERS substrates are highly important properties for fabrication DNA hybridization assay. Typical assay steps include: culturing of the sample, modification of SERS surface, immobilization of single-stranded oligonucleotide (ssDNA probe) on the modified surface, performing hybridization, washing and reading the results. The processing time can be long (up to 32h).

Figure 58 shows the SERS spectra for adsorbed $ST_{20}N2$ DNA sequence (after washing). The concentration of DNA was 10^{-6} M. The spectra were collected after 20 min, 60 min, 2 h, 6 h and 36 h of storage in ambient desktop conditions. The data in **Figure 58** contains results from the spectra of three similar experiments on different pieces of the same substrate. The SERS study revealed the excellent reproducibility and stability of our surface.

The SERS spectra of DNA display the two major bands. The 731 cm^{-1} band is assigned to a breathing mode; and the multi-component band peaking at 1330 cm^{-1} is assigned to mixed in-plane stretching motions of the six-member ring (ring skeleton vibration).[271] The intensity

of the strongest band at 731cm^{-1} was reduced approximately by only 10% after 36 hours of keeping the surface on the shelf. We cannot detect any peak shift or appreciable change of intensity of other DNA bands. These results demonstrate outstanding stability characteristics enabling clear and unambiguous detection of DNA.

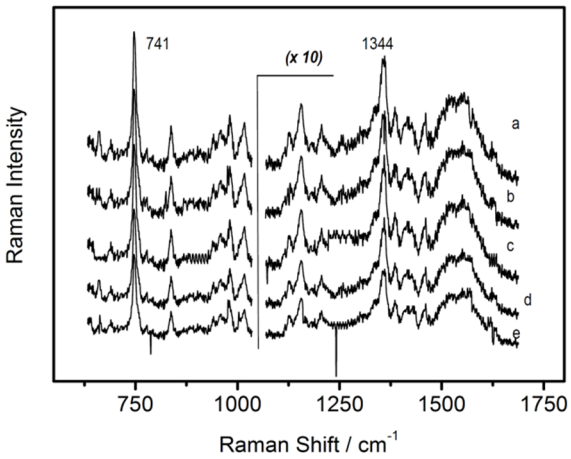

Figure 58 SERS spectra of $ST_{20}N2$ DNA sequence (SHC_6TTTTTTTTTTTTTTTTTTTTGCG GCAATCAGGTTGACCGTACATCATAGCAGGACTAGTTGGTCGCAGTC) adsorbed from 10^{-6} M concentrations obtained after (a) 20 min, (b) 60 min, (c) 2 h, (d) 6 h and (e) 36 h of storage in ambient conditions.

5.3. Conclusions

A successfully designed and conducted multi-step "bottom-up" procedure of preparation a functional surface of desired properties is presented. It is based on formation of net-like structures of **Au NPs**. **GaN** nanowires were grown on such matrix using the CVD method according to the VLS mechanism. The **Au NPs** structures acted as a catalyst, determining distribution of the **GaN** nanowires at the surface. Such scaffolds were afterwards utilized as substrates for deposition of gold microflowers. The procedure led to a new, stable SERS platform offering very good sensitivity and reliable reproducibility of results. It combined the mechanical endurance provided by the **GaN** nanowires with great enhancement factor allowed by specific distribution of gold microflowers on top of them. It was demonstrated how beneficial for the properties of the final structure the merging of different surface modification techniques was. In consecutive steps of self-assembly, relatively simple procedures can be used to obtain complex structures of controllable morphology. Selective decoration of surface with nanoscale objects and spatial control over the self-assembly process are of particular importance for material science.

6. Results: Phase transitions in monolayer formed by hyperbranched polyester with alkyl-terminated branches at the air/water interface

Molecular films of polymers spread at the air/water interface and their transfer onto solid substrates have been the subject of extensive research for many years. Thin films of polymers are used in variety of applications in the fields of optics, biosensors, coatings, microlithography and electronics. Many types of synthetic polymers and biopolymers have been studied as monolayers at the air/water interface and on solid substrates.[272] In recent years Langmuir and Langmuir-Blodgett molecular films of amphiphilic dendritic polymers have been also investigated.[276-284]

Highly branched dendritic macromolecules with a complex architecture and a large number of surface functional groups are a relatively new class of polymers. Their properties are different from those of linear polymers of the same molecular mass. Dendritic macromolecules show lower flexibility, a significant chain-end group effect, lower viscosity in solutions and a high solubility in common solvents. The two main classes of dendritic macromolecules are random hyperbranched polymers and dendrimers. As opposed to dendrimers random hyperbranched polymers are in fact mixtures of species differing in molecular weight and the degree of branching. Dendrimers and hyperbranched polymers have similar properties. Nevertheless hyperbranched polymers have more possibilities of potential applications, because they are less expensive and simple to produce.

In contrast to dendrimers, hyperbranched polymers can be easily prepared in a one-pot procedure by means of single monomer methodology or double-monomer methodology.[273] Many commercially available compounds can be used as monomers in these systems, which should extend the availability and accessibility of hyperbranched polymers with various end groups, architectures and properties.[274] The properties of hyperbranched polymers are affected by the nature of the backbone, functionality of terminal groups, the degree of branching, the chain length between branching points, and the molecular weight distribution.[275]

End-capping of the hydrophilic dendritic macromolecules with hydrophobic alkyl chains makes the modified molecules amphiphilic. These macromolecular amphiphiles form well defined monolayers both at the air/water interface and on solid substrates. Most of the

research reported in the literature concern modified dendrimers of different generations. Sayed-Sweet *et al.*[276] investigated poly (amidoamine) (PAMAM) dendrimers modified with aliphatic chains with 8, 10 and 12 carbon atoms. The authors showed that the properties of the modified PAMAM dendrimers at the air/water interface strongly depend on dendrimer generation. In their experiments the length of the terminal alkyl chains did not significantly influence the surface area occupied by the dendrimer molecules at the collapse point. The authors also proved that modified dendrimers with guest molecules placed in the interior void space were able to form monolayers at the air/water interface. Schenning *et al.*[277] investigated poly-(propylene imine) dendrimers modified with palmitoyl chains, alkyl chains containing azobenzene chromophore and adamantane. From Langmuir experiments the authors concluded that the dendrimer molecules were able to rearrange themselves to form monolayers. The dendrimer core of the molecule was in contact with the water subphase and the alkyl terminal chains were all pointing towards the air, forming a parallel – packed hydrophobic layer.

The transfer of the third-generation PAMAM dendrimer end-capped with dodecyl chains onto hydrophobic silicon wafers was investigated by Tanaka *et al.*[278] At the beginning the dendrimer molecules were in contact with the surface through alkyl chains. The authors suggested that during the drying process the silicon surface became hydrophilic. At the same time the PAMAM molecules turned upside down. Poly (propylene imine) dendrimer modified with dialkyl sulfide chains self-organized into monolayers in the same fashion as dendrimers end-capped with alkyl chains.[279] Investigations of the surface behavior of multidendron structures were also reported in the literature. Saville *et al.*[280,281] studied the structure and kinetics of surface phase transitions in monolayers formed by polyether bidendrons based on 3, 5-dihydroxybenzyl alcohol. The authors investigated the influence of the molecular weight and compression rate on the shape of Langmuir isotherms. Pao *et al.*[282] investigated second- and third-generation polyether monodendrons with end groups functionalized with hydrophobic $C_{12}H_{25}$ alkyl tails and a hydrophilic ester or crown ether in the core. X-ray reflectivity data suggested that at higher surface pressures the alkyl tails were extended and perpendicular to the surface of the water.

The structure of monolayers formed by the amphiphilic dendrimer macromolecules raises the question of the surface behavior of hyperbranched polymers. Are the similarities of

dendrimers and hyperbranched polymers big enough for polymers to form supramolecular structures at surfaces and interfaces analogous to dendrimers?

Zhai *et al.*[283] investigated the influence of the degree of hydrophobic substitution of the end groups of second generation hyperbranched polyesters on the behavior at the surfaces and the air/water interface. The polyesters were functionalized with stearic acid. The experiments showed that at high surface pressure, the alkyl tails became arranged in an up-right orientation with dense liquid-crystalline like ordering of the quasi-hexagonal type. The authors suggested that in contrast to modified dendrimers irregular branching and random attachments of the terminal alkyl tails in hyperbranched polymers prevented the formation of regular lateral ordering and crystallization of the alkyl tails within Langmuir monolayers. Ornatska *et al.*[284] investigated the formation of the monolayer at the air/water interface by the hyperbranched polymer Boltorn H40 modified with palmitoyl chloride and the transfer of the monolayer onto the silicon substrate. The polymer used in the experiments had 80 % terminal hydroxyl groups substituted with palmitic acid. As reported by the authors, the modified polyester formed a stable monolayer at the air/water interface. Uniform dense Langmuir-Blodgett monolayers with an effective thickness of 3 – 4 nm were observed for the polymer molecules transferred onto the solid substrate at different surface pressures.

The current state of knowledge leaves the influence of temperature and the length of the alkyl terminal tail on the properties of thin films of hyperbranched polymers unknown. In this contribution the surface behavior of polyester with the terminal hydroxyl end groups esterified with a mixture of eicosanoic and docosanoic acid is described. The terminal tails of the studied polyester are much longer than in the other studies reported in the literature. Presented results together with the literature reports give the opportunity to elucidate the significance of the length of the terminal alkyl tails for the process of monolayer formation. This contribution also aims at an understanding of the influence of temperature on monolayer formation by modified hyperbranched polyesters at the air/water interface.

6.1. Results and Discussion

6.1.1. Characterization of polymer

Studies presented in this chapter focused on the self-assembly behavior of hyperbranched polymer **Boltorn H3200** at the air/water interface and on solid substrates. The polymer was

the hyperbranched polyester Boltorn H30 (Perstorp AB) with terminal OH groups functionalized with a mixture of eicosanoic and docosanoic carboxylic acids. The structure of this hyperbranched macromolecule is presented schematically in **Figure 59**. The molecular mass and the number of terminal OH groups of a hyperbranched polyester depended on the degree of polymerization. The core polymer (Boltorn H30) used in this study was a third generation polyester synthesized from 2,2-bis (hydroxymethyl) propionic acid (bis-MPA) with ethoxylated pentaerythriol as the core molecule. The structure of the core polyester with the terminal OH groups was characterized by ^{1}H NMR spectroscopy. Analysis of the NMR data revealed that the polymer molecule consisted on average of 15.4 monomeric units and had 19.3 OH terminal groups. The number average molecular weight of the unmodified polymer was estimated to be 2080 g mol^{-1}. From the methylene signals of the bis-MPA the degree of branching (DB) was estimated to be 0.45. The value of DB indicated that the structure of Boltorn H30 resembled a star – like polymer. The characterization of the polyester presented here is in agreement with the literature data reported for the same material.[285,286]

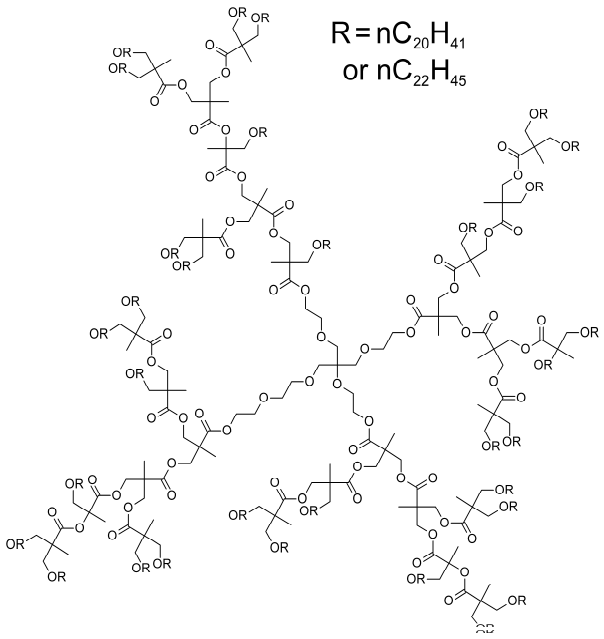

Figure 59 2D sketch of the third generation polyester with end groups modified with eicosanoic and docosanoic carboxylic acids.

The structure of polyesters with substituted terminal OH groups (**Boltorn H3200**) was also analyzed by ^{1}H NMR spectroscopy. The number of substituted terminal groups was determined. It was estimated that over 98 % of OH groups reacted. Within the accuracy of the

characterization method it was assumed that all the terminal groups of polyester H30 were esterified with the fatty acids.

^{13}C NMR spectra of polyester **H3200** in dichloromethane with the addition of $Cr(acac)_3$ were measured. From the spectra the average length of the alkyl tail attached to the terminal OH group was estimated. The terminal alkyl chain on average consisted of one methyl group and 19.5 methylene groups. ^{1}H NMR and ^{13}C NMR spectra for polymers H30 and **H3200** are not shown.

In summary the number average molecular weight of polymer **H3200** estimated from NMR measurements was 8200 g mol^{-1}. The number average molecular weight (M_n), weight average molecular weight (M_w) and polydispersity index (PI) estimated from GPC MALS measurements were 8400 g mol^{-1}, 17600 g mol^{-1}, and 2.1 respectively. The number average molecular weights obtained from NMR and GPC measurements agreed reasonably well. Throughout this study the M_n obtained from NMR analysis was used to estimate the number average surface area occupied by the polymer molecule.

6.1.2. Monolayers at the air/water interface at low surface concentrations

The hyperbranched polyester functionalized with fatty acids forms an amphiphilic compound with well-defined and separated polar and hydrophobic fragments. The internal part of the polyester molecule consists of hydrophilic carbonyl and alkoxy groups, while the terminal aliphatic chains form hydrophobic external shell. When placed at the air/water interface the internal part of the macromolecule prefers to be in contact with the water subphase. The hydrophobicity of these macromolecules depends on the length of the terminal alkyl chains.

In the experiments presented in this paragraph the behavior of the monolayers formed by the modified hyperbranched polyesters at high surface areas per molecule (low surface concentrations) was studied. The experiments were performed in the static mode, *i.e.* portions of the polymer were successively deposited on the surface of the water keeping the total surface area of the trough constant. After deposition of a portion of the polymer the system was equilibrated for a period of about 30 minutes. Then the surface pressure was measured. The results of the static mode measurements performed at room temperature (296 K) are presented **Figure 60**.

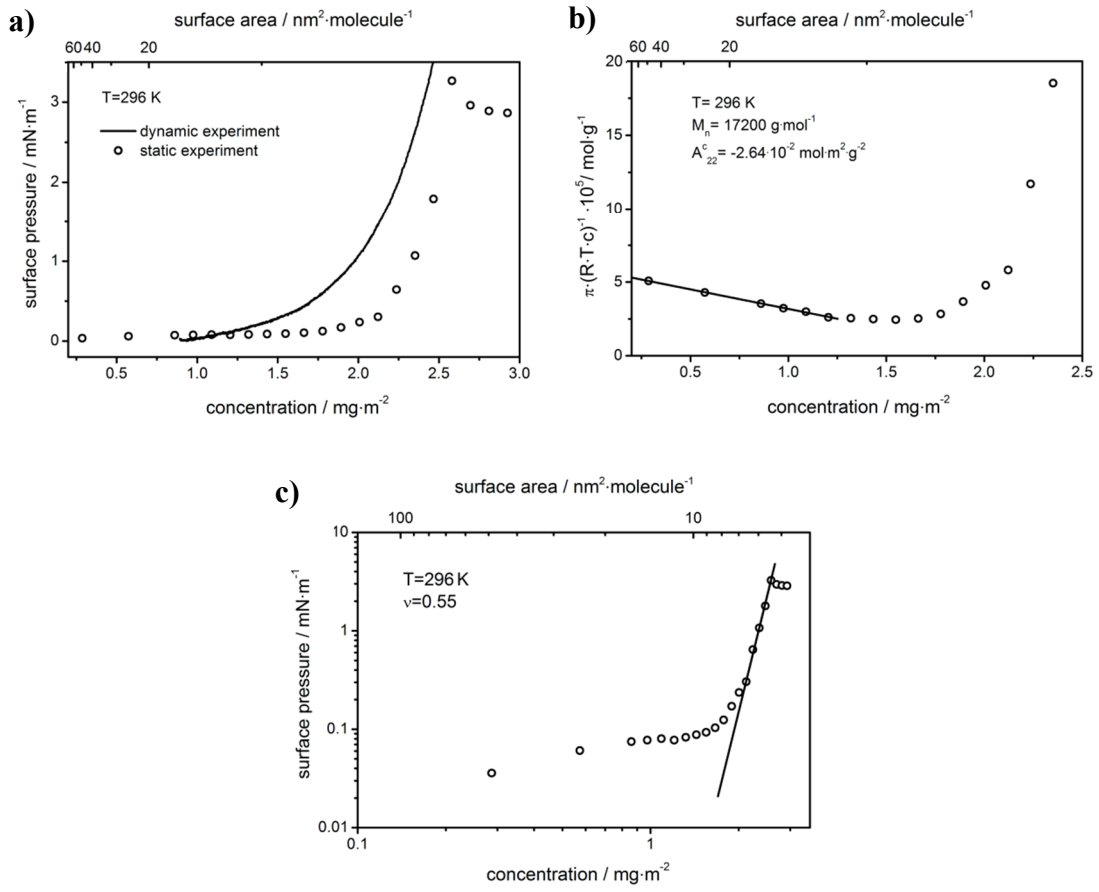

Figure 60 a) Surface pressure – surface concentration $\pi(c)$ isotherm at 296 K for polyester **H3200**, **b)** plot of π/RTc versus surface concentration, **c)** logarithmic plot of surface pressure π versus surface concentration c.

The $\pi(c)$ data obtained in the static mode (open circles) are shown in **Figure 60a**. A typical monotonic dependence of the surface pressure on the surface concentration was observed. At surface concentrations up to 1.8 mg m^{-2} (7.57 nm^2 molecule^{-1}) the changes of surface pressure on the deposition of the portions of the polymer were very small. Beyond this concentration the surface pressure started to increase and finally at about 2.5 mg m^{-2} (6.81 nm^2 molecule^{-1}) a steep surface pressure increase was observed. The crossover from the dilute (gas-like) regime to the intermediate (semi-dilute, analogue of the liquid expanded phase) regime occurred at an overlap surface concentration c^* = 1.8 mg m^{-2}. From the overlap concentration c^* obtained from the $\pi(c)$ data at a temperature of 296 K the radius of gyration R_g was estimated according to the formula:

$$c^* = \frac{M_n}{\pi R_g^2 N_A} \qquad \textbf{Equation 15}$$

where N_A – the Avogadro number. At the overlap concentration a polymer molecule occupied on average surface area of about 7.6 nm^2 and R_g was found to be 1.6 nm.

In **Figure 60a** the results of measurements performed by the dynamic method are also shown for comparison. The Langmuir isotherm obtained in dynamic mode was shifted to higher surface pressures. Similar effect was reported by Hilles *et al.*[287] In presented case the difference between the isotherms obtained by both methods was not as pronounced.

At low surface concentration, in the intermediate concentration regime $c<c^*$, the surface pressure may be expressed by a virial expansion truncated to the first order term: [288]

$$\pi = RT\left[\frac{c}{M_n} + A_{22}^c(T)c^2 + \ldots\right] \qquad \textbf{Equation 16}$$

M_n is the number average molecular weight of a chemical species present at the surface. $A^c{}_{22}$ is the second virial coefficient with the second subscript referring to the dimensionality of the system. From the **Equation 16** it is clear that both M_n and $A^c{}_{22}$ can be estimated from a plot of π/RTc versus c. This was done in **Figure 60b** where the data points of **Figure 60a** were plotted on these coordinates. The estimated number averaged molecular weight from surface measurements was about 17200 g mol^{-1}. This value was higher than the number averaged molecular weight obtained from the NMR and GPC characterizations. The effect led to the conclusion that the polymer molecules formed aggregates at the air/water interface even at very low surface concentrations. The negative sign of the surface second virial coefficient indicated that the air/water interface at 296 K was a poor solvent for the polyester **H3200**. The effect was attributed to a limited penetration of water into the polyester kernel of the polymer molecule. Strong interactions of the polyester molecules with each other and weak interactions with the water surface certainly influenced the structure of the monolayer, phase transitions occurring in the monolayer and a mechanism of a collapse.

The data presented in **Figure 60a** showed that the deposition of the next portion of the polymer at the interface above a concentration of 2.5 mg m^{-2} resulted in a lowering of surface pressure. This observation suggested that the structure of the monolayer formed above the overlap concentration finally prevented the additional portion of the material from being smoothly spread at the surface of the water. As a result the static method was not appropriate for the investigation of Langmuir molecular films of polyester **H3200** at higher surface concentrations.

The logarithmic plot of surface pressure π versus surface concentration c is presented in **Figure 60c**. The scaling theory was originally worked out for linear polymers. It predicted that within the intermediate regime (an analogue of the semi-dilute regime in bulk polymer solutions) the relation between surface pressure and surface polymer concentration could be expressed by:[288]

$$\pi \propto c^{y} \qquad \textbf{Equation 17}$$

where $y = 2\nu/(2\nu\text{-}1)$ and ν - Flory's exponent for the radius of gyration. The ν exponent obtained by fitting the experimental data to **Equation 17** was equal 0.55. This result again indicated that the air/water interface was a poor or Θ solvent for the polyester **H3200**. Thus the measurements in dilute and intermediate regimes gave consistent results.

In the above considerations validity of the **Equation 17** and the scaling theory for the hyperbranched polymers at the air/water interface is assumed. The virial expansion of the surface pressure is obtained by a purely phenomenological procedure. No information about the structure of the polymer molecules is introduced. Thus the conclusions drawn from application of **Equation 17** to the hyperbranched polyester placed at the air/water interface are entirely justified. However, the scaling theories for polymers in solutions and at interfaces are derived assuming linear structure of macromolecules. At concentrations higher than the overlap concentration the chains overlap and entangle. The behavior of hyperbranched macromolecules in solutions and at interfaces is different than linear polymers. At concentrations higher than the overlap concentration these molecules do not penetrate each other but rather contract. As a result they do not entangle and mainly interact through the terminal functional groups. Nevertheless, it seems that the scaling relation obtained for the hyperbranched polyester follow the same scaling low as found for chain macromolecules in the semi-dilute region at the air/water interface.

6.1.3. Monolayers at the air/water interface at high surface concentrations

The experiments presented in the previous paragraph (**Figure 60**) focused on the behavior of the monolayers at high surface areas per molecule (low surface concentrations). The experiments were performed in the static mode. It was shown that in these experiments the high surface concentration (low surface area per molecule) region was not accessible. Langmuir experiments in high concentration regime were performed in the dynamic mode. Langmuir isotherms were recorded with simultaneous surface potential measurements and

BAM observations. Surface pressure (π) – surface area per molecule (A) isotherms are presented in **Figure 61**.

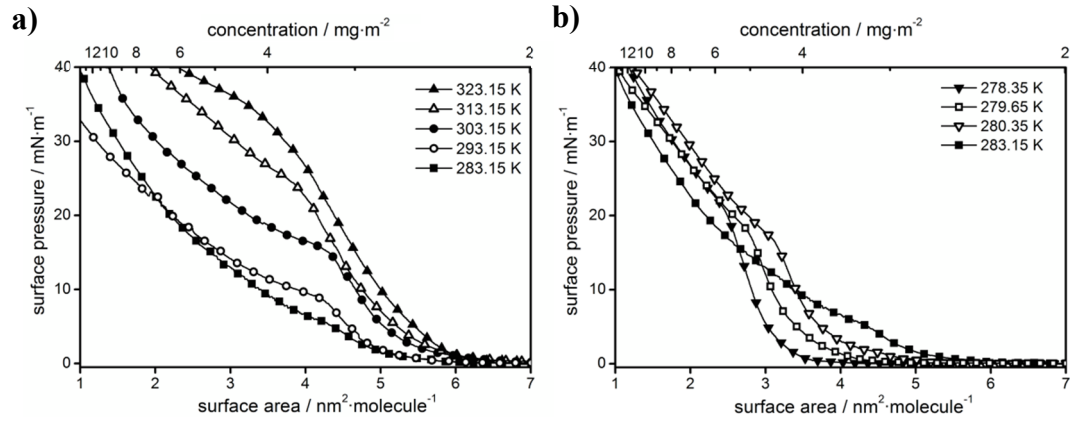

Figure 61 Surface pressure – area isotherms for polyester **H3200** at different temperatures: **a)** high and medium temperature regions, **b)** low temperature region.

All the isotherms obtained were repeatable, what was an indication that stable monolayers were formed at the air/water interface. At low surface area per molecule the surface pressure was small. The compression of the monolayer resulted in a steep surface pressure increase. Further compression resulted in a steep surface pressure increase. During this process the structure of the monolayer was changed to the liquid condensed type. Further compression caused that eventually the Langmuir $\pi(A)$ curves bent. Beyond the bend the isotherms continued with a smaller slope. All the measured $\pi(A)$ isotherms had a characteristic shape with a change in the slope occurring after the initial steep surface pressure increase.

From the course of the $\pi(A)$ curves depicted in **Figure 61** two temperature regimes were distinguished: the high temperature region (283.15 K – 323.15 K) and the low temperature region (278 K – 280 K). At temperatures equal to or higher than 283.15 K the lift-off surface area, at which the π value started to increase, slightly depended on temperature. On the contrary, the slope of the initial surface pressure increase significantly depended on temperature. In the high temperatures regime the higher the temperature the steeper was the slope of the $\pi(A)$ curves. It was also shown that lowering of the temperature from 323.15 K to 283.15 K resulted in a disappearance of the bend (*e.g.* compare the isotherms at 283.15 K and 313.15 K). Lowering of the temperature below 283.15 K gave rise to the appearance of the bend on the $\pi(A)$ curve but at much lower surface area per molecule. This temperature effect suggested that structural changes in the monolayer occurred.

At temperatures lower than 283.15 K the shape of the $\pi(A)$ curves was very similar to that observed at higher temperatures (see **Figure 61b**). There was, however, a significant difference: the lift-off surface area significantly depended on temperature (decreases with decreasing temperature), while the slope was almost independent of temperature. As it was mentioned, in this temperature region the surface areas per molecule at the bend on the $\pi(A)$ curves was much lower than those at higher temperatures. Formation of multilayered aggregates is a possible explanation of the effect. At low temperatures the aggregates were likely to form already at low surface concentrations just after deposition of the polymer at the interface.

The polar core of the polymer **H3200** molecule is flexible and the spatial arrangement of the terminal tails determines the surface area occupied by the whole molecule. Thus taking the known cross sectional surface area per alkyl chain in the monolayer state as 0.205 nm^2, one can estimate the average surface area of the polyester **H3200** molecule to be approximately 4 nm^2 $molecule^{-1}$. This is the lowest possible value of the average surface area per molecule in the monolayer formed by this polymer at the air/water interface.

In performed experiments in the high temperature region the isotherms started to bend at the surface area per molecule of about 4.5 nm^2 $molecule^{-1}$. According to above considerations, in this region all the polymers molecules were incorporated into the monolayer. Thus the onset of the bends on the isotherms corresponded to the compact arrangements of the macromolecules in the monolayer. It was a straightforward conclusion that at this point the polymer molecules arranged into monolayer started to explore the third dimension. A common name for such a process is a collapse.

The two-dimensional film on compression finally reaches its stability limit and explores the third dimension via collapse. The mechanism of the collapse was studied carefully for lipids, fatty acids, alcohols and esters.[112,289] For detailed description on this phenomenon see **Chapter 1.3.3.1.**

The $\pi(A)$ isotherms obtained for the polyester **H3200** (**Figure 61**) did not show any plateau region. Beyond the bend the isotherms showed a steady increase in the surface pressure upon compression. The shape of the isotherms indicated the change of the structure of the monolayer during the collapse. Although the hyperbranched polyester molecules resembled in some respect lipid molecules the collapse mechanism was probably different. The tendency of

the polyester molecules to aggregation and their comparatively weak affinity to the water surface, as was discussed in the previous chapter, probably gave rise to a unique mechanism of the 2D to 3D transition. The fact that polymer was multicomponent systems might also influence the mechanism of the collapse.

6.1.4. Brewster angle microscopy and surface potential

Figure 62 shows the Langmuir isotherm obtained in the dynamic mode at 296 K together with BAM images and surface potential measurements. The BAM images obtained below the bend and above the bend at the onset of collapse are shown in **Figure 62b**. The numbers in **Figure 62a** indicate the points at the isotherm at which the BAM images were taken. The BAM image taken at a surface pressure around 0 mN m^{-1} (image 1) revealed that the polymer formed pieces of the condensed phase floating at the water surface. The condensed phase formed sharp-edged panes resembling ice-floe. The islands of the condensed phase were randomly distributed in size. The panes of the condensed phase were in equilibrium with the surface gas phase at this temperature. The direct phase transition from the gas phase to the condensed phase was also observed in monolayers of fatty acids.[290,291] From the BAM images in **Figure 62b** it was concluded that the floes of the condensed phase had a uniform texture and thickness. This observation justified the conclusion that in the condensed phases the aliphatic tails were perpendicular to the surface of the water. The islands of the condensed phase merged upon compression. BAM image 2 in **Figure 62b** obtained at about 2 mN m^{-1} illustrates these processes. The increase of the surface pressure to about 3 mN m^{-1} resulted in the formation of a uniform monolayer (image 3). On further pressure increase no visible changes in the structure of the monolayer was observed. Close to the bend the process of collapse started (image 4 in **Figure 62b**). The rigid monolayer fractured along straight strips. This proved the formation of multilayered aggregates at the air side of the interface. The BAM images obtained in the static mode experiments at surface concentrations close to these marked in **Figure 62a** showed the same overall picture of the processes occurring at the interface (not shown).

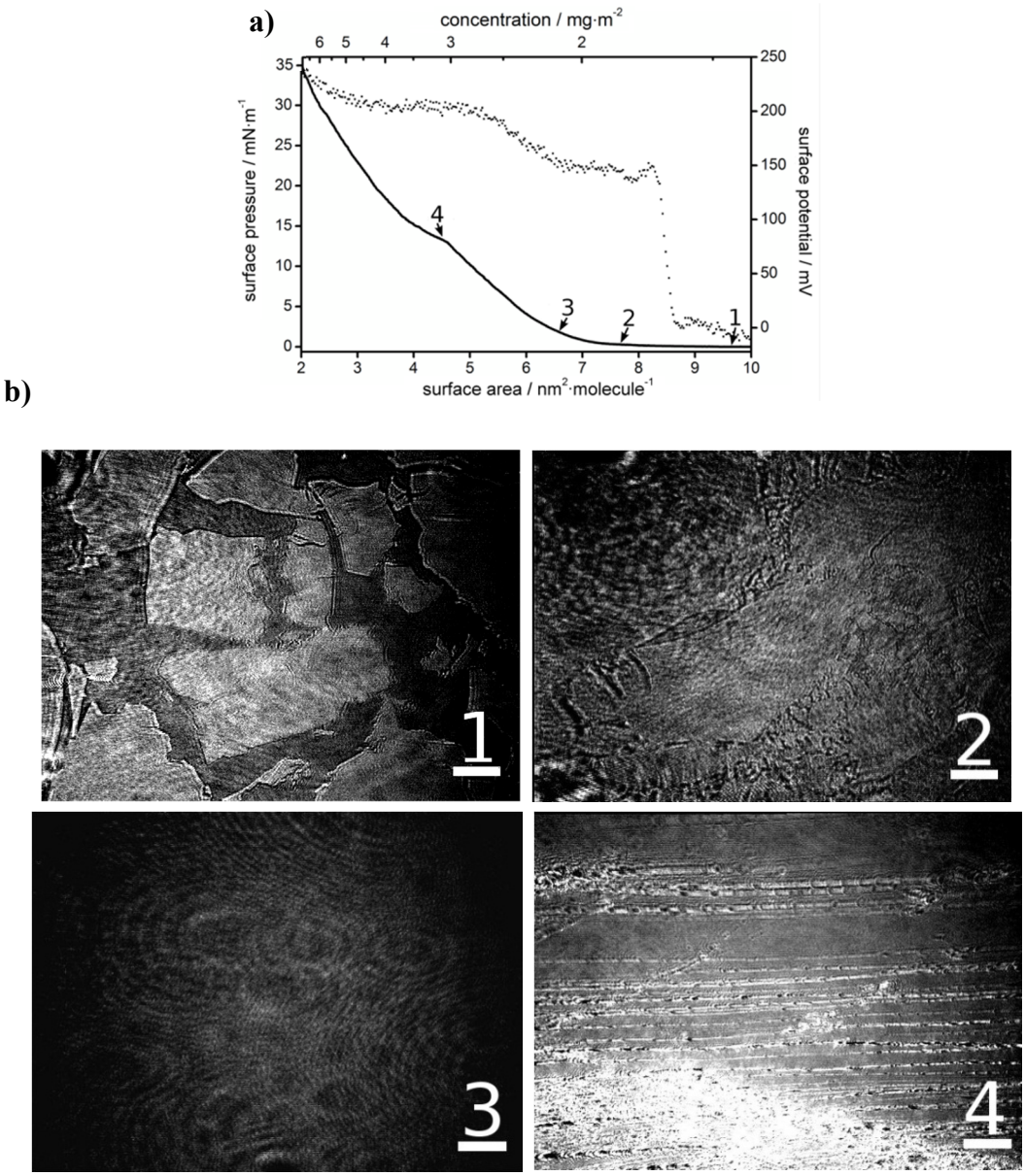

Figure 62 Surface pressure – area isotherm for polyester **H3200** at 296 K, **a)** compression pressure – area isotherm and related surface potential: solid line – Langmuir isotherm, solid points – surface potential, **b)** BAM images of **H3200** monolayers at the air/water interface for pressures indicated in picture a. Scale bars 500 µm.

The formation of panes of the condensed phase at the air/water interface is unusual for monolayers of polymers. The formation of structures of this type has been reported for long chain carboxylic acids. BAM images of monolayers of stearic acid[292] and 7-(2-antryl) heptanoic acid[293] at the air/water interface presented by Angelova *et al.*[292,293] showed similar floe-like structures as those observed in this study. In contrast to results presented here, their BAM images revealed different tilt directions of the aliphatic chains in

different panes. Comparison of obtained results with the results of Angelova *et al.*[292,293] justified two important conclusions: (1) the terminal aliphatic chains of the polymer **H3200** dominated the process of the formation of the condensed phases; (2) in the monolayer, the terminal aliphatic tails were perpendicular to the surface of water. These conclusions are in line with the literature reports.[282-284]

Simultaneously with the surface pressure the surface potential was measured using the Kelvin-electrode method. **Figure 62a** shows the course of the surface potential as a function of surface area per molecule on compression of the **H3200** monolayer at 296 K. At larger areas per molecule up to 8.5 nm^2 $molecule^{-1}$ the surface potential was small. This indicated that the panes of the condensed phase were sparsely distributed at the surface of the water. On compression the area available for the panes diminished and finally some of them enter the focal area of the electrode. At this moment a jump in surface potential was observed. On further compression the surface potential rose slowly indicating merging of the panes. The process was completed at the area per molecule corresponding to the bend on the $\pi(A)$ isotherm. Compression beyond the bend did not influence the surface potential. This behavior was consistent with the overall picture of monolayer formation by the polyester molecules described above. At higher temperatures there was no jump on the surface potential curves (not shown). Nevertheless a fast and steep continuous increase of the surface potential was observed during compression at temperatures higher than 303 K. The surface potential reached a plateau just before the bend on the $\pi(A)$ curve similar to the behavior observed at lower temperatures.

The BAM images of polyester H3200 monolayers at 279.65 K and 323.15 K together with corresponding $\pi(A)$ isotherms are presented in **Figure 63**. At low temperatures multilayered aggregates of the polymer molecules were also present at the interface, as shown in images 1 and 2 in **Figure 63b.** The BAM images of the surface phases at 323.15 K clearly showed that at very low surface pressure (image 3 in **Figure 63b**) liquid phase was in equilibrium with the gas phase at the interface. As π increased, the amount of the gas phase decreased (image 4 of **Figure 63b**). At π = 3 mN m^{-1} uniform monolayer was formed (image 5 in **Figure 5b**). Further surface pressure increase caused collapse of the monolayer (image 6 in **Figures 5b**). Since the monolayer was fluid at temperature 323.15 K, the mechanism of the collapse was apparently different than that at temperature 296 K. The BAM image 6 (**Figure 5b**) suggested that at the collapse aggregates in the form of vesicles were formed.

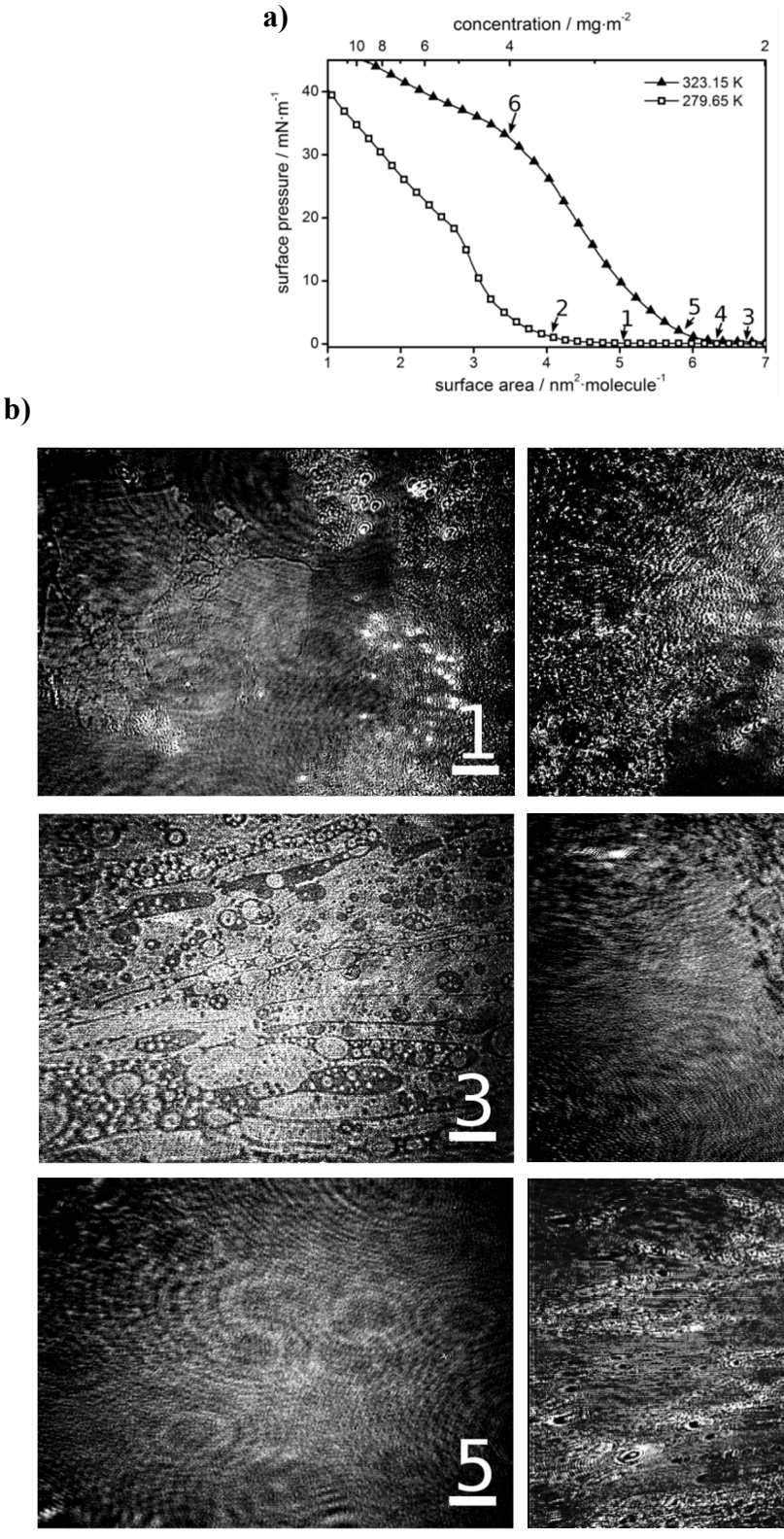

Figure 63 a) Surface pressure – surface area isotherms of polyester **H3200** measured on compression at two temperatures 279.15 K and 313.15 K, **b)** BAM images of **H3200** monolayers at the air/water interface recorded at the points indicated in **a**. Scale bars 500 μm.

6.1.5. Phase transitions

Phase transitions in Langmuir monolayers have been extensively investigated. In particular structures and phase transitions of the monolayers of fatty acids, fatty acids esters and long chain aliphatic alcohols at the air/water interface are well established.[294] For these systems gaseous, liquid expanded, liquid condensed and solid phases are observed. In the liquid condensed and solid phases molecules are aligned parallel to each other. The difference between the phases is in the orientation of the chains. They are either tilted or perpendicular with respect to the water surface. The phase transitions in monolayers of long chain amphiphilic compounds are usually of the first order. Temperatures and pressures of the phase transitions depend on the length of the alkyl tail.

Structure of molecular films formed by linear polymers at the air/water interface differs from the structure of monolayers of fatty acids. In these systems macromolecules lie flat at the surface of water and typically gel, glass, layering or liquid – solid transitions are observed. As can be expected behavior of dendritic polymers (dendrimers and hyperbranched polymers) with the terminal groups modified with alkyl tails at the air/water interface differs from the behavior of linear polymers. It has been proven that dendritic polymers form stable monolayers. However, Up to now no general view on the structure and phase transitions in molecular films formed by these molecules has been presented.

As discussed in the presiding chapter, our study of the morphology of polyester H3200 monolayers performed by means of BAM imagining showed that the morphology was similar to those observed for fatty acids. These results indicated that functionality of the terminal groups controlled the formation of the hyperbranched polyester monolayer. It was expected that the end groups functionality influenced also the surface phase transitions in the monolayers. However, the types and schemes of the phase transitions in the polyester monolayers were not necessarily the same as in the fatty acid monolayers.

The changes of the structure of the polyester monolayer with temperature at low surface pressure ($\pi \approx 0$ mN m^{-1}) were observed by means of BAM. The results are shown in **Figure 64**. The experiment was started at about 323 K. The monolayer was liquid. Then the temperature was decreased and the changes in the structure of the monolayer were detected. With temperature decreases the oval drops of the liquid phase disappeared. **Figure 64** shows an emerging condensed phase with sharp edges upon temperature decrease. There were also

voids of irregular shape seen at the interface. When the temperature reached 289.15 K panes of the condensed phase were formed. This experiment clearly showed that the phase transition in the monolayer of the polyester **H3200** at the air/water interface occurred between the liquid and the condensed phases.

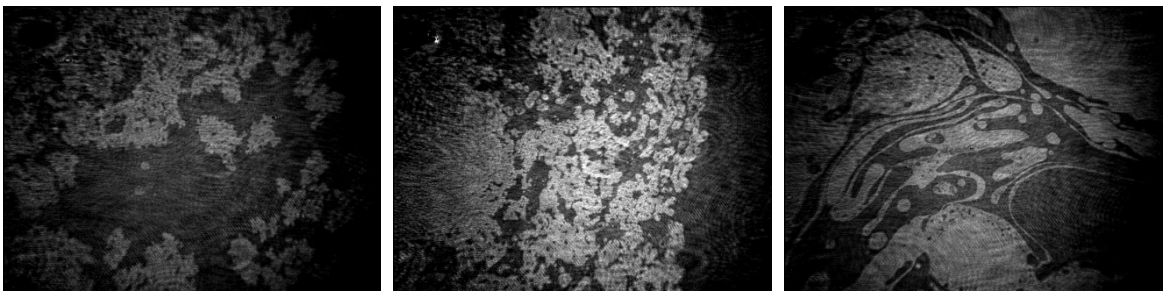

(a) 289 K (b) 313 K (c) 323 K

Temperature

Figure 64 BAM images of surface phase transition occurring with temperature decrease.

In **Figure 65** the change of surface area with temperature at constant surface pressure of about 4 mN m^{-1} is presented. A surface area per molecule step increase between 293 K and 303 K is clearly visible. This fact indicates that the phase transition in the monolayer observed on the BAM images in **Figure 64** is of the first order.

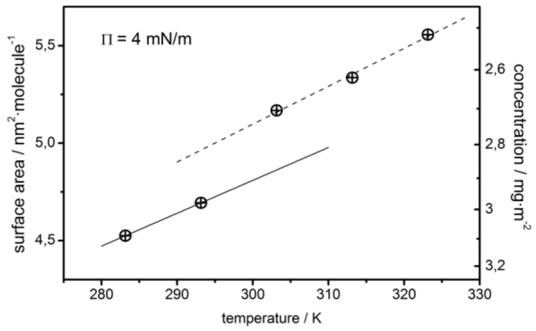

Figure 65 Surface area per molecule versus temperature at constant surface pressure of $\pi = 4$ mN m^{-1}.

Figure 66 shows the static elasticity (**Equation 6**) as a function of surface area per molecule calculated along the $\pi(A)$ isotherms presented in **Figure 61**. In all temperatures one maximum at the elasticity curve was observed. The curves started with a relatively low value at a higher surface area and in the high temperature range reached maxima at the surface area equal about 4.5 nm^2 $molecule^{-1}$. The maximum corresponded to the point of inflection on the $\pi(A)$

isotherm. At this point the molecules were in the most compact arrangement possible for the monolayer. It was also the point where collapse started giving rise to the band at the $\pi(A)$ curve. The surface area at the maximum was practically independent of temperature in the range 283 K – 323 K. Compression of the monolayer beyond the inflection point resulted in a steep decrease of the elasticity modulus as a result of the collapse. Then the elasticity modulus stabilized at low level.

The elastic modulus at the onset of the collapse was constant at temperatures in the range 323.15 K – 303.15 K. It decreased with decreasing temperature from 293.15 K to 283.15 K, then again increased with further temperature decrease below 283.15 K. The changes in the elastic properties of the monolayer corresponded to the changes of the surface area per molecule at the phase transition presented in **Figure 65**. The behavior of the elastic modulus as a function of temperature also suggested that between 293 K and 303 K the phase transition occurred.

The changes in the elastic properties of the monolayer suggested that structure of the monolayer changed and what follow the mechanisms of the collapse in the three temperature ranges were different. At the highest temperatures (323 K – 303 K) the monolayer was fluid. The surface areas corresponding to onset of the collapse in the high temperature region were about 4.5 nm^2 $molecule^{-1}$. This value indicated the compact arrangement of the polymer molecules in the monolayer at the onset of the collapse. Since the polyester molecules were not soluble in water and the interface was for them a poor solvent (as shown in the previous chapters), it was plausible that over this temperature range the collapse occurred via buckling. This was consistent with the BAM observations presented in the preceding chapter.

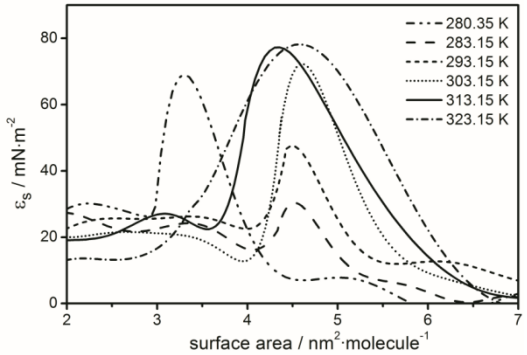

Figure 66 The static elasticity *(ε_s)* calculated along the $\pi(A)$ curves at different temperatures.

During the experiments over the temperature range 293 K – 283 K the monolayer was below the temperature of the phase transition (see **Figure 65**). In this temperature regime the polymer molecules present at the interface self-assembled into monolayer without excess of the surface pressure. Hence the surface pressure needed for the formation of the monolayer was lower and the apparent compressibility modulus was lower (higher compressibility) than for the films at higher temperatures. At temperature of about 280 K aggregation of the high molecular mass fractions of the polyester started just after deposition of the polymer solution at the interface and even before evaporation of the solvent. These aggregates built into the monolayer. In this situation the molecular film formed at the interface contained multilayer structures just from the beginning. As a result the apparent surface area per molecule was smaller than for the closed packed arrangements of the molecules in the monomolecular layer observed at higher temperatures.

Observations made on the influence of temperature on the process of spreading of the polymer solution at the air/water interface supported the presented supposition. The solution used in the experiments was stored at room temperature and not in a refrigerator, as it is usually done in case of chloroform solutions. When cooled down to about 4°C during overnight refrigeration, the solution became turbid. When used for the $\pi(A)$ measurements performed at room temperature gave isotherms strongly shifted towards smaller values of surface area per molecule. The solution removed from the refrigerator and kept at room temperature finally homogenizes. Ten minutes after clarification, the solution was deposited onto the surface of water. The isotherm recorded at 296 K (the temperature of the water subphase) resembled those recorded at 278 K. Isotherms recorded after 2, 6 and 12 hours were still shifted toward lower surface areas per molecule. Not until 24 hours after low temperature incubation were the isotherms repeatable and not shifted. Similar behavior was observed for freshly prepared solutions, for which the dissolution of the polymer through sonication of the sample was not good enough. After 10 minutes of sonication the shift of the isotherms was still observed. The experiments showed that apart from sonication it was necessary to keep the samples at room temperature at least for twelve hours to obtain repeatable isotherms. The explanation for this behavior is in line with the observations presented above. At low temperatures the aggregation of the polyester molecules occurred in the solution that is spread over the surface of the subphase. In fact it did not matter how the aggregates appear at the interface: from the spread solution; or formed due to low temperature of the subphase. The final results in both cases were the same: the three dimensional

aggregates occupied on average smaller area per molecule in comparison to molecules arranged into monolayer.

6.1.6. Reversibility of Langmuir isotherms

Figure 67 shows the compression and decompression isotherms and related BAM images at 296 K. The compression – decompression experiments clearly showed that the compression process was not reversible at this temperature.

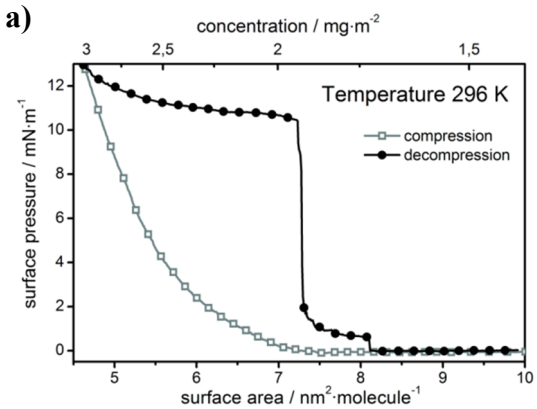

Figure 67 a) Compression and decompression $\pi(A)$ isotherms at 296 K: black solid squares and solid black line – decompression, grey open squares and a solid grey line – compression, **b)** BAM images of **H3200** monolayers at the air/water interface taken at 8 mN m^{-1} during compression (1) and decompression (2). Scale bars 500 μm.

Figure 67a shows the $\pi(A)$ curve recorded on expansion at 296 K. Expansion began at about 12 mN m^{-1}, just before the bend on the isotherm - after formation of the uniform monolayer. Expansion of the surface area from about 4.7 nm^2 $molecule^{-1}$ to 7.5 nm^2 $molecule^{-1}$ almost did not change the surface pressure. The BAM image taken during expansion did not show any detectable changes in the structure of the monolayer (image 1in **Figure 67b**). As can be seen

in **Figure 67a** the monolayer expanded beyond 7.5 nm^2 $molecule^{-1}$ cracked. At the same time a sudden drop of the surface pressure was observed. The crack of the monolayer may be clearly seen in image 2 in **Figure 67b**. The mechanism of the fracture of the monolayer during expansion could be explained as follows. During compression, just before the bend on the $\pi(A)$ isotherm, where the formation of the monolayer is completed, the polymer molecules were organized into the most compact arrangement. However, the air/water interface was not a perfectly flat plane. It fluctuated and as a result surface waves were created. The large plane of the polyester monolayer was not perfectly stiff and fluctuated along with the surface of the water. Close to the bend the monolayer was bounded by the barriers and this prevented it from breaking. When the barriers started to move back the large plane of the monolayer, still intact, but detached from the barriers, floated freely on the water surface. The surface area and the structure of the floe did not change; as a result the measured surface pressure did not change too. The movement of the barriers induced larger surface fluctuations. Now the monolayer was not supported by the barriers and the freely floating large plane of the monolayer, being fragile, finally broke into pieces. The size of the pieces depended on the size of the surface fluctuations. This reasoning was additionally supported by the fact that the breaking of the monolayer occurred at a random surface area per molecule in repeated experiments.

An experiment of expansion of the monolayer started beyond the bend was also performed. The result is presented in **Figure 68**. Expansion was started at about 15 mN m^{-1} just after the bend of the $\pi(A)$ curve. The increase of the surface area per molecule resulted in a smooth pressure decrease down to 7 mN m^{-1}. During this process, strips of the monolayer unfolded and again formed a uniform molecular film. Then the film cracked. A sudden pressure drop on the $\pi(A)$ curve was observed, similar as in the decompression experiments started before the bend. Repeated expansion experiments were qualitatively identical although the particular values of the surface area and surface pressure at the crack were different.

During the expansion experiments the surface potential remained constant at the level reached at the end of the process of monolayer formation. An example of the results is presented in **Figure 68**. The constant value of the surface potential during decompression till to a very large area per molecule indicated that the monolayer broke into floe-like pieces. At the same time the panes of the condensed phase remained in the focal area of the electrode. In each

pane the polyester molecules were tightly bounded through terminal groups and the tails remained straighten with the position perpendicular to the surface of the water.

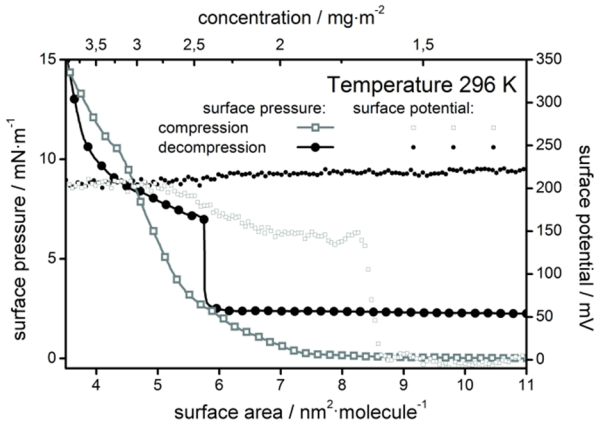

Figure 68 Surface pressure – area isotherm and related surface potential for polyester **H3200** at 296 K. Grey curves and open points – compression (grey curve and open circles – $\pi(A)$ isotherm, open squares – surface potential). Black curves and solid points – decompression (black curve and solid circles – $\pi(A)$ isotherm, solid squares – surface potential).

The influence of temperature on the shape of the expansion isotherms was also investigated. The results are presented in **Figure 69**. The difference in the course of the isotherms below and above the phase transition temperature was evident especially in the decompression run. At 296 K (**Figure 67a**) a sudden jump in the surface pressure due to fracture of the monolayer was observed. At 323.15 K (**Figure 69c**) the surface pressure decreased monotonically during expansion as it was expected for liquid monolayer. At 303.15 K and 313.15 K (**Figure 69 a** and **b**), when more time was needed for the panes to "melt" and spread over the water surface, the isotherms gradually decreased to zero surface pressure. The decompression isotherm at 303.15 K decreased very slowly since this temperature was close to the transition temperature and melting of the monolayer and spreading of the polymer molecules at the interface were very slow.

At lower temperatures the decompression curves run always above the compression isotherm. In view of the information presented in the literature the course of the decompression isotherms for the polyester monolayer is very unusual. In the ideal case, when isotherms are completely reversible the decompression isotherms follow exactly the compression $\pi(A)$ curves. It is a consequence of a perfect spread out of the molecules forming the monolayer with decreasing surface pressure. If during the decompression monolayer does not split into

separate molecules and aggregates are present at the interface, the surface pressure is lower than during the compression process at the same surface area per molecule. The effect is a result of a smaller amount of species present at the interface.

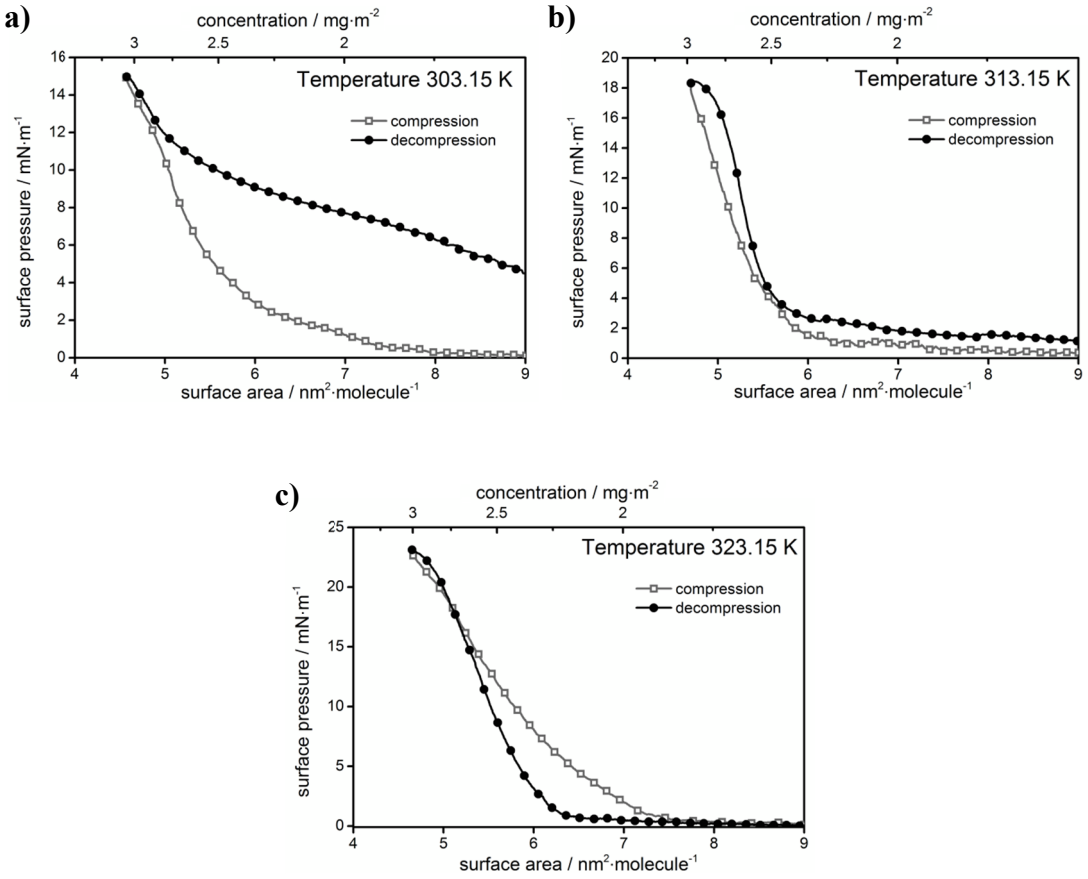

Figure 69 Compression and decompression surface pressure – surface area isotherms at three temperatures. Grey curves and open points – compression. Black curves and solid points – decompression.

The monolayer of the polymer **H3200** formed at lower temperature did not spread during decompression. It detached from the barriers and remained intact. The surface pressure remained at a high level and it was almost constant because the freely floating monolayer had the same structure as at the end of the compression process. The sudden drop of the surface pressure corresponded to the break of the monolayer into a number of small panes as was revealed by BAM observations. Such floe – like panes spread over the whole available area of the water surface. The fact that the surface pressure did not always drop to 0 mN m^{-1} might be caused by the attachment of some of smaller panes to the surface pressure sensor (**Figure 68**). The increase of the temperature resulted in improved spreading of the molecules forming the monolayer upon decompression. At 303 K the process of the spreading of the monolayer occurred. However, it was slow because the film was closed to the phase transition and just

started to "melt". As a result the decompression curve was still above the compression curve. At temperatures much higher than the phase transition temperature, *e.g.* 323 K, with decreasing surface pressure the fluid monolayer spread out at the interface like the liquid film. As a result decompression curve lied below the compression $\pi(A)$ curves (**Figure 69c**).

6.1.7. Langmuir-Blodgett molecular films

Within this study, LB-transfer of a monolayer of H3200 from the air/water interface onto silicon and mica substrates were performed. The silicon wafers and freshly cleaved mica were used. The measurements of the contact angle of a water drop placed on the surfaces indicated that surfaces of both silicon and mica substrates were really hydrophilic. The monolayers were transferred at a temperature of about 296 K during the upstroke of vertically placed substrates. The transfer of the monolayer was conducted before the onset of the collapse at π = 10 mN m^{-1}. An AFM image of the surface of the silicon substrate after the transfer of the monolayer is presented in **Figure 70**. AFM observation revealed that the prevailing part of the surface of the substrate was covered with the monolayer.

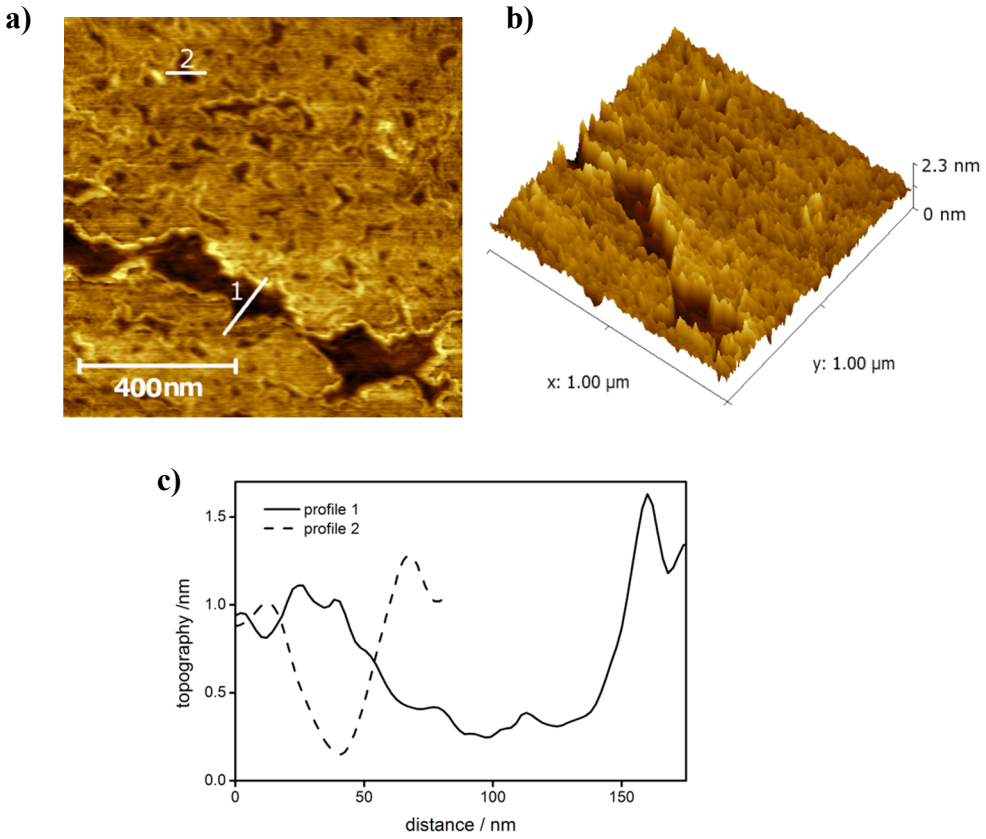

Figure 70 a, b) AFM images of the Langmuir-Blodgett monolayer for polymer **H3200** deposited at the silicon substrate at a surface pressure 10 mN m^{-1} and a temperature of 296 K, **c)** cross sections of the monolayer along the lines indicated in picture **a**.

As it is shown in **Figure 70a** the structure of the monolayer transferred onto the silicon substrate was not uniform. Upon compression the pieces of the phase formed at the interface started to interact. However, they did not merge perfectly leaving voids in the monolayer clearly visible in the AFM images. **Figure 70c** shows the height profiles along the lines indicated in **Figure 70a**. The height of the monolayer obtained from AFM measurement was about 2 nm. From the geometry of the chemical bonds in aliphatic hydrocarbons it was estimated that the length of the fully extended terminal tails in polymer H3200 was in the range of from 2.6 to 2.8 nm. It was reasonable to assume that the hydrophilic interior of the polymer lied flat on the silicon surface. Thus the thickness of the LB film of the polyester should be greater than 3 nm. In this case agreement between the experimental and the calculated height of the aggregates was poor and further investigations were needed.

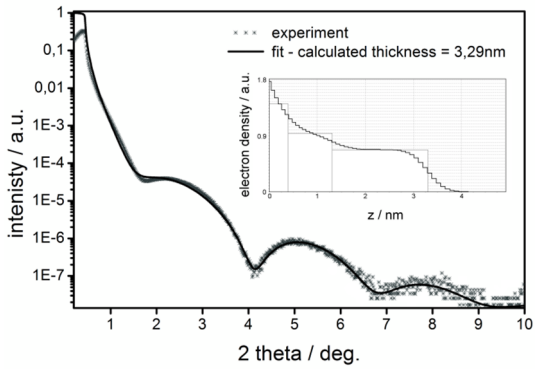

Figure 71 X-ray reflectivity data for the Langmuir-Blodgett monolayer of polymer **H3200** deposited at the silicon substrate at a surface pressure 10 mN m^{-1} and at temperature of 296 K. Grey crosses – experimental points, black curve – fit, inset shows the electron density profile used for fitting procedure.

In the next step X-ray reflectivity (XRR) studies of the sample were performed. The experimental and simulated XRR profiles are presented in **Figure 71**. Well-developed intensity curves with well-defined minima were obtained. The CPK model was used for modeling of molecular structures and estimation of molecular dimensions. The reflectivity data was analyzed using the box model of the electron density profile.[190] For the simulation purposes the polymer film was divided into three sublayers of different electron densities. The thickness of each sublayer was estimated from the geometry of the molecule. Final result of the fits gave the average total thickness of the polymer layer equal 3.3 nm. The thickness of the waterlogged part of the polyester interior was about 0.3 nm. The intermediate part of the polyester interior had a thickness of about 1 nm. The external part of the monolayer composed of the aliphatic tails had a thickness of about 2 nm. It was difficult to determine precisely the

position of the connection between the tail and the interior of the polymer. The thickness of the aliphatic sublayer was in good agreement with the length of the aliphatic tail estimated from the geometry of the hydrocarbon chain.

The transfer of **H3200** monolayer onto the mica substrate was performed at the same conditions as for the deposition of the polymer onto the silicon substrate, *i.e.* upstroke at $\pi = 10$ mN m^{-1} and at a temperature of 296 K. The AFM images of the surface of mica after the transfer showed similar morphology as in case of films transferred onto silicon. The surface was almost completely covered with the polymer monolayer of uniform thickness with some voids remaining after merging of the panes.

The monolayer was also transferred onto the silica substrate at temperature of 323 K. The transfer was conducted during the upstroke of vertically placed substrate. In the first experiment the monolayer was transferred before the collapse, at π = 27 mN m^{-1}. A noncontact AFM image of the surface of the silicon substrate after the transfer of the monolayer is presented in **Figure 72**. At this temperature the voids were also visible in the transferred monolayer. Although they were significantly smaller than those observed at lower temperature.

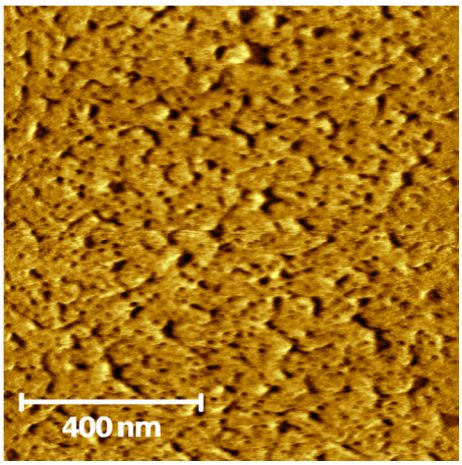

Figure 72 AFM image of the Langmuir-Blodgett monolayer of polymer **H3200** deposited at the silicon substrate at a surface pressure 27 mN m^{-1} below the onset of the collapse and a temperature of 323 K.

In the second experiment performed at temperature 323 K the monolayer was transferred after the collapse, at π = 37 mN m^{-1}. A non-contact AFM image of the surface of the silicon substrate after the transfer of the monolayer is presented in **Figure 73**. The folds (buckles)

and structures resembling vesicles are clearly seen. This observation supports the supposition that at higher temperatures folding was the mechanism of the collapse.

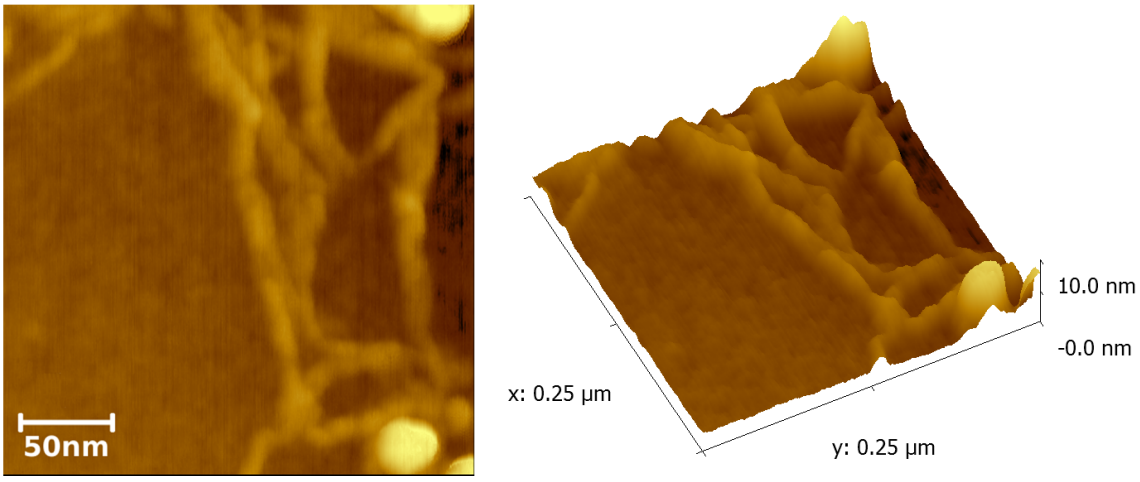

Figure 73 AFM image of the Langmuir-Blodgett monolayer of polymer **H3200** deposited at the silicon substrate at a surface pressure 37 mN m^{-1} after the collapse; temperature 323 K.

6.2. Conclusions

Langmuir film experiments at the air/water interface demonstrate that the polymer **H3200** molecules are able to arrange themselves into monolayers. The hydrophilic interior of the macromolecules is in contact with the water subphase and the alkyl chains are arranged perpendicular to the interface forming a hydrophobic layer. The self-aggregation of the polymer **H3200** molecules at the air/water interface stem from the properties of the terminal alkyl terminal groups. The structure of the monolayer depends also on temperature. At higher temperatures (> 303 K) the monolayer forms a liquid surface phase. In the temperature range 293 K – 303 K a phase transition in the monolayer occurs. The transition from a condensed surface phase to the liquid phase occurs with a step change of the surface area per molecule. This effect indicates that the phase transition is of the first order. The transition is clearly seen in BAM images and exerts influence on $\pi(A)$ isotherms, elastic modulus and course of the decompression isotherms. This type of the phase transition is for the first time found in monolayers formed by polymers.

At lower temperatures below 293 K the collapse occurs via fracturing and formation of the 3D structures at the air side of the interface. This collapse is irreversible, and the collapsed materials do not incorporate into the monolayer as the surface pressure is decreased. At higher

temperature (*e.g.* 323 K) the collapse of the monolayer occurs through the buckling mechanism. The BAM images taken at the interface and the AFM images of the collapsed monolayer transferred onto the solid substrate support this conclusion.

The polymer **H3200** monolayers were transferred onto solid substrates. The AFM images of the molecular films transferred onto the solid substrates show that the structure of the monolayer is not uniform. There are places at the surface densely covered by the polymer molecules, but also there are voids in the monolayer. The thickness of the monolayer obtained from the XRR measurements confirms that the terminal aliphatic chains of the polymers **H3200** molecules are arranged perpendicular to the surface of the substrate.

SUMMARY AND CONCLUSIONS

7. Summary and conclusions of the thesis

Thin films became the hot topic in 1920s and 1930s. Langmuir and Blodgett work in General Electric's laboratories resulted in creation of multilayer antireflective coatings on glass. The first great achievement of utilization of thin films in field of material chemistry was the world's first 100% transparent, or truly "invisible," glass. Nonreflective glass eliminated distortions from reflected light in a wide variety of optical equipment including eyeglasses, telescopes, microscopes, cameras and projector lenses. After a first wave of great interest this seemed to be the end of the development of the thin films. The Nobel Prize was awarded to Langmuir and researchers believed that nothing more was left to explore. The comeback of the surface chemistry to the mainstream of science occurred in the beginning of 1980s. Development of the experimental techniques allowed the observations of the matter down to one molecule or even atom. It became possible to study the alignment of the molecules and to control the formation of nanostructures. Thin films appeared to be important part of newly born nanotechnology.

Several research projects were described in presented thesis. Two main ideas of Langmuir-Blodgett (LB) technique were explored. First the physicochemical properties of novel classes of compounds (bolaamphiphiles and hyperbranched polymers) in 2D systems were investigated. Secondly, utilization of LB for material preparation was presented, *i.e.* fabrication of platform for surface enhanced Raman spectroscopy (SERS).

- **Chapter 3** is devoted to thin films of partially fluorinated bolaamphiphiles of different shapes. The compression/decompression cycles during Langmuir experiments were reversible and reproducible. This was caused by the reversible layering transition and formation of ordered multilayer stacks at air/water interface. In the following experiments it appeared that compression is not necessary for partially fluorinated bolaamphiphiles to form ordered trilayer films both on water and solid substrates. Such structures were prepared according to simple drop casting, due to true self-assembly. The tendency of bolaamphiphiles for self-assembly was used to prepare ordered films of gold nanoparticles.
    - **Chapter 3.2.** Layering transitions from monolayer to multilayer films were described. The monolayers did not collapse during compression. Ordered lamellar structures were formed instead. The balance between rigidity and flexibility of the molecules was the key factor opposing irreversible aggregation of the molecules. The properties of molecules

were adjusted by partial fluorination and by changing the general geometry of the molecules (X-, T- and anchor-shaped). Several peaks and plateaus were observed in the Langmuir isotherms of the investigated compounds. The first plateau always corresponded to the formation of a trilayer films. Further compression gave different results depending on the shape and degree of fluorination of the molecules. Only partially fluorinated compounds formed well defined multilayers created in reversible process. Anchor-shaped bolaamphiphiles formed a trilayer and, subsequently, a 9-layer film due to a *double roll over* mechanism. This was the first experimental proof of such subsequent process of 9-layer film formation. In contrast, when the trilayer films of X-shaped bolaamphiphiles were compressed, 5-layer and 7-layer films were created. For this process new mechanism of multilayers formation was proposed. X-ray photoelectron spectroscopy (XPS) and X-ray reflectometry (XRR) was used to evaluate the thickness and molecular alignment of the layers. Perfect fits of the XRR data to theoretical equations supported the conclusion that the multilayers were well-ordered lamellar structures. The multilayer films with a thickness of up to nine layers were transferred onto solid substrates in a single step procedure. The ordering of the films was not disturbed during the transfer. These investigations led to general understanding of multilayer formation in Langmuir-Blodgett systems. The main part of the results presented in **Chapter 3.1** was published in *Soft Matter* (**2012**). The XRR analyses constituted significant part of the publications in *Chemical Communications* (**2010**) and *Chemistry – A European Journal* (**2011**).

- **Chapter 3.3.** In the next step of studies it was found that the compression was not needed to form ordered trilayer stacks of bolaamphiphiles. Partially fluorinated bolaamphiphiles of different shapes showed a tendency for spontaneous self-assembly into well-defined layered films at the air/water interface and on solid substrates. The developed method of preparation of such films was very simple and effective. Precisely calculated volume of solution of known concentrations was spread (drop casted) directly onto the surface of water or silicon wafer. Analysis of XRR patterns revealed no differences between films prepared with use of drop casting (DC) and via typical Langmuir-Blodgett technique. However only in case of trilayer films. Irrespective of expected thickness of drop casted films only a trilayer was detected by XRR as an ordered part of the film. The excessive molecules formed random aggregates, which were located on top of lamellar trilayers. In LB experiments stacks of thickness up to nine molecular layers were found. The ordering

of the trilayer was induced by the hydrophilic surface. This influence was effective only in relatively short range. Therefore no thicker films were formed as a result of DC process. Nevertheless, such simple procedure of preparation of well-ordered thin films may significantly facilitate and improve the preparation processes of organic electronic materials. Results of this project are currently in preparation for publication.

- **Chapter 3.4.** The exceptional tendency of bolaamphiphiles for self-assembly was utilized. Drop casted films composed of mixtures of bolaamphiphiles and **Au NPs** exhibited enhanced ordering when compared to films of pure **Au NPs**. The patent application submitted to Polish Patent Office in **2011** was based on this phenomenon (*P-395009*).

- **Chapter 3.5.** The self-assembly properties of gold nanoparticles with covalently attached bolaamphiphilic ligands (**B-Au NPs**) were described. Uniform films were formed over large areas upon simple drop casting. The films consisted of densely packed nanorings of diameter of around 30 nm, with the **B-Au NPs** at the rim and an empty interior. The manuscript presenting this part of the thesis is currently in preparation for publication in *Chemical Communications*.

- In **Chapter 4** formation of net-like structures of gold nanoparticles (**Au NPs**) in a matrix of liquid crystalline amphiphile4`-n-octyl-4-cyanobiphenyl (**8CB**) at the air/water interface was described. After initial compression to at least 18 mN m^{-1}, decompression of the Langmuir film of a mixture containing both components (**8CB** and **Au NPs**) resulted in development of net-like structures. The average size of a unit cell of the net was easily adjustable by changing the surface pressure during the decompression of the film. The net-like patterns of different, adjusted average unit cell areas were transferred onto solid substrates (Langmuir-Blodgett method). SEM and XRR proved that the patterns were not disturbed over large areas of the solid substrates. XRR data revealed lifting of the **Au NPs** from the surface during the formation of the film. A molecular mechanism of formation of the net-like structures was proposed and discussed. The manuscript describing formation of net-like patterns in **8CB** matrix was recently accepted for publication in Journal of Nanoparticle Research (**2012**). Also the described method of surface coverage was submitted as patent application to Polish Patent Office in **2011** (*P-397169*).

- **Chapter 5.** Innovative application of a true “bottom-up” approach was reported. In this thesis, three consecutive self-assembly steps were utilized for the formation of complex SERS

platform. First the Langmuir-Blodgett technique was used to deposit gold nanoparticles on the solid substrate. Thus prepared surfaces were afterwards used as substrates in the chemical vapor deposition process of **GaN** nanowires growth. On such scaffolding, a third step of material fabrication was performed. **Au MFs** deposited from solution preferably appeared at the top of the GaN nanowires and not in the cavities in between. The obtained morphology of the final material was controlled at each step of the preparation process to tailor its properties for desired purposes. Prepared surfaces were tested as SERS platforms. The enhancement factor was around 10^7 in case of *p*-mercaptobenzoic acid (***p*-MBA**). Presented platforms were also suitable for biological and biomedical applications. The label-free detection of DNA was demonstrated. Obtained substrates gave the reproducible SERS spectra both across a single platform and between different platforms. The average spectral correlation coefficients (Γ) was 0.87. Moreover, the obtained material proved to be very stable. The presented complex structure demonstrated therefore advantages of the two surface functionalization concepts it comprised: 1) GaN scaffold and 2) **Au MFs** coverage. Proposed approach eliminated their major drawbacks. It combined high SERS enhancement factor of **Au MFs** deposited on flat surface and good durability of microflowers deposited on a surface completely covered with nanowires, which were almost not SERS active. First the patent application was submitted (*P-397249*) in **2011**. Very recently the results presented in **Chapter 5** were also submitted as scientific paper to *Chemistry of Materials*.

- **Chapter 6.** Langmuir and Langmuir-Blodgett molecular films of hyperbranched polyester with alkyl-terminated branches (**H3200**) were studied using surface pressure and Kelvin potential measurements, Brewster Angle Microscopy (BAM), X-Ray Reflectivity (XRR), and Atomic Force Microscopy (AFM) over a temperature range of 278 – 323 K. At the air/water interface experiments were performed using two different strategies (modes), *i.e.* static and dynamic modes. Amphiphilic hyperbranched polyesters formed stable and well defined monolayers at the air/water interface. Experiments performed at small surface concentrations (large surface area per molecule) in the static mode showed that the air/water interface was a poor or Θ solvent for polyester **H3200**. In the temperature range of 283 – 313 K already from very low surface pressures ice floe – like structures of a condensed phase were formed as revealed by BAM. The floes of the condensed phase merged at higher surface pressures and the uniform monolayer was formed. Temperature dependence of the area per molecule at constant surface pressure of 4 mN m^{-1} indicated that a phase transition occurred in the monolayer. The results of the surface pressure (π) – surface area per molecule (A)

measurements, supported by the BAM images, performed at different temperatures justified a conclusion that the phase transition from the condensed phase to a surface liquid phase occurred between 293 K and 303 K. Compression – decompression $\pi(A)$ experiments performed at lower temperatures showed that the compression process was not reversible. The $\pi(A)$ experiments performed at higher temperatures clearly showed that the compression process became reversible at 323 K. The monolayers were transferred onto silicon and mica substrates using the Langmuir-Blodgett procedure. The transferred molecular films were characterized with use of the AFM and XRR. The results obtained indicated that alkyl terminal tails of the polyester were arranged perpendicularly to surface of the substrate and the hydrophilic core of the polymer was in contact with the substrate. Results presented in this chapter were recently submitted for publication in *Langmuir*.

8. Literature

1. a) Pankhurst, Q. A.; Connolly, J.; Jones, S. K.; Dobson, J. *J. Phys. D: Appl. Phys.* **2003**, *36*, 167, b) Sun, S.; Weller, D.; Murray, C. B. *Springer Ser. Surf. Sci.* **2001**, *41*, 249, c) Murray, C. B.; Sun, S.; Gaschler, W.; Doyle, H.; Betley, T. A.; Kagan, C. R. *IBM J. Res. Dev.* **2001**, *45*, 47.
2. a) Pericet-Camara, R.; Papastavrou, G.; Borkovec, M. *Langmuir* **2004**, *20*, 3264, b) Leite, F. L.; Riul, A., Jr.; Herrmann, P. S. P. *J. Adhes. Sci. Technol.* **2003**, *17*, 2141.
3. a) Petroff, P. M.; Lorke, A.; Imamoglu, A. *Phys. Today* **2001**, *54*, 46, b) Empedocles, S. A.; Neuhauser, R.; Shimizu, K.; Bawendi, M. G. *Adv. Mater.* **1999**, *11*, 1243, c) Julien, F. H.; Alexandrou, A. *Science* **1998**, *282*, 1429, d) McEuen, P. L. *Science* **1997**, *278*, 1729.
4. a) Alkaisi, M. M.; Blaikie, R. J.; McNab, S. J. *Adv. Mater.* **2001**, *13*, 877, b) Lewis, A. *Phys. World* **2001**, *14*, 25, c) Jiang, J.; Bosnick, K.; Maillard, M.; Brus, L. *J. Phys. Chem. B* **2003**, *107*, 9964, d) Levene, M. J.; Korlach, J.; Turner, S. W.; Foquet, M.; Craighead, H. G.; Webb, W. W. *Science* **2003**, *299*, 682.
5. a) Bao, J.; Bragas, A. V.; Furdyna, J. K.; Merlin, R. *Nat. Mater.* **2003**, *2*, 175, b) Cleland, A. N.; Aldridge, J. S.; Driscoll, D. C.; Gossard, A. C. *Appl. Phys. Lett.* **2002**, *81*, 1699, c) Leuenberger, M. N.; Loss, D. *Nature* **2001**, *410*, 789 d) Bayer, M.; Hawrylak, P.; Hinzer, K.; Fafard, S.; Korkusinski, M.; Wasilewski, Z. R.; Stern, O.; Forchel, A. *Science* **2001**, *291*, 451.
6. a) Wang, W.; Lee, T.; Reed, M. A. *Phys. Rev. B: Condens. Matter* **2003**, *68*, 035416/1., Binnig, G.; Rohrer, H. *IBM J. Res. Dev.* **2000**, *44*, 279, b) Stroscio, J. A.; Eigler, D. M. *Science* **1991**, *254*, 1319.
7. a) Torchynska, T. V. *J. Appl. Phys.* **2002**, *92*, 4019 b) Yanson, A. I.; Bollinger, G. R.; Van Den Brom, H. E.; Agrait, N.; Van Ruitenbeek, J. M. *Nature* **1998**, *395*, 783.
8. Galatsis, K.; Wang, K. L.; Ozkan, M.; Ozkan, C. S.; Huang, Y.; Chang, J. P.; Monbouquette, H. G.; Chen, Y.; Nealey, P.; Botros Y. *Adv. Mater.* **2010**, *22*, 769.
9. Novoselov K. S.; Geim A. K.; Morozov S. V.; Jiang D.; Zhang Y.; Dubonos S. V.; Grigorieva I. V.; Firsov A. A. *Science* **2004**, *306*, 666.
10. Feynman, R. P. *Eng. Sci.* **1960**, *23*, 22, reprint *J. Micromech. Systems* **1992**, *1*, 60.
11. Gribbin, J.. *Richard Feynman: A Life in Science*, Dutton, **1997**, p. 170.
12. Taniguchi, N. *Proc. Intl. Conf. Prod. London, Part II British Society of Precision Engineering* **1974**.

13. a) Drexler E. *Nanosystems: Molecular Machinery, Manufacturing, and Computation. MIT PhD thesis*. New York: Wiley. ISBN 0471575186, **1991**, b) Drexler, E. *Engines of Creation: The Coming Era of Nanotechnology*, Doubleday, **1986**.
14. Zsigmondy, R. *Colloids and the Ultramicroscope*, J.Wiley and Sons, NY, **1914**.
15. Langmuir, I. *J. Am. Chem. Soc.* **1917***, 39*, 1848.
16. a) Blodgett, K. B. *J. Am. Chem. Soc.* **1935**, *57*(6), 1007, b) K. B. Blodgett, I. Langmuir, *Phys. Rev.* **1937**, *54*, 964.
17. Binnig, G.; Rohrer H. *IBM J. Res. Dev.* **1986**, *30*, 4.
18. Eigler D. M.; Schweizer E. K. *Nature* **1990**, *344*, 524.
19. *International Technology Roadmap for Semiconductors* **2005** edn, available online at <http://public.itrs.net/>.
20. *Understanding Moore's Law: Four Decades of Innovation*, ed. D. C. Brock, Chemical Heritage Foundation, Philadelphia, PA, **2006**.
21. Lu W.; Lieber C. M. *Nature Materials* **2007**, *6*, 841.
22. Balaz, P. *Mechanochemistry in Nanoscience and Minerals Engineering*, Springer-Verlag Berlin Heidelberg **2008.**
23. Levinson, H. J. *Principles of Lithography*, SPIE Press, Bellingham, WA, **2001**.
24. Alexe, M.; Harnagea C.; Hesse D. *J. Electroceram*. **2004**, *12*, 69.
25. a) Urban, G. *Sens. Actuators* **1999**, 74, 219, b) Chang H. *J. Vac. Sci. Technol.* **1975**, *12*, 1271.
26. a) Mullenborn, M.; Dirac H.; Petersen, J. W. *Appl. Surf. Sci.* **1995**, 86, 568, b) Amer, M. S.; Dosser, L.; LeClair S.; Maguire, J. F. *Appl. Surf. Sci.* **2002**, *187*, 291.
27. Junno, T.; Deppert, K.; Montelius, L.; Samuelson, L. *Appl. Phys. Lett.* **1995**, *66*, 3627.
28. Euliss, L. E.; DuPont, J. A.; Gratton, S.; DeSimone, J. *Chem. Soc. Rev.* **2006**, *35*, 1095.
29. a) Rasmussen, A.; Gaitan, M.; Locascio, L. E.; Zaghloul, M. E. *J. Microelectromech. Syst.* **2001**, *10*, 286, b) Laugere, F.; Guijt, R. M.; Bastemeijer, J.; van der Steen, G.; Berthold, A.; Baltussen, E.; Sarro, P.; van Dedem, G. W. K.; Vellekoop, M.; Bossche, A. *Anal. Chem.* **2003**, *75*, 306, c) Pandraud, G.; Koster, T. M.; Gui, C.; Dijkstra, M.; van den Berg, A.; Lambeck, P. V.; *Sens. Actuators, A—Physical* **2000**, *85*, 158.
30. a) Munson, M. S.; Cabrera, C. R.; Yager, P. *Electrophoresis,* **2002**, *23*, 2642, b) Kamholz, A. E.; Weigl, B. H.; Finlayson, B. A.; Yager, P. *Anal. Chem.*, **1999**, *71*, 5340.

31. a) Auroux, P. A.; Iossifidis, D.; Reyes, D. R.; Manz, A. *Anal. Chem.* **2002**, *74*, 2637, b) Veenstra, T. T.; Lammerink, T. S. J.; Elwenspoek, M. C.; van den Berg, A. *J. Micromech. Microeng.* **1999**, *9*, 199.

32. Dendukuri, D.; Tsoi, K.; Hatton, T. A.; Doyle, P. S. *Langmuir* **2005**, *21*, 2113.

33. Xu, S. Q.; Nie, Z. H.; Seo, M.; Lewis, P.; Kumacheva, E.; Stone, H. A.; Garstecki, P.; Weibel, D. B.; Gitlin, I.; Whitesides, G. M.; *Angew. Chem., Int. Ed.* **2005**, *44*, 724.

34. Yu, B.; Meyyappan, M. *Solid-State Electronics* **2006**, *50*, 536.

35. a) Frank, D. J.; Dennard, R. H.; Nowak, E.; Solomon, P.; M. Taur,; Y. Wong. H.-S. P. *Proc. IEEE* **2001**, 89, 259, b) Likharev, K. K. *Nano and Giga Challenges in Microelectronics* (editors J. Greer, A. Korkin, J. Labanowski) Elsevier, Amsterdam, **2003**, 27–68.

36. See articles in the *Nanoscale Materials* Special Issue, *Acc. Chem. Res.* **1999**, *5.*

37. a) Whitesides, G. M.; Mathias, J. P.; Seto, C. T. *Science* **1991**, *254*, 1312; b) Kiely, C. J.; Fink, J.; Brust, M.; Bethell, D.; Schiffrin, D. J. *Nature* **1998**, *396* 444, c) Li, M.; Schnablegger, H.; Mann, S. *Nature* **1999**, *402*, 393, d) Pileni, M.-P. *J. Phys. Chem. B* **2001**, *105,* 3358, e) Fendler, J. H. *Chem. Mater.* **2001**, *13,* 3196, f) Sanchez, C.; Soler-Illia, G. J. D. A.; Ribot, F.; Lalot, T.; Mayer, C. R.; Cabuli, V. *Chem. Mater.* **2001**, *13*, 3061.

38. Moriarty, P. *Rep. Prog. Phys.* **2001**, *64*, 297.

39. a) McEuen, P. L.; Fuhrer, M. S.; Park, H. *IEEE Trans. Nanotechnol.* **2002**. *1*, 78, b) Lieber, C. M. *Mater. Res. Soc. Bull.* **2003**, *28*,486.

40. Love, C.; Estroff, L.; A. Kriebel, J. K.; Nuzzo, R. G.; Whitesides, G. M. *Chem. Rev.* **2005**, *105*, 1103.

41. Bjørnholm, T.; Greve, D. R.; Reitzel, N.; Hassenkam, T.; Kjæer, K.; Howes, P. B.; Larsen, N. B.; Bøgelund, J.; Jayaraman, M.; Ewbank, P. C.; McCullough, R. D. *J. Am. Chem. Soc.* **1998**, *120*, 7643.

42. Bjørnholm, T.; Hassenkam, T.; Reitzel, N.; *J. Mater. Chem.*, **1999**, *9*, 1975.

43. a) Philp, D.; Stoddart, J. F. *Angew. Chem. Int. Ed.* **1996**, *35*(11), 1155, b) Lehn, J. M. *Angew. Chem. Int. Ed.* **1990**, *29*(11), 1304.

44. Hung, A. M.; Noh, H.; Cha, J. N. *Nanoscale* **2010**, *2*, 2530.

45. Fernandez-Lopez, S.; Kim, H.-S.; Choi, E. C.; Delgado, M.; Granja, J. R.; Khasanov, A.; Kraehenbuehl, K.; Long, G.; Weinberger, D. A.; Wilcoxen, K. M.; Ghadiri, M. R. *Nature* **2001**, *412*, 452.

46. Bossmann, S. H.; Janik, K.; Pokhrel, M. R.; Heinz, C.; Niederweis, M. *Surf. Interface Anal.* **2004**, 36, 127.

47. a) Hyun, J.; Kim, J.; Craig, S. L.; Chilkoti, A. *J. Am. Chem. Soc.* **2004**, *126*, 4770, b) Riemenschneider, L.; Blank, S.; Radmacher, M. *Nano Lett.* **2005**, *5*(9), 1643.

48. a) Hong, J.; Quake, S. *Nat. Biotechnol.* **2003**, *21*(10), 1179, b) Zhu, H.; Snyder, M. *Curr. Opin. Chem. Biol.* **2003**, *7*(1), 55, c) Lipshutz, R. J.; Fodor, S. P.; Gingeras, T. R.; Lockhart, D. J. *Nat. Genet.* **1999**, *21*, 20.

49. Chow, D. C.; Johannes, M. S.; Lee, W.-K.; Clark, R. L.; Zauscher, S.; Chilkoti, A. *Nano today* **2005**, 30.

50. Bisoyi, H. K.; Kumar, S. *Chem. Soc. Rev.* **2011**, *40*, 306.

51. *Handbook of Liquid Crystals*, ed. Demus, D.; Goodby, J.; Gray, G. W.; Spiess, H.-W.; Vill, V.; Wiley-VCH, Weinheim, **1998**, vol. 1–3.

52. Adamson, A. W.; Gast, A. P. Physical Chemistry of Surfaces, 6th ed.; Wiley-Interscience: New York, **1997**.

53. O'Neill,; M. Kelly, S. M. *Adv. Mater*. **2011**, *23*, 566.

54. a) Sekitani, T.; Yokota, T.; Zschieschang, U.; Klauk, H.; Bauer, S.; Takeuchi, K.; Takamiya, M.; Sakurai, T.; Someya, T. *Science* **2009**, *326*, 1516, b) Anariba, F.; McCreery, R. L. *J. Phys. Chem. B* **2002**, *106*, 10355.

55. a) Metzger, R. M. *J. Mater. Chem.* **2008**, *18*, 4364, b) Metzger, R. M.; Chen, B.; Hopfner, U,; Lakshmikantham, M. V.; Vuillaume, D.; Kawai, T.; Wu, X. L.; Tachibana, H.; Hughes, T.; V. Sakurai, H.; Baldwin, J. W.; Hosch, C.; Cava, M. P.; Brehmer, L.; Ashwell, G. J. *J. Am. Chem. Soc*. **1997**, *119*, 10455.

56. Urdampilleta, M.; Klyatskaya, S.; Cleuziou, J-P.; Ruben, M.; Wernsdorfer, W. *Nature Mater.* **2011**, *10*, 502.

57. Metzger, R. M. *Chem. Rev*. **2003**, *103*, 3803.

58. Iler, R. K. *J. Colloid Interface Sci.* **1966**, *21*, 569;

59. a) Decher, G.; Hong, J. D. *Macromol. Chem. Macromol. Symp.*, **1991**, *46*, 321, b) Decher, G.; Hong, J. D. *Ber. Bunsen-Ges. Phys. Chem*. **1991**, *95*, 1430, c) Decher, G.; Hong, J. D.; Schmitt, J. *Thin Solid Films*, **1992**, *210*, 831.

60. Boccaccini, A. R.; Cho, J.; Roether, J. A.; Thomas, B. J. C.; Minay, E. J.; Shaffer, M. S. P. *Carbon* **2006**, *44*, 3149.

61. Ulman, A. *An Introduction to Ultrathin Organic Films: From Langmuir-Blodgett to Self-assembly*, Academic Press, Boston, **1991**.

62. Gaines Jr., G. L. *Insoluble monolayers at Liquid-Gas Interfaces*, Interscince Publishers, New York, **1966**.

63. Nuzzo, R. G.; Allara, D. L. *J. Am. Chem. Soc.* **1983**, *105*, 4481.

64. Bain, C. D.; Whitesides, G. M. *J. Am. Chem. Soc.* **1989**, *111*, 7164.

65. a) Bain, C. D.; Evall, J.; Whitesides, G. M. *J. Am. Chem. Soc.* **1989**, *111*, 7155, b) Bain, C. D.; Whitesides, G. M. *Science* **1988**, *240*, 62.

66. a) Stranick, S. J.; Atre, S. V.; Parikh, A. N.; Wood, M. C.; Allara, D. L.; Winograd, N.; Weiss, P. S. *Nanotechnology* **1996**, *7*, 438, b) Stranick, S. J.; Parikh, A. N.; Tao, Y. T.; Allara, D. L.; Weiss, P. S. *J. Phys. Chem.* **1994**, *98*, 7636.

67. a) Xia, Y.; Whitesides, G. M. *Angew. Chem., Int. Ed. Engl.* **1998**, *37*, 550, b) Michel, B.; Bernard, A.; Bietsch, A.; Delamarche, E.; Geissler, M.; Juncker, D.; Kind, H.; Renault, J. P.; Rothuizen, H.; Schmid, H.; Schmidt-Winkel, P.; Stutz, R.; Wolf, H. *IBM J. Res. Dev.* **2001**, *45*, 697.

68. a) Liu, G.-Y.; Xu, S.; Qian, Y. *Acc. Chem. Res.* **2000**, *33*, 457, b) Kraemer, S.; Fuierer, R. R.; Gorman, C. B. *Chem. Rev.* **2003**, *103*, 4367, c) Ginger, D. S.; Zhang, H.; Mirkin, C. A. *Angew. Chem., Int. Ed. Engl.* **2004**, *43*, 30.

69. a) Shadnam, M. R.; Kirkwood, S. E.; Fedosejevs, R.; Amirfazli, A. *Langmuir* **2004**, *20*, 2667, b) Klauser, R.; Hong, I. H.; Wang, S. C.; Zharnikov, M.; Paul, A.; Goelzhaeuser, A.; Terfort, A.; Chuang, T. J. *J. Phys. Chem. B* **2003**, *107*, 13133, c) Sun, S.; Chong, K. S. L.; Leggett, G. J. *J. Am. Chem. Soc.* **2002**, *124*, 2414, d) Behm, J. M.; Lykke, K. R.; Pellin, M. J.; Hemminger, J. C. *Langmuir* **1996**, *12*, 2121.

70. a) Geyer, W.; Stadler, V.; Eck, W.; Golzhauser, A.; Grunze, M.; Sauer, M.; Weimann, T.; Hinze, P. *J. Vac. Sci. Technol., B* **2001**, *19*, 2732, b) Weimann, T.; Geyer, W.; Hinze, P.; Stadler, V.; Eck, W.; Golzhauser, A. *Microelectron. Eng.* **2001**, *903*, 57, c) Golzhauser, A.; Eck, W.; Geyer, W.; Stadler, V.; Weimann, T.; Hinze, P.; Grunze, M. *Adv. Mater.* **2001**, *13*, 806.

71. Berggren, K. K.; Bard, A.; Wilbur, J. L.; Gillaspy, J. D.; Helg, A. G.; McClelland, J. J.; Rolston, S. L.; Phillips, W. D.; Prentiss, M.; Whitesides G. M. *Science* **1995**, *269*, 1255.

72. Bernt, P.; Kurihara, K.; Kunitake, T. *Langmuir*, **1992**, *8*, 2486.

73. Lvov, Y.; Ariga, K.; Onda, M.; Ichinose, I.; Kunitake, T. *Colloids Surf., A,* **1999**, *146*, 337.

74. a) Lvov, Y.; Decher, G.; Mohwald, H. *Langmuir*, **1993**, *9*, 481, b) Decher, G.; Lvov, Y.; Schmitt, J. *Thin Solid Films* **1994**, *244*, 772, c) Korneev, D. Lvov, Y.; Decher, G.;

Schmitt, J.; Yaradaikin, S. *Physica B* **1995**, *213*, 954, d) Hoogeveen, N. G.; Stuart, M. A. C.; Fleer, G. J.; Bohmer, M. R. *Langmuir* **1996**, *12*, 3675, e) Chen, W.; McCarthy, T. J. *Macromolecules* **1997**, 30, 78.

75. a) Fou, A. C.; Onitsuka, O.; Ferreira, M.; Rubner, M.; Hsieh, B. R. *J. Appl. Phys.* **1996**, *79*, 7501, b) Stockton, W. B. Rubner, M. F. *Macromolecules* **1997**, *30*, 2717.
76. Lvov, Y.; Yamada, S.; Kunitake, T. *Thin Solid Films* **1997**, *300*, 107.
77. a) He, J.-A.; Valluzzi, R.; Yang, K.; Dolukhanyan, T.; Sung, C.; Kumar, J.; Tripathy, S. K.; Samuelson, L.; Balogh, L.; Tomalia, D. A. *Chem. Mater.* **1999**, *11*, 3268, b) Khopade, A. J.; Caruso, F. *Langmuir* **2002**, *18*, 7669.
78. a) Lvov, Y.; Ariga, K.; Kunitake, T. *Chem. Lett.* **1994**, 2323, b) Lvov, Y.; Ariga, K.; Ichinose, I.; Kunitake, T. *J. Am. Chem. Soc.* **1995**, *117*, 6117, c) Lvov, Y.; Ariga, K.; Ichinose, I.; Kunitake, T. *Thin Solid Films* **1996**, *285*, 797, d) Onda, M.; Lvov, Y.; Ariga, K.; Kunitake, T. *Jpn. J. Appl. Phys.(Part 1)* **1997**, *36*, 1608, e) Ariga, K.; Onda, M.; Lvov, Y.; Kunitake, T. *Chem. Lett.* **1997**, 25, f) Caruso, F.; Furlong, D. N.; Ariga, K.; Ichinose, I.; Kunitake, T. *Langmuir* **1998**, *14*, 4559, g) Lvov, Y.; Lu, Z.; Schenkman, J. B.; Zu, X.; Rusling, J. F. *J. Am. Chem. Soc.* **1998**, *120*, 4073, h) Beissenhirtz, M. K.; Scheller, F. W.; Lisdat, F. *Anal. Chem.* **2004**, *76*, 4665, i) He, P.; Hu, N.; Rusling, J. F. *Langmuir* **2004**, *20*, 722, j) Sultana, N.; Schenkman, J. B.; Rusling, J. F. *J. Am. Chem. Soc.* **2005**, *127*, 13460, k) Shutava, T. G.; Kommireddy, D. S.; Lvov, Y. *J. Am. Chem. Soc.* **2006**, *128*, 9926, l) Qi, Z.; Honma, I.; Ichihara, M.; Zhou, H. *Adv. Funct. Mater.* **2006**, *16*, 377.
79. a) Lvov, Y.; Decher, G.; Sukhorukov, G. *Macromolecules* **1993**, *26*, 5396, b) Decher, G.; Lehr, B.; Lowack, K.; Lvov, Y.; Schmitt, J. *Biosens. Bioelectron.* **1994**, *9*, 677, c) Lang, J.; Liu, M. *J. Phys. Chem. B* **1999**, *103*, 11393, d) Shi, X.; Sanedrin, R. J.; Zhou, F. *J. Phys. Chem. B* **2002**, *106*, 1173, e) Chen, X.; Ling, J.; Liu, M. *Thin Solid Films* **2002**, *409*, 227, f) Luo, L.; Liu, J.; Wang, Z.; Yang, X.; Dong, S.; Wang, E. *Biophys. Chem.* **2001**, *94*, 11, g) Johnston, A. P. R.; Mitomo, H.; Read, E. S.; Caruso, F. *Langmuir* **2006**, *22*, 3251, h) Yamauchi, F.; Koyamatsu, Y.; Kato, K.; Iwata, H. *Biomaterials* **2006**, *27*, 3497, i) Ishibashi, A.; Yamaguchi, Y.; Murakami, H.; Nakashima, N. *Chem. Phys. Lett.* **2006**, *419*, 574.
80. a) Lvov, Y.; Onda, M.; Ariga, K.; Kunitake, T. *J. Biomater. Sci., Polym. Ed.* **1998**, *9*, 345, b) Voigt, A.; Lichtenfeld, H.; Sukhorukov, G. B.; Zastrow, H.; Donath, E.; Baumler, H.; Mohwald, H. *Ind. Eng. Chem. Res.* **1999**, *38*, 4037, c) Qiu, X.; Leporatti, S.; Donath, E.;

Mohwald, H. *Langmuir* **2001**, *17*, 5375, d) Serizawa, T.; Yamaguchi, M.; Akashi, M. *Biomacromolecules* **2002**, *3*, 724, e) Constantine, C. A.; Mello, S. V.; Dupont, A.; Cao, X. H.; Santos, D.; Oliveira, O. N.; Strixino, F. T.; Pereira, E. C.; Cheng, T. C.; Defrank, J. J.; Leblanc, R. M. *J. Am. Chem. Soc.* **2003**, *125*, 1805, f) Thierry, B.; Winnik, F. M.; Merhi, Y.; Silver, J.; Tabrizian, M. *Biomacromolecules* **2003**, *4*, 1564, g) Shutava, T. G. Lvov, Y. *J. Nanosci. Nanotechnol.* **2006**, *6*, 1655.

81. a) Kotov, N. A.; Dekany, I.; Fendler, J. H. *J. Phys. Chem.* **1995**, *99*, 13065, b) Ariga, K.; Lvov, Y.; Onda, M.; Ichinose, I.; Kunitake, T. *Chem. Lett.* **1997**, *125*, c) Lvov, Y.; Ariga, K.; Onda, M.; Ichinose, I.; Kunitake, T. *Langmuir* **1997**, *13*, 6195, d) Lvov, Y.; Rusling, J. F.; Thomsen, D. L.; Papadimitrakopoulos, F.; Kawakami, T.; Kunitake, T. *Chem. Commun.* **1998**, 1229, e) Cassagneau, T.; Fendler, J. H.; Mallouk, T. E. *J. Am. Chem. Soc.* **1998**, *120*, 7848, f) Ostrander, J. W.; Mamedov, A. A.; Kotov, N. *J. Am. Chem. Soc.* **2001**, *123*, 1101, g) Zhang, H.; Zhou, Z.; Yang, B.; Gao, M. *J. Phys. Chem. B* **2003**, *107*, 8, h) Koo, H. Y.; Yi, D. K.; Yoo, S. J.; Kim, D.-Y. *Adv. Mater.* **2004**, *16*, 274, i) Tian, S.; Liu, J.; Zhu, T.; Knoll, W. *Chem. Mater.* **2004**, *16*, 4103, j) Han, B.-H.; Manners, I.; Winnik, M. A. *Chem. Mater.* **2005**, *17*, 3160, k) Ko, H.; Jiang, C.; Tsukruk, V. V. *Chem. Mater.* **2005**, *17*, 5489, l) Shchukin, D. G.; Zheludkevich, M.; Yasakau, K.; Lamaka, S.; Ferreira, M. G. S.; Mohwald, H. *Adv. Mater.* **2006**, *18*, 1672, m) Salgueirino-Maceira, V.; Correa-Duarte, M. A.; Spasova, M.; Liz-Marzan, L. M.; Farle, M. *Adv. Mater.* **2006**, *16*, 509, n) Liang, Z.; Dzienis, K. L.; Xu, J.; Wang, Q. *Adv. Funct. Mater.* **2006**, *16*, 542.

82. a) Lvov, Y.; Ariga, K.; Ichinose, I.; Kunitake, T. *Langmuir* **1996**, *12*, 3038, b) Mamedov, A.; Ostrander, J.; Aliev, F.; Kotov, N. A. *Langmuir* **2000**, *16*, 3941, c) Zhou, Y.; Hu, N.; Zeng, Y.; Rusling, J. F. *Langmuir* **2002**, *18*, 211.

83. a) Sasaki, T.; Ebina, Y.; Watanabe, M.; Decher, G. *Chem. Commun.* **2000**, 2163, b) Sasaki, T.; Ebina, Y.; Tanaka, T.; Harada, M.; Watanabe, M.; Decher, G. *Chem. Mater.* **2001**, *13*, 4661, c) Wang, L.; Sasaki, T.; Ebina, Y.; Kurashima, K.; Watanabe, M. *Chem. Mater.* **2002**, *14*, 4827, d) Wang, Z.-S.; Sasaki, T.; Muramatsu, M.; Ebina, Y.; Tanaka, T.; Wang, L.; Watanabe, M. *Chem. Mater.* **2003**, *15*, 807, e) Wang, L.; Omomo, Y.; Sakai, N.; Fukuda, K. I.; Nakai, I.; Ebina, Y.; Takada, K.; Watanabe, M.; Sasaki, T. *Chem. Mater.* **2003**, *15*, 2873, f) Wang, L.; Ebina, Y.; Takada, K.; Sasaki, T. *J. Phys. Chem. B* **2004**, *108*, 4283, g) Zhou, Y.; Ma, R.; Ebina, Y.; Takada, K.; Sasaki, T. *Chem. Mater.* **2006**, *18*, 1235, h) Osada, M.; Ebina, Y.; Funakubo, H.; Yokoyama, S.; Kiguchi,

T.; Takada, K.; Sasaki, T. *Adv. Mater.* **2006**, *18*, 10238, i) Li, L.; Ma, R.; Ebina, Y.; Iyi, N.; Sasaki, T. *Chem. Mater.* **2005**, *17*, 4386.

84. Lee, G. S.; Lee, Y.-J.; Yoon, K. B. *J. Am. Chem. Soc.* **2001**, *123*, 9769.

85. Mitsui, T.; Yamaguchi, K.; Takeoka, Y.; Rikukawa, M.; Sanui, K. *Chem. Commun*. **2002**, 1094.

86. a) Ichinose, I.; Tagawa, H.; Mizuki, S.; Lvov, Y.; Kunitake, T. *Langmuir* **1998**, *14*, 187, b) Ariga, K.; Lvov, Y.; Ichinose, I.; Kunitake, T. *Appl. Clay Sci.* **1999**, *15*, 137.

87. a) Ramsden, J. J.; Lvov, Y.; Decher, G. *Thin Solid Films* **1995**, *254*, 246, b) Toutianoush, A.; Tieke, B. *Macromol. Rapid Commun.* **1998**, *19*, 591, c) Locklin, J.; Youk, J. H.; Xia, C.; Park, M.-K.; Fan, X.; Advincula, R. C. *Langmuir* **2002**, *18*, 877.

88. a) Ichinose, I. Fujiyoshi, K. Mizuki, S. Lvov, Y. Kunitake, T. Chem. Lett., 1996, 257, b) Ariga, K.; Sasaki, Y.; Horiguchi, H.; Horiuchi, N.; Kikuchi, J. *Soft Chemistry Leading to Novel Materials Defect and Diffusion Forum*, ed. Agarwala, R. P. Trans Tech Publication, Zurich, **2001**, *191*, p. 35.

89. a) Cooper, T.; Campbell, A.; Crane, R. *Langmuir* **1995**, *11*, 2713, b) Ariga, K.; Lvov, Y.; Kunitake, T. *J. Am. Chem. Soc.* **1997**, *119*, 2224, c) Araki, K.; Wagner, M. J.; Wrigton, M. S. *Langmuir* **1996**, *12*, 5393, d) Kometani, N.; Nakajima, H.; Asami, K.; Yonezawa, Y.; Kajimoto, O. *Chem. Phys. Lett.* **1998**, *294*, 619, e) Clark, S. L.; Handy, E. S.; Rubner, M. F.; Hammond, P. T. *Adv. Mater.* **1999**, *11*, 1031, f) Kaschak, D. M.; Lean, J. T.; Waraksa, C. C.; Saupe, G. B.; Usami, H.; Mallouk, T. E. *J. Am. Chem. Soc.* **1999**, *121*, 3435, g) Tedeschi, C.; Caruso, F.; Mohwald, H.; Kristein, S. *J. Am. Chem. Soc.* **2000**, *122*, 5841, h) Rousseau, E.; Van der Auweraer, M.; De Schryver, F. *Langmuir* **2000**, *16*, 8865, i) Tedeschi, C.; Mohwald, H.; Kirstein, S. *J. Am. Chem. Soc.* **2001**, *123*, 954, j) Das, S.; Pal, A. J. *Langmuir* **2002**, *18*, 458, k) Van Cott, K. E.; Guzy, M.; Neyman, P.; Brands, C.; Heflin, J. R.; Gibson, H. W.; Davis, R. M. *Angew. Chem., Int. Ed.* **2002**, *41*, 3236, l) Lee, D.-C.; Morales, G. M.; Lee, Y.; Yu, L. *Chem. Commun.* **2006**, 100, m) Chen, H.; Zeng, G.; Wang, Z.; Zhang, X.; Peng, M.-L.; Wu, L.-Z.; Tung, C.-H. *Chem. Mater.* **2005**, *17*, 6679.

90. Ariga, K.; Hill, J. P.; Ji, Q. *Phys. Chem. Chem. Phys.* **2007**, *9*, 2319.

91. Tang, Z.; Wang, Y.; Podsiadlo, P.; Kotov N. A. *Adv. Mater.* **2006**, *18*, 3203.

92. a) Yoo, D.; Shiratori, S. S.; Rubner, M. F. *Macromolecules* **1998**, *31*, 4309, b) Shiratori, S. S.; Rubner, M. F. *Macromolecules* **2000**, *33*, 4213.

93. Franklin, B *Philosophical Transactions of the Royal Society* **1774**, *64*, 445.

94. Pockels, A. *Nature* **1891**, *46*, 437.

95. Langmuir, I.; Schaefer, V. J. *J. Am. Chem. Soc.* **1938**, *60*, 2803.

96. Wilhelmy, L *Angew. Physik* **1863**, *119*, 117.

97. Halperin, K.; Ketterson, J. B.; Dutta, P. *Langmuir* **1989**, *5*, 161.

98. Petkov, J. T.; Gurkov, T. D.; Campbell, B. E.; Borwankar R. P. *Langmuir* **2000,** *16,* 3703.

99. a) Sucker, C. *Kolloid Z.* **1963**, *190*,146, b) Grunfeld, F. *Rev. Sci. Instrum.* **1993**, *64*, 548.

100. Somasundaran, P.; Danitz, M.; Mysels K. J. *J. Coll. Int. Sci.* **1974**, *48*, 410.

101. Iwahashi M.; Maehara N.; Kaneko Y.; Seimiya T.; Middleton S. R.; Pallas N. R.; Pethica B. A. *J. Chem. Soc., Faraday Trans. 1* **1985**, *81,* 973.

102. Girard-Egrot, A.P.; Blum, L.J. *Langmuir-Blodgett technique for synthesis of biomimetic lipid membranes*, in *Fundamental biomedical technologies* **2007** Springer Science+Business Media, LLC: New York.

103. Davies, J. T.; Rideal, E. K. *Interfacial phenomena,* Accademic Press, New York, **1963**.

104. Xue, J.; Jung, C. S.; Kim, M. W. *Phys. Rev. Lett.* **1992**, *69*, 474.

105. Ibn-Elhaj, M.; Möhwald, H.; Cherkaoui, M. Z.; Zniber, R. *Langmuir* **1998**, *14*, 504.

106. Hsiung, H.; Shen, Y. R. *Phys. Rev. A* **1986**, *34*, 4303.

107. Flannery D.; James S. W.;Tatam R. P.; Ashwell G. J. *Opt. Lett.* **1997**, *22*, 567, b) Flannery D.; James S. W.; Tatam R. P.; Ashwell G. J. *Appl. Opt.* **1999**, *38*, 7370.

108. a) Glasgow B. J.; Marshall G.; Gasymov O. K.; Abduragimov A. R.; Yusifov T. N.; Knobler C. M. *Investig. Ophthalmol. Vis. Sci.* **1999**, *40*, 3100, b) Greiner J. V.; Glonek T.; Korb D. R.; Booth R.; Leahy C. D. *Ophthalmol. Res.* **1996**, *28*, 44.

109. a) Grace A.; Kwok P.; Hawke M. *Otolaryngol. Head Neck Surg.* **1987**, *96*, 336, b) Hills B. A. *Arch. Otolaryngol.* **1984**, *110*, 3.

110. a) Veldhuizen R.; Nag K.; Orgeig S.; Possmayer F.; *Biochim. Biophys. Acta* **1998**, *1408*, 90, b) Yu S. H.; Possmayer F. *J. Lipid Res.* **2003**, *44*, 621, c) Goerke J.. *Biochim. Biophys. Acta* **1974**, *344*, 241.

111. a) Tchoreloff P.; Gulik A.; Denizot B.; Proust J. E.; Puisieux F. *Chem. Phys. Lipids* **1991**, *59*, 151, b) Gopal A. *The collapse of phospholipid Langmuir monolayers: implications for biological surfactant*. **2004**, PhD thesis. Univ. Chicago.

112. a) Ries H.; Swift H. *Langmuir* **1987**, *3*, 853, b) Siegel S.; Honig D.; Vollhardt D.; Mobius D. *J. Phys. Chem.* **1992**, *96*, 8157, c) Lipp M. M.; Lee K. Y. C.; Zasadzinski J. A.; Waring A. J. *Science* **1996**, *273*, 1196, d) Birdi K.; Vu D. *Langmuir* **1994**, *10*, 623.

113. a) Notter R. H.; Tabak S. A.; Mavis R. D. *J. Lipid Res.* **1980**, *21*, 10, b) Liu H.; Lu R. Z.; Turcotte J. G.; Notter R. H. *Colloid Interface Sci.* **1994**, *167*, 378.

114. a) Ding J. Q.; Takamoto D. Y.; von Nahmen A.; Lipp M. M.; Lee K. Y. C.; Waring, A. J.; Zasadzinski J. A. *Biophys. J.* **2001**, *80*, 2262, b) Takamoto D. Y.; Lipp M. M.; von Nahmen A.; Lee K. Y. C.; Waring A. J.; Zasadzinski J. A. *Biophys. J.* **2001**, *81*, 153.

115. Clements J. A. *Physiologist* **1962**, *5*, 11.

116. Lee K. Y. C. *Annu. Rev. Phys. Chem.* **2008**, *59*, 771.

117. a) Bourdieu L.; Daillant J.; Chatenay D.; Braslau A.; Colson D.. *Phys. Rev. Lett.* **1994**, *72*, 1502, b) Saint-Jalmes A.; Graner F.; Gallet F.; Houchmandzadeh B.. *Europhys. Lett.* **1994**, *28*, 565.

118. a) Hu J. G.; Granek R. *J. Phys. II* **1996**, *6*, 999, b) Milner S. T.; Joanny J. F.; Pincus P. *Europhys.Lett.* **1989**, *9*, 495.

119. Ries Jr., H. E.; Kimbali, W. A. *J. Phys. Chem.* **1955,** *59,* 94.

120. Rapp, B.; Gruler, H. *Phys. Rev. A* **1990**, *42*, 2215.

121. de Mul, M. N. G.; Mann, J. A. *Langmuir* **1994**, *10*, 2311.

122. de Mul, M. N. G.; Mann, J. A. *Langmuir* **1995**, *11*, 3292.

123. Ibn-Elhaj, M.; Riegler, H.; Möhwald, H.; Schwendler, M.; Helm, C. A. *Phys. Rev. E* **1997**, *56*, 1844.

124. Ibn-Elhaj, M.; Riegler, H.; Möhwald, H. *J. Physique* **1996**, *6*, 969.

125. Gallani, J.-L.; Bourgogne, C.; Nakatsui, S. *Langmuir* 2004, **20**, 10062.

126. Ries, Jr, H. E. *Nature* **1979**, *281*, 287.

127. González-Delgado, A. M.; Pérez-Morales, M.; Giner-Casares, J. J.; Muñoz, E.; Martín-Romero, M. T.; Camacho, L. *J. Phys. Chem. B* **2009,** *113,* 13249.

128. Plehnert, R.; Schröter, J. A.; Tschierske, C. *Langmuir* **1998**, *14*, 5245.

129. de Mul, M. N. G.; Mann, J. A. *Langmuir* **1998**, *14*, 2466.

130. Friedenberg, M. C.; Fuller, G. G.; Frank, C.; W. Robertson, C. R. *Langmuir* **1994**, *10*, 1251.

131. Modlińska, A.; Inglot, K.; Martyński, T.; Dąbrowski, R.; Jadżyn, J.; Bauman, D. *Liq. Cryst.* **2009**, *36*, 197; see also other references of the same authors quoted in there.

132. Schmitz, P.; Gruler, H. *Europhys. Lett.* **1995**, *29*, 451.

133. Guyot-Sionnest, P.; Hsiung, H.; Shen, Y. R. *Phys. Rev. Lett.* **1986**, *57*, 2963.

134. Olenik, I. D.; Kocevar, K.; Musevic, I.; Rasing, T. *Eur. Phys. J. E* **2003**, *11*, 169.

135. Yamamoto, T. Taguchi, D. Manaka, T. Iwamoto, M. *J. Chem. Phys.* **2005**, *122,* 164703.

136. a) Thomy, A.; Duval, X.; Regnier, J. *Surf. Sci. Rep.* **1981**, *1*, 1, b) Ball, P. C.; Evans, R. *J. Chem. Phys.* **1988,** *89*, 4412.

137. Brezesinski, G.; Mohwald H. *Adv. Coll. Int. Sci.* **2003**, 100, 563.

138. Cardenas, M.; Nylander, T.; Jonsson, B.; Lindman, B. *J. Coll. Int. Sci.* **2005**, *286*, 166.

139. Juskowiak, B.; Paczesny, J. *J. Coll. Int. Sci.* **2012**, *365*, 150.

140. Ahuja, R. C.; Caruso, P. L.; Mobius D. *Thin Solid Films* **1994***, 242*, 195.

141. Souza, S. M. B. Chaimovich, H. Politi, M. J. *Langmuir* **1995***, 11*, 1715.

142. Koelsch, P.; Viswanath, P.; Motschmann, H.; Shapovalov, V. L.; Brezesinski, G.; Möhwald, H.; Horinek, D.; Netz, R. R.; Giewekemeyer, K.; Salditt, T.; Schollmeyer, H.; von Klitzing, R.; Daillant, J.; Guenoun P. *Colloids and Surfaces A: Physicochemical and Engineering Aspects* **2007**, *303(1–2)*, 110.

143. Binks*,* B. P. *Adv. Coll. Int. Sci.* **1991***, 34*, 343.

144. Hughes A. V.; Goldar A.; Gerstenberg M. C.; Roser S. J.; Bradshaw J. *Phys. Chem. Chem. Phys.* **2002**, *4*, 2371.

145. Tamm L. K.; McConnell H. M. *Biophys. J.* **1985**, *47*, 105.

146. Sakka, S.; Kamyak, K. *J. Non-Crystalline Solids* **1982**, *48*, 31.

147. Seshan, K. *Handbook of Thin Film Deposition, Processes and Technologies* **2002** (2nd Edition), Noyes Publication, New York.

148. Fuhrhop, J. H.; Wang, T. *Chem. Rev.* **2004**, *104*, 2901.

149. Tschierske, C. *Chem. Soc. Rev.* **2007**, *36*, 1930.

150. a) Kolbel, M.; Beyersdorff, T.; Cheng, X.; H. Tschierske, C.; Kain, J.; Diele, S. *J. Am. Chem. Soc.* **2001**, *123*, 6809, b) Cheng, X.; Prehm, M.; Das, M.; K. Kain, J.; Baumeister, U.; Diele, S.; Leine, D.; Blume, A.; Tschierske, C. *J. Am. Chem. Soc.* **2003**, *125*, 10977, c) Prehm, M.; Liu, F.; Baumeister, U.; Zeng, X.; Ungar, G.; Tschierske, C. *Angew. Chem.* **2007**, *119*, 8118, d) Prehm, M.; Gotz, G.; Buerle, P.; Liu, F.; Zeng, X.; Ungar, G.; Tschierske, C. *Angew. Chem.* **2007**, *119*, 8002, e) Prehm, M.; Enders, C.; Anzahaee, M. Y.; Glettner, B.; Baumeister, U.; Tschierske, C. *Chem. Eur. J.* **2008**, *14*, 6352, f) Kieffer, R.; Prehm, M.; Pelz, K.; Baumeister, U.; Liu, F.; Hahn, H.; Lang, H.; Ungar, G.; Tschierske, C. *Soft Matter* **2009**, *5*, 1214.

151. a) Kieffer, R.; Prehm, M.; Glettner, B.; Pelz, K.; Baumeister, U.; Liu, F.; Zeng, X.; Ungar, G.; Tschierske, C. *Chem. Commun.* **2008**, *33*, 3861, b) Glettner, B.; Liu, F.; Zeng, X.; Prehm, M.; Baumeister, U.; Walker, M.; Bates, M. A.; Boesecke, P.; Ungar, G.;

Tschierske, C. *Angew. Chem., Int. Ed.* **2008**, *47*, 9063, c) Cheng, X.; Dong, X.; Wei, G.; Prehm, M.; Tschierske, C. *Angew. Chem., Int. Ed*. **2009**, *48*, 8014.

152. a) Glettner, B.; Liu, F.; Zeng, X.; Prehm, M.; Baumeister, U.; Ungar, G.; Tschierske, C. *Angew. Chem.* **2008**, *120*, 6169, b) *Angew. Chem. Int. Ed.* **2008**, *47*, 6080.
153. Ungar, G.; Tschierske, C.; Abetz, V.; Hołyst, R.; Bates, M. A.; Liu, F.; Prehm, M.; Kieffer, R.; Zeng, X.; Walker, M.; Glettner, B.; Zywocinski, A. *Adv. Funct. Mater.* **2011**, *21*, 1296.
154. Jana, N. R.; Peng, X. *J. Am. Chem. Soc.* **2003**, *125*, 14280.
155. Kalsin, A. M.; Fiałkowski, M.; Paszewski, M.; Smoukov, S. K.; Bishop, K. J. M.; Grzybowski, B. A. *Science*, **2006**, *5772*, 420.
156. Nørgaard, K.; Weygand, M. J.; Kjaer, K.; Brust, M.; Bjørnholm, T. *Faraday Discuss.* **2004**, *125*, 221.
157. Wójcik M. *Synteza i właściwości fizykochemiczne ligandów ciekłokrystalicznych pochodnych 4,4`-bifenylu, do modyfikacji powierzchni nanocząstek złota* PhD Thesis **2011** Warsaw University.
158. Brust, M.; Walker, M.; Bethell, D.; Schiffrin, D. J.; Whyman, R. J. *J. Chem. Soc., Chem. Commun.* **1994**, 801.
159. Templeton, A. C.; Hostetler, M. J.; Kraft, C. T.; Murray, R. W. *J. Am. Chem. Soc.* **1998**, *120*, 1906.
160. Dass, A. Holt, K. Parker, J. F. Feldberg, S. W. Murray, R. W. *J. Phys. Chem. C* **2008**, *112*, 20276.
161. a) Wagner, R. S.; Ellis, W. C. *Appl. Phys. Lett.* **1964**, *4*, 89; b) Wu, Y.; Yang, P. *J. Am. Chem. Soc.* **2001**, *123*, 3165.
162. Brown, K. R.; Natan, M. J. *Langmuir*, **1998**, *14*, 726.
163. Winkler, K.; Kamińska, A.; Wojciechowski, T.; Hołyst, R.; Fiałkowski, M. *Plasmonics* **2011**, *6(4)*, 697.
164. Parratt, L. G. *Phys. Rev.* **1954**, *95*, 359.
165. a) Authier, A. *X-ray and Neutron Diffraction* NATO ASI Series, **1996**, b) Holy, V.; Pietsch, U.; Baumbach, T. *High Resolution X-ray Scattering. From Thin Films to Lateral Nanostructures* 2-nd Edition, Springer-Verlag, New York, **2004**.
166. Jablonski, A. *Anal. Sci.* **2010**, *26*, 155.
167. Barhoumi, A.; Zhang, D.; Tam, F. *J. Am. Chem. Soc.* **2008**, *130*, 5523.
168. Turberg, M. P.; Brady, J. E. *J. Am. Chem. Soc.* **1988**, *110*, 7797.

169. a) Li, M.; Acero, A. A.; Huang, Z.; Rice, S. *Nature* **1994**, *367*, 151, b) Krafft, M. P.; Goldmann, M. *Curr. Opin. Colloid Interface Sci*., **2003**, *8*, 243, c) Gaines Jr., G. L. *Langmuir* **1991**, *7*, 3054.

170. de Gracia Lux, C.; Gallani, J.-L.; Waton, G.; Krafft, M. P. *Chem. Eur. J.* **2010**, *16*, 7186.

171. a) Broniatowski, M.; Dynarowicz-Łątka, P. *J. Colloid Interface Sci.* **2006**, *299*, 916, b) Broniatowski, M.; Dynarowicz-Łątka, P. *Langmuir* **2006**, *22*, 6622.

172. Riess, J. G. *Curr. Opin. Colloid Interface Sci.* **2009**, *14*, 294.

173. Gerber, F.; Krafft, M. P.; Vandamme, T. F.; Goldmann, M.; Fontaine, P. *Artif. Cell Blood Sub.* **2007**, *35*, 211.

174. Krafft, M. P.; Giulieri, F.; Fontaine, P.; Goldmann, M. *Langmuir* **2001**, *17*, 6577.

175. Lo Nostro, P. *Curr. Opin. Colloid Interface Sci.* **2003**, *8*, 223.

176. a) De Rosa, M.; Gambacorta, A.; Gliozzi, A. *Microbiol. Rev.* **1986**, 70, b) Benvegnu, T.; Brard, M.; Plusquellec, D. *Curr. Opin. Colloid Interface Sci.* **2004**, *8*, 469, c) Sprott, G. D. *J. Bioenerg. Biomembr*. **1992**, *24*, 555, d) Gambacorta, A.; Gliozzi, A.; de Rosa, M. *World J. Microbiol. Biotechnol.* **1995**, *11*, 115, e) Yamauchi, K.; Kinoshita, M. *Prog. Polym. Sci.* **1993**, *18*, 763.

177. Hentrich, F.; Tschierske, C.; Zaschke, H. *Angew. Chem.* **1991**, *103*, 429.

178. Kohler, K.; Forster, G.; Hauser, A.; Dobner, B.; Heiser, U. F.; Ziethe, F.; Richter, W.; Steiniger, F.; Drechsler, M.; Stettin, H.; Blume, A. *J. Am. Chem. Soc.* **2004**, *126*, 16804.

179. Meister, A.; Weygand, M. J.; Brezesinski, G.; Kerth, A.; Drescher, S.; Dobner, B.; Blume, A. *Langmuir* **2007**, *23*, 6063.

180. a) Schröter, J. A.; Plehnert, R.; Tschierske, C.; Katholy, S.; Janietz, D.; Penacorada, F.; Brehmer, L. *Langmuir* **1997**, *13*, 796, b) Plehnert, R.; Schröter, J. A.; Tschierske, C.; *Langmuir* **1999**, *15*, 3773.

181. Mizoshita, N.; Seki, T. *Langmuir* **2005**, *21*, 10324.

182. Bunz, U. H. F. *Macromol. Rapid. Commun.* **2009**, *30*, 772.

183. Jatsch, A.; Schillinger, E.-K.; Schmid, S.; Bäuerle, P. *J. Mater. Chem.* **2010**, *20*, 3563.

184. Lorenz, C. D.; Travesset, A. *Langmuir* **2006**, *22,* 10016.

185. Gallani, J.-L.; Mery, S.; Galerne, Y.; Guillon, D. *J. Phys. Chem. B* **2004**, ***108***, 11627.

186. a) Cheng, X. H.; Das, M. K.; Diele, S.; Tschierske, C. *Angew. Chem. Int. Ed. Engl.,* **2002**, *41*, 4031, b) Prehm, M.; Cheng, X. H.; Diele, S.; Das, M. K.; Tschierske, C. *J. Am. Chem. Soc.* **2002**, *124*, 12072, c) Prehm, M.; Diele, S.; Das, M. K.; Tschierske, C. *J. Am. Chem. Soc.* **2003**, *125*, 614, d) Patel, N. M.; Dodge, M. R.; Zhu, M. H.; Petschek, R. G.;

Rosenblatt, C.; Prehm, M.; Tschierske, C. *Phys. Rev. Lett*. **2004**, *92*, 015501, e) Patel, N. M.; Syed, M. I.; Rosenblatt, C.; Prehm, M.; Tschierske, C. *Liq. Cryst.* **2005**, *32*, 55.

187. a) Tweet, D. J.; Hołyst, R.; Swanson, B. D.; Stragier, H.; Sorensen, L. B. *Phys. Rev. Lett.* **1990**, *65*, 2157, b) Hołyst, R. *Phys. Rev. A* **1991**, *44*, 3692.
188. Taylor, D. M.; Bayes, G. F. *Mater. Sci. Eng. C* **1999**, *8-9*, 65.
189. a) Broniatowski, M. Vila-Romeu, N. Dynarowicz-Łątka, P. *J. Fluorine Chem.* **2006**, *127*, 909, b) Bunn, C. W.; Howells, E. R. *Nature* **1954**, *174*, 549.
190. a) Helm, C. A.; Möhwald, H.; Kjaer, K.; Als-Nielsen, J. *Europhys. Lett.* **1987**, *4*, 697, b) Bosio, L.; Benattar, J. J.; Rieutord, F. *Revue Phys. Appl*. **1987**, *22*, 775.
191. Israelachvili, J.; Gee, M. L. *Langmuir* **1989**, *5*, 288.
192. a) Marmur, A.; Bittoun, E. *Langmuir* **2009,** *25,* 1277, b) Marmur, A. *Langmuir* **2003**, *19,* 8343, c) Cassie A. B. D. *Discuss. Faraday Soc.* **1948**, *3*, 11.
193. Janssen, D.; De Palma, R.; Verlaak, S.; Heremans, P.; Dehaen, W. *Thin Solid Films* **2006**, *515*, 2433.
194. Wyszogrodzka, M.; Haag, R. *Biomacromol*. **2009**, *10*, 1043.
195. Chidsey, C. S. D.; Loiacono, D. N. *Langmuir* **1990**, *6*, 682.
196. Diversified Enterprises <http://www.accudynetest.com/polytable_03_print.html>
197. Li, Y.; Pham, J. Q.; Johnston, K. P.; Green, P. F. *Langmuir* **2007**, *23*, 9785.
198. Polster, D.; Graaf, H.; Baumgärtel, T.; von Borczyskowski, C.; Benedikt, U.; Auer, A. A. *Langmuir* **2010**, *26*, 8301.
199. a) Hąc-Wydro, K.; Flasiński, M.; Broniatowski, M.; Dynarowicz-Łątka, P.; Majewski, J. *J. Phys. Chem. B* **2010**, *114,* 6866, b) Rapaport, H.; Kuzmenko, I.; Lafont, S.; Kjaer, K.; Howes, P. B.; Als-Nielsen, J.; Lahav, M.; Leiserowitz, L. *Biophys. J.* **2001**, *81*, 2729.
200. a) Gershfeld, N. L.; Tajima, K. *Nature* **1979**, *279*, 708, b) Tajima, K.; Gershfeld, N. L. *Biophys. J.* **1985**, *47*, 203, c) Marsh, D. *Chem. Phys.Lipids* **2006**, *144*,146.
201. a) Strobel, M.; Kita-Tokarczyk, K.; Taubert, A.; Vebert, C.; Heiney, P. A.; Chami, M.; Meier W. *Adv. Funct. Mater.* **2006**, *16*, 252, b) Dermody, D. L.; Crooks, R. M.; Kim, T. *J. Am. Chem. Soc*. **1996**, *118*, 11912, c) Dermody, D. L.; Lee, Y.; Kim, T.; Crooks, R. M. *Langmuir* **1999**, *15*, 8435.
202. a) Cladis, P. E.; Guillon, D.; Bouchet, F. R.; Finn, P. L. *Phys. Rev. A* **1981**, *23*, 2594, b) Guillon, D.; Cladis, P. E.; Stamatoff, J. *Phys. Rev. Lett.* **1978**, *41*, 1598, c). Urban, S.; Przedmojski, J. Czub, J. *Liq. Cryst.* **2005**, *32*, 619.
203. Krafft, M. P.; Riess, J. G. *Chem. Rev.* **2009,** *109,* 1714.

204. a) El Abed, A.; Pouzet, E.; Fauré, M.-C.; Sanièr, M. ; Abillon, O. *Phys. Rev. E* **2000**, *62*, 5895, b) El Abed, A.; Fauré, M.-C.; Pouzet, E.; Abillon, O. *Phys. Rev. E* **2002**, *65*, 051603.

205. a) Elemans, J. A. A. W.; Lei, S.; De Feyter, S. *Angew. Chem*. **2009**, *48*, 7298, b) Kühne, D.; Klappenberger, F.; Decker, R.; Schlickum, U.; Brune, H.; Klyatskaya, S.; Ruben, M.; Barth, J. V. *J. Am. Chem. Soc.* **2009**, *131*, 3881.

206. Ozawa, H.; Kawao, M.; Tanaka, H.; Ogawa, T. *Langmuir* **2007**, *23*, 6365.

207. Hutchinson, T. O.; Liu, Y.-P.; Kiely, C.; Kiely, C. J.; Brust, M. *Adv. Mater.* **2001**, *13*, 1800.

208. Schön, G.; Simon, U. *Colloid Polym. Sci.* **1995**, *273*: 101.

209. a) Panigrahi, S.; Basu, S.; Praharaj, S.; Pande, S.; Jana, S.; Pal, A.; Kumar Ghosh, S.; Pal, T. *J. Phys. Chem. C* **2007**, *111*, 4596, b) Cheong, S.; Watt, J. D.; Tilley, R. D. *Nanoscale* **2010**, *2*, 2045.

210. a) Pasquato, L.; Pengo, P.; Scrimin, P. *J . Mater. Chem*. **2004**, *14,* 3481, b) Zhong, H.; Lei, X.; Hun, X.; Zhang, S. *Chem. Commun*. **2009**, *45*: 6958, c) Song, S.; Qin, Y.; He, Y.; Huang, Q.; Fan, C.; Chen, H.-Y. *Chem. Soc. Rev.* **2010**, *39*, 4234.

211. Wu, H.; Wexler, D.; Liu, H.; Savadogo, O.; Ahn, J.; Wang, G. *Mater. Chem. Phys.* **2010**, *124*, 841.

212. Moulin, E.; Sukmanowski, J.; Schulte, M.; Gordijn, A.; Royer, F. X.; Stiebig, H. *Thin Solid Films* **2008**, *516*, 6813.

213. Yin, G.; Xue, W.; Chen, F.; Fan, X. *Colloid. Surface. A* **2009**, *340*, 121.

214. Wang, Y.; Zhu, L.; Zhang, Y.; Yang, M. *J. Nanopart. Res.* **2010**, *12*, 1821.

215. a) Kim, S.-H.; Lim, J.-M.; Lee, S.-K.; Heo, C.-J.; Yang, S.-M. *Soft Matter* **2010**, *6*, 1092, b) Yan, B.; Thubagere, A.; Premasiri, W. R.; Ziegler, L. D.; Negro, L. D.; Reinhard, B. M. *ACS Nano* **2009**, *3*, 1190.

216. Sbrana, F.; Parodi, M. T.; Ricci, D.; Di Zitti, E. *Mater. Sci. Eng. C* **2002**, *22*, 187.

217. Yu, P.; Yan, J.; Zhang, J.; Mao, L. *Electrochem. Commun.* **2007**, *9*, 1139.

218. Markovich, G.; Collier, C. P.; Henrichs, S. E.; Remacle, F.; Levine, R. D.; Heath, J. R. *Acc. Chem. Res*. **1999**, *32*, 415.

219. Reincke, F.; Kegel, W. K.; Zhang, H.; Nolte, M.; Wang, D.; Vanmaekelbergh, D.; Möhwald, H. *Phys. Chem. Chem. Phys.* **2006**, *8*, 3828.

220. Wang, M.-H.; Hu, J.-W.; Li, Y.-J.; Yeung, E. S. *Nanotechnology* **2010**, *21*, 145608.

221. a) Lopes, W. A.; Jaeger, H. M. *Nature* **2001**, *414*, 735, b) Minelli, C.; Hinderling, C.; Heinzelmann, H.; Pugin, R.; Liley, M. *Langmuir* **2005**, *21*, 7080, c) Shenhar, R.; Jeoung, E.; Srivastava, S.; Norsten, T. B.; Rotello, V. M. *Adv. Mater.* **2005**, *17*, 2206, d) van Herrikhuyzen, J.; Janssen, R. A. J.; Meijer, E. W.; Meskers, S. C. J.; Schenning, A. P. H. J. *J. Am. Chem. Soc.* **2006**, *128*, 686, e) van Herrikhuyzen, J.; George, S. J.; Vos, M. R. J.; Sommerdijk, N. A. J. M.; Ajayaghosh, A.; Meskers, S. C. J.; Schenning, A. P. H. J. *Angew. Chem., Int. Ed.* **2007**, *46*, 1825.

222. a) Braun, E.; Eichen, Y.; Sivan, U.; Ben-Yoseph, G. *Nature* **1998**, *391*, 775, b) Jiang, L.; Zhang, H.; Zhuang, J.; Yang, B.; Yang, W.; Li, T.; Sun, C. *Adv. Mater.* **2005**, *17*, 2066, c) Deng, Z.; Mao, C. *Nano Lett.*, **2003**, *3(11)*, 1545.

223. Patolsky, F.; Weizmann, Y.; Lioubashevski, O.; Willner, I. *Angew. Chem., Int. Ed.* **2002**, *41*, 2323.

224. Ugarte, D.; Chatelain, A.; de Heer, W. A. *Science* **1996**, *274*, 1897.

225. a) Chen, S. *Langmuir* **2001**, *17*, 2878, b) Guo, Z.; Zhang, Y.; Huang, L.; Wang, M.; Wang, J.; Sun, J.; Xu, L.; Gu, N. *J. Colloid Interface Sci.* **2007**, *309*, 518, c) Krichevski, O.; Markovich, G. *Langmuir* **2007**, *23*, 1496, d) Zhang, Y. X.; Zeng, H. C. *J. Phys. Chem. B*, **2006**, *110*, 16812.

226. Lau, C. Y.; Duan, H.; Wang, F.; He, C. B.; Low, H. Y.; Yang J. K. W. *Langmuir* **2011**, *27*, 3355.

227. a) Oettel, M.; Dominguez, A.; Dietrich, S. *J. Phys.: Condens. Matter* **2005**, *17*, 337, b) Imperio, A.; Reatto, L.; Zapperi, S. *Phys. Rev. E* **2008**, *78*, 021402, c) Chen, W.; Tan, S.; Huang, Z.; Ng, T.-K.; Ford, W. T.; Tong, P. *Phys. Rev. E* **2006**, *74*, 021406, d) Sear, R. P.; Chung, S.-W.; Markovich, G.; Gelbart, W. M.; Heath, J. R. *Phys. Rev. Lett.*, **1999**, *59*, 6255.

228. a) Moleller, M.; Spatz, J. P.; Roescher, A. *Adv. Mater.* **1996**, *8*, 337, b) Sainsbury, T.; Ikuno, T.; Okawa, D.; Pacile, D.; Frechet, J. M. J.; Zettl, A. *J. Phys. Chem. C* **2007**, *111*, 12992, c) Porter, M. D.; Bright, T. B.; Allara, D. L.; Chidsey, C. E. D. *J. Am. Chem. Soc.* **1987**, *109*, 3559.

229. a) Martin, J. E.; Wilcoxon, J. P.; Odinek, J.; Anderson, R. A.;Provencio, P. *J. Phys. Chem. B* **2003**, *107*, 430, b) Kim, B.; Tripp, S. L.; Wei, A. *J. Am. Chem. Soc.* **2001**, *123*, 7955, c) Leff, D. V.; Brandt, L.; Heath, J. R. *Langmuir* **1996**, *12*, 4723 d) Yamamoto, M.; Nakamoto, M. *J. Mater. Chem.* **2003**, *13*, 2064, e) Prasad, B. L. V.; Stoeva, S. I.; Sorensen, C. M.; Klabunde, K. *J. Chem. Mater.* **2003**, *15*, 935.

230. Kanehara, M.; Kodzuka, E.; Teranishi T. *J. Am. Chem. Soc.* **2006**, *128*, 13084.

231. Zirbs, R.; Kienberger, F.; Hinterdorfer, P.; Binder, W. H. *Langmuir* 2005, 21, 8414.

232. Gonzalez-Valls, I.; Lira-Cantu, M. *Energy Environ. Sci.* **2009**, *2*,19.

233. Lux, K. W.; Rodriguez, K. J. *Nano Lett.* **2006**, *6*, 288.

234. Wang, L.; Shi, X.; Kariuki, N. N.; Schadt, M.; Wang, G. R.; Rendeng, Q.; Choi, J.; Luo, J.; Lu, S.; Zhong, C. J. *J. Am. Chem. Soc.* **2007**, *129*, 2161.

235. Yao, H.; Kojima, H.; Sato, S.; Kimura, K. *Langmuir* **2004**, *20*, 10317.

236. Lohmueller, T.; Bock, E.; Spatz, J. P. *Adv. Mater.* **2008**, *20*, 2297.

237. Sistach, S.; Rahme, K.; Périgno n, N.; Marty, J.-D.; Lauth-de Viguerie, N.; Gauffre, F.; Mingotaud, C. *Chem. Mater.* **2008**, *20(4)*, 1221.

238. Schultz, D. G.; Lin, X.-M.; Li, D.; Gebhardt, J.; Meron, M.; Viccaro, P. J.; Lin B. *J. Phys. Chem. B* **2006**, *110,* 24522.

239. Tao, A.; Sinsermsuksakul, P.; Yang P. *Nature Nanotechnology* **2007**, *2*, 435.

240. Kumar, M.; Pathak, A.; Singh, M.; Singla M. L. *Thin Solid Films* **2010**, *519*, 1445.

241. Wen, M.; Qi, K. E. H.; Li, L.; Chen, J.; Chen, Y.; Wu, Q.; Zhang T. *J. Nanopart. Res.* **2007**, *9*, 909.

242. Laskar, I. R.; Watanabe, S.; Hada, M.; Yoshida, H.; Li, J.; Iyoda T. *Surf. Sci.* **2009**, *603*, 625.

243. Garcia, R.; Perez, R. *Surf. Sci. Rep.* 2002, 47, 197.

244. Ruiz, V.; Nicholson, P. G.; Jollands, S.; Thomas, P.; Macpherson, J. V.; Unwin, P. R. *J. Phys. Chem. B*, **2005**, *109*, 19335.

245. a) Ohara, P. C.; Gelbart, W. M. *Langmuir* **1998**, *14*, 3418, b) Vossmeyer, T.; Chung, S.-W.; Gelbart,W. M.; Heath, J. R. *Adv. Mater.* **1998**, *10*, 351.

246. Maillard, M.; Motte, L.; Pileni, M. P. *Adv. Mater.* **2000**, *13*, 200.

247. Khanal, B. P.; Zubarev, E. R. *Angew. Chem. Int. Ed.* **2007**, *46*, 2195.

248. Deegan, R. D.; Bakajin, O.; Dupont, T. F.; Huber, G.; Nagel, S. R.; Witten, T. A. *Nature* **1997**, *389*, 827.

249. a) Zhou, W. L.; He, J. B.; Fang, J. Y.; Huynh, T. A.; Kennedy, T. J.; Stokes, K. L.; O'Connor, C. J. *J. Appl. Phys.* **2003**, *93*, 7340, b) Govor, L. V.; Bauer, G. H.; Reiter, G.; Shevchenko, E.; Weller, H.; Parisi, J. *Langmuir* **2003**, *19*, 9573, c) Guo, Q.; Teng, X.; Yang, H. *Nano Lett.* **2004**, *4*, 1657, d) Liu, Z.; Levicky, R. *Nanotechnology* **2004**, *15*, 1483.

250. Grimme S. *Angew. Chem. Int. Ed.* **2008**, *47(18)*, 3430.

251. Sanchez, C.; Boissière, C.; Grosso, D.; Laberty, C.; Nicole, L. *Chem. Mater.* **2008**, *20*, 682.

252. Sun, L.; Wei, G.; Song, Y.; Wang, L.; Guo, C.; Sun, Y.; Li, Z. *Chem. Lett.* **2007**, *36*, 610.

253. Petit, C.; Taleb, A.; Pileni, M.-P. *Adv. Mater.* **1998**, *10(3)*, 259.

254. Srivastava, S.; Kotov, N. A. *Soft Matter*, **2009**, *5*, 1146.

255. Favier, F.; Walter, E. C.; Zach, M. P.; Benter, T.; Penner, R. M. *Science* **2001**, *293*, 2227.

256. Charrier, A.; Candoni, N.; Thibaudau, F. *J. Phys. Chem. B* **2006**, *110*, 12896.

257. Kane, J.; Inan, M.; Saraf, R. F. *ACS Nano* **2010**, *4(1)*, 317.

258. Hansen, C. R.; Westerlund, F.; Moth-Poulsen, K.; Ravindranath, R.; Valiyaveettil, S.; Bjørnholm, T. *Langmuir*, **2008**, *24*, 3905.

259. Hassenkam, B. T.; Nørgaard, K.; Iversen, L. Kiely, C. J.; Brust, M. *Adv. Mater.* **2002**, *14*, 1126.

260. Mogilevsky, A.; Volinsky, R.; Dayagi, Y.; Markovich, N.; Jelinek, R. *Langmuir*, **2010**, *26*, 7893.

261. Poulin, P.; Stark, H.; Lubensky, T. C.; Weitz, D. A. *Science*, **1997**, *275*, 1770.

262. Vijayaraghavan, D.; Kumar, S. *Mol. Cryst. Liq. Cryst.*, **2009**, *508*, 101.

263. Nielsen. L. K.; Bjørnholm, T.; Mouritsen, O. G. *Nature*, **2000**, *404*, 352.

264. Yuan, M.; Zhan, S.; Zhou, X.; Liu, Y.; Feng, L.; Lin, Y.; Zhang, Z.; Hu, J. *Langmuir*, **2008**, *24*, 8707.

265. a) Jensen, P. *Rev. Mod. Phys.* **1999**, *71*, 1695, b) Taylor, M. D. R.; Moriarty, P.; Brust, M. *Chem. Phys. Lett.* **2001**, *348*, 27.

266. Ko, H.;Singamaneni, S.;Tsukruk, V. V. *Small* **2008**, *4 (10)*, 1576.

267. Nie, S.; Emery, S. R. *Science* **1997**, *275*, 1102.

268. a) Jeanmaire, D. L.; Van Duyne, R. P. *J. Electroanal. Chem.* **1977**, *84*, 1, b) Fleischman, M.; Hendra, P. J.; McQuillan, A. J. *Chem. Phys. Lett.* **1974**, *26*, 163, c) Albrecht, M. G.; Creighton, J. A. *J. Am. Chem. Soc.* **1977**, *99*, 5215.

269. a) Alvarez-Puebla, R. A.; Liz-Marzan, L. M. *Chem. Soc. Rev.* **2012**, *41*, 43, b) Zou, S. L.; Schatz, G. C. *Chem. Phys. Lett.* **2005**, *403*, 62, c) Qin, L.; Zou, S.; Xue, C.; Atkinson, A.; Schatz, G. C.; Mirkin, C. A. *P. Natl. Acad. Sci. USA* **2006**, *103*, 13300.

270. Park, H.; Lee, S. B.; Kim, K.; Kim, M. S. *J. Phys. Chem.*, **1990**, *947*, 576-579.

271. a) Law, S. M.; Eritja, R.; Goodman, M. F.; Breslauer, K. *J. Biochem.* **1996**, *35*, 12329, b) Grajcar, L.; Baron, M. H. *J. Raman Spectrosc.* **2001**, *32*, 912, c) Grajcar, L.; Huteau, V.; Dinh, T. H.; Baron, M. H. *J. Raman Spectrosc.* **2001**, *32*, 1037, d) Otto, C.; Van den Tweel, T. J. J.; de Mul, F. F. M.; Greve, J. J. *Raman Spectrosc.* **1986**, *17*, 289, e) Lecomte, S.; Baron, M. H. *Biospectroscopy* **1997**, 3, 31, f) Chumanov, G.; Cotton, T. M. *SPIE Conference on Biomedical Applications of Raman Spectroscopy* **1999**, *3608*, 204.

272. a) Kumaki, J. *Macromolecules* **1988**, *21*, 749, b) Gaines Jr., G. L. *Langmuir* **1991**, *7*, 834, c) Brinkhuis, R. H. G.; Schouten, A. J. *Macromolecules* **1991**, *24*, 1487, d) Kaku, M.; Hsiung, H.; Sogah, D. Y.; Leavy, M.; Rodriguez-Parada, J. M. *Langmuir* **1992**, *8*, 1239, e) Ringard-Lefebvre, C.; Baszkin, A. *Langmuir* **1994**, *10*, 2376, f) Li, B.; Wu, Y.; Liu, M.; Esker, A. R. *Langmuir* **2006**, *22*, 4902, g) Li, B.; Esker, A. R. *Langmuir* **2007**, *23*, 2546, h) Li, H.; Sachsenhofer, R.; Binder, W. H.; Henze, T.; Thurn-Albrecht, T.; Busse, K.; Kressler, J. *Langmuir* **2009**, *25*, 8320.

273. Gao, C.; Yan, D. *Prog. in Polym. Sci.* **2004**, *29*, 183.

274. a) Fréchet, J. M. J.; Tomalia, D. A. *Dendrimers and other dendritic polymers*, West Sussex Wiley, **2001**, b) Gao, C.; Yan, D. *Prog. in Polym. Sci.* **2004**, *29*, 183, c) Voit, B. *J. Polym. Sci. Part A: Polym. Chem.* **2000**, *38*, 2505.

275. Malmstrom, E.; Johansson, M.; Hult, A.; *Macromol Chem. Phys.* **1996**, *197*, 3199.

276. Sayed-Sweet, Y.; Hedstrand, D. M.; Spinder, R.; Tomalia, D. A. *J. Mat. Chem.* **1997**, *7*, 1199.

277. Schenning, A. P. H. J.; Elissen-Roman, C.; Weener, J-W.; Baars, M. W. P. L.; van der Gaast, S. J.; Meijer, E. W. *J. Am. Chem. Soc.* **1998**, *120*, 8199.

278. Tanaka, K.; Dai, S.; Kajiyama, T.; Aoi, K.; Okada, M. *Langmuir* **2003**, *19*, 1196.

279. Liebau, M.; Janssen, H. M.; Inoue, K.; Shinkai, S.; Huskens, J.; Sijbesma, R. P.; Meijer, E. W.; Reinhoudt, D. N. *Langmuir* **2002**, *18*, 674.

280. Saville, P. M.; White, J. W.; Hawaker, C. J.; Wooley, K. L.; Frechet, J. M. J. *J. Phys. Chem.* **1993**, *97*, 293.

281. Saville, P. M.; Reynolds, P. A.; White, J. W.; Hawaker, C. J.; Frechet, J. M. J.; Wooley, K. L.; Penfold, J.; Webster, J. R. P. *J. Phys. Chem.* **1995**, *99*, 8283.

282. Pao, W-J.; Stetzer, M. R.; Heiney, P. A.; Cho, W-D.; Percec, V. *J. Phys. Chem. B* **2001**, *105*, 2170.

283. Zhai, X.; Peleshanko, S.; Klimenko, N. S.; Genson, K. I.; Vaknin, D.; Vortman, M. Ya.; Shevchenko, V. V.; Tsukruk, V. V. *Macromolecules* **2003**, *36*, 3101.

284. Ornatska, M.; Peleshanko, S., Genson, K. L.; Rybak, B.; Bergman, K. N.; Tsukruk, V. V. *J. Am. Chem. Soc.* **2004**, *126*, 9675.

285. Zagar, E.; Zigon, M. *Macromolecules* **2002**, *35*, 9913.

286. Zagar, E.; Zigon, M.; Podzimek S. *Polymer* **2006**, *47*, 166.

287. Hilles H.; Maestro A.; Monroy F.; Ortega F.; Rubio R. G.; Velarde M. G. *J. Chem. Phys.* **2007**, *126*, 124904.

288. a) Vilanove R.; Rondelez F. *Phys. Rev. Lett.* **1980**, *45*, 1502, b) Takahashi A.; Yoshida A.; Kawaguchi M. *Macromolecules* **1982**, *15*, 1196, c) Kawaguchi M.; Yoshida A.; Takahashi A. *Macromolecules* **1983**, *16*, 956, d) Vilanove R.; Poupinet D.; Rondalez F. *Macromolecules* **1988**, *21*, 2880.

289. a) Ybert, C.; Lu, W.; Moller, G.; Knobler, C. M. *J. Phys. Chem. B* **2002**, *106*, 2004, b) Lu, W.; Knobler, C. M.; Bruinsma, R. F. *Phys. Rev. Letters* **2002**, *89*, 146107, c) Courier, C.; Knobler, C. M.; Daillant, J.; Chatenay, D. *Langmuir* **2002**, *18*, 9434, d) Hatta, E.; Fischer, Th. M. *J. Phys. Chem. B* **2002**, *106*, 589, e) Lipp, M. M.; Lee, K. Y. C.; Takamoto, D. Zasadzinski, J. A.; Waring, A. J. *Phys. Rev. Letters* **1998**, *81*, 1650.

290. Moore, B. G.; Knobler, C. M.; Akamatsu, S.; Rondalez, F. *J. Phys. Chem.* **1990**, *94*, 4588.

291. Knobler, C. M. *Science* **1990**, *249*, 870.

292. Angelova, A.; Vollhardt, D.; Ionov R. *J. Phys. Chem.* **1996**, *100*, 10710.

293. Angelova, A.; van der Auweraer, M.; Ionov, R.; Vollhardt, D.; de Schryver, F. C. *Langmuir* **1995**, *11*, 3167.

294. Kaganer, V. M.; Mohwald, H.; Dutta, P. *Rev. Modern Phys.* **1999**, *71*, 779.